MAGNETOENCEPHALOGRAPHY: TECHNICAL IMPROVEMENTS IN IMAGE CO-REGISTRATION AND STUDIES OF VISUAL CORTICAL OSCILLATIONS

Peyman Adjamian

Doctor of Philosophy

Aston University

November 2002

ASTON UNIVERSITY

MAGNETOENCEPHALOGRAPHY: TECHNICAL IMPROVEMEN IN IMAGE CO-REGISTRATION AND STUDIES OF VISUAL CORTICAL OSCILLATIONS

PEYMAN ADJAMIAN

Doctor of Philosophy

2002

The work presented in this thesis is divided in two distinct sections. In the first, functional neuroimaging technique of Magnetoencephalography (MEG) is described ar new technique is introduced for accurate combination of MEG and MRI co-ordi systems. In the second part of this thesis, MEG and the analysis technique of SAM are u to investigate responses of the visual system in the context of functional specialisa within the visual cortex.

In chapter one, the sources of MEG signals are described, followed by a b description of the necessary instrumentation for accurate MEG recordings. This chapte concluded by introducing the forward and inverse problems of MEG, techniques to s the inverse problem, and a comparison of MEG with other neuroimaging techniques.

Chapter two provides an important contribution to the field of research with M Firstly, it is described how MEG and MRI co-ordinate systems are combined localisation and visualisation of activated brain regions. A previously used co-registra methods is then described, and a new technique is introduced. In a series of experiment is demonstrated that using fixed fiducial points provides a considerable improvement in accuracy and reliability of co-registration.

Chapter three introduces the visual system starting from the retina and ending v the higher visual areas. The functions of the magnocellular and the parvocellular pathw are described and it is shown how the parallel visual pathways remain segreg throughout the visual system. The structural and functional organisation of the visual co is then described.

Chapter four presents strong evidence in favour of the link between consci experience and synchronised brain activity. The spatiotemporal responses of the vi cortex are measured in response to specific gratings. It is shown that stimuli that ind visual discomfort and visual illusions share their physical properties with those that ind highly synchronised gamma frequency oscillations in the primary visual cortex.

Finally, chapter five is concerned with localisation of colour in the visual cortex this first ever use of Synthetic Aperture Magnetometry to investigate colour processin the visual cortex, it is shown that in response to isoluminant chromatic gratings, the hig magnitude of cortical activity arise from area V2.

Keywords: Magnetoencephalography; Synthetic Aperture Magnetometry (SAM); MEG/EEG-MRI co-registration; Functional specialisation; Visual discomfort and Visua illusions; Oscillatory gamma activity, colour localisation.

Dedication

This thesis is dedicated
to my parents Manouchehr and Fatimeh,
to my sister Parisa,
and to Ian D. Johnston.

Acknowledgement

The work described in this thesis was carried out by the author, with the following exceptions:

Chapter 2. The experiments were carried out under the guidance of Dr. Arjan Hillebrand and Dr. Gareth Barnes. The simulation described in experiment 2 was carried out by Dr. Gareth Barnes.

Signed:

I have received many sources of support and assistance during my time at Aston. I would like to thank my supervisor, Dr. Ian Holliday for the guidance, and for providing me the opportunity to carry out this work.

Special thanks must go to Dr. Gareth Barnes and Dr. Arjan Hillebrand for supervision of experiments in chapter 2 and for their generosity to devote so much of their time to provide valuable feedback and advice, throughout the years. Also, thank you both for making the MEG lab so enjoyable to work in.

I am also grateful to Dr. Krish Singh, who never refused a request for help, or to provide guidance, and to pass on his knowledge and experience on analysis techniques.

Thanks must also go to my fellow postgraduates, and in particular Andy Turvey, Pamela Madden, Vanessa Parson, Alison Fisher, and Sian Worthen, plus all other postgrads who, at one point or other, were my contemporaries and who helped make the good times what they were and the hard times more bearable.

But most significant of all are four individuals without whom I would not be here today: to my parents and my sister, as everything I achieve in life is down to the sacrifices they made for me; and to Ian D. Johnston for his unwavering support and encouragement and for being a second father to me throughout my journey in foreign lands.

TABLE OF CONTENTS

FIGURES

CHAPTER 1

CHAPTER 2

CHAPTER 3

CHAPTER 4

CHAPTER 5

TABLES

CHAPTER 2

CHAPTER 3

CHAPTER 4

CHAPTER 5

Chapter 1. The Principles of Magnetoencephalography

1.1 Introduction

Magnetoencephalography (MEG) is a neuroimaging technique that provides an adequate understanding of the function of the brain because of its ability to localise sources of electric and magnetic activity with an excellent temporal and ever-improving spatial resolution. The first MEG recording was carried out by David Cohen using a one-sensor magnetometer (Cohen, 1968). MEG is a non-invasive technique for estimating the sources of intracranial currents by measuring the neuromagnetic fields outside the head. The electrical signals from a group of firing neurons in the brain constitute a small, but detectable, electrical current across the scalp, which is measured as potential difference between scalp electrodes with the electroencephalogram (EEG). The electrical current, in turn, generates a magnetic field, which can be measured outside the head with the MEG. Therefore, MEG is based on the principle that the time-varying magnetic fields produced by current flow are capable of inducing currents in detection coils placed outside the head. The magnitude of these signals is infinitesimal compared to the earth's magnetic field, requiring highly sensitive cryogenic devices for their successful detection and extraction from background noise. The output waveforms are similar in appearance to EEG and can be recorded either as continuous traces or as averaged event-related responses.

In this chapter, the generation of MEG signals is briefly discussed followed by instrumentation that is required for effective neuromagnetic recording. The final parts of this chapter are concerned with the forward and inverse problems and their influence upon the spatial resolution of MEG. This is followed by a brief review of a number of techniques used to solve the inverse problem. The novel MEG inversion technique of Synthetic Aperture Magnetometry is then described with emphasis upon its advantages over other source reconstruction algorithms. Finally, the advantages and disadvantages of MEG over other neuroimaging modalities are described by comparison to EEG, fMRI, and PET.

1.2 The Source of MEG Signals

The MEG signals are magnetic fields outside the head that are produced by electrical currents within the head. Just like an electric current passing through a wire generates a magnetic field, so does an ionic current within the brain. When a region of the brain is activated, a *primary current* source is produced due to the movement of ions. In addition to this primary current, a secondary or a *volume current*, which is a passive *ohmic current*, is set up in the periphery such that there is no build-up of charge. Both the primary currents and the volume currents generate a magnetic field. However, volume currents occur outside the head, as will be discussed in subsequent sections.

1.2.1 The neurons of cortical grey matter

The cerebral cortex consists of 6 layers of neurons that are organised parallel to its surface with layer 1 being the most superficial. The two principal groups of neurons are the *stellate* and the *pyramidal cells*. The pyramidal cells bodies (figure 1-1a and 1-1b) are mainly found in layer 3 of the cerebral cortex are larger than stellate cells, and their dendrites spread parallel to each other (Wikswo, 1989).

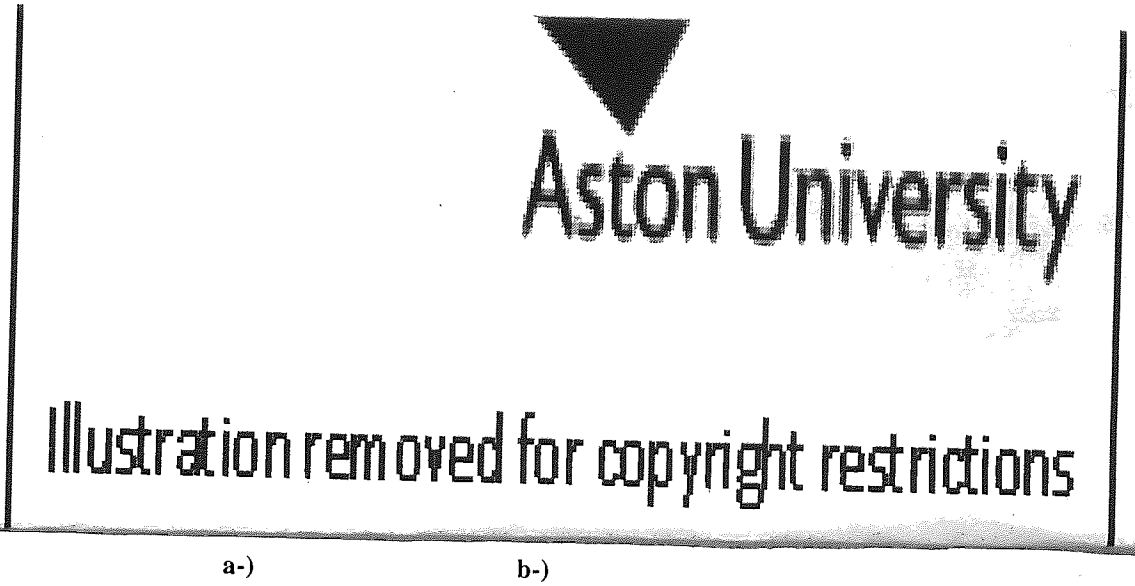

a-) b-)

Figure1-1. **(a)** A single pyramid neuron with its apical dendrite towards the surface of the cortex; **(b)** a population of pyramid cells in layer 3, stretching parallel to each other and perpendicular to the cortical surface. From Wikswo (1989).

Stellate cells populate layers 2, 4, and 5, are smaller in size, and cannot produce a measurable magnetic field. On the other hand, the pyramidal cells generate a significant magnetic field outside the head when activated, as they stretch in a direction perpendicular to the cortical surface. Because of this, the electrical current flow is also produced in a direction perpendicular to the cortical surface (Wikswo, 1989).

The source of electrical currents of the brain, and hence the magnetic fields, lie in the neurons of the cortical grey matter (MEG signals are mainly due to cortical currents and do not directly apply to subcortical structures). The neuronal membrane is selectively permeable, controlling the exchange of ions between the inside and the outside of the cell. It also maintains an electrical gradient that is necessary for neuronal firing. When the neuron is not stimulated, it maintains an electrical polarisation, or a resting potential, which is the result of unequal distribution of ions between the inside and the outside of the neuron. This causes a negative electrical potential of approximately –70mV inside the neuron compared to its outside. During a resting potential, the concentration gradient of ions is such that sodium (Na^+) is over ten times more concentrated on the outside than on the inside of neuronal membrane, while potassium (K^+) is over twenty times more concentrated inside the neuron than outside. However, because the body possesses more sodium than potassium ions in total, Na^+ concentration is much greater outside the cell compared to the K^+ concentration inside, and hence the inside is more negatively charged, due mainly to the existence of chloride (Cl^-) ions. The purpose of this negative resting potential is to prepare the neuron for a rapid response to stimuli and is maintained through a protein complex known as the sodium-potassium pump (Kalat, 1992).

In general, two types of neuronal activity can be discriminated which are important in the generation of measurable electromagnetic field currents. These are the *action potential* and the *postsynaptic potential*, both of which are related to the flow of Na^+ and K^+ ions between the inside and the outside of the cell.

1.2.2 The action potential

The polarisation of a neuron can be altered by either a negative charge, which increases the polarisation causing hyperpolarisation, or by a positive charge, which causes depolarisation. If the depolarising current is sufficiently strong to reach a certain threshold (approximately –40mV), the membrane produces a large response and causes an action potential (figure 1-2). This alters the permeability of the neuronal membrane for certain ions allowing mainly sodium to cross the membrane. When the neuron is depolarised, an axial current flow is induced within the axon that is caused by local excess of positive charge. This causes an accumulation of positive charge near the end of the arrow as shown in figure 1-3. The excess of positive charges at this point causes an outward flow of currents that return to the place of depolarisation origin through the extracellular space. Similarly, during the repolarisation process, the ions return to their original place, inducing an intracellular flow of negative currents. An action potential lasts for approximately 1msec.

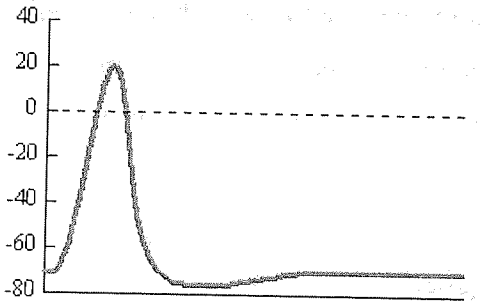

Figure 1-2. The action potential. Depolarisation of neuronal membrane beyond the threshold produces a disproportionately large response.

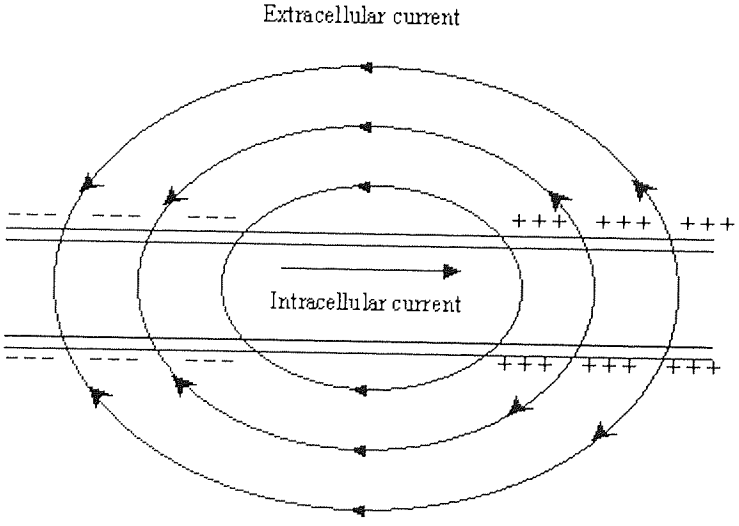

Figure 1-3. Intracellular and Extracellular current flow associated with depolarisation of the action potential.

The strength of an action potential is sustained and does not fade with distance, as each point along the membrane regenerates the action potential in much the same way as it was generated by the initial impulse. When an action potential causes the flow of sodium along a point on the membrane, that point becomes positively charged with respect to its adjacent areas. The positive charge then flows down the axon and crosses the membrane in a new location, and as it moves further down the axon it depolarises the neighbouring areas of the membrane. If the depolarisation is sufficient to reach the threshold (approximately –40 mV), the permeability of the membrane in this area will be altered and the ions flow to the cells, causing them to fire an action potential of their own (Figure 1-4). In this way the action potential is propagated, passing like a wave along the axon. For a more detailed description of this process see Wikswo (1989).

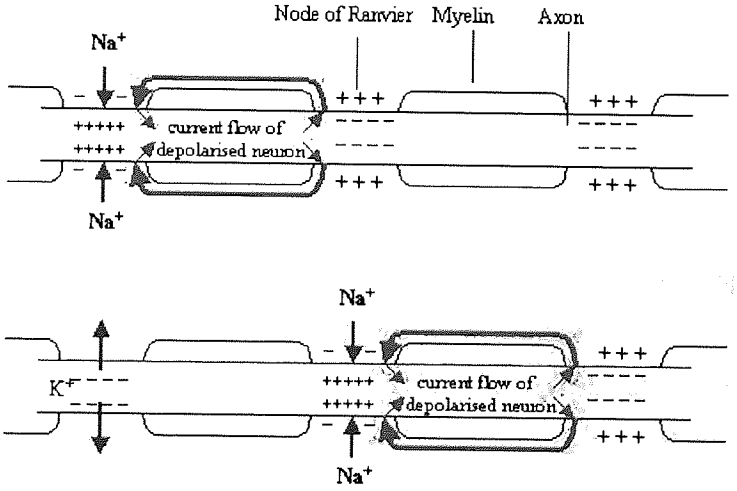

Figure 1-4. The principle of propagation that drives neuronal connectivity is responsible for an action potential. The arrows indicate direction of ionic flow

1.2.3 The postsynaptic potential (PSP)

Neuronal depolarisation is regenerated in a neighbouring neuron as the presynaptic neuron delivers a synaptic transmission to the postsynaptic neuron. When the action potential reaches a synapse, it causes an accumulation of positive charges on the presynaptic membrane due to the intracellular current. Some of this charge then moves across the synapse to arrive at the postsynaptic neuron, causing a new action potential. This movement of ions to the postsynaptic neuron also produce a steady potential distribution

that extends beyond the spatial limits of the synapse itself producing the postsynaptic potential. Unlike an action potentials that is always depolarisation, PSP may be either a depolarisation (excitatory) or a hyperpolarisation (inhibitory), while the strength of the current flow decreases with distance from the synapse. An excitatory postsynaptic potential (EPSP) occurs when sodium ions enter the cell, while an inhibitory postsynaptic potential (IPSP) results from potassium ions leaving the cell or chloride ions entering the cell. Swinney and Wikswo (1980) provide a detailed description of the complex processes occurring at the level of single neurons that lead to the origin of the measurable electromagnetic fields.

PSP activity is a slower process than the action potential and the consequent current distribution related to a PSP lasts for several tens, or even hundreds, of milliseconds. Additionally, PSP activity can be synchronised across many neurons. On the other hand, the repolarisation process is not synchronous across a sufficient number of neurons in order to produce a detectable magnetic field. Furthermore, the action potential is too short and hence there can be no signal summation. MEG, therefore, measures the response of the postsynaptic neuron and the PSP in particular. The measured magnetic field is the summation of the non-propagating EPSP or IPSP at the postsynaptic terminals. The pyramidal cells are aligned in parallel columns, orthogonal to the cortical surface (Okada, 1982), while the generated PSP has duration of approximately 100ms with a peak value of approximately 10mV (Romani, 1989). Therefore, both *spatial and temporal summation* is possible when sufficient synapses (about 10^6) are activated in relative synchrony (Nunez, 1986). This summed activity creates a change in the magnetic field that is strong enough for detection by MEG. At a typical measurement distance, which is at least 2 cm from the source, many current configurations seem dipolar. In other words, the synchronous activity forms a current dipole layer, which can be considered as a single current dipole when observed from a distance much larger than the dimensions of the area of active cortex. The unit strength of a dipole is expressed as A*m (amper*meter). For a more comprehensive account of the neurogenesis of evoked magnetic fields see Okada (1989).

1.3 Neuromagnetic Instrumentation

The firing of a single neuron is obviously insufficient to produce a measurable magnetic field outside the head, mainly due to source currents in neighbouring neurons that flow in opposite direction. Therefore, the synchronous firing of tens of thousands of neurons is required, occupying an area of several mm^2. Each mm^2 of the cortical surface is estimated to cover 100,000 neurons (Rockel et al. 1980), and although only half are pyramid cells, an adequate electric or magnetic field is generated for measurement. However, even a large population of neurons can still create only very weak magnetic currents that are many orders of magnitude smaller than the earth's magnetic field, thus requiring highly sensitive sensors as well as a significant reduction in interference from environmental and other sources of disturbance. In the next sections, the essential requirements for MEG recording are described.

1.3.1 The SQUID

A main requirement for measuring the magnetic fields of the brain is magnetic field detectors of high sensitivity. The neuromagnetic field created by the activity of cortical neurons is in the femtoTesla range and typically as weak as 10^{-12} tesla, which is weaker than both the earth's static magnetic field of about 0.5×10^{-4} tesla (see figure 1-5), as well as the urban fluctuating magnetic background of about 10^{-7} tesla. Because of the extremely small magnitude of magnetic fields to be detected, MEG signals are first detected by super-conducting pick-up coils and then coupled into *Superconducting*

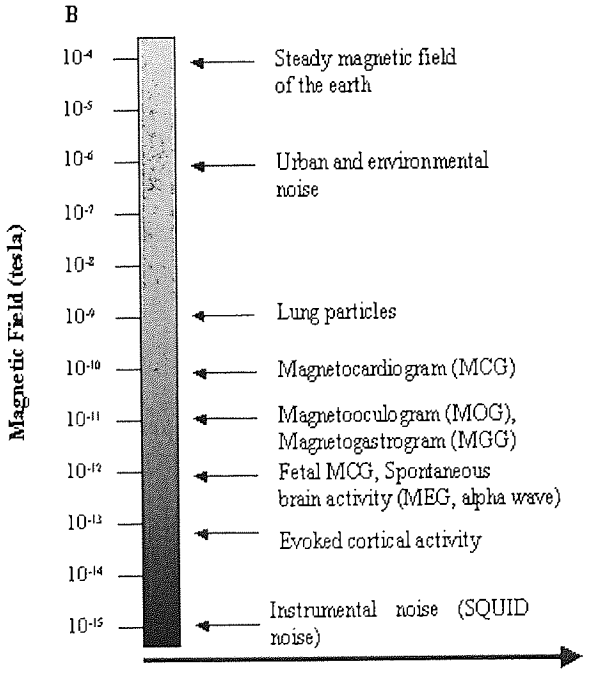

Figure 1-5. Comparisons of field strengths versus frequency

QUantum Interference Devices, or *SQUIDs*, that are highly sensitive to small magnetic fields (Zimmerman, 1977). The superconductive state is the state where electric resistance is zero. Materials that become superconducting at very low temperatures lose their resistance to the flow of electrical currents and can thus be used to measure very small potentials induced by changes in magnetic flux. Therefore, SQUIDs operate at cryogenic temperatures (Tc = 4 K or -269°C) and are contained in a liquid helium (LHe) dewar. Essentially, a SQUID sensor converts the magnetic flux into voltage such that alterations in the magnetic flux result in voltage changes across the SQUID circuitry. It can be shown that the voltage is non-linear and periodic with the changing flux (Swithenby, 1980). The magnetic flux is then measured by counting the number of voltage steps. It consists of a superconducting ring interrupted by one or two weak links, or Josephson (1962) junctions, which limit the flow of the supercurrents. Two types of SQUID have been used, the rf SQUIDs and the dc SQUIDs. The more commonly used SQUID in magnetometers contain two junctions and is referred to as dc SQUID because of their high sensitivity and low noise level (Clarke et al., 1976).

1.3.2 Flux transformers

The magnitude of magnetic fields is given as the number of lines of magnetic force, or *magnetic flux density*. Since SQUIDs are very sensitive to variations in magnetic field, the magnetic flux is fed into it by means of a transformer, which shields the SQUIDs from unwanted noise. This consists of a pick-up coil, which coupled with the SQUID, forms an entirely superconducting loop called the *flux transformer*. The flux transformer is often constructed as a gradiometer that measures the gradient of the magnetic field rather then the magnetic field itself (Vrba, 1997). The purpose of using gradiometers is to cancel unwanted sources of interference. There are complementary techniques for cancellation of noise, which will now be described in some detail.

1.3.3 Noise reduction techniques

An essential requirement for MEG measurement is the suppression of magnetic background noise. Commonly, a combination of magnetic shielding and gradiometer devices are used.

1.3.3.1 Magnetic shielding

Significant outside disturbances and magnetic noise is caused by environmental factors such as moving vehicles, radio and television frequencies, and the ever-present geomagnetic and power line fields, all of which produce significantly greater magnetic fields than the brain. This type of magnetic background can be counteracted in a magnetically shielded room (MSR) where one or more layers of a high permeability alloy such as μ-metal provide effective ferromagnetic shielding against low frequencies of urban magnetic noise. An increase in the number of wall layers improves the degree of shielding. In addition, a layer of a high conductivity metal such as aluminium is used to shield against higher frequency fields. These fields induce Eddy currents that create magnetic fields that are of opposite direction and hence cancel the noise fields in the material (Cuffin and Cohen, 1977).

1.3.3.2 Gradiometers

Shielding only attenuates the external magnetic fields and does not provide defence against magnetic field disturbances that arise inside the MSR such as muscle artefacts, the heart, and other internal organs. For instance, the heart generates a field that is at least two orders of magnitude greater than that created by the cortical neurons (Hamalainen et al., 1993). Therefore, another way to suppress noise is to use gradiometers, which measure the gradient of the magnetic field instead of the magnetic field itself. The principle of noise rejection by gradiometers is based on the following: the magnetic field is first measured by two coils formed in winding loops. As these loops are wound in opposite directions, they cancel out the homogenous part of the field. The magnetic field falls off as the square of

distance. As distant sources produce more homogenous fields than nearby sources, for a gradiometer sensitivity to nearby sources is greater (Carelli and Foglietti, 1983). In other words, distant magnetic fields induce virtually identical currents in the two coils giving no net output from the gradiometer. Magnetic fields due to sources near (about a baseline away) to the pick-up coil will induce a considerably larger current in the pick-up than compensation coil leading to a net gradiometer output. Therefore, by measuring the spatial gradient rather than the overall magnitude of a magnetic field, it is possible to accentuate signals from sources near the detection system, while minimising the contribution from stronger distant sources (Vrba, 1997). Advanced gradiometers reduce background noise further by incorporating more coils in different locations, forming higher order gradiometers.

Various gradiometer configurations are shown in figure 1-6. The coil at one end is called a pickup coil and the coil wound in opposite direction is called compensation coil. This arrangement is known as a first-order gradiometer and the distance between the two coils is called the baseline. A simple magnetometer pick-up coil (1-6a) is rendered useless in blocking nearby noise sources such as the heart. A first-order axial gradiometer (1-6b) is insensitive to homogenous magnetic fields. This is effective in measuring the non-homogenous magnetic fields of nearby sources. A second-order axial gradiometer, as that shown in 1-6c, further improves the cancellation of magnetic fields produced by distant sources. It consists of two first-order gradiometers connected together in opposite directions such that the pick-up coil is insensitive to gradients of homogenous and uniform fields alike.

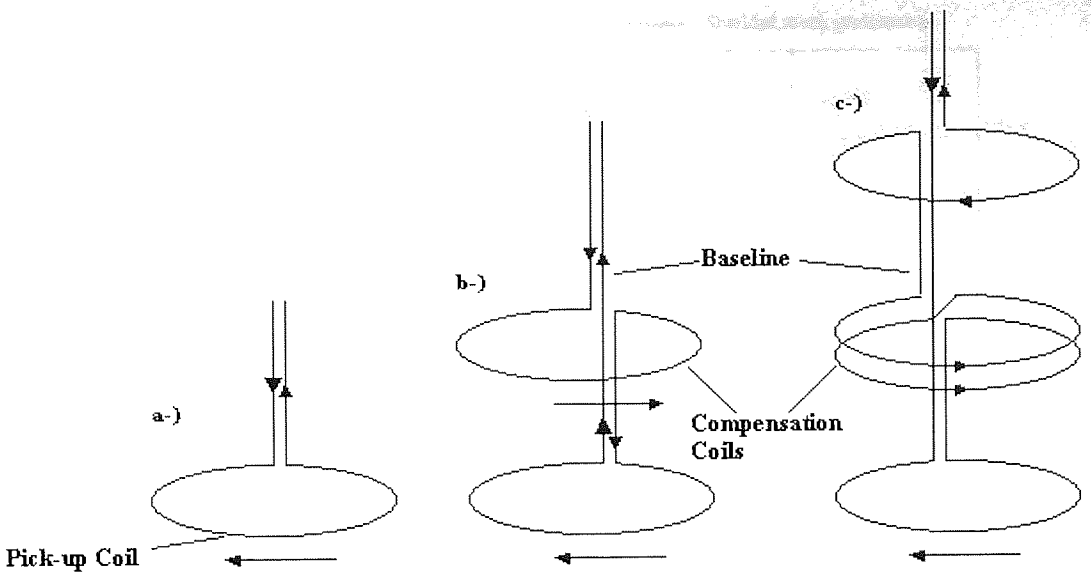

Figure 1-6. Various types of flux transformers: **(a)** simple magnetometer (pick-up coil); b-) first-order axial gradiometer; **(c)** second-order axial gradiometer.

An example of the effect of gradiometer configuration on the strength of the measured noise is shown in figure 1-7 demonstrating the reduction of disturbance by a passenger car with and without MSR. A simple magnetometer in the open environment is sensitive to disturbance caused by a passenger car at a distance of several kilometres. On the other hand, a first order gradiometer in the open environment would only be sensitive to disturbances at several hundred meters. In a shielded room, a second order gradiometer is as effective as a third order gradiometer in the open environment. In a shielded room, noise reduction is equivalent to increasing the gradiometer order by one (Vrba et al., 1994). Therefore a third order gradiometer in open environment offers better protection than a shielded lower order gradiometer. Higher order gradiometer hardware requires large spacing between coils, which is not possible in large array multi-channel systems. Therefore synthetic gradiometers are constructed to further suppress environmental noise (Vrba et al., 1994).

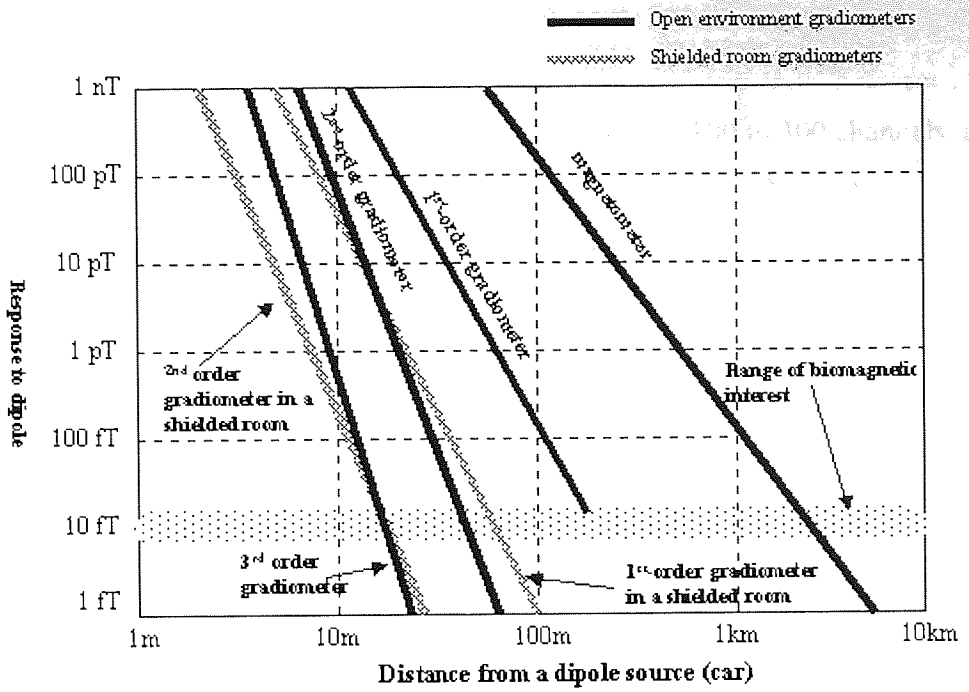

Figure 1-7. Example of noise rejection by gradiometers with and without MSR. Dipole signal as a function of distance. A magnetometer would detect a 10fT signal at a distance of several km from dipole, while a 3rd-order gradiometer would detect a 10fT signal only when the dipole approaches a distance of 20m. In a shielded room, noise reduction is equivalent to increasing the gradiometer order by one such that a shielded 3rd-order gradiometer would detect a 10fT signal only if the distance from the dipole is approximately 10m. Redrawn from CTF Systems Manual, with permission.

1.4 The Aston Neuromagnetometer

State-of-the-art neuromagnetometers contain between 100 to 300 channels, allowing for simultaneous recording of signals all over the scalp. At Aston University's Neurosciences Research Institute, research is conducted using a 151-channel CTF Omega system (CTF Systems Inc., Port Coquitlam, Canada) housed inside a MSR (figure 1-8). The MEG sensors are uniformly distributed, in a grid (figure 1-9a), over the inner surface of the helmet-shaped dewar filled with liquid helium and cover the entire head (figure 1-9b). Average inter-channel spacing is approximately 3.1 cm. A 2cm diameter and 5cm baseline first-order axial gradiometers are employed, which is the optimum choice for maximizing the signal-to-noise ratio of brain signals in realistic environments. Each gradiometer is connected to a low-noise planar DC SQUID and coupled with their flux transformers. The SQUIDs are placed in the cryogenic insert with vacuum linings that minimise the interaction of outside heat with the LHe environment. Facility is provided for simultaneous EEG recording using low magnetic noise electrodes that plug into a head box mounted near the patient support. The system comprises of a reclining chair, which can be replaced by an extended seat for studies in various modes, such as sleep, while the helium-containing dewar can be reclined accordingly. For presentation of certain types of stimuli such as in vision studies, the stimulus generator is placed outside the MSR and projected through a window in the room and onto an adjustable mirror inside the room.

The microvolt signals of MEG are transmitted through an amplifier, which provide an output signal in the volt range. Once detected by the SQUIDs, and after initial amplification, the SQUID signals are further processed in the data collection system. Conditioning electronics are used to transform the quantum periodic signals of the SQUIDs into a linear representation of the magnetic field. The data acquisition system allows the acquisition of many channels simultaneously at a sample rate of up to 2500Hz, which is high enough to measure the brain activity of interest.

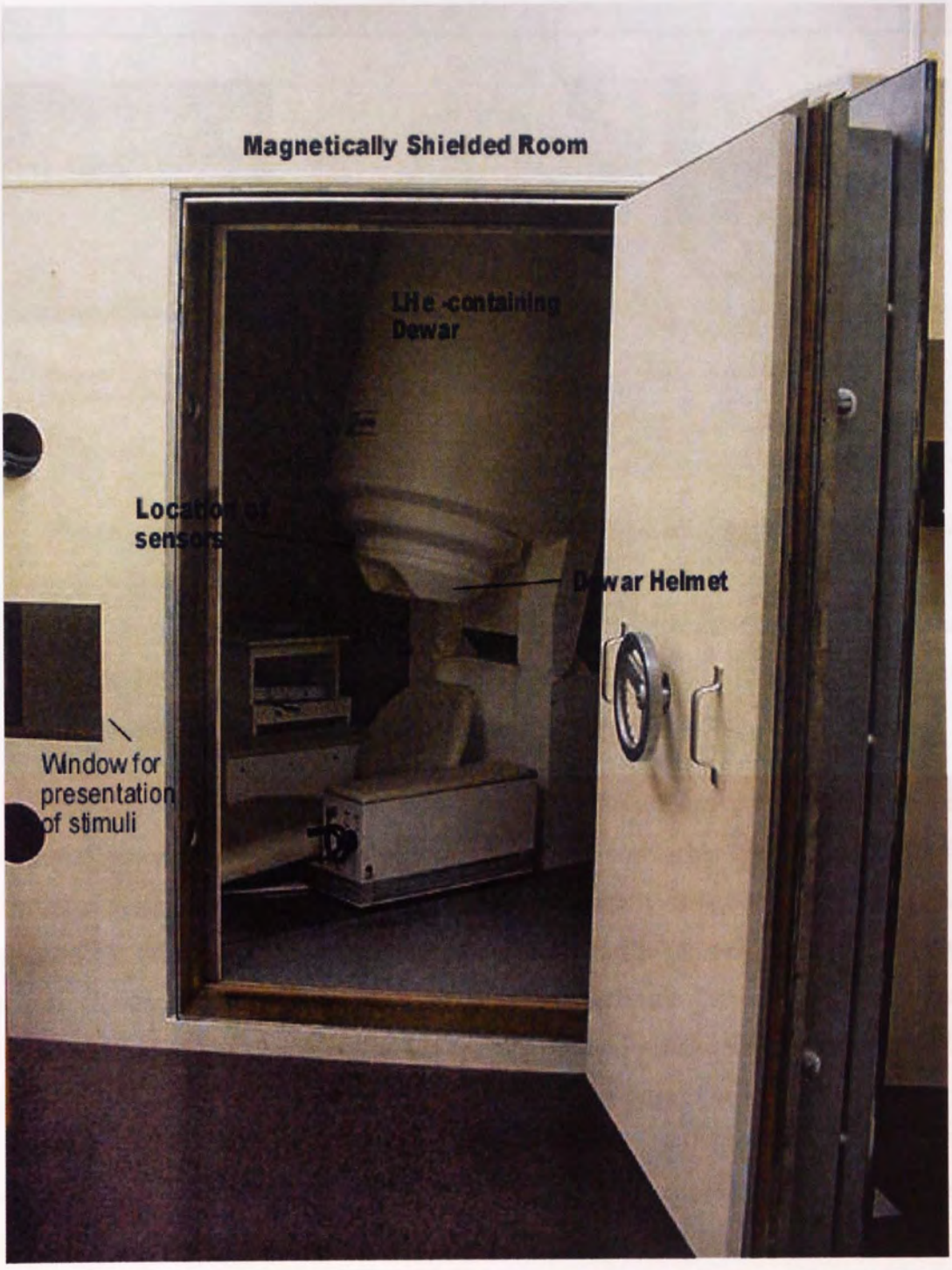

Figure 1-8. The Aston CTF Omega 151-channel Neuromagnetometer in a magnetically shielded room. The stimuli are projected from the outside through a window in the shielded room and onto a mirror inside the room.

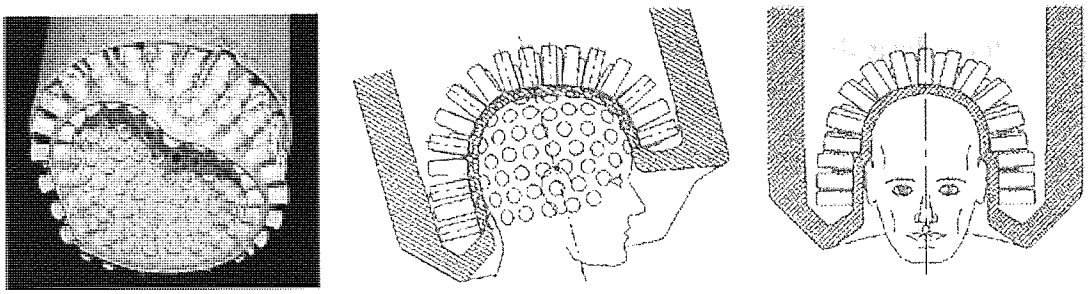

a) b)

Figure 1-9. a) the grid containing the magnetic field sensors; and **b)** schematic diagram of the MEG sensor array. Reproduced from CTF Systems Inc. with permission

The results of MEG data analysis can be overlaid on an image of the brain, often obtained by magnetic resonance imaging (MRI), in order to relate cortical function to its structure. A successful correlation relies on accurate co-registration between anatomical and functional data and is achieved by combining the head co-ordinate system from the two modalities. Details of this procedure will be given in the next chapter.

The aim of bioelectromagnetism, is to estimate the primary currents that are driven by neuronal processes. However, there is no direct relationship between the magnetic field measured at the sensor level and the potential distribution. This is because the data is also influenced by secondary currents, or the ohmic currents in the periphery of the volume conductor (Hamalainen et al., 1993). In order to estimate the total current density, information regarding the conductivity of the volume conductor as well as the electric field strength in the conductive medium is required. The relationship between the total current density and the magnetic field distribution can be solved by applying *Maxwell's equations.* The interested reader is referred to Hamalainen et al. (1993) for the mathematical basis of this relationship. The ultimate aim of MEG is to discover which areas of the brain generate this magnetic field. In order to estimate the neuronal sources that generate the magnetic field of interest, one must solve the inverse and the forward problems, which will be briefly described in the following sections.

1.5 The Inverse Problem

In EEG and MEG, accurate localisation of cortical activity depends on the ability to make reasonable estimates about the number, spatial configuration, location, strength, and time-course of the neuronal currents that give rise to the magnetic field. The problem of estimating the region of the source of brain activity is of paramount importance in improving the spatial resolution of EEG and MEG. However, there is not a unique solution to this problem as there can be an infinitely large number of sources that produce the same electric potential or magnetic field (Scherg and Berg, 1991; see Sarvas, 1987 for a comprehensive review). This so-called *bioelectromagnetic inverse problem* for MEG and EEG is thus referred to as *non-unique*. In other words, given exact MEG/EEG data, there could be an infinite number of different three dimensional source distributions that could have exactly produced the measured signals. This problem is heightened by magnetically silent sources in that, unlike *tangential sources* that are detected by both MEG and EEG (Wood 1985), *radial sources* do not produce a magnetic field outside the head (Cohen and Cuffin, 1983) thus remaining undetected by MEG. Similarly, if two dipoles with the same orientation and direction are relatively close to each other, compared to the distance at which they are measured, the resulting field will be indistinguishable from the field of a single dipole (Balish and Muratore, 1990).

Because of the non-uniqueness of the inverse solution, it is necessary to describe a model for the sources, as well as for the head, in order to limit the possible source distributions, such that a "constrained inverse solution" is solved (Nunez, 1986). One such way is to add *a priori* information, or assumptions about the number and location(s) of active brain regions. *A priory* assumptions introduce constraints based on temporal as well as spatial information, thus limiting the orientation of the sources, or making assumptions regarding the time of onset/offset of stimuli and cortical activity over time (Aine et al., 1989). However, such *a priori* information merely provide a unique solution within the frame of the constraints used while a solution to the non-uniqueness of inverse problem in general still remains. In order to solve the inverse problem, one must solve the forward problem, described in the next section.

1.5.1 The Forward problem

The forward problem is the problem of estimating the amount of brain activations at the level of the sensors and computing the output of the sensors due to sources in the brain as accurately as possible. The source of the electromagnetic data is obtained by reducing the differences between the measured and the predicted signals. By making certain assumptions and simplifications (such as modelling the shape of the head as a homogenous volume conductor and modelling the magnetic field as a dipolar current source) the magnetic field in the sensors can be computed using volume conductor theory based on the law of Biot and Savart. A full description of the mathematical principles related to the computation of the forward problem is given by Sarvas (1987). which are briefly described below.

1.5.2 Volume Conductor Models

1.5.2.1 Creating a spherically homogenous head model

The pattern of extracellular currents is affected by the conductivity and shape of the surrounding medium, which consists of several components, including the cerebral tissue, the scalp, and the skull. With a spherically homogenous head model, the magnetic field does not depend on the conductivity of the head itself. Volume currents do not affect the component of the magnetic field that is normal to the sphere, such that recorded magnetic fields reflect the intracellular currents only. In order to reconstruct the source of underlying activations, it is necessary to model such a complex medium accurately. In MEG and EEG, the source maybe restricted to a volume, often a sphere, which represents the head. This is often achieved by a model consisting of a set of concentric spheres that represent the scalp, the skull, and the brain (De Munck, 1989). The spheres have to be fitted to the head in such a way that it provides an adequate description of its curvature. This is obtained by using a segmented image of the head from an MR image. De Munck (1989) provides a comprehensive description of this procedure. The EEG requires three or four concentric spheres with differing conductivities to represent the brain and the surrounding medium. In

contrast, with the MEG, the head can be modelled using a single homogenous sphere representing the inner boundary of the skull, which approximates the circumference of the head compartment as accurately as possible. It is possible to use a single sphere because concentric spherical layers do not disturb the magnetic field produced by a current dipole source in the sphere (Williamson and Kaufman, 1981). But this is not always achievable (e.g. when the current sources are in the temporal area) in which case more realistic modelling with boundary element method (BEM) or finite element method (FEM) is applied. For more details on these methods, the reader is referred to Hamalainen and Sarvas (1989).

One important implication of spherical head model is that the radial component of the magnetic field is due to the primary currents and not the volume currents throughout the conductive medium, which cancel due to spherical symmetry (Cuffin, 1986). Therefore, only tangential current dipoles contribute to the magnetic field outside, while the radial sources are externally silent making no contribution to the measured magnetic fields (Cohen and Cuffin, 1983). This leads to certain important implications: a) dipoles located at the centre of a homogenous, spherically symmetric volume conductor cannot be detected by magnetic measurements; b) because pyramidal neurons are perpendicular to the cortical surface, only those located inside the fissures of the cortex are magnetically detectable. This does not cause a significant limitation at least as far as the primary sensory areas (visual, somatosensory, and auditory) are concerned since they are mainly located within the fissures (Hamalainen et al., 1993). More recently, Hillebrand and Barnes (2002) have shown that the direction of a source does not affect the detection of MEG signals; rather it is the depth of sources, which is a more significant factor.

1.5.3 Source Models

In the following sections, several algorithms that are commonly used to find a solution to the bioelectromagnetic inverse problem are described. These techniques can be divided in two general categories: those for localisation of *discrete sources*, and those for localisation of *distributed sources*. However, it must be emphasised that neither group of

techniques is a solution to the non-uniqueness of the inverse problem, but that each uses a different approach to locate the sources of brain signals as accurately as possible.

1.5.3.1 The Equivalent Current Dipole (ECD)

As described in section 1.2.3, the neural activity can be considered as a single current dipole at the measurement distance in which case it can be most simply modelled as a dipolar field. Therefore, the *equivalent current dipole* (ECD) model is commonly used to find a solution to the inverse problem and to approximate the flow of electromagnetic currents in a small area. The aim is to fit one or a few ECDs to the observed field distribution. The optimal solution is reached by approximating the measured and theoretical field patterns in a least square sense. The final solution is the reconstructed source of electromagnetic brain activity. In a fixed dipole model, the orientation of dipoles can be varied or it can be fixed, and it is assumed that they are at a fixed position during a given time interval while their strength varies over time. Another model is that of a moving dipole whereby dipoles are allowed to change their orientation, strength, and position over time, thus fitting more than one independent dipole across time. A comprehensive account of the theoretical background of these models is given by Sarvas (1987).

A current dipole is described by a set of parameters that define its position, orientation, and strength within the head. When recording brain activity with MEG or EEG, the ongoing background signals and spontaneous brain activity are a source of noise. When using sensory stimuli that produce a clear evoked response, the signals must be averaged so that these evoked responses can become distinguished from the background noise. Ideally, signals should be recorded over a large area of the brain with sensors that are no more than 2 cm apart (Hamalainen et al., 1993). For an adequate signal-to-noise ratio it is necessary to record evoked responses to the same stimulus many times to increase the strength of a signal relative to the noise in the signals. Once the dipole fitting procedure is complete, the location of the ECDs can be displayed on a co-registered MRI of the subject.

One extension to the ECD fitting procedure is the *Monte Carlo* analysis (Medvick et al., 1989) in which randomly generated errors are added to the recorded magnetic fields as though they occurred during the measurment process, and the sources are reconstructed for each. This is repeated a large number of times (~100) to reconstruct an approximate distribution of the dipole parameters for the perturbed fields. The 95% ellipsoid based on the distribution of the dipole locations provides a measure of the stability of the source reconstruction with respect to noise.

However, the current dipole procedure is relevant in situations where there exists a clear evoked response to time- and phase-locked stimuli in the recorded signals. One limitation of MEG has been that the measurement of higher order cognitive functions such as memory and language are not easily feasible because such activities are modulated by input from various regions of the brain that cannot be adequately and directly correlated with external events. On the other hand, sensory or motor responses are well synchronised with external stimuli. Therefore, MEG has been best suited for studies of sensory responses mainly arising from the surface of the cortex. An increasing number of analytical techniques are now available that allow processing of data with high spatial resolution. These techniques are based on increasing the number of sensors, which often exceed 100. By increasing the number of scalp locations from which activity can be recorded, the average inter-sensor distance is greatly reduced. As a result, the spread of activation from discrete cortical sources can be brought into focus. The usefulness of spatial sampling techniques for EEG is limited since the spatial details of electrical sources are distorted by the highly resistive nature of the skull. On the other hand, magnetic responses are electrical epiphenomena, which occur outside the head because the skull has limited effect on magnetic field topography. By means of sophisticated spatial analysis techniques, and in addition to a high concentration of sensors, it is possible to obtain an accurate map of the spatial topography of brain magnetic fields. In the next sections, some alternatives to the single ECDs are described with regard to their assumptions, advantages, and disadvantages over other techniques currently in use. Subsequently, it becomes clear that one such technique, SAM, provides a more adequate estimation of the electromagnetically active sources of the brain.

1.5.3.2 Multiple Signal Classification (MUSIC)

A *single ECD* is used under the assumption that the recorded electromagnetic activity is the result of a single current source. However, when multiple sources are active, the assumptions of a single ECD model are invalid. In these situations, multiple dipole models can be used with multiple latencies as an alternative, resulting in significant improvement in accuracy of source localisation (Achim, 1995). But the problem with this strategy is the increase in the number of unknown parameters, since the time-series of each source as well as dipole orientation and location must be estimated (George et al., 1991). One solution is to use the *multiple signal classification* (MUSIC) algorithm to localise multiple dipolar sources from the data (Mosher et al., 1991). MUSIC uses a single dipole to scan through a grid confined to a three dimensional *source space*. The forward model for a dipole at each location is projected against a *signal subspace* or a *noise subspace* determined from the MEG or EEG data. MUSIC identifies sources with minimum forward projection onto the noise subspace or those with maximum forward projection onto the signal subspace rank. It has been shown that instead of testing all possible dipole orientations for each location, it is possible to perform an eigenvalue decomposition (Singular Value Decomposition or SVD) to identify the optimum orientation of the dipole (Mosher et al., 1992). The most important assumption of MUSIC is that the measured signal is the consequence of a number of sources that are always less than the number of sensors. In other words, that the measured magnetic field is generated by a few discrete sources of activity. It also assumes that the signal and noise subspaces can be separated.

One major problem of MUSIC is the difficulty in choosing the locations that give the best projection onto the signal subspace. An improved version of the algorithm, Recursive MUSIC (R-MUSIC), was later developed to counter this and other limitations of the original algorithm. A description of the improved algorithm is beyond the scope of this brief introduction and the interested reader is referred to Mosher and Leahy (1998) for a detailed account of R-MUSIC.

Nevertheless, numerous limitations of MUSIC remain: normally there is no clear separation between the signal and the noise subspaces. Therefore it is not possible to extract the signal subspace accurately. Consequently, the calculated source location may not be the true one. Furthermore, the maximum number of sources that can be reconstructed is equal to the number of sensors. Due to noise in the data, the rank is even smaller than the number of measurements. This can be a serious problem for low channel MEG/EEG systems while modern systems are not hindered by this limitation. Finally, it remains to be proven whether the algorithm is also suitable for distributed sources.

1.5.3.3 Minimum-Norm Least-Squares (MNLS) Inverse Approach

MUSIC is based on the assumption that the measured electromagnetic activity is the consequence of discrete sources. But this may not always be the case, particularly when a distributed source is located on the convolutions of the cortical surface. The minimum-norm least-squares (MNLS) approach is an algorithm that can reconstruct the properties of source current distribution based on a set of measurements. The first distributed source model was the simple minimum-norm solution introduced by Hämäläinen and Ilmoniemi (1984). Its aim was to release the constraints imposed by the dipole model by resorting to a distributed source solution making minimal assumptions about the source. The solution is made unique by selecting the current distribution with minimum overall source power. In effect, MNLS looks for an inverse estimation that minimises the residual error, such that the sum of squares of the differences between the measured field pattern and that from the predicted field has minimum power among all least-squares solutions (Wang, 1993). *A priori* assumptions are required in order to define a source space in which a set of dipoles approximate the primary current distribution. It is also assumed that the image space (the source space defined by *a priori* assumptions) is at the same location as the true source space that produced the magnetic field (but this is not always the case due to, for example, MEG/MRI co-registration errors (see chapter 2)). MNLS requires many sensors in order to obtain an adequately detailed image of the reconstructed source. Furthermore, source estimation with MNLS creates a bias towards solutions nearest to the sensors, due to the minimum norm constraints. Finally, for discrete sources, the solutions are spread out,

producing blurred images of a point source, which makes the interpretation of the data more difficult (Hari, 1991).

1.5.3.4 Low Resolution Electromagnetic Tomography (LORETA)

Low Resolution Electromagnetic Tomography (LORETA) is an algorithm that avoids some of the problems associated with the MNLS approach, such as the bias towards superficial source distributions. It was originally formulated by Pasqual-Marqui et al. (1994) and attempts to obtain more localised solution than the minimum-norm solution. LORETA finds the inverse solution that maximises only the synchronisation of strength between neighbouring neuronal populations. The method assumes that the current distribution is smooth (rather than a limited number of dipolar points). The smoothness of all the possible current is found by applying a minimum spatial Laplacian. LORETA, indeed, produces a blurred image of a point source. Therefore, it has a relatively low spatial resolution and the result is still a distributed source. Consequently, two simultaneously active nearby sources can be misleadingly represented as a single source.

1.5.3.5 Focal Underdetermined System Solver (FOCUSS)

The Focal Underdetermined System Solver (FOCUSS) (Gorodnitsky et al., 1992) can also overcome the problem of biasing associated with MNLS. The FOCUSS algorithm starts by finding the minimum-norm solutions with an additional weight on the solution and iteratively updates the previously obtained solution. Solutions are concentrated around the best-fitting sources until they are resolved. Once the rank of the weighted basis matrix reaches a number less than that of the measurements, the algorithm has converged. It is claimed that the FOCUSS algorithm can resolve both the depth and extent of cortical sources. The only problem with the algorithm is that in order to converge to the correct solution, the initial solution will have to be as precise as possible (Gorodnitsky and Rao, 1997). If not, subsequent iterations may also be inaccurate. Therefore, although the algorithm will always find a localised solution, it is not necessarily the correct one.

1.6 Synthetic Aperture Magnetometry (SAM)

Synthetic aperture Magnetometry (SAM) is a minimum variance beamformer, which provides tomographic images of the alterations in cortical power within selected frequency bands and within pre-determined active and passive states. Inverse solutions such as ECD do not provide information regarding alterations in source power. SAM is essentially a noise reduction technique, based on the spatial selectivity of the gradiometer being more sensitive to the nearby, rather than the distant, sources (Robinson and Vrba, 1998). For each voxel in the brain, source power is estimated by minimising signal power due to all other sources. Each voxel is scanned with a fixed array of weighted channels, or sensors, using an *optimal spatial filter* for that voxel. An *optimal weight* is calculated for each voxel based on the statistics of the data such that it attenuates distant fields while enhancing those from nearest sources. This spatial filter provides a measure of source power in each voxel as a function of time, using the *weighted sum of all the MEG sensors*. Therefore, the output is a *synthetic depth electrode* or a *virtual electrode* that has the same millisecond temporal resolution as the original MEG signals. The entire timeseries can be divided into active and passive states and Fourier analysis can be performed to calculate the power in each frequency band. Because spontaneous MEG signals are produced by more sources than there are sensors, SAM only reveals sources that have a high signal-to-noise-ratio and contribute to a significant proportion of the overall signal. A MEG beamformer uses amplitude information rather than phase inhomogeneities that arise from neuronal propagation (Robinson and Vrba, 1998). Furthermore, unlike signal space projection techniques (e.g. MUSIC), noise sources do not confound with target source, but they become suppressed by the spatial filter.

The main advantage of SAM as an analytical technique of MEG is that it does not rely on averaging many short epochs, each of which must be time- and phase-locked to the stimulus presentation. SAM uses the covariance of the recorded data and therefore the presence of a clear evoked response is no longer a requirement, hence the data is still time-locked to the stimulus, but not phase-locked. Furthermore, unlike dipole fitting, *a-priori* assumptions regarding the number of active sources are no longer required, instead of

which volumetric images are constructed with 'hotspots' representing locations of significant difference between the active and passive epochs. SAM also gives MEG the resolution to examine sensory, or motor, as well as cognitive brain activity even without magnetic shielding (Robinson, 1997).

One characteristic of the brain is its ability to alternate between a synchronised and a desynchronised state, representing changes in cortical power due to external events. These changes in brain states reflect high and low amplitude signals and are referred to as *event-related synchronisation* (ERS) and *event-related desynchronisation* (ERD), respectively (Pfurtscheller and Lopes Da Silva, 1999). This important feature of the brain is discussed in more detail in section 3.9. One important advantage of SAM is that the investigation of these differences between brain states during pre-specified passive and active states is made possible within pre-specified frequency bands. The difference in cortical power during active and passive states can be calculated with *t* statistics using all the recorded passive and active epochs. For each voxel in the brain this procedure is repeated, generating a 3-dimensional *differential current density map* (DCDM). These can then be superimposed on an anatomical image of the subject's own brain (an MR image). SAM, therefore, provides a method for studying higher-level cognitive tasks, such as language and memory, which last for many seconds and are not phase-locked to the stimulus. With this MEG analysis technique, it has become possible to perform traditional boxcar paradigms that have previously been used with fMRI and PET only (Singh et al., 2001). These advantages are the motivation for choosing SAM as the preferred technique to analyse the data in the final two chapters of this thesis that relate to visual function.

It must be re-emphasised that despite its advantages, SAM is not an inverse solution, but that it is a beamformer that circumvents the inverse problem (Robinson and Vrba, 1998). SAM has a major disadvantage that perfectly synchronised sources are not detected as they cancel each other out. But sources with highly correlated time courses are unlikely to occur (particularly for studies consisting of time windows that last some seconds) and this is mainly a problem for conventional evoked-potential studies where cortical responses are perfectly phase-locked to the onset of the stimulus. This is precisely

the reason why SAM is most suited to time-locked, but not phase-locked data that run over long epochs. It has been shown that temporal correlation must be relatively high (>0.7) for cancellation to take place, and it is highly unlikely for two or more areas of the brain to maintain high temporal correlation with millisecond precision over the entire course of the epoch of interest (Van Veen et al.1997).

1.6.1 Grouping of SAM functional volumes

Using SPM99, it is possible to construct an average of a group of SAM pseudo t images. In functional neuroimaging, statistical analyses of data is voxel-based such that at each voxel, a statistic representing the induced effect of stimuli for that voxel is computed, thus creating a statistic image or statistical parametric map (SPM). The entire array of the image voxels is in this way assessed in order to identify all regions affected by experimental stimuli. As described above, SAM provides precisely such an activation map. This means that the data can be co-registered with the subject's own MRI, spatially normalised, and averaged to form a group image. Spatial normalisation transforms each subject's data into the 3-dimensional anatomical co-ordinate space of Talairach and Tournoux (1988). This allows comparable co-ordinates to be given for foci in each subject. Therefore, as with fMRI studies where images from individual subjects can be used for group statistical analysis, SAM images too, once spatially normalised and averaged, can be used for statistical analysis of data from a group of subjects (Singh et al., 2002).

SPM is a parametric test with which it is assumed that the data is normally distributed and uses variances created within each subject's data. The effect of the stimulus is thus assessed at each voxel independently, which can then be transformed from t-statistic into Z-scores and into probabilities. This is referred to as a fixed-effects model group SAM analysis (Singh et al., in press), representing the simplified effects of the averaged responses from all the subjects. However, it is known that the spatial distribution of ERD/ERS can be highly variable between subjects particularly since many studies employ low number of subjects. Consequently, the assumption of a normal distribution is violated as a consequence of which a significantly higher activation of any given area in one subject

compared to the rest, may distort other sources of activity from the remaining subjects in the group. For this reason, a non-parametric permutation analysis (SnPM) of the averaged image of interest is also used, which does not require assumptions regarding normality, or compliance to particular spatial distribution. Nichols and Holmes (2002) provide a detailed description of non-parametric methods of statistical analysis for use in function neuroimaging, while Singh et al., (in press) describe how the technique can be adapted for use with SAM.

The resulting SAM averages, as well as individual SAM images, can then be adapted for visualisation on a template brain. One limitation of SPM/SnPM method is that the data is visualised on one such template representation of the brain that has been transformed into co-ordinate space of Talairach and Tournoux (1988). The normalisation of the brain does not give adequate information regarding highly localised activations, such as those inside the sulci or the gyri, which are variable in position in different individuals. Therefore, the normalisation procedure only gives good information regarding low spatial frequency activation maps that are less detailed (Singh et al., in press).

Group SAM studies are further problematic in that they are open to a number of interpretations regarding areas of significant activation (Singh et al., in press). An activated cortical area in a group study may represent a spatial location that is consistently activated in all subjects, but only weakly. This means there maybe other areas with more significant activation but their locations maybe so spatially variable in each individual that they are no longer significant after normalisation to template space. On the other hand, a significantly active region of cortex on a template brain may be considered as an important area for processing of the given task in its own right. Therefore care must be taken when interpreting data driven from groups (Singh et al., in press).

1.7 Justification for choosing SAM as the preferred inversion technique

None of the inversion techniques described in this chapter can offer a unique and satisfactory solution to the bioelectromagnetic inverse problem. Each method involves formulation of certain assumptions, while constraints must be applied that limit the number of solutions. Therefore, comparison between these techniques can only be made in the context of the feasibility of assumptions and the nature of the constraints. Consequently, a technique is only optimal under these conditions and its superiority depends on the type of information that is required from the data. The method chosen for the type of studies in chapters 4 and 5 of this work is SAM because it makes the least number of assumptions and is ideal for the type of induced effects associated with the experimental stimuli.

The most appealing features of SAM as an inverse technique are:

- Unlike techniques that incorporate the use of dipoles, SAM does not require *a priori* assumptions about the number of active sources.
- SAM does not require a high signal-to-noise ratio, as it does not rely on signal averaging. Therefore, studies into the effect of non-phase-locked stimuli become possible.
- Unlike techniques where each solution is based on the previous one (e.g. FOCUSS), estimates of power change for each voxel in SAM is independent of all other voxels, and can be made sequentially without influencing other sources.
- Unlike methods that use signal space projection (e.g. MNLS) where nearby sources interfere with the output of the filter for target location, SAM uses beamformers that take advantage of the entire MEG sensor array in order to produce spatial filters.
- As the data covariance is used to obtain the solutions, task-related changes of spectral power can be obtained between active and passive states in terms of ERD and ERS.
- Given anatomical information, spatial normalisation can be applied to each set of data for use in standard template space and group statistical maps (SPMs) of activity can be calculated.

On the other hand, SAM has only a few limitations. One major problem that is characteristic of beamformer techniques is that spatially separate sources that are synchronous will be self-cancelling. But as discussed earlier, it is unlikely for two sources to maintain high temporal correlation over any length of time and this is mainly a problem for traditional evoked response paradigms. In theory, this problem can be largely overcome by using longer epochs. The longer the stretch of data, the less likely it will be for two sources to remain synchronous over its entire course. This makes SAM more suitable for studying cognitive tasks, which have so far been a domain of fMRI and PET techniques. Another problem of SAM is that the resulting images are spatially smooth and inhomogeneous, requiring statistical flattening before multiple comparisons can be made between sets of data (Barnes and Hillebrand, 2003). Therefore, care must be taken when interpreting the data.

Throughout this work, and in each of the chapters where SAM is applied, its merits are again highlighted. This will further substantiate its suitability both in the context of experimental paradigms employed and in terms of the type of information we hope to obtain from the data.

1.8 Comparison of MEG to other neuroimaging modalities

1.8.1 Comparison of MEG and EEG

From a broad perspective that includes all the neuroimaging modalities, the similarities between EEG and MEG far outweigh their differences. Although the MEG and EEG traces are produced by a common source, a MEG map over the head has a different spatial pattern compared to the EEG map, which may reveal additional sources of cortical activity (Cohen and Cuffin, 1983). The EEG measures the difference in voltage, or potential, between two electrode sites across the scalp one of which is placed at an electrically silent location to act as a reference point. The problem with reference points, however, is that no electrode site is completely electrically silent. Yet, a topographic map representing the distribution of electrical potential over the head can be constructed from such a recording. But unlike a topographic map of the MEG, it is not possible to assume that the source of cortical activity lies between the regions of maximum and minimum extrema. This is because the location of the reference electrode determines the position of the zero potential, and therefore, any change in the location of reference electrode changes the location of the zero line.

This problem of EEG is compounded by the poor conductivity of the skull and the surrounding tissue, such that the scalp current potentials cannot be considered a true reflection of the brain's electrical events, contributing an estimated 5% to the extracranial measured magnetic field only (Hamalainen and Sarvas, 1989). Therefore, in order to estimate the amount of current between adjacent electrodes and accurately interpret the EEG signals, precise knowledge of the thickness and conductivity of the scalp and skull is required. On the other hand, a simple magnetometer measures the absolute magnitude of the magnetic field without requiring a reference. The scalp and skull contribute approximately 5% to the extracranial measured magnetic field only (Hamalainan and Sarvas, 1989). An advantage of MEG over EEG therefore is that neuromagnetic signals penetrate the skull and scalp without any significant distortion. As a result, the spatial resolution of MEG is potentially higher than that of EEG.

MEG and EEG measure different neuronal populations. The EEG records dipoles oriented in any direction but it is more sensitive to a radially oriented dipole when a tangential dipole is also present (Cohen and Cuffin, 1983). On the other hand, the MEG is primarily sensitive to tangentially oriented dipoles because in a spherically symmetric volume conductor, a radially oriented dipole does not produce a magnetic field outside the volume conductor (De Munck, 1989). For EEG, the pattern of the topographic map changes depending on the presence of radial or tangential dipoles. The pattern of a MEG topographic map does not change. The distribution of the magnetic field for a tangential dipole in a homogenous, spherically symmetric volume conductor is shown in figure 1-10. For a tangential dipole, the map of the magnetic field consists of two extrema; a maximum and a minimum, where the magnitude, direction, and position of the dipole inside the sphere are related to the characteristics of the pattern (Williamson and Kaufman, 1987; Romani et al., 1982). The dipole lays half way between the negative and positive field extrema.

The low spatial resolution of EEG and low-channel MEG systems reflects the fact that activity is recorded at only a small number of scalp sites. The spatial detail obtained from conventional EEGs is so inadequately global that functional traces can only be meaningfully interpreted in terms of the underlying functional neuroanatomy at the level of entire brain.

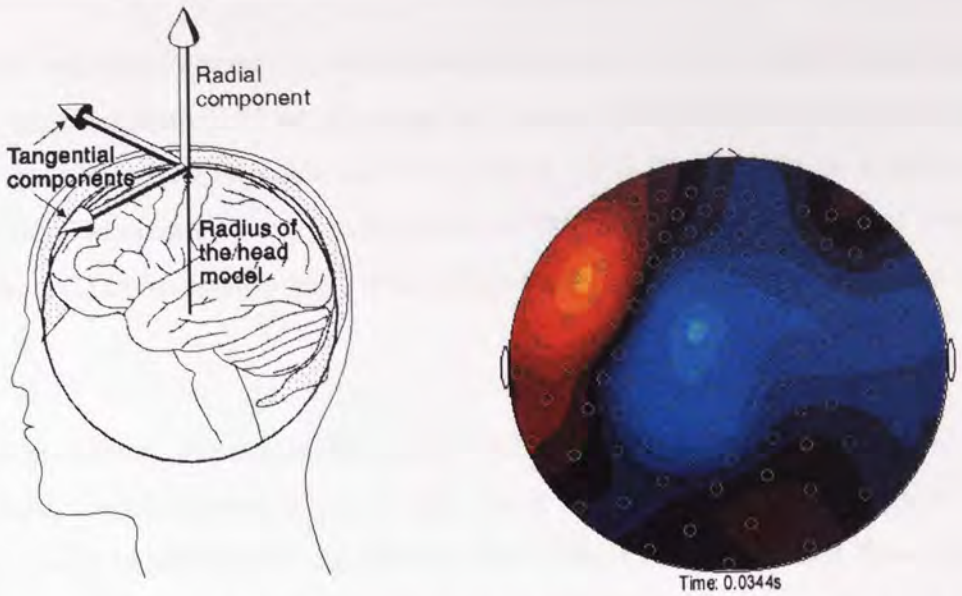

Figure 1-10. On the left, the difference between radial and tangential sources in their orientation (from Malmivuo et al, 1997); the magnetic field produced by a radial current dipole is zero outside the sphere. Only tangential current dipoles can produce a magnetic field outside the sphere. A colour coded topographic map of a magnetic field pattern at 34ms (on the right) recorded for the onset of electrical stimulation applied to the median nerve of the right hand. A dipolar field is clearly apparent, indicating that the source of cortical activity can be probably modelled by a single equivalent current dipole in the left somatosensory cortex. Such topographic maps depict the distribution of signal power at the sensors and not that of the sources. Source reconstruction can be achieved by applying, for example, equivalent current dipole procedures.

1.8.2 Comparison of MEG and fMRI

The difference between MEG and other imaging techniques such as functional magnetic resonance imaging (fMRI) and positron emission tomography (PET) is that it provides estimates of magnitude and direction of net current flow. MEG is a direct measure of neuronal activity within the brain. fMRI and PET however are based on correlates of neural currents such as haemodynamic and/or metabolic changes, which are only secondary consequences to changes in cortical activity. They are based on the assumption that local metabolic changes are indirectly related to increased neuronal function. These techniques are slower and only indirectly measure the electrical activity of the brain. PET is an invasive technique that involves the injection of small radioactive traces into the blood stream, which on reaching the brain reveal areas with increased regional cerebral blood flow (rCBF) presumably caused by increased activity of the underlying neurons. fMRI is a

non-invasive technique whereby a radiofrequency magnetic field is applied to the patient placed in a static magnetic field while a large coil outside detects weak radio signals arising from the head. Blood oxygenation level dependent (BOLD) in fMRI is a method for visualising haemodynamic changes using levels of blood oxygen as indicator of increased activity. The BOLD contrast is high when oxygenation of the blood is decreased (Aine, 1995).

The spatiotemporal resolution of the fMRI signal has been the cause of some debate. Firstly, it must be ascertained whether the BOLD signals reflect changes of blood flow in the large blood vessels, or whether they reflect changes in the finer mesh of vascular network known as the parenchyma. Identifying the vascular source of BOLD signals has important implications for the spatial resolution of the fMRI method since oxygenation levels in large veins could reflect activity that emanates from large areas of the brain, in which case they represent the average activity over these regions and thus the neural resolution will be poor. Some evidence suggests that most of the signal arises from the cortical capillaries (Menon et al., 1995), and others have localised fMRI signals with a precision of 1.1 mm (Engel et al., 1997), which suggests that a significant portion of the signal arises from vessels that serve a small region of the brain. Moreover, retinotopic mapping of the visual cortex with fMRI, to be described in chapter 3, has revealed that signals change position smoothly rather than alternating between large veins, thus indicating that at least as far as the visual cortex is concerned, the signals originate at the smaller veins. However, a spatial resolution of about 1.5 mm is not sufficient to measure certain structures such as the orientation and ocular dominance columns of V1. Furthermore, the temporal resolution of the fMRI BOLD signal is not ideal in accurately resolving the sub-millimetre responses of cortical neurons, given also that they are secondary phenomena during which many cortical responses can take place. Boynton et al., (1996) measured the temporal response of the fMRI signal in calcarine cortex using various visual stimuli and estimated that the temporal filter has a delay of roughly 5 seconds, measuring from the initial latency of response and including the peak.

When compared to fMRI and PET, MEG has the following advantages and disadvantages: MEG is a totally non-invasive technique that directly measures the electromagnetic responses of the brain, providing excellent temporal, and reasonable spatial resolution. The presence of signals is evidence of cortical activity, and apart from signal averaging, there is no need for complicated statistical analyses. Interpretation of fMRI data is hindered by the complex relationship between changes in BOLD signals and the underlying neural activity. On the other hand, MEG is a victim of the non-uniqueness of the inverse problem and does not provide information regarding the extent of cortical activation. Therefore, the spatial resolving power of MEG does not match that of fMRI and PET. However, recent applications of beamformer techniques to analysis of MEG data, such as SAM, have improved the spatial resolution MEG. MEG signals are easily contaminated by noise as a result of which MEG requires a magnetically silent environment for high quality data. Figure 1-12 offers a summary of the spatial and temporal resolutions of each brain imaging modality.

Figure 1-11. Spatial and temporal resolution of experimental neuroimaging techniques, among which MEG offers the best temporal resolution. From CTF Systems Inc.

1.9 Conclusion

Magnetoencephalography is a neuroimaging technique that can be used in a wide variety of research situations. Compared to other, more commonly used, neuroimaging techniques such as fMRI and PET, MEG is a direct measurement of the ongoing brain activity. It can lead to a better understanding of functioning of neuronal networks because of its ability to provide excellent temporal and reasonable spatial resolution, although the use of beamformer techniques in MEG data analysis has improved upon the latter. The localisation of sources within the brain has to be presented with reference to anatomical and structural information obtained from other modalities, such as MRI. This is the scope of the next chapter in which the results of numerous experiments provide evidence for improved accuracy and reliability of a MEG/MRI co-registration technique.

Chapter 2. The Co-registration of MEG and MRI Co-ordinate Systems

2.1 Introduction

Co-registration of neuroimaging data obtained from two different modalities can cause a number of problems, most commonly associated with the accuracy of the procedure. The ultimate aim of neuroimaging techniques is to provide information regarding the precise location of the sources of brain activity and enable researchers and clinicians to relate the function of the brain to its structure. Because MEG and EEG are functional modalities that provide mainly the temporal aspect of brain activity, it is necessary to relate this functional data to the underlying neuronal activation. Therefore, accurate co-registration of MEG/EEG data with MR images is required. An accurate co-registration is particularly important in clinical assessment and pre-surgical identification of the loci of interest.

At Aston University, we have utilised a bite-bar for co-registration of MEG with MRI. This technique, though efficient, has been problematic in a number of ways, which are concerned both with its accuracy as well as its ease of use and implementation. In this chapter, an improved co-registration method will be described, which, based on the previous bite-bar approach, provides greater accuracy for combining structural data obtained from MRI with functional data from MEG or EEG. The methods involved in co-registration are first described and the procedure for co-registration using the previous technique as well as the technique using the new bite-bar is described. In a number of experiments, designed to test the reliability and accuracy of co-registration procedures, it is demonstrated that the new method is far superior to other techniques that use head-based reference points, currently in practice elsewhere.

2.2 Methods and aims of MEG/MRI co-registration

Essentially, co-registration of MEG with MRI requires the transformation of two sets of data into a single co-ordinate system. The co-registration of anatomical scans is often volume-based, where a statistical comparison of intensity values is sufficient for co-registration. Fitzpatrick et al. (1998) have described a technique for co-registration of anatomical scans from two different modalities, which is used to identify targets of interest pre-surgically. This technique is based on markers fixed to the bones of a patient undergoing surgery, which Fitzpatrick and colleagues claim to be the most accurate co-registration technique. However, this approach is obviously unsuitable for purely research purposes. There are two alternative methods for co-registration of MEG/EEG with MRI: those based on fiducial markers (George et al., 1989; Wieringa, 1993, PhD thesis; Fuchs et al., 1995) and those based on surface matching (Pelizzari et al., 1989; Schwartz et al., 1996; Huppertz et al., 1998). These methods are introduced in the following sections. But first, co-registration of data from MEG/EEG with MRI requires that the co-ordinates for the location of the source areas in MEG/EEG be converted into the co-ordinate system of the MRI scan. The former are represented by either current dipoles or SAM functional volumes (where this analytical technique is applied), while the latter are structural images of the subjective brain. Therefore, the two co-ordinate systems have to be taken into account, which will now be briefly described.

2.2.1 Co-ordinate systems

2.2.1.1 The MEG head co-ordinate system

In a CTF magnetometer, the head co-ordinate system is defined by the X- and Y-axes running through anatomical landmarks. The origin of the co-ordinate system is located as equidistant as possible from the ears while the Z-axis is perpendicular to X and Y, pointing to the top of the head. The nasion (NA), and the right and left preauricular (PA) points are often used as identifiable landmarks (De Munck, 1989) with the origin half way across the line between the left and the right points. The Y-axis runs towards the left PA (PAL) while the X-axis runs from the origin to NA. In a reversed head system, the inion

and the right PA (PAR) can also be used. Figure 2-1 demonstrates the MEG head co-ordinate system and its relationship to the location of head localisation coils that together serve as fiduciary landmarks.

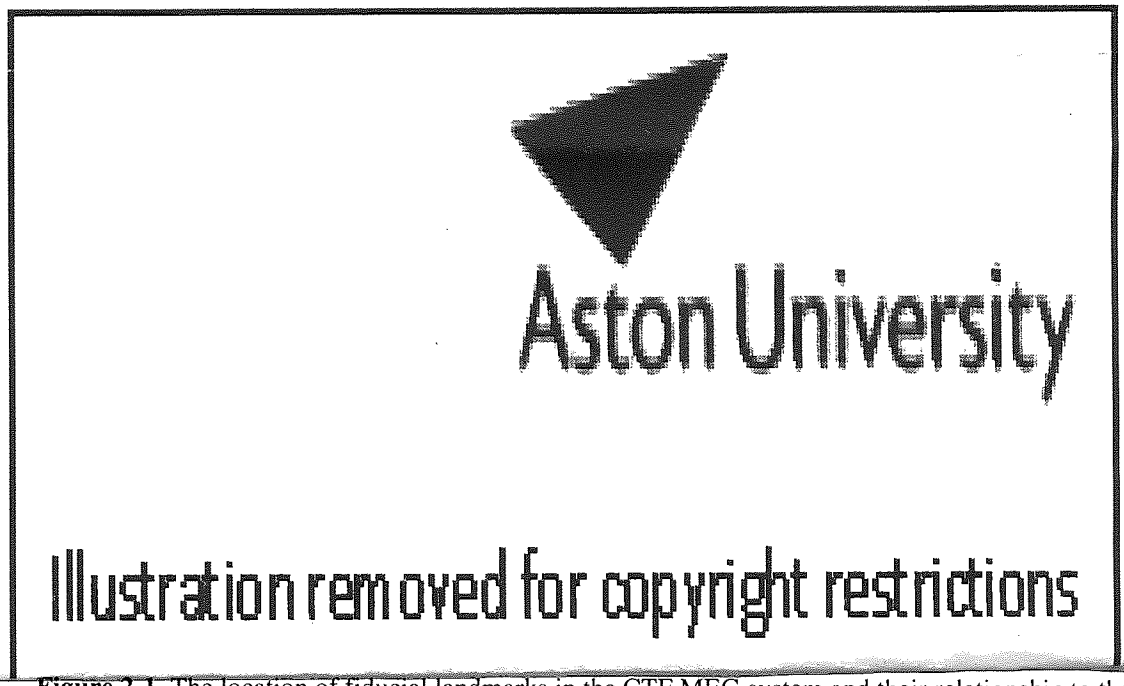

Figure 2-1. The location of fiducial landmarks in the CTF MEG system and their relationship to the head co-ordinate system. Note that a right-handed co-ordinate system is used. From CTF Systems Inc.

2.2.1.2 The MRI co-ordinate system

In an MRI dataset, the scanned area can be viewed as a cube that contains the head with each voxel having its own Cartesian co-ordinates with Z reflecting the number of slices. All co-ordinates can run from 0 to 255 in slices of one mm.

2.2.2 Co-registration based on fiducial landmarks

Co-registration of MEG/EEG with MRI is often based on anatomical landmarks, or fiducial points, the positions of which are first identified in both modalities and then co-registered with one another (George et al., 1989, Wieringa, 1993, PhD thesis). The fiducial points are based on easily recognisable anatomical landmarks, such as the nasion and the right and left preauricular points. The markers used to define these landmarks are called

fiducial markers. The fiducial markers are defined by a 3D digitiser, which is used to identify the fiducial points and define a co-ordinate system, referred to as the MEG co-ordinate system. In the MRI scan, the same anatomical landmarks are identified by using the MRI slices where the location of fiducials can be marked with oil filled capsules, which are easily identifiable in the MR scanner. The co-registration of fiducial locations is based on the assumption that the skull is a rigid object, and thus a rigid-body transformation is applied using a simple rotation and translation to align the markers in the two modalities. This alignment is achieved by a least squares fitting procedure that minimises the Euclidean distance between the two sets of data points. George et al. (1989), and Fuchs et al. (1995) provide detailed description of the fitting procedure. However, using this technique, errors in co-registration can amount to several millimetres (Fuchs et al., 1995; Schwartz et al., 1996) due to identification of points in both modalities. Huppertz et al. (1998) have shown that repeated digitisation of anatomical landmarks could cause significant variations in localisation, and become particularly large when measured by different experimenters. Also, the size of the capsules further complicates the accurate alignment of fiducial landmarks.

2.2.2.1 Errors of interest

Errors in co-registration bias the localisation algorithm by causing errors in MRI positioning, which can ultimately lead to uncertainties regarding the precise location of cortical activation (Schwartz et al. 1996). An ideal co-registration technique, therefore, is one whereby the errors between the two sets of data are minimized as far as possible. The following measures are of paramount importance:

- Target registration error (TRE): co-registration requires the alignment of certain targets of interest such as activated brain regions, or cortical lesions and epileptic foci for surgical and diagnostic applications. Thus TRE is defined as the Euclidean distance between corresponding points, other than the fiducial points, in both modalities after registration. Examples of these are epileptogenic foci or the precise location of the tightly adjacent visual areas.

- Fiducial registration error (FRE): the accuracy of co-registration, in turn, depends on accurate co-registration of fiducial point. FRE is defined as the root mean squared Euclidean distance between corresponding fiducial points after registration (Singh et al., 1997). Fitzpatrick et al. (1998) observed that a small FRE can generate a large TRE and is therefore a poor indicator of the accuracy of co-registration.
- Fiducial localisation error (FLE): In a Monte Carlo simulation study of MEG/MRI co-registration, Singh et al. (1997) have shown that TRE increases with distance from the fiducial locations, and is dependent on the error in localising the fiducial markers (Fitzpatrick and West, 2001). FLE is defined as the error in locating the fiducial markers (Maurer et al. 1998). A minimum FLE is thus an important requirement for an effective co-registration technique.

It follows from the last point, that TRE is proportional to the error in localising the fiducial points, or FLE. TRE increases if the target point is further away from the principal axis. Moreover, increasing the number of fiducial locations has little effect on improving TRE unless they are placed as far away from each other as possible (Singh et al., 1997). One important way in which the accuracy of co-registration can be improved therefore is to minimise FLE as far as possible, and to increase the number of fiducial locations and the distance between them. Schwartz et al., (1996) have found that repeated localisation of a fiducial point on the skin produces a mean error of approximately 1.5mm. Using a bite-bar, Singh et al. (1997) have reported variability of FLE errors for the NA and the PAL notch to be 3.74mm and 4.46mm respectively, when localised with a 3D digitiser.

The alignment of fiducial markers and their accurate localisation alone is not sufficient for co-registration since it has been shown that head surfaces in the two modalities also require accurate alignment (Bamidis and Ioannides, 1996). Furthermore, Fitzpatrick et al. (1998) have shown that fiducial alignment is a poor indicator of target registration accuracy. For these reasons, it is necessary to incorporate and perform a surface matching technique in order to align the two surfaces defined in the MRI and MEG co-ordinate systems.

2.2.3 Co-registration based on surface matching

In addition to co-registration of landmarks, a surface matching technique can also be applied, which aligns two head surfaces defined in the MEG and MRI co-ordinate systems (Pelizzari et al., 1989; Schwartz et al., 1996; Huppertz et al., 1998). Surface matching was first used for registration of CT, MR, and PET images by Pelizzari et al (1989) and subsequently adapted by several other groups for MEG/EEG-MRI co-registration (Schwartz et al. 1996; Bamidis and Ioannides, 1996; Huppertz et al. 1998). In this technique, co-registration is performed by aligning two sets of data that represent the head surfaces defined in the MEG and MRI co-ordinate systems. The procedure of obtaining the head shapes in the two co-ordinate systems is now described.

2.2.3.1 Segmentation: Extraction of skin surface from MRI

The objective of segmentation is to obtain a connected set of voxels, extracted from the MRI, which describes the scalp surface as accurately as possible. Since the skin surface used in co-registration is directly derived from the segmentation procedure, errors in segmenting the head shape will introduce unwanted inaccuracies in registration. Therefore, different steps, such as thresholding and erosion, are taken to remove the background noise, obliterate holes in the head shape not connected to the skin surface, and removes weak connections and further artefacts from the MRI volume. A detailed description of this procedure is beyond the scope of this thesis but is provided by Schwartz et al. (1996).

2.2.3.2 Head shape extraction in the MEG co-ordinate system

The surface of the scalp in the MEG co-ordinate system is commonly obtained by the Polhemus Isotrak 3D digitiser (manufactured by Kaiser Aerospace Inc.), which consists of an emitter that sends out magnetic signals, and a pen-shaped receiver, which mark the fiducial points. This produces a set of independent 'hat' points (Pelizzari et al., 1989), which define the head surface, and should be as similar as possible to the one segmented from the subject's MRI. Care must be taken to avoid errors caused by pressure from the digitising pen, which can deform the scalp surface.

The actual surface matching is performed in MATLAB. In this stage, the 'hat' points are first placed as closely as possible on the segmented MRI surface as an appropriate starting point following which a co-registration matrix is computed. This defines the cost-function by minimising the Euclidean distance between each of the two nearest points (Schwartz et al., 1996). Techniques for fast computation and optimisation are incorporated in the minimisation algorithm, which accelerate the process and increase its precision (Huppertz et al., 1989; and Schwartz et al., 1996). One technique that is used to determine the distance between the two sets of points is to calculate a look-up table (Huppertz et al., 1989). This calculation is performed once and before the start of the actual surface matching. Each voxel within the 3D image cube corresponds to each cell of the table containing the relative distance of the voxel to the nearest point on the MRI-segmented head surface. The matching error between the two head surfaces is calculated as the average of the relative distances obtained from the look-up table at the position of the transformed 3D co-ordinates of the 3D-scanned head-surface points. By adjusting the transformation parameters, the cost function is minimised and is given by the mean relative distance between the two sets of points (Huppertz et al., 1989).

An example of surface matching is shown in figure 2-2a, b, and c. In these illustrations, the points in green represent the head surface obtained by the 3D digitisation procedure (the 'hat' points), while the red points represent the segmented head shape derived from the MRI. The independent 'hat' points are first manually superimposed on the points representing the MRI-derived head shape. By running the optimisation algorithm, the nearest distance between the two sets of points is reached, represented in the lower illustration by the blue points. A more detailed account of all these procedures is provided by Huppertz et al. (1998) and Schwartz et al. (1996).

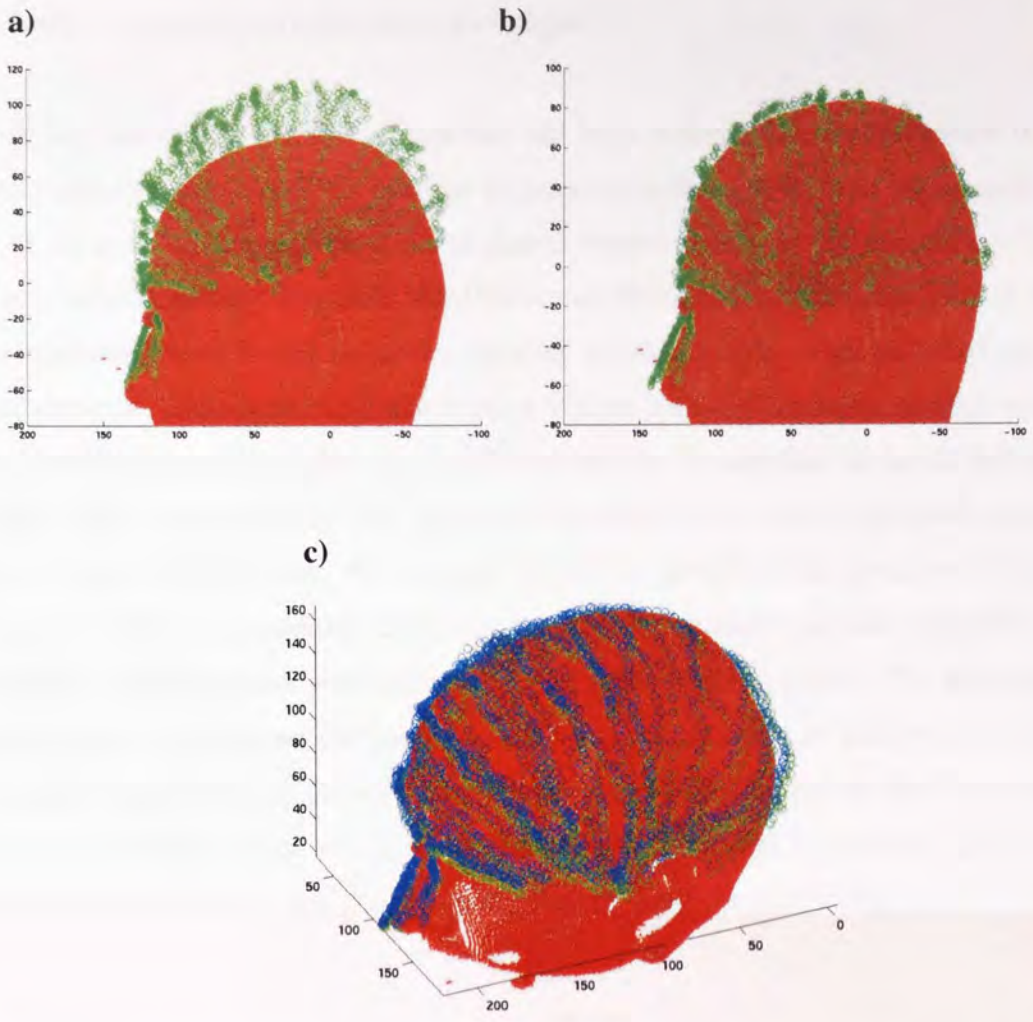

Figure 2-2. Different stages of surface matching as performed at Aston. The digitised 'hat' points of the head (green circles) are superimposed on the MRI-derived head shape (red circles). The points as first recorded **(a)** are then adjusted manually as closely as possible to one another **(b)**. After running the surface matching algorithm **(c)**, the distance between the two sets of points is minimised by a fast computation and optimisation technique. The 'hat' points after optimisation are represented by the blues circles.

Pelizzari et al. (1989) have demonstrated the accuracy of surface matching technique to be on the order of two image pixels, while Huppertz et al. (1998) found the test-retest reliability of between 1.4 and1.8 mm. Generally, methods of co-registration based on surface matching are more reliable than those using fiducial markers alone. Our co-registration technique at Aston is essentially based upon surface matching combined with alignment of fiducial landmarks. In the following sections, it is described how the position of fiducial points is determined in the MEG co-ordinate system and how they are co-registered with the MRI data using the surface matching technique.

2.3 Methods of applied co-registration technique

In our laboratory at Aston, a bite-bar has been utilised for co-registration of MRI and MEG data (Figure 2.2). This bite-bar is made of a sheet of acrylic with small holes drilled in its arms as fiducial points, and dental thermoplastic for forming the subject's dental impression. Initially, and with the 19-channel MEG system formerly used at Aston, the co-registration was based on these fiducial markers, with large oil-filled capsules attached above the smaller holes, which became visible in the MR images. Outside the MRI scanner, the bite-bar was attached to a rigid wooden arm to stabilise the head. Before and after each MEG measurement the positions of these holes were digitised using the Polhemus Isotrak 3D digitiser, the average of which identified the location of fiducial points in the MEG co-ordinates. Once the location of markers in both modalities was determined, a transformation was reached by alignment of the markers. The advantage of the bite-bar was that because the head was stabilised, errors due to movement were less likely to occur during an MEG recording. Furthermore, the problem of identification and alignment of oil-filled points based on landmarks, as described in section 2.3.2, is thus eliminated. Further detail of this procedure is given by Singh et al. (1997).

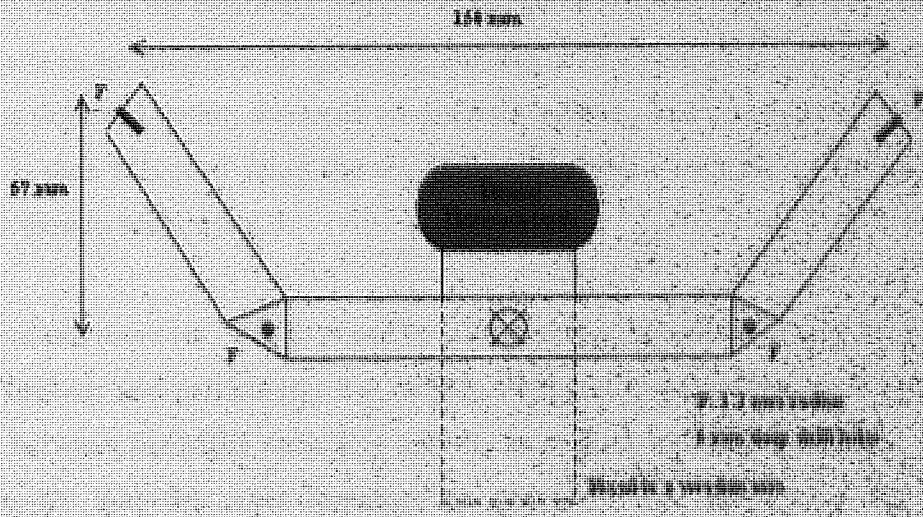

Figure 2.3. Schematic of the design of the bite-bar used at Aston. 'F' represents each fiducial point to which oil-filled markers are attached, becoming visible in the MR scanner. These points are also digitised in the MEG co-ordinate system.

This co-registration procedure was then modified with the acquisition of the 151-channel whole-cortex MEG system (CTF Systems Inc.) with which it was no longer possible to digitise the bite-bar based fiducial points in the MEG environment since the entire head is placed inside the dewar helmet. Instead, the position of the head with respect to the MEG sensors was determined using a set of small solenoid head-based localisation coils (Ahlfors and Ilmoniemi, 1989). Using a Velcro band these coils are attached to the circumference of the head and near the discrete, and easily identifiable, anatomical points of NA, PAL and PAR. Before and after each MEG recording, the locations of these coils are determined by the sensors by a signal that is sent through the coils. Because the number of sources is known and the signal produces a magnetic field with high enough signal-to-noise ratio, the location of the coils is easily determined. The position of the coils in the MEG co-ordinate system was thus obtained from the averaged coil locations, calculated from the pre- and post-MEG measurements, and was used for the co-registration procedure.

After the completion of MEG recording, the subject is removed from the MEG system with the coils remaining on the circumference of the head. These locations are then digitised with the Polhemus with the bite-bar mounted onto a rigid wooden arm to stabilise the head. Subsequently, the Velcro band was gently removed and the surface of the scalp was obtained by running the digitising pen across the surface of the head. In this procedure, the Polhemus acts as an intermediate technique and the head localisation coils and the scalp surface are thus digitised within the same co-ordinate system. The co-registration of MEG and MRI data is then achieved using the transformation found with the surface matching procedure described in section 2.2.3.

This method, however, was exposed to potential inaccuracies and was tiresome for both the experimenter and particularly the subject. Potential inaccuracies could arise from the movement between the MEG recording and the head digitisation sessions as it was not possible to ensure that the coils remained in precisely the same locations on the circumference of the head throughout. The relationship between error in localisation of fiducial points and target registration accuracy was described in section 2.2.2. Furthermore, because a Velcro band containing the three coils was attached to the circumference of the head, it caused tightness around the skull due to the restricted size of the helmet and many

subjects complained of the discomfort, particularly during lengthy experiments. Also, because the position of the anatomy-based coils was not the same for each recording session, this method required that the entire co-registration procedure be repeated following each MEG recording of the same subject.

2.4 The purpose of this study

The aim of this present work was to devise a new co-registration method in order to overcome the inefficiencies encountered with the previous technique. An ideal technique should primarily aim to increase the accuracy of localising the fiducial points and assist the ease with which co-registration is performed. A new bite-bar was thus designed comprised of fixed magnetic coil fiducial locations in order to reduce the FLE and FRE, thus increasing target registration accuracy. The advantage of fixing the coils is that the co-ordinate system is not based upon arbitrary and operator dependant fiducial points that are attached to loosely defined landmarks (e.g. nasion and the preauricular points), but rather on those that are permanently fixed in relation to the subject's skull. Furthermore, it will be shown how this new technique eliminates parts of the co-registration procedure where unwanted errors commonly occur, and increase the ease of use for both the subject and the experimenter.

2.5 Methods

Bite-bar design

With the help of technical staff at Birmingham Dental Hospital, a new bite-bar was designed and crafted (Figure 2-4) to incorporate a number of significant differences to that described by Singh and colleagues (1997). The new design incorporates a removable dental plate, which is personalised by obtaining the dental profile of each user. The fiducial points used comprise 5 solenoid coils: three co-planar coils, referred to for convenience as the nasion (NA), the left pre-auricular (PAL), and the right pre-auricular (PAR), reflecting their general position around the head. These are positioned symmetrically on the arms of the bite-bar, such that the nasion coil is placed between the left and the right preauricular points. The coils are fixed to the bite-bar mechanically using nylon bolts and screws. There are also two additional coils, equidistant from the nasion coil, which are raised by 5.6 cm. The purpose of this design is to further increase target registration accuracy. The purpose of this adjustment will be illustrated by the results of experiment 2.

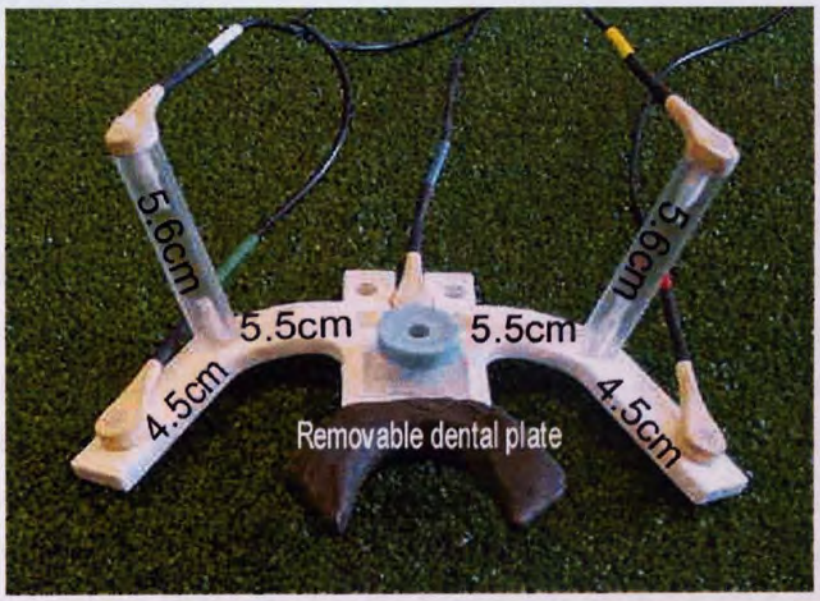

Figure 2-4. The bite-bar with the coils attached. The measurements indicate the distances between the coil locations on the same plane. The PAL and PAR coils are on the extreme arms of the device while the NA coil is located half way between. Two additional coils are raised by 5.6 cm with respect to the other coils. The removable dental plate carries the subject's dental impression.

MEG data acquisition

At the start of the MEG data acquisition, the bite-bar is firmly held in the mouth while the coils are activated for localisation. After the localisation and during MEG recording, the bite-bar need not remain in the mouth and can be removed by the subject until the data acquisition is complete, at which point the bite-bar is replaced for the re-localisation of the coils. The purpose of repeating the coil localisation is to detect any head movements during the MEG recording and the calculated mean of the coil locations is used for the co-registration procedure. Therefore, an advantage of the new bite-bar over the old procedure is that the coils are no longer positioned on the circumference of the head, becoming liable to errors caused by scalp displacement in the MEG helmet. This helps to decrease the possibility of inaccurate localisation resulting from the displacement of the coil locations from the instability of the headband. Also by removing the Velcro band from the head, the MEG recording becomes more comfortable for the subject.

Problems caused by the Polhemus

The Polhemus 3D digitiser is an external device that can be used to determine the location of the head coils independently from the MEG sensors. It provides a common co-ordinate system whereby the digitised co-ordinates are registered with those determined in the MEG co-ordinate system by minimising the Euclidean distance between the corresponding points. Clearly, for the most precise registration of the corresponding points it is essential that the head coils be localised as accurately as possible. One major disadvantage of using the Polhemus to determine the location of the coils, therefore, is that errors caused by localisation and registration of these points is not trivial. When using the Polhemus 3D digitiser to determine the location of the coils or to obtain the head points, a number of potential problems may arise. For the head points needed in surface matching, the digitising pen must not be applied firmly against the skin, since the deformation of the latter will cause dissimilarities with the scalp surface obtained from MRI and cause inaccuracies in matching the two sets of points. This is particularly critical for areas around the nose and the eyes (Huppertz et al., 1998). Furthermore, when digitising the coils, the pressure from the digitising pen can cause displacement errors, which are exaggerated in

directions where the coil is not supported by bony structures (Hillebrand, 2000, PhD Thesis). Therefore we attempted to eliminate the inaccuracies caused by the 3D digitisation process by replacing this component of the co-registration process with a technique that localises the coils and obtains the head shape directly using the MEG system itself.

Using a fourth coil for head digitisation

De Munck et al. (2001) have introduced a technique for registration of MEG with EEG that can also be used for head digitisation and does not require the use of an external 3D digitiser. They have developed a strategy to simultaneously activate a set of coils using the MEG sensors. Three coils are attached to the head at roughly the left and right preauricular points and the nasion, while a fourth coil is moved along different locations on the scalp to digitise EEG electrodes or to obtain the shape of the head. At each point, the coils are activated simultaneously for 2 s and their position is localised by fitting a magnetic dipole function on the MEG signals that are generated. The position of the head points is thus determined with respect to the MEG detectors. The data can then be mapped directly onto other modalities without the need for an intermediate procedure.

We adopted a variation of this approach for bite-bar coil localisation and digitisation of the head surface. An extra localising coil, calibrated in the MEG system, was used to digitise the head of each subject below the MEG helmet by placing it on different locations on the surface of the scalp. A trigger button was pressed at each scalp location with which all the coils were activated and their position was determined with respect to the MEG sensors. The distance of the bite-bar from the MEG sensors was approximately 30 to 40 cm. Our preliminary results showed a major problem in the accuracy of the coil localisation caused by the fact that the extra coil was much closer to the MEG sensors than were the bite-bar coils and hence the latter set of coils were not localised accurately. Consequently, simultaneous activation of all the coils produced interference from the bite-bar coils with one another and with localising the fourth coil. To alleviate the problem, the bite-bar was fixed to a rigid wooden arm and held firmly in the mouth by the subject who sat stationary below the MEG helmet. The technician then collected the head points by placing the extra coil on arbitrary locations on the surface of the head. At each location, the

extra coil was activated and its position localised in the MEG co-ordinate system. This procedure was repeated 300 times in order to obtain sufficient number of scalp points. The position of the bite-bar-based coils was determined separately before and after the collection of head points. This was done by holding the fourth coil away from the subject and the bite-bar, and activating the coils twenty times before and after collection of the head points in order to obtain an estimate of their average location and hence determine the position of the head. It is assumed, therefore, that there is no head movement and that all coils are in the same co-ordinate system However, it was soon noticed that this procedure too was beset with the problem of accurate localisation of the bite-bar coils. Many points were wrongly localised to the extent that the resulting head shape contained many outliers, commonly around 50 out of 300, as shown in figure 2-5a. When the outliers were removed, the head shape resembled that in figure 2-5b. This component of the co-registration procedure was thus abandoned and the Polhemus Isotrak was retained for digitisation of the coils and the scalp surface outside the MEG room. Attempts were therefore made to find ways of improving the accuracy of digitisation using the Polhemus.

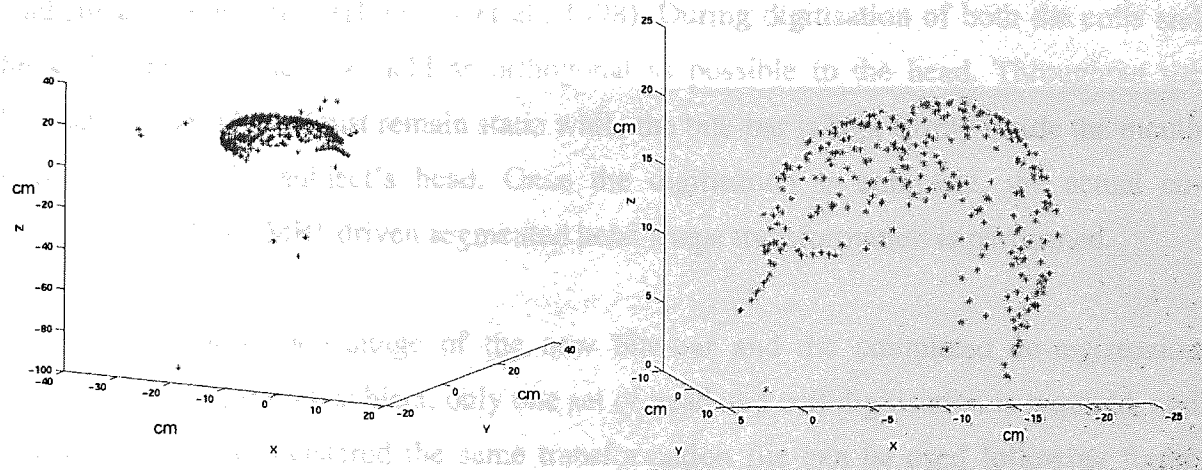

a) **b)**

Figure 2-5. Head shape points as obtained with the MEG sensors using the fourth coil procedure. **(a)** 300 head points showing the position of the activated fourth coil on the scalp. Note the outliers caused by erroneous localisation of the fourth coil. **(b)** Head shape after the outliers were removed from the data.

Head digitisation with the Polhemus

Following the problems described above, the 3D digitiser was retained for the purpose of fiducial localisation and scalp digitisation. Using the Polhemus device, each coil location is repeatedly digitised with the bite-bar firmly attached to a wooden frame. The fiducial coils are 4.5mm thick and the centre of the coils is determined by nylon screws that are raised 2.25mm from the base of the coils. A small dent is created at the centre of each screw so that the same location is consistently digitised as accurate as possible. Hillebrand (2000, PhD Thesis) used the Polhemus Isotrak device to digitise the location of fiducial coils on the circumference of the head and found that FLE decreased by repeating the digitisation and using the mean locations. Therefore, to increase the accuracy of fiducial localisation, each coil is digitised three times and the mean location is used for the co-registration procedure. Subsequently, the Polhemus pen is run slowly over the surface of the head to obtain a set of scalp surface points (typically > 1000). Because the head is almost spherical, points around the eyes and the nose are particularly important for accurate head surface registration (Huppertz et al., 1998). During digitisation of both the coils and the scalp, the pen must be held as orthogonal as possible to the head. Throughout the digitisation, the subject must remain static while the bite-bar is kept firmly inside the mouth in order to fix the subject's head. Once the digitisation is complete, the actual co-registration with the MRI-driven segmented head-shape transformation is performed.

An important advantage of the new bite-bar and the completed co-registration procedure is that for each subject, only one set of head and coil digitisation is required, and once the data is co-registered the same transformation file can be used following future MEG recordings, provided that the subject uses same dental plate. This saves considerable time compared to the previous technique with which the coils where fastened to the circumference of the head and their location was different for each MEG recording.

Experiment 1: *An estimate of errors due to bite-bar repositioning*

Accuracy of the new procedure after repeated repositioning was tested by firmly attaching a reference coil to the subject's inion and measuring the movement of the bite-bar coils in relation to this fixed inion coil. Four human subjects and a phantom device were tested. For each subject, 10 MEG recordings of 30-second duration were collected. Between each 30 seconds of MEG recording, the subject was instructed to remove the bite-bar and reposition it for the next recording. For the phantom recording, the bite-bar was firmly attached to a support and placed under the MEG helmet in approximately the same position as a subject's head, and the inion coil was attached to the support at about the location of the inion. Using a stationary object provides an unbiased estimate of the residual error produced by noise in the MEG sensors and the coil localisation algorithm, against which errors due to head movement can be assessed. The bite-bar-based fiducial locations as well as the inion coil were activated before and after each recording and their positions recorded. The mean displacement of the inion coil with respect to the head coils is calculated using the positions of all coils after each recording.

Results

Figure 2-6 represents the mean shift in position of the bite-bar coils with respect to the inion coil, due to repeated (N=10) removal and repositioning of the bite-bar, for the 4 subjects. This is drawn against the corresponding values derived from the phantom device. The averaged displacement due to repositioning of the bite-bar inside the mouth were less than 0.5mm which, when compared to the residual movement of 0.18mm, is symptomatic of the stability of the bite-bar position during MEG acquisition over repeated recordings.

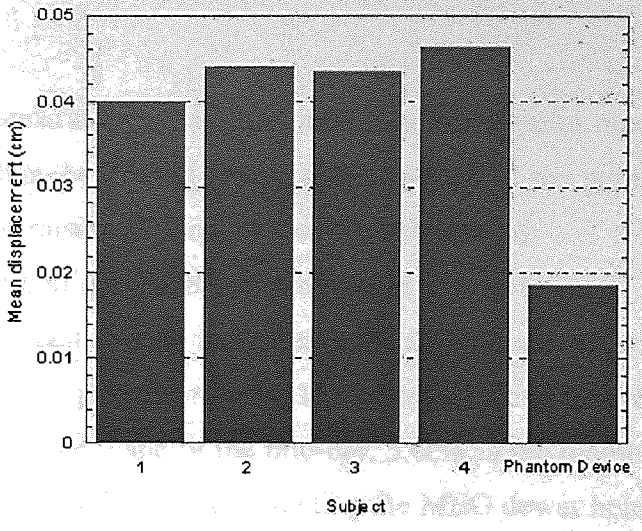

Figure 2-6. The mean absolute error for bite-bar displacement after repeated (N=10) repositioning of the bite-bar. The error measured with the phantom device indicates residual error due to noise in the MEG sensors and the algorithm that reconstructs the coil locations.

Experiment 2: *Effect of bite-bar configuration on TRE as a function of distance*

In a Monte Carlo simulation of MRI/MEG co-registration, Singh and colleagues (1997) found a dependency on distance for TRE, such that locations in the brain that are furthest from the fiducial points are subject to increasingly greater co-registration error. Since the fiducial points are placed in close proximity and are almost in the same plane, it follows that small errors in determining their locations will cause greater errors at distant locations. We therefore tested the effect of increasing both the number of fiducial locations as well as the distance between them. Thirty localisations of the bite-bar were collected at different locations beneath the MEG sensors. The mean location of the bite-bar was obtained from these recordings and was used as a hypothetical model of the bite-bar. In a computer simulation of fiducial locations, increasing errors were assumed and added to these points for both a 3- fiducial point, and a 5-fiducial model of the bite-bar. The effect of these errors on the TRE at a point near the inion was estimated for all thirty locations of the bite-bar and the mean was computed. It was expected that adding extra fiducial locations in a different reference plane would decrease FRE and subsequently TRE.

Results

Figure 2-7a demonstrates that as FLE increases, the 5-point model of the bite-bar produces smaller errors than the 3-point model at the position of the inion coil. Figure 2-7b demonstrates the effect of raising the location of the 4th and 5th coil when the offset is 6 cm. Compared with the 3-coil design, the improvement is a factor of 2. The improvement in accuracy of locating distant targets increases with an increase in height of the raised coils. In this case 2 coils are placed on poles that extend 5.6cm, above the plane of the others, and perpendicular to the plane of the bite-bar. 5.6cm is the maximum displacement above the plane that can be added without contacting the MEG dewar helmet.

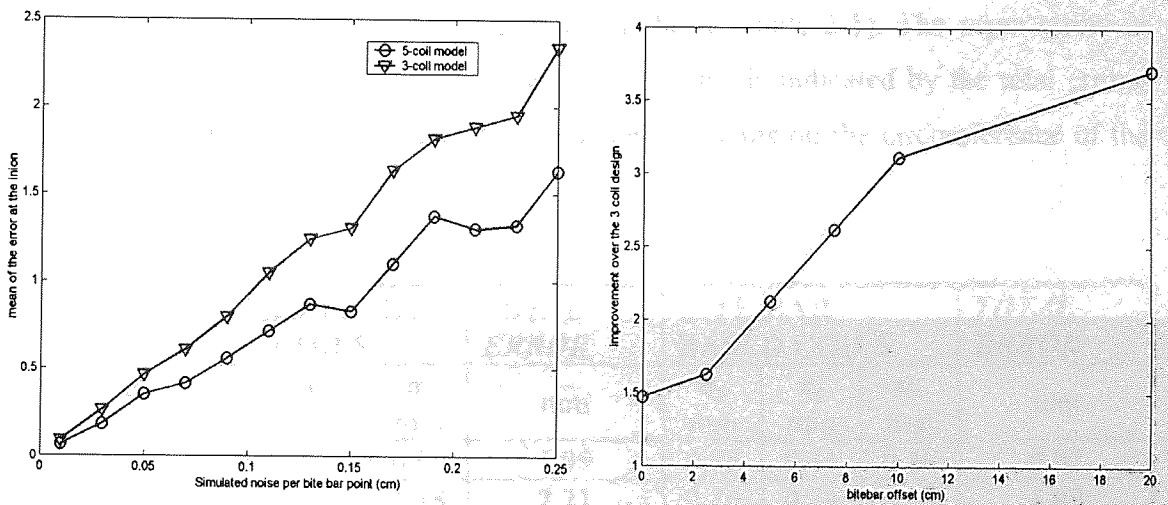

a-) b-)

Figure 2-7. Simulated estimates of improvement in TRE by adding fiducial locations **(a)** errors are smaller and increase less rapidly with the 5-fiducial model than with the conventional 3-fiducial model when the noise per bite-bar point is increased; **(b)** improvement factor at the location of the inion coil as a result of raising two fiducial locations with a certain offset (compared to the 3-coil design).

Experiment 3: An estimate of FLE

Because a small FLE is of utmost importance in the accuracy of co-registration, it is crucial that the fiducial markers are localised as accurately as possible. The accuracy of fiducial localisation using the new bite-bar was tested by repeating the digitisation procedure of the coils and head 15 times. Commonly, and for a single digitisation

procedure, the position of each coil is determined 3 times with the Polhemus digitiser and the average position is used for co-registration. This procedure was repeated 15 times for both the new bite-bar and the previous method with which the coils were placed on the circumference of the head. To obtain an estimate of FLE, the total error, ε, was calculated for each digitised fiducial location by $\varepsilon=\sqrt{\sigma^2_x+\sigma^2_y+\sigma^2_z}$, with σ_x, σ_y, and σ_z the standard deviation in x, y, and z direction respectively.

Results

With the fiducial points fixed to the bite-bar, errors were considerably smaller than when coils are placed on the circumference of the head (Table 2-1). The mean errors in localising the coils are smaller for the new` bite-bar. This is indicated by the total errors, which are reduced by ~1mm compared to localising the coils on the circumference of the head.

	HEAD-BASED COILS			*TOTAL ERROR*	BITE-BAR BASED COILS			*TOTAL ERROR*
Fiducial Coil	σ_x mm	σ_y mm	σ_z mm	mm	σ_x mm	σ_y mm	σ_z mm	mm
NA	1.32	1.19	0.90	**1.99**	0.78	0.41	0.40	**0.97**
PAL	1.58	1.00	1.18	**2.21**	0.76	0.54	0.57	**1.09**
PAR	1.30	1.04	0.81	**1.85**	1.03	0.67	0.56	**1.35**
Extra Coil L					0.87	0.16	0.87	**1.24**
Extra Coil R					0.96	0.23	0.64	**1.17**

Table 2-1. Standard deviations and total error of nasion (NA), left pre-auricular (PAL), and right pre-auricular (PAR), digitised with the Polhemus, with coils on the circumference of the head and on the bite-bar. For the bite-bar-based method, the standard deviations and the total error of the raised coils was obtained as well.

Experiment 4: *An estimate of co-registration reliability*

For both methods, co-registration with the subject's MRI was performed separately for each digitised set of data. A point on the calcarine fissure (i.e. a point furthest from the location of the coils) was selected on one co-registered MRI and its location was noted in terms of MRI voxels in the three coronal, sagittal, and axial views (the voxel size is

1x1x1mm). The MEG co-ordinates for this target location are constant for all the co-registrations. This target location was then located based on the MEG co-ordinates in all other co-registered MRIs and the x, y, and z co-ordinate was noted for each.

Results

The stability of the completed co-registration procedure is represented by the mean displacement of the marker after each co-registration. With the new bite-bar the displacement is considerably smaller than that found with the coils around the circumference of the head (Table 2-2). The standard deviation of marker locations within each co-registered MRI is smallest in the direction orthogonal to the plane of the bite-bar. The total errors over repeated co-registrations for the two techniques are 9.2mm for the head-based fiducials and 4.3mm for the bite-bar based fiducials.

	MRI SLICES FOR MARKER LOCATION					
	Head-based Coils			**Bite-bar-based Coils**		
	Coronal	*Sagittal*	*Axial*	*Coronal*	*Sagittal*	*Axial*
1	236	128	143	233	133	144
2	161	126	161	236	137	146
3	249	128	166	233	136	150
4	244	131	160	233	137	141
5	247	134	173	233	131	143
6	243	131	162	232	131	143
7	242	121	156	233	132	146
8	242	118	159	231	135	141
9	244	130	159	231	133	141
10	243	122	162	232	135	142
11	241	116	161	234	137	142
12	244	122	159	235	134	148
13	247	128	167	232	139	144
14	242	133	155	229	136	139
15	241	131	155	231	139	140
Std	**3.08**	**5.55**	**6.66**	**1.50**	**2.62**	**3.06**
Total Error		**9.20 mm**			**4.30 mm**	

Table 2-2. MRI voxel co-ordinates for the same marker location in the calcarine fissure in each co-registered MRI (the voxel size is 1x1x1mm). The columns on the left show marker locations with co-registration performed with coils placed on the circumference of the head, while the columns on the right represent marker locations when co-registration was performed using the new bite-bar-based method.

It was thought that perhaps this error is largely caused by the surface matching component of the co-registration procedure seeing that FLE produces such negligible errors, as indicated by the results in Table 2-1. This possibility was examined by repeating the 15 co-registrations using only a single set of fiducial locations with the 15 separate sets of head shapes. This set of fiducial locations was obtained from the average of the 15 sets of fiducial digitisations. As before, a point on the calcarine fissure was selected on one co-registered MRI and its location was noted on the MRI voxels. It was expected that the total error of 4.30mm would be somewhat reduced since the small errors caused by fiducial localisation were now removed from the 15 co-registrations.

MRI voxel co-ordinates and the average marker displacement are shown in table 2-3 . The total error using a single set of fiducial locations is 4.50mm, which when compared to the 4.30mm as shown in the table above, shows no improvement. This is surprising since having used a single set of fiducial locations for the 15 co-registered MRIs, it was expected that some error should be removed from the total marker displacement.

MRI SLICES FOR MARKER LOCATION

	Coronal	*Sagittal*	*Axial*
1	236	132	143
2	239	139	150
3	239	132	150
4	237	133	143
5	236	132	142
6	236	133	142
7	237	136	148
8	237	136	148
9	233	134	144
10	237	135	147
11	235	139	144
12	239	136	150
13	234	136	143
14	233	135	142
15	233	133	142
Std	**2.12**	**2.31**	**3.23**
Total Error		**4.50 mm**	

Table 2-3. MRI voxel co-ordinates for the same marker location in the calcarine fissure in each co-registered MRI using a single set of fiducial locations.

***Experiment 5:** Target registration accuracy*

Target registration accuracy and stability was determined in a simple functional mapping experiment. We used a median nerve stimulation paradigm with one subject. In order to evoke a clear response from the subject's cortex, the electrical pulse stimulus was set to twice the subject's threshold. 200 epochs of half-second duration were collected. The procedure was repeated 15 times between which the subject was requested to remove the bite-bar and reposition the head below the MEG helmet. After eliminating artifact-contaminated trials, the data was passed through an 80Hz low-pass filter and averaged. The 100ms pre-trigger period was used for DC offset correction. To estimate the source of the sensory evoked responses, a single equivalent current dipole (ECD) (see section 1.5) was fit to the peak of the averaged sensory evoked responses, typically occurring at 34ms post stimulus onset. A spherical head model was fitted to the subject's scalp outline obtained from the MRI, to describe the curvature of the head as accurate as possible. This ECD model is often used as an inverse solution that estimates the sources of electromagnetic signals (Cohen and Cuffin, 1979; de Munck, 1989). For each of the 15 runs, the data was analysed using Monte Carlo simulations (see section 1.5) to estimate the stability of the reconstructed sources with respect to noise in the data. The same procedure was repeated 15 times for the previous co-registration method with the coils on the circumference of the head. For both methods, ECDs were fitted and the mean displacement of the dipoles and the Monte Carlo volumes were noted.

Results

The results of source reconstruction using equivalent current dipole modelling for source localisation of median nerve stimulation are shown for the 15 runs in table 2-4, while figure 2-8 depicts their position on an axial view of the brain. The improvement over the previous technique with which the fiducials coils are placed on the circumference of the head (Table 2.4) is relatively small. The Monte Carlo volumes represent the confidence ellipsoid containing 95% of all the estimates of each dipole. An ideal co-registration method is one with which the volume of the 95% confidence ellipsoid is smallest. In this

case, the bite-bar based fiducials yield the smallest confidence volumes (Table 2-4). Also note that the majority of volumes overlap (Figure 2-8).

MRI SLICES FOR DIPOLE LOCATIONS								
	Head-based Coils				**Bite-bar-based Coils**			
Dipole	*Coronal*	*Sagittal*	*Axial*	MC Vol. cm^3	*Coronal*	*Sagittal*	*Axial*	MC Vol. cm^3
1	169	100	90	0.70	157	85	85	0.04
2	167	102	90	0.28	162	89	87	0.18
3	165	97	88	0.29	157	91	87	0.06
4	165	98	84	1.20	160	85	80	0.19
5	169	100	90	0.21	168	85	84	0.11
6	173	92	95	0.25	160	87	86	0.05
7	166	97	87	0.59	163	89	90	0.11
8	165	96	86	0.33	160	88	88	0.03
9	165	92	86	1.30	161	91	85	0.04
10	165	97	89	0.37	168	92	87	0.18
11	161	93	97	0.58	161	86	89	0.04
12	158	96	89	0.21	162	91	88	0.14
13	165	94	87	0.12	164	88	83	0.29
14	164	97	80	0.21	160	87	90	0.10
15	166	94	83	0.50	171	93	89	0.27
Mean	165.47	96.33	88.07	0.48	162.27	88.47	86.53	0.12
StDev	3.44	2.97	4.30	0.35	4.01	2.67	2.77	0.08
Total dipole displacement		**6.26 mm**				**5.55 mm**		

Table 2-4. MRI voxel co-ordinates for the location of dipoles. The columns on the left show dipole locations when the experiment was carried out with the coils on the circumference of the head, while columns on the right show dipole locations when using the new bite-bar-based method. The Monte Carlo volumes represent the 95% confidence ellipsoids and are smaller for the results obtained with the new bite bar.

Figure 2-8. Equivalent current dipole locations reconstructed from 15 MEG recordings projected onto a single MRI slice. The confidence volume for each location activated by median nerve stimulation is represented by yellow ellipses. The cloud formed by the dipoles represents intra-recording variability and co-registration errors, whereas the Monte Carlo Volumes depict uncertainties due to noise in the data.

2.6 General Discussion

The combination of techniques described in this paper provides a novel procedure for co-registering MEG/EEG results with MRI. We have demonstrated that placing fiducial coils on a rigid dental bite-bar improves the accuracy of co-registration. Using fixed fiducial locations has improved fiducial localisation error and, compared to the method that employs head-based fiducials, the errors are in the order of 1 mm (Table 2-1), which may be considered as errors caused by the Polhemus digitiser. The main errors in localisation of the coils when the latter are located on the circumference of the head are caused by movement due to the pressure from the digitising pen (Hillebrand, 2000, PhD Thesis). Target registration error is therefore considerably improved upon by using the new design, which can be considered a direct result of improvement in fiducial localisation accuracy.

It has been shown that errors in localising the fiducial coils cause an error in target co-registration, magnified by a factor of 6 for targets that are located furthest away from the coils (Singh et al., 1997; Hillebrand, 2000, PhD Thesis). As we have shown here, and also suggested by Singh et al., (1997), the introduction of extra fiducial coils in a different reference plane improves the accuracy of co-registration and cortical targets of interest are therefore more accurately registered (Figure 2-7a). Unfortunately, it is not possible to further elevate the position of these coils with some MEG systems, such as ours, since the head dewar restricts the physical space available. Figure 2-7a indicates an improvement by a factor of 2 in TRE as direct result of raising two of the coil locations by 6 cm.

The high rate of reproducibility, and test-retest reliability, of the bite-bar is shown by results of experiment 1 (Figure 2-6) as well as consistent dipole locations in experiment 4 (Table 2-4, Figure 2-8). The position of the bite-bar deviates by less than 0.5mm after subsequent removals and the errors are remarkably little more than that obtained from the phantom device (Figure 2-6). The results of experiment 4 indicate that the deviation of same target location maybe limited to within one gyrus, illustrating the accurate reproducibility of the technique. The main errors in reproducibility of the co-registration procedure maybe related to the alignment of head-shapes from the Polhemus and that extracted from the segmented MRI. As shown in figure 2-6, the movement of the bite-bar,

and hence the fiducial coils, has a reliable stability of less than 0.5 mm while the mean FLEs in table1 shows the accuracy with which the coils can be localised.

The majority of dipole volumes shown in figure 2-8 overlap. Table 2-4 shows that although the Monte Carlo volumes are smaller using the new bite-bar, there is little improvement in source localisation accuracy. Recently, Shaefer et al. (2002) tested the test-retest reliability of EEG source localization of somatosensory evoked potentials (SEPs) over an extended time period and found mean standard deviation of the dipole locations that were 5.21 mm in the x, 5.98 mm in the y and 4.22 mm in the z direction. Therefore, their total accuracy of source reconstruction is 8.98 mm. This is less accurate than the total errors of 6.25 mm and 5.55 mm we found for both our tested techniques. The errors could be partly due to co-registration error and partly explained by the fact that such errors maybe an inherent characteristic of such source reconstruction paradigms. It should also be noted that errors in the co-registration procedure could be further minimised by developing enhanced algorithms to improve the accuracy of the surface matching technique.

Figure 2-9 depicts the total error attributed to the different methods tested in the series of studies described here. The graph shows that co-registration with the new bite-bar produces an overall improvement of ~7mm over the method with which the fiducial points are arbitrarily based on the circumference of the skull.

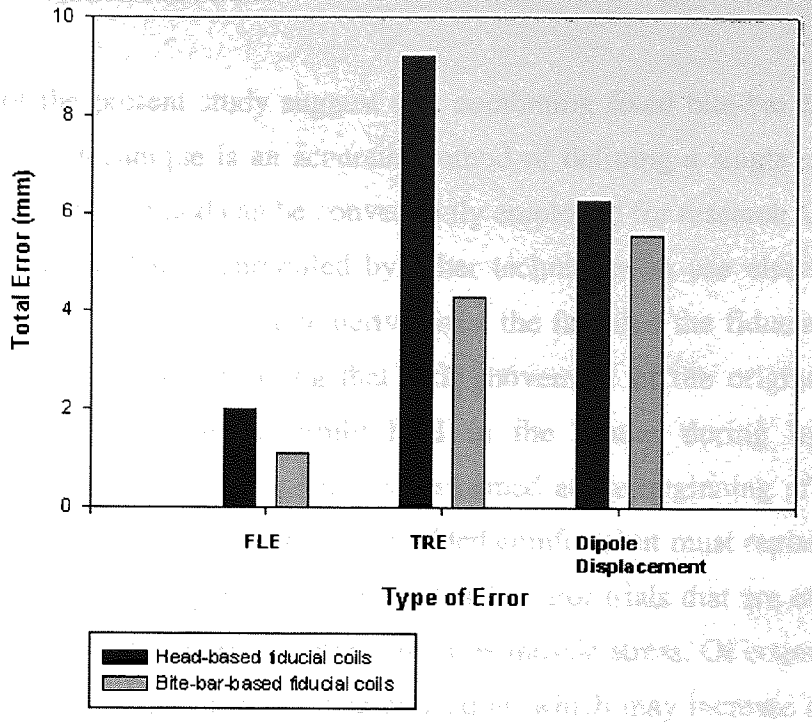

Figure 2-9. Comparison of the overall errors produced by the two co-registration techniques. For FLE, the average of the errors at NA, PAL, and PAR are plotted. The biggest improvement occurs for the repeatability of co-registration as shown by the stability of TRE.

For many clinical applications, such as diagnosis and surgical removal of epileptogenic foci, localisations with millimetre accuracy are highly desirable. It must be noted that this technique can be applied to EEG as well as MEG since the latter is often equipped for simultaneous recording of the patient's EEG. The benefit of this procedure for administrative purposes is that once co-registration is performed for each subject, the same co-ordinate transformation can be applied following subsequent recordings provided that there are no alterations in the subject's dental characteristics.

2.7 Conclusion and Recommendations

The results of the present study suggest that combining fixed bite-bar based coils with a surface matching technique is an accurate method of defining a single co-ordinate system for MEG/MRI. This method can be conveniently employed for research and clinical purposes with an accuracy that is unrivalled by other techniques in use elsewhere. The numerous advantages of the new technique derive from the fact that the fiducial coils are fixed to the arms of the bite-bar, ensuring that little movement of the original position occurs provided that the bite-bar is firmly held in the mouth during localisation. Furthermore, after the localisation of the head is performed at the beginning of each data collection, the subject can remove the bite-bar for added comfort, but must replace it at the end of the data collection for the purpose of re-localisation. For trials that are of extended duration this is particularly advantageous since it reduces muscle stress. Of course the bite-bar may remain in the mouth during MEG data collection, which may increase accuracy a little further at the risk of some discomfort. The advantage of this approach is that the coils could be activated repeatedly to track movement of the head. Subsequently a technique for head correction can be devised and implemented. One method that can be implemented to track head movement during MEG measurement is the use of markers on specific landmarks around the skull. The lens of a 3D camera can then be fixated on these markers to track their displacement to reflect the movement of the head, which can then be corrected in the dataset.

One major success of fMRI as a brain imaging technique has been its ability to distinguish between the visual areas through a process known as retinotopic mapping (see section 3.8.1). With MEG, however, this success has not been attainable primarily because of traditional methods of analysis such as dipole fitting. Novel procedures such as SAM (described in section 1.6) can now be used to perform retinotopic mapping of the visual cortex. Since the visual areas are tightly adjacent, the accuracy of the new co-registration technique is invaluable in identifying each visual area from the other.

Chapter 3: The Visual Pathways, Functional Specialisation, and the Significance of Cortical Oscillations

3.1 Introduction

The primate visual system consists of several parallel processing systems whose specific functional properties and combined output contribute to the fundamental aspects of visual perception. The earliest of these systems begins in the retina. The light that enters the eye initiates a chain of events in two distinct types of photoreceptor cells whose pathways remain segregated throughout the system, including the highest visual areas. Variations in light intensity, spatial or temporal, that reach the eye are the most important aspect of retinal images, while vision itself is a product of the brain. In this chapter, structural and functional organisation of the retinal photoreceptor cells are described with particular emphasis on the two different types of ganglion cells whose specific properties are an important first stage in initiating the segregated pathways that convey different information to the brain. This is followed by a description of the pathways as they arrive in the visual cortex. Along the way, the functional specificity of the pathways is emphasised. The pathways arrive in the primary visual cortex, which acts as a segregator of pathways. It will be demonstrated how each pathway projects to different areas of the visual cortex and how this division is related to the function of each area. The concept and logic of functional specialisation in the visual cortex is introduced along the way with particular reference to perception of colour and motion.

This chapter is concluded by describing the concept of perceptual binding in terms of the dynamics of brain activity. EEG and MEG signals provide information regarding synchronised activity of underlying neuronal networks. The literature regarding the functional significance of neural synchronisation is finally reviewed with particular reference to the frequency of recorded cortical oscillations.

3.2 Functional organisation of the mammalian retina

The human retina is about 250 μm thick and is a highly organised structure consisting of multiple layers of cell bodies and synaptic interactions. The light that enters the eye is focused onto the fovea, which forms a depression in the retina with a diameter of around 1500 μm (Dowling, 1987). This light is then absorbed by the rod and cone photoreceptor cells. The light from any fixation point in space is directly projected onto its centre, the foveola. Detailed studies of the retina have revealed that it does more than simply convert light signals into neural activity. The intricate neuronal interconnectivity and the various layers of cells, however, suggests that light signals are selectively processed before the information is sent to the brain where they are further analysed to form conscious perception of colour, contrast, depth, form etc.

However, the neuronal machinery of the retina is unique in a number of ways. Morphologically, the most obvious difference between the brain and the retina is the presence, in the latter, of photoreceptors and their photosensitive elements that convert light photons into electrical events. Furthermore, unlike neurons in the central nervous system whose action potentials occur as all-or-none phenomena, the impulses of the retinal neurons are graded slow potentials that depend upon stimulus properties such as luminance, colour, and shape. The principal computations of the retina, therefore, are carried out in analogue form, and a conversion to digital output is only achieved at the last stage of retinal synaptic interactions by the ganglion cells whose transfer of impulses through the optic nerve activates neurons in the brain.

Contemporary knowledge regarding the general features of retinal histology is derived from classical works by Ramon y Cajal (1892, cited in Rodieck, 1973) and Polyak (1941). They revealed important information regarding the intricate architecture and specific functional properties of rod and cone photoreceptors. In short, the mammalian retina consists of three basic layers: the outer nuclear layer (ONL), the inner nuclear layer (INL), and the ganglion cell layer (GCL). Figure 3-1 depicts a light micrograph of a section through the retina. The retina is apposed to the pigment epithelium that lines the back of the

eye and is filled with the pigment melanin. One remarkable feature of the eye is that the photosensitive elements contact the pigment epithelium directly while the other cellular layers are closer to the lens. Consequently, light must travel through all the neuronal layers of the retina before striking the photoreceptors.

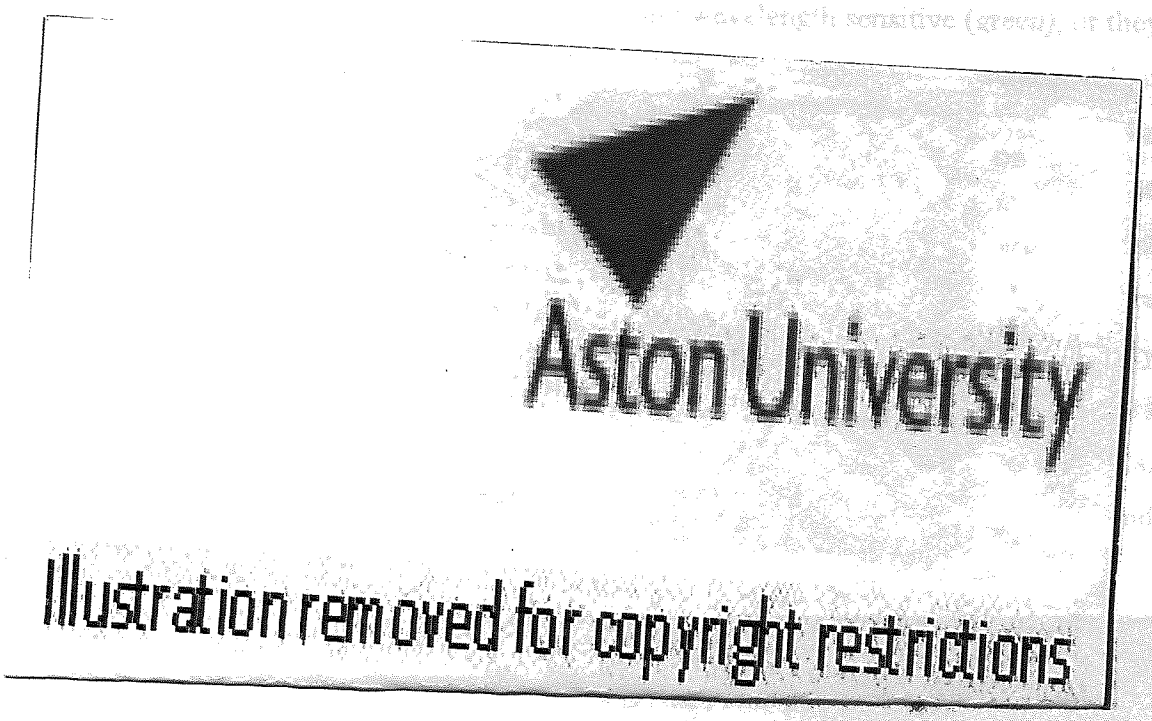

Figure 3-1 A light micrograph of a cross section through the human retina. PE, Pigment epithelium; IS, photoreceptor inner segments; ELM, external limiting membrane; ONL, outer nuclear layer (contains cell bodies of rods and cones); OPL, outer plexiform layer (contains synapses between rods and cones and second order neurons); INL, inner nuclear layer (contains cell bodies of horizontal, amacrine, bipolar, interplexiform cells); IPL, inner plexiform layer (synapses of third-order neurons); G, ganglion cell layer (contains cell bodies of ganglion cells); OFL, optic fibre layer (axons of ganglion cell layers); ILM, internal limiting membrane. (From Cohen, AI: The retina. In Moses, RA, and Hart, WM, Jr, eds: *Adler's physiology of the eye: clinical application*, ed 8, St Louis, 1987, Mosby.)

3.2.1 Functional characteristic of rod and cone photoreceptors

The human retina consists of an average of 57.4 million rods and 3.3 million cones (Panda-Jonas et al., 1994). Rods mediate dim-light or night vision whereas cones are active in bright light and perform better than rods in all visual tasks except the detection of dim stimuli. Consequently, total loss of rods leads to night blindness whereas those who lose cone function are effectively blind. The photoreceptor cells utilise four different photopigments, which are capable of trapping photons. The rod photoreceptors contain a

pigment called rhodopsin while the other three pigments are found in the cones and are collectively referred to as iodopsin. These photopigments differ mainly in their sensitivity to wavelengths of light and are referred to as red, green, or blue cones, based on the part of the spectrum that their photopigments absorb. In other words, the photopigments are either S, or short wavelength sensitive (blue), M, or medium wavelength sensitive (green), or they are L, or long wavelength sensitive (red). Consequently, the cone system mediates colour vision whereas the rod system is achromatic. The highest population of cones is in the fovea with approximately 200,000 cones/mm^2; this density rapidly declines towards the periphery of the retina. On the other hand the density of rods at the fovea is nil, but increases rapidly with distance and peaks at around 3mm either side of the fovea where there are approximately 150,000 rods/mm^2. This concentration of rods declines less rapidly in the periphery than does the cone density (Panda-Jonas, 1994). The rod photoreceptors are responsible for our sensitivity to light as they mediate vision at low illumination levels. Cones mediate vision at daylight levels and are responsible for good visual acuity and colour perception. Illumination levels at which rods alone are sensitive are described as scotopic, and levels at which cones alone function are referred to as *photopic*.

The concentration of cones in the fovea is partly responsible for the higher spatial resolution of the cone system in comparison to the rod system. As mentioned earlier, rods and cones do not fire action potentials but respond to light with graded changes in membrane potential. Rods respond slowly, which prevents them from resolving light flicker faster than about 12 Hz. Conversely, the response of cones is much more rapid and they can detect flicker of up to 55Hz. Subsequently, the cone system is capable of resolving greater temporal resolution of images (Dowling, 1987). Table 3-1 summarises the differences between rod and cone neural systems.

Rod Photoreceptors	Cone Photoreceptors
High sensitivity;	Lower sensitivity;
Specialised for night vision;	Specialised for day vision;
Contains a single photopigment called rhodopsin;	Contains 3 types of photopigments collectively called iodopsin;
Contain more photopigment;	Contain less photopigment;
Low temporal resolution;	High temporal resolution;
Sensitive to scattered light;	Sensitive to direct axial rays;
High amplification, capable of detecting single photons;	Low amplification, incapable of detecting weak light rays;
Rod Neural System	**Cone Neural System**
Low acuity as a result of a highly convergent pathways and its absence in foveola;	High acuity as a result of less convergent and more divergent pathways and high concentration in the foveola;
Achromatic and insensitive to variations in wavelength;	Chromatic and capable of detecting light of different parts of the spectrum;

Table 3-1: Differences between the rods and cones and their neural systems.

3.2.2 Phototransduction

When light strikes the photoreceptor cells, the energy is transferred from photons to photopigments and the absorption of light by the latter causes hyperpolarisation of the cell membrane. This brings about the most fundamental process in the perception of visual images that occurs in the outer segment of the retina, namely the process of *phototransduction.* This is the conversion of light energy into electrical signals and is the hyperpolarising response of rod and cone photoreceptors to light. In short, it refers to retina's ability to detect light of a retinal image through its photoreceptors. By transforming this light into chemical energy, the chain of neural events that leads to the perception of images is initiated. Each cell in the visual pathway responds to light directed at a specific area of the retina. This region of space in which stimuli affect the neuron's activity is the *receptive field* (RF) of that neuron.

The light that enters the photoreceptors is communicated to the brain by a network of cells within the retina that form the INL. These cells are organised in two interconnecting but directionally distinct pathways known as vertical (or direct), and horizontal (or lateral) pathways, due to the directions of information flow.

3.2.3 The vertical pathways of the retina

3.2.3.1 Bipolar cells

The rod and cone photoreceptors synapse to a type of second-order vertical neurons known as bipolar cells that initiate the first step in parallel rod and cone pathways. The term bipolar refers to the fact that the cell body is situated between the dendritic end and the axon terminal end. The discovery that the rod bipolar cells contact only the rod photoreceptors and the cone bipolar cells connect only to cones (Boycott and Wassle, 1991) support the existence of segregated rod and cone pathways throughout the retina.

3.2.3.2 Ganglion cells

As the output neurons of the retina, ganglion cells are the last stage of processing before signals are sent to the brain. The dendrites of the bipolar cells receive input from the photoreceptor while the axon ends make synaptic contact to third-order vertical neurons known as ganglion cells. These are retinal neurons whose cell bodies lie in the IPL; their dendrites receive synapses from amacrine and bipolar cells. In short, the inputs of the bipolar cells are integrated by the dendrites of the ganglion cells, where they are converted to action potentials that travel down the axons. These then make up the bundle of neurons that forms the optic nerve, terminating in the lateral geniculate nucleus (LGN) and the superior colliculus. Ganglion cells receive specific synaptic connections from the bipolar cells such that they form two major pathways, which remain segregated through to the LGN (Schiller and Malpeli, 1977; Schiller et al., 1986). Certain properties of ganglion cells are crucial in the way visual stimuli are perceived and communicated to higher-order visual areas and are described in some detail later.

3.2.4 The lateral pathways of the retina

The organisation of vertical pathways described above would indicate that the output of the ganglion cells to the brain is a direct reflection of the amount of light absorbed through the photoreceptors' connection with the bipolar cells. If this were the case, light falling on neighbouring photoreceptors would have little or no conscious perception. However, there are lateral pathways at two levels of the retina, meaning that the input into the vertical pathways from a group of photoreceptors is indirectly influenced by inputs from neighbouring photoreceptors.

3.2.4.1 Horizontal cells

Horizontal cells are the interneurons of the outer retina, which is a layer of neurons that make connections between neighbouring photoreceptors (Boycott and Kolb, 1973). These cells form the first of the lateral pathways and mediate between the photoreceptor

and the bipolar cell layers. In the vertical pathway, the input from the photoreceptors to the bipolar cells is the result of a direct flow of signals as well as input from the neighbouring photoreceptors as mediated by the horizontal cells.

3.2.4.2 Amacrine cells

The amacrine cells in the inner retina form the second of the lateral pathways. They are situated between the bipolar cell and ganglion cell layers of the vertical pathways. Amacrine cells receive input from the bipolar cells as well as other amacrine cells and their output is mainly to other amacrine cells, ganglion cells and even to other bipolar cells. There are a number of different types of amacrine cells with the *A-II* and the *A-17* type cells being the most important components of the scotopic or rod visual pathway in the human retina (Kolb, 1994).

3.3 Structural and functional properties of retinal ganglion cells

The evidence for the computations carried out by the retina is found in the receptive field properties of ganglion cells and their selective sensitivity to patterns of light and dark. The receptive field (RF) of a ganglion cell is that area of retinal where stimulation of photoreceptors causes either an increase or decrease in of the ganglion cell's firing rate. Ganglion cell receptive fields have a centre and an antagonistic surround. Kuffler (1953) investigated the RF properties of ganglion cells by exposing the eye to small spots of light and found circular RFs that vary in size across the retina. In the fovea, where visual acuity is greatest, the RFs are smaller with centres that are only a few minutes of arc. In the periphery of the retina, where acuity is low, the RFs are larger.

Physiological and anatomical investigations have also revealed several distinct classes of ganglion cells within the primate retina whose parallel functioning results in the perception of a unified visual scene (Schiller, 1986). For this reason they are often thought of parallel processing channels (DeYeo and Van Essen, 1988; Livingstone and Hubel, 1988). The most important of ganglion cells are the *midget* (Pβ) and the *parasol* (Pα) types that dominate the primate retina (Polyak, 1941), constituting about 70% and 10% of the total ganglion cells respectively (Watanabe and Rodieck, 1989). The most obvious difference between these two categories of ganglion cells concerns their size and the spread of their dendrites, as shown in figure 3-2.

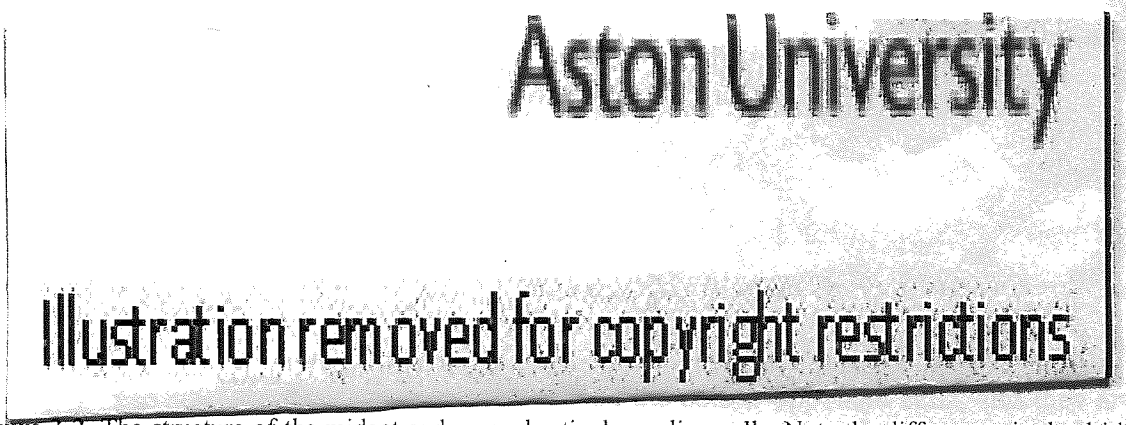

Figure 3-2. The structure of the midget and parasol retinal ganglion cells. Note the differences in dendritic spread between the two categories of cells. Redrawn from Kolb (1994).

Each subgroup of ganglion cells projects to a different layer of the LGN and subserves different functional roles: parasol cells play an important role in the perception of fast flicker and motion, whereas the midget cells are important in form and colour perception (Schiller and Logothetis, 1990; Schiller et al., 1990a, 1990b). The parasol and midget ganglion cells initiate two major channels that contribute greatly to many important aspects of vision: the broadband and the colour-opponent channels respectively (Schiller and Logothetis, 1990). These pathways project to different laminae of LGN; the broadband cells connect to the magnocellular (M) layers, whereas the colour-opponent pathway projects to the parvocellular (P) layers. For this reason they are also referred to as magnocellular (M) and parvocellular (P) pathways respectively.

The retinal ganglion cells of these pathways can be divided into two populations: those that are stimulated and those that are inhibited. ON-centre cells are excited (depolarised) when light is directed to the centre of their receptive field, and they are inhibited when light hits their surround. On the other hand, OFF-centre cells are inhibited (hyperpolarised) when light is directed to the centre of their receptive field, and are excited when light is directed at their centre. This is because these cells have concentric *antagonistic centre-surround organization* with the surround being inhibitory. The P cells have small receptive fields and have colour coding properties. Their colour-opponent organisation means that while the centre maybe stimulated by one colour, another activates the surround. This interaction is based on the three types of cone inputs introduced earlier: the S, M, and L wavelength receptors. In contrast, M cells have larger receptive fields and do not discriminate colour. The basic properties and differences of these types of cells are depicted in Figure 3-3 (Schiller and Logothetis, 1990a).

The RF centre region of the broadband cells is believed to receive input from all three types of cone photoreceptors, whereas the colour-opponent cells receive their input from only one cone type (Wiesel and Hubel, 1966; Gouras, 1968). On the other hand, the RF surround of both types of cells receives equal input from all cones (Wassle, et al.1989). The RF of the broadband cells is much larger than the colour-opponent cells, and they are much more sensitive to slight differences in luminance information. The response latencies

of these cells also differ from each other; whereas colour-opponent cells respond in a sustained fashion to the stimulation, the response of the broadband cells is transient.

The RF properties of single cells at different levels of the visual system indicate that the colour-opponent channel is involved in colour vision as well as the perception of high spatial frequency patterns, whereas the broad-band system is involved in the perception of motion and low contrast stimuli (Livingstone and Hubel, 1987a; Schiller and Logothetis, 1990; Schiller et al., 1990a). In the following sections, the functional specificity of the visual pathways is discussed with particular reference to the division of functionally distinct areas within visual cortex.

a.)

Colour-opponent system Broad-band system

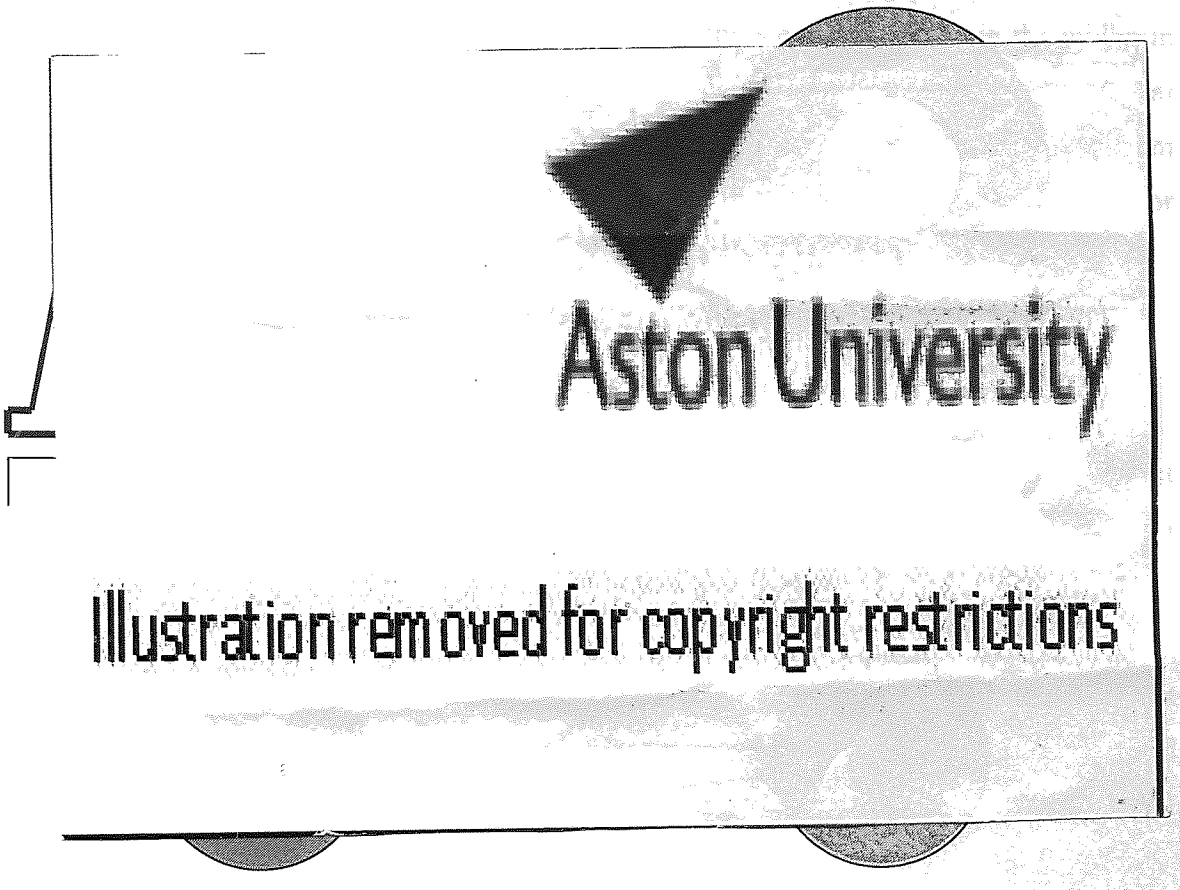

Figure 3-3. The various properties of retinal ganglion cells: (a) R, G, b, indicate different cone type inputs. Colour-opponent cells have small receptive fields and their centre receive input from just one cone type whereas their surround receives input from all cone types. The cumulative-response histogram indicates the sustained fashion in which these cells respond to light stimulation. The broad cells have large receptive fields and receive equal input from all cone types in both centre and surround regions of their receptive fields. Their light-evoked responses are transient. Blue cones are shown in lower case 'b' as the ratio of blue cones to the rest is 1:10. (b) ON-centre cells respond when maximally when the entire centre is stimulated which causes the inhibition of their surround region. Light that falls on the surround inhibits the centre region of the OFF-centre ganglion cells. Redrawn from Logothetis et al. (1990a).

3.4 The Retino-Cortical Visual Pathways

The major retinal output exits the eye via the optic nerve and cross over at the optic chiasm in a very specific fashion. Once the pathways have crossed at the chiasm, they form the optic tract. Around 10% of retinal ganglion cell outputs enter a nucleus in the midbrain known as the superior colliculus while the rest send axons that terminate in the lateral geniculate nucleus (LGN). Cowey and Perry (1980) found that almost all the outputs from the parasol and midget ganglion cells enter the LGN, with none going to the superior colliculus.

3.4.1 Functional properties of the visual pathways

Anatomical and physiological properties of cells in the P and M pathways suggest that they perform different roles in visual processing (Merigan et al., 1989). There are a vastly greater number of retinal ganglion cells in the P pathway (~80%) than in the M pathway (~10%), and because of their colour opponent properties, they are believed to respond to form as well as colour. Neurons in the M pathway, however, have high contrast sensitivity and greater temporal resolution and are believed to respond best to motion and luminance (Merigan et al., 1989; Schiller et al., 1990a, Schiller et al., 1990b).

3.4.2 The Lateral Geniculate Nucleus (LGN)

Seemingly, the lateral geniculate nucleus (LGN) acts as a relay station that conveys information from the retina to the visual cortex. The LGN is a subcortical thalamic structure either side of the midbrain, with remarkable specificity of axonal connections that reflect the input and the properties of corresponding retinal ganglion cells. Figure 3-4 depicts the laminar organisation of the LGN. The retinal input from the two eyes is segregated in distinct layers of the LGN. A slice through this nucleus reveals 6 distinct subdivisions with four upper and two lower layers. Because the cells in the latter are larger, they are called the magnocellular layers while the upper four divisions are referred to as the parvocellular layers due to the smaller size of the cells they contain. One distinctive feature

of the LGN is that the inputs from the two eyes remain segregated such that the nerve fibres coming from the contralateral eye terminate in layers 6, 4, and 1, while the ipsilateral fibres end in layers 5, 3, and 2 (Fries, 1981). Furthermore, there is a remarkable retinotopic organisation such that adjacent points on the retina project to adjacent points in each layer of the LGN. The back of each LGN contains neurons whose receptive fields are near the fovea while the peripheral retina is mapped towards the front of the nucleus (Fries, 1981).

Figure 3-4. The parvocellular and magnocellular layers of the lateral geniculate nucleus (left). The nerve fibres from each eye terminate at different layers. The image on the right shows the nerve fibres from the contralateral eye, which terminate in layers 6, 4, and 1. From Merigan and Maunsell, 1990.

The cells of the LGN inherit their properties from the retina. The receptive fields of retinal ganglion cells and the cells of the LGN to which they project are strikingly similar. Because there is little convergence from retinal ganglion cells onto LGN cells, the distinction between ON and OFF receptive field centres is maintained, as are other properties such as colour opponency and contrast sensitivity. Most cells in the P layers have certain degree of wavelength specificity as opposed to those in the M layers which are not colour specific but respond to motion stimuli (Wiesel and Hubel, 1966). The connections between the pathways that leave the LGN and the visual cortex are highly detailed and specific. In summary, the outputs from the P layers of LGN arrive at layer 4C of V1 from where they connect to layers 2 and 3. Here, they divide to form two subpathways: one feeds the blob cells and is thus concerned with colour; the other feeds the interblob cells and is concerned with form. On the other hand, the M lamina of LGN connect to layer 4B of V1

and divide to produce two subpathways: one feeds the direction as well as orientation selective cells of layer 4B and is thus concerned with motion; the other only feeds the orientation selective cells of 4B and is thus only concerned with form perception (Zeki, 1993).

In spite of the wealth of knowledge regarding the structure of the LGN, establishing its role in visual function has remained an enigma. Guillery (1979) presents an excellent review of the LGN and its development. The close similarity between the receptive fields of ganglion cells and the LGN cells to which they project suggests that little or no further processing of visual signals occurs in the latter and that it merely acts as a relay station between the retina and the visual cortex. It has been suggested that rather than altering the receptive field properties, the LGN regulates the strength and the flow of visual signals to the cortex (Steriade and Llinas, 1988). Others have suggested that the LGN may simply be regarded as a 'sorting' centre that separates the crossed and uncrossed fibres that had been mixed up in the optic tract (Guillery, 1979). What is certain is that the basic function achieved by this highly organised lamination is clearly to keep the retinal inputs from the two eyes separate. This would imply that integration of inputs from the eyes, to give the perception of a unified field of vision, is primarily a function of visual cortex.

The differences between the functions of M and P pathways have been extensively studied at the geniculate. Perhaps the best and most comprehensive findings regarding the functional properties of the retinocortical pathways at the level of LGN are derived from lesion studies in macaque monkeys (e.g. Merigan, 1989; Merigan and Maunsell, 1990; Schiller et al., 1990a). Merigan (1989) and Merigan and Maunsell (1990) employed a method whereby the colour-opponent or the broadband system was blocked following the administration of the toxin acrylamide. Schiller et al. (1990a) trained monkeys to perform visual discrimination or detection tasks and rewarded their responses based on saccadic eye movement. They injected quantities of the neurotoxin ibotenic acid to create small lesions in either the magnocellular or the parvocellular portions of the LGN. They then presented stimuli on the impaired locations of the visual field. The results of these studies are briefly described below.

3.4.2.1 Parvocellular LGN (PLGN) lesions

PLGN lesions led to severe deficits in colour discrimination to the point that the animal could no longer discern colour at all. However, the ability to detect small colour stimuli on an isoluminant background remained intact. It was concluded that PLGN lesions impair the capacity for colour discrimination in that the animal is unable to assign colour values to different wavelengths but the ability to 'see' stimuli based on wavelength differences remained intact. They suggested that the P pathway is essential for colour discrimination, and although the M pathway lacks the capacity to differentiate on the basis of wavelength, it is capable of providing information for 'seeing' colour stimuli. Form vision, including shape, texture, and pattern were severely compromised following PLGN lesions but only when the stimuli were set at high spatial frequencies. Low spatial frequency stimuli produced considerably less pronounced deficits in form perception.

3.4.2.2 Magnocellular LGN (MLGN) lesions

MLGN lesions have no effect on colour and form discrimination tasks but the perceptions of flicker and motion were most dramatically affected. At high spatial frequencies, MLGN lesions produced significant deficits in detection of monochromatic as well as heterochromatic (red/green) flicker. This indicated that the broadband system determines the temporal aspect of flicker perception. For motion detection, a random array of dots was presented that included a small area where dots moved at different temporal rates. It was found that when the moving dots appeared at the M-lesioned location of the visual field, there was no perception of movement. However, performance improved linearly with an increase in contrast and/or a decrease in the temporal aspect of the stimulus. As a results if these findings, Schiller and colleagues (1990a and 1990b) have suggested that although the M pathway is essential for the perception of motion, the parvocellular system is capable of sustaining some aspects of motion perception at high levels of contrast.

3.4.3 The projections of LGN

The parvocellular and magnocellular pathways remain segregated on exit from the LGN, forming the optic radiation and arriving at the primary visual cortex, or visual area 1 (V1). The axons of the ganglion cells that originate in the nasal part of the retina cross over to the opposite or contralateral hemisphere, whereas those that originate in the temporal retina terminate in the same or ipsilateral hemisphere. This partial crossing over of the optic nerves is referred to as decussation (Zeki, 1993). Thus, fibres from the temporal retina of the right eye and the nasal retina of the left eye pass over to the right LGN and so look at the left half of the field of view. Conversely, fibres from the nasal retina of the right eye and the temporal retina of the left eye terminate in the left LGN, which therefore view the right half of the field of vision.

3.5 The organisation of the primate visual cortex

Most primates are highly visual creatures and a vast area of the entire cerebral cortex is devoted to analysing and integrating the highly complex and multi-faceted type of retinal information. The visual areas have been identified using several criteria, including topographic organisation, neuronal response properties, anatomical connections, architectonics, and perceptual deficits resulting from lesions (Maunsell and Newsome, 1987) although the results can be contradictory. For instance, any two visual areas may contain the same retinotopic organisation while their neuronal connectivity and architecture may reveal little else in common. This uncertainty further emphasises the complexity in identification and localisation of specific areas while the picture emerging from the subdivisions within the visual cortex is as yet not complete. Consequently, it is likely that our understanding of the subdivisions of the visual cortex will change with time as new areas are identified (Van Essen et al., 1993).

In the macaque monkey, a total of 32 visually related areas have been implicated (Van Essen, et al; 1993), which comprise an estimated 54% of the entire cerebral neocortex, including parts of the frontal lobe, the posterior half of the parietal lobe, the ventral half of the temporal lobe, and the entire occipital lobe (Felleman and Van Essen, 1991). Figure 3-6 depicts an unfolded map of the entire visual cortex where the regions implicated in vision are shown in colour.

Figure 3-5. A two-dimensional, unfolded map of cerebral cortex in the right hemisphere of the macaque monkey. The coloured regions on the map and on the lateral and medial brain views include 32 visual areas, 25 of which are predominantly or exclusively visual in function while the other 7 are involved in other functions such as polysensory or visuomotor functions. They occupy an estimated 54% of the cerebral neocortex. Copied from Van Essen et al. (1990).

3.5.1 The primary visual cortex (V1)

Area V1 is also known as Brodmann's Area 17, or the *striate* area, so called because its cytoarchitecture forms a large striation, called the *stria of Gennari* consisting of cortical axons. V1 is a multi-layered structure about 2mm thick that lies at the pole of the occipital lobe. It has a columnar organisation and is segregated into six layers based on density and shape of neurons as well as variation in interconnections to the rest of the visual cortex, which are highly complex and specific. In summary, Layer 1, or the neuropil consists of mainly axons, dendrites, and synapses. Layers 2 and 3 are often grouped together and referred to as the *superficial layers* and consist of cell bodies and dendritic interconnections. The columns are specially prominent in layers 2 and 3 and form 'blobs', separated by a more lightly staining region of 'interblobs'.

Most of the incoming fibres from LGN terminate in layer 4 of V1. Layer 4 has multiple connections with many other cortical areas and for this reason it has been divided into several layers. A row of darkly staining patches constitutes layer 4A, followed by the lightly staining layer 4B, and a more darkly staining layer 4C. Layer 4C has a complicated structure and is further subdivided to receive input from the magnocellular and parvocellular lamina of the LGN with the former projecting to the upper layer 4Cα and the latter to the lower 4Cβ. Cells of layer 4Cβ send connections to layers 2 and 3. Layer 4B receives large input from 4Cα and sends its output to extrastriate areas. Layer 5 consists of relatively less cell bodies compared to the other layers and sends its input back to the superior colliculus. Layer 6 is densely populated with cells and sends a large output back to the LGN (Lund, 1988).

Felleman and Van Essen (1991) propose that in general forward outputs to other cortical areas come from the superficial layers and terminate in layer 4 while the feedback projections come from deep layers to terminate in layers 1 and 6. Indeed the organisation of V1 and particularly the cells within the blob and interblob regions have different functional properties as they project to different destinations in the cortex. The functional significance

of this organisation will be discussed in the section relating to functional organisation of visual cortex.

3.5.2 The extrastriate cortex

The surrounding area of V1 corresponds to Brodmann's Areas 18 and 19, or the *prestriate (*or *extrastriate)* areas. Clare and Bishop (1954) confirmed the existence of visual areas other than the primary visual cortex, which they referred to as 'association areas'. Hubel and Wiesel (1962) recorded from the cat's visual cortex and specifically Brodmann areas 18 and 19, which lie adjacent to V1, and found a highly complex variety of cells similar in architecture to V1. This indicated a hierarchical chain of events involved in visual processing. Further evidence for the existence of visual areas in the periphery of V1 was based on anatomical work with the brain of Old World macaque monkey (Zeki, 1969, 1971). It was found that V1's highly detailed retinotopical map is projected in a similarly detailed, point-to-point manner to some regions of the visual association cortex. In contrast, other areas of the association cortex contained less precise projections from V1 implying that the retinal topography created in them is also less precise.

Studies of the visual cortex in many species have shown that the extrastriate cortex comprises a mosaic of visual areas that can be distinguished by several anatomical, functional, and physiological criteria (reviewed by Zeki, 1978a; Cowey, 1979; Van Essen, 1985). It is now well established that outside the primary visual cortex, there are multiple areas in which the retina is independently represented and the nature of this retinal representation is different from that in V1 and differs from area to area. Furthermore, the receptive fields of cells in the association areas are larger and their areas are smaller in size than V1 (Hubel and Wiesel, 1962).

3.5.2.1 Area V2

Area V2 corresponds to Brodmann area 18 and is situated within an area of uniform cytoarchitecture and for this reason, it is not distinguishable from the immediately surrounding cortex of the same cytoarchitectonic structure. Its position, therefore, is revealed by its metabolic or cytochrome oxidase architecture. V2 consists of alternate thick and thin *dark stripes*, separated from each other by lightly staining, or *pale interstripes* that run perpendicular to the border between V1 and V2. This structure is unique to area V2 and has important functional implications and will be discussed in the section relating to functional specificity. The striped regions are relay points for the three major pathways that pass through V1, projecting to different extrastriate areas (Zeki and Shipp, 1988; Van Essen et al., 1992) and form systems that appear to process distinct types of visual information.

Just as adjacent retinal points connect with adjacent points in V1, resulting in a detailed point-to-point map of the visual scene in the latter, adjacent points in V2 also receive detailed connections from adjacent points in V1 that result in a detailed topographical map of the visual scene in V2 (Zeki, 1969; Cragg, 1969). This pattern of connectivity from V1 to V2 is such that the upper field of view, or the lower contralateral retinal quadrant, is mapped in the lower part of V2 while the lower field of view, or the upper contralateral retinal quadrant, is mapped in its upper part (Van Essen and Zeki, 1978). In man, much of area V2 lies on the medial surface that surrounds the striate cortex. The part of V2 on which the upper retina (or the lower visual field) is mapped, borders the upper lip of the calcarine sulcus. Similarly, the part of V2 on which the lower retina (or the upper visual field) is represented lies in the border of lingual gyrus.

3.5.2.2 Area V3

Area V3 lies on the medial side of the brain surrounding area V2 and like the latter, it lies within Brodmann's area 18 having a ventral and a dorsal part. In the macaque, V3 lies on the cuneus and the lingual gyrus where the latter represents the upper visual field and the former representing the lower visual field (Van Essen and Zeki, 1978). Area V3A

extends dorsally across the brain and although its architecture has not been adequately investigated, it shares certain functional characteristics with V3. It does not receive a direct input from V1, but instead it receives strong input from V3. Because of the functional similarities between V3 and V3A, they are collectively referred to as the A3 complex. In the human brain, neither the location nor even the existence of V3 has been confirmed (Zeki, 1993).

3.5.2.3 Area V4

In the macaque, area V4 is situated on the lateral side of the brain bordering area V3A. The main input into V4 arrives from V2 although it also receives direct input from that region of V1 with foveal representation (Zeki, 1978b). Much like V3, area V4 has a further subdivision, referred to as V4A, where the properties of cells are very similar to those in V4 itself. For this reason, the two areas are collectively referred to as area V4 complex (Zeki, 1977). V4A receives the majority of its input from V4, a small amount from V2, and none at all from V1.

3.5.2.4 Area V5

Lying buried within the superior temporal sulcus, also referred to as MT, on the anterior side of V4, and extending laterally on the side of the brain is area V5 (Dubner and Zeki, 1971). It received direct input from V1 and projects to a number of locations in its immediate surrounding. These areas do not have inputs from V1 and share certain physiological characteristics with V5 itself, such as specific response to certain kinds of motion (Dubner and Zeki, 1971).

3.5.3 Retinotopic organisation

The projections from each LGN terminate in the ipsilateral V1 such that the cortex of each hemisphere receives signals from the contralateral half of the field of view (Zeki, 1993). If activity is recorded from any given region of the cortical surface in V1, the cells

of that region will have receptive fields at a given position in visual space, meaning that the input is from a given region of the retina. In other words, adjacent points of the field of vision correspond to adjacent retinal points, which are mapped at adjacent points in V1. This produces a *topographic map* of the retina within the primary visual cortex (Hubel and Wiesel, 1977). The receptive field size of each cell indicates that central vision occupies more of the cortical surface in V1, as they are smaller in the part of the cortex representing central vision (centre of gaze) and increase in size with a move to periphery of the retina. This is thought to be proportional to the importance of central vision since it is needed to observe finer details of a visual scene (Zeki, 1977).

V1 projects in a point-to-point fashion to area V2 such that the latter is also topographically organised although this organisation is somewhat different to that in V1 (Hubel and Wiesel, 1977). This difference is manifest by the size of receptive fields in V2, which are generally larger although, as in V1, the size increases with departure from central vision. Other visual areas too seem to have a certain degree of retinotopic organisation.

In V3 cells have larger receptive fields than the preceding areas but much like the latter, receptive field size of cells increases away from the central vision. The receptive fields of cells in areas V4 and V5 are larger still but they do not possess the same topographic organisation as those in V1 or V2 (Maunsell and Van Essen, 1987). Recordings from successive cells in V4 and V5 show that the receptive fields of most cells are in roughly the same region of visual space. This fact, in addition to the large size of receptive fields in these areas, indicates that the retinal maps created in them are not as clear as those in V1 or V2. Zeki (1975) used the term 'crude' to refer to the maps of the retina created in V4 and V5, a position from which he later retracted to emphasise that '...maps in the brain are precise enough as they need to be to undertake their function with efficiency' (Zeki, 1993). In other words, unlike the topographic map in V1, the maps in V4 and V5 (if they are topographic maps at all) are less precise as they represent particular types of activity, namely colour and motion processing that occur in the field of view (Zeki, 1993). The mapping of the retina in V4 occurs with a unique difference to that in all other areas. In V4, only the central 40 degrees of retina is mapped which in the latter corresponds

to the foveal region where the concentration of cones required for colour vision is emphasised and become less concentrated with a move to peripheral regions (Van Essen and Zeki, 1979). This organisation is described in more detail when discussing colour perception in chapter 5.

3.6 Functional specialisation within the visual cortex

In reviewing the visual pathways, Hubel and Wiesel (1979) observed:

"The lateral geniculate cells in turn send their axons directly to the primary visual cortex. From there, after several synapses, the messages are sent to a number of further destinations: neighbouring cortical areas and also several targets deep in the brain.... the primary visual cortex is in no sense the end of the visual path. It is just one stage, probably an early one in terms of the degree of abstraction of the information it handles."

Over the past few decades, there have been a number of hypotheses regarding the perceptual significance of extrastriate visual areas as well as the role of V1 in segregating the variety of incoming stimuli (Zeki, 1975; Van Essen 1985; Livingstone and Hubel, 1987a). In particular, there has been the notion that individual visual areas are responsible for detailed computation of specific perceptual features such as colour, shape, form, motion, and depth, and that area V1 is the first recipient of pathways entering the visual cortex where they become isolated and diverted to specialised areas (Livingstone and Hubel, 1987a). In the following sections, the organisation of V1 and functional specificity of the extrastriate areas are briefly described. Because area V5 in the extrastriate cortex was the first specialised area to be identified, the description of functional specialisation in the visual cortex begins with the extrastriate cortex.

3.6.1 The extrastriate cortex

The extrastriate areas differ in the types of visual information they process. Anatomical and functional investigations of rhesus monkey prestriate visual cortex have reinforced the idea that different areas within it have remarkably different populations of functional cells, thus providing further evidence for the theory of functional specialisation within the visual cortex (Shipp and Zeki, 1985). Evidence for selective processing of visual information was provided by Zeki and his colleagues following their investigations of the visual cortex of the macaque monkey (Dubner and Zeki, 1971; Zeki, 1974a).

3.6.1.1 Area V5

Dubner and Zeki (1971) found that a region of cortex in the superior temporal sulcus contains an abundance of neurons that are selective for the direction of stimulus motion but not so selective for colour or form. This area was first identified in the owl monkey and was referred to as the middle temporal visual area (MT) or the motion area of the superior temporal sulcus with its homologue being area V5 (Zeki, 1983a, 1983b) in humans and the macaque monkey (Zeki, 1993).

This in fact was the first area whose function was studied in some detail (Zeki, 1974b). It was found that 90% of the cells in area V5 of the rhesus monkey respond to motion in a particular direction but not to its opposite or a null direction. In other words the majority of cells in area V5 were directionally selective and neither the intensity nor the colour of the spots of light seemed to alter the response of cells in this area. The cell's response depended solely upon the direction of movement within its receptive field independent of other attributes.

3.6.1.2 Area V4

Zeki (1973, 1977) found that the cells in area V4 of the macaque are colour selective, that is, they responded to lights of some wavelengths better than others. Additionally, these cells were also found to be orientation selective many of which were wavelength selective as well. This area contains few cells that are involved in detecting the direction of motion. Further evidence from a number of other studies has confirmed that form, colour, and wavelength selectivity is overwhelmingly emphasised within area V4 (Desimone and Schein, 1987). The homologue of this area in humans is the region of lingual and fusiform gyri (Zeki, 1993)

3.6.1.3 Area V3

Zeki (1978c) identified area V3 whose cells responded to lines of specific orientation regardless of both the colour of the lines and the colour of the background on which these lines were presented. Zeki (1978c) speculated that since orientated lines are important components of the form of objects, then area V3 is involved in processing of the form of visual stimuli.

3.6.2 The primary visual cortex and area V2

If V1 acts as a segregator of signals, and if the theory of functional specialisation in the extrastriate areas is to be upheld, then certain amount of specialisation must also exist in the areas that provide their inputs (Zeki and Shipp, 1988). It is therefore logical that some degree of specialisation exists within V1 itself such that cells concerned with colour processing are separated from cells that process form or motion.

As mentioned earlier, V2 receives point-to-point projections from V1 and its cytoarchitecture is very similar to the rest of Brodmann's area 18 making it hard to distinguish from the rest of the extrastriate cortex. Much like V1, area V2 also contains subgroupings of cells that are functionally distinct and which project to the same extrastriate areas (V3, V4, and V5) as V1. The common feature of the functionally distinct extrastriate areas is that they all receive their inputs from V1 and the surrounding area V2 (Cragg, 1969; Zeki, 1969). The primary visual cortex receives most of the visual input to the brain and sends parallel outputs to a number of specialised visual areas (Zeki, 1978a; 1978c). Confirmation of the role of V1 in segregating the various kinds of visual information relating to colour, form, motion, and depth has come from a number of anatomical studies (Zeki, 1978a; Livingstone and Hubel, 1984; Shipp and Zeki, 1985). The distinct structural composition of V1 with its uniquely diverse laminar cytoarchitecture of blobs and interblobs suggested that each region must possess a different function. According to Roe and Ts'o (1995), there are 3 separate visual maps in V2 since its physiology reveals functionally heterogeneous populations of cells. Within the thin stripes,

there is a colour map; within the thick stripes, there is a directional map; and within the interstripes, there is an orientation map. In other words, cells that are wavelength selective, orientation selective, and direction selective are found within it. These maps are devoted to a different attribute and are all contained within the overall map of V2. It is therefore feasible to also think of area V2 as a segregator that sends separate and distinct signals to different specialised areas each of which attends to different attributes of the visual scene (Zeki, 1993). Furthermore, since V1 and V2 contain representations of the same submodalities of vision, it can be logically inferred that cells processing particular types of signals in each area are connected with each other in such a way that wavelength selective cells of V1 connect specifically with wavelength selective cells in V2 and so on.

Highly specific connections exist between the functionally distinct groups of cells of V1 and V2. In particular, the blobs in layers 2 and 3 of V1 connect to the thin stripes of V2 while layer 4B connects with the thick stripes, and the interblobs connect with interstripes (Livingstone and Hubel, 1987b). Furthermore, it has been shown that the thick stripes of V2 connect with areas V3 and V5 while the thin stripes connect with area V4 (Shipp and Zeki, 1989a and 1989b).

Shipp and Zeki (1985) found that just like the blob cells of V1 and the cells of area V4 to which they project, the thin stripes of V2 are primarily wavelength selective. Similarly, it was found that just like the interblobs of V1 to which they connect, the interstripes of V2 are orientation but not wavelength selective. The interstripes also project to area V4 where orientation and wavelength selective cells coexist, and hence there maybe an overlap between the interstripe and thin stripe projections to V4 (De Yeo and Van Essen, 1988). Moreover, just like layer B4 of V1 where cells are predominantly orientation as well as direction selective, cells in the thick stripes of V2 to which they connect are also direction as well as orientation selective. Finally, just like the cells in layer B4, it was expected that the thick stripes would project to V3 and V5 where cells are predominantly orientation and direction selective respectively, which indeed has been shown to be the case (Shipp and Zeki, 1985; De Yeo and Van Essen, 1985, Hubel and Livingstone, 1987b).

3.7 The logic of M and P connections in the cortex

The M and P pathways have different destinations in the visual cortex. Because of their properties, it has been suggested that the major cortical input of the P pathway is to the colour and form areas of the visual cortex whereas the inputs of the M pathway are mainly to the motion centres (Maunsell and Newsome, 1987, Livingstone and Hubel, 1988). According to De Yeo and Van Essen (1988), the parvocellular-interblob (P-I) system is characterised by a high incidence of orientation selectivity but contains many cells that are wavelength selective and seems to be specialised for the detection of high-resolution static form and shape using either colour contrast or brightness contrast edges and the ability to see details of stationary objects and scenes. However, although cells in this system respond to both luminance and colour-contrast borders they are not likely to be involved in the perception of colour. The parvocellular-blob (P-B) system is characterised by cells that are predominantly wavelength selective but orientation selective and direction selective cells are much less common. P-B is therefore specialised for colour but not with movement, stereopsis, or shape discrimination (Livingstone and Hubel, 1988). Finally, the magnocellular-thick-stripe (M-I) system is characterised by cells that are direction selective but includes many cells that are selective for orientation and disparity. The M-I system is therefore specialised for motion and spatial relationships and contributes to detection of stereoscopic depth. The cells in this pathway are insensitive to colour and therefore respond poorly to borders and contours that are only perceived based on colour contrast (Zeki, 1983a).

Livingstone and Hubel (1987a, 1988) have emphasised the segregation of pathways extending to higher visual areas. A diagram of these independent pathways is shown in Figure 3-7. According to this model, the magno-recipient layers of V1 project to thick stripes of V2 and to the higher cortical visual area V5, also called medial temporal (MT). The parvo-recipient upper layers of V1 that are divided into blobs and interblobs project to different areas. The interblobs project to the pale interstripes of V2 (Livingstone and Hubel, 1988). On the other hand, the blob system may receive input from the magno as well as the parvo system (Livingstone and Hubel, 1987a and 1987b) and project to the thin stripes in

V2. Notably, the pathways seem to remain independent in their projections to higher cortical areas: the thick stripes project to area MT and the thin stripes to area V4; and the projections of the interstripes are unclear.

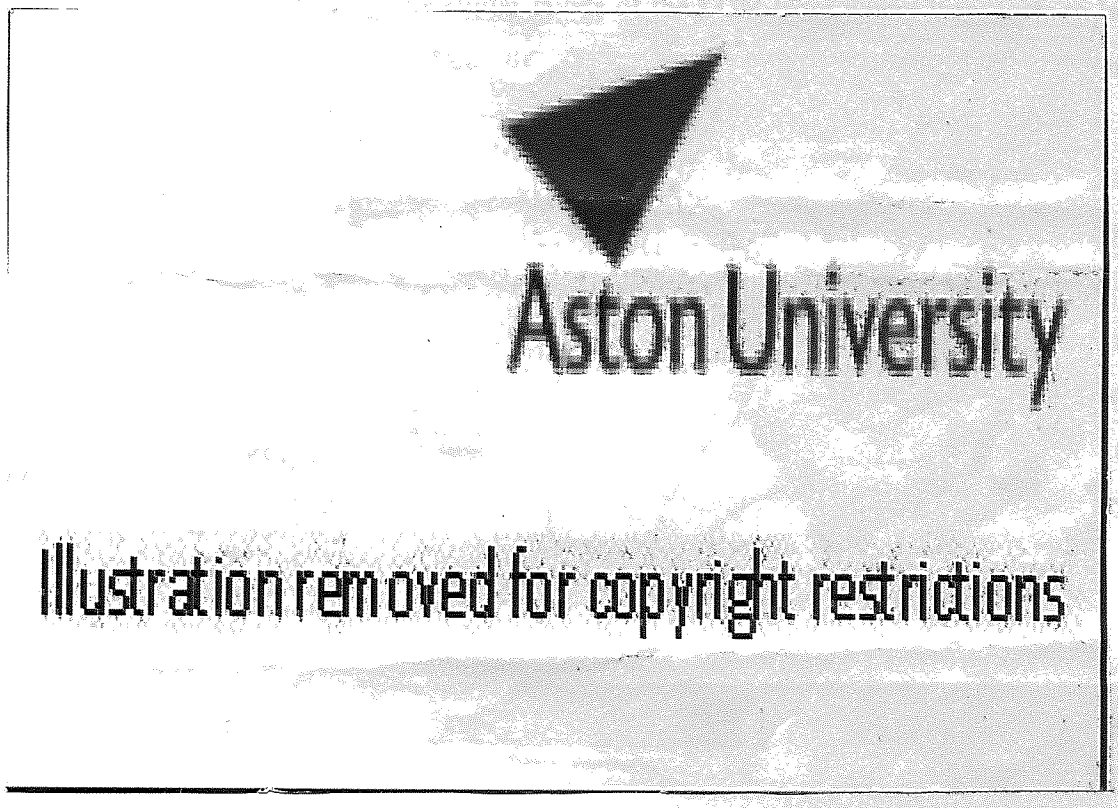

Figure 3-6. The functional segregation of the primate visual system, showing the pathways at their origin in the retinal ganglion cells, through to the LGN, the layers of V1, V2, and projections to higher areas. (Reproduced from Livingstone and Hubel, 1988)

The magnocellular pathway arrives at the layer 4Cα of V1 and then projects to layers 4B and 6. From there it leads to the thick stripes of V2, then to area V3, and then to area V5 or MT. MT projects to MST and other areas concerned with visuospatial function. The parvocellular system subdivides to form two distinct patterns of connectivity. The first of these enters V1 through layer 4Cβ, then to the interblobs of layer 2 and 3 in V1, then to the pale stripes of V2, to V4 and finally to the inferior temporal cortex (ITC). The second subdivision projects to the blobs of layers 2 and 3 in V1, then to the thin stripes of V2, and then to area V4 and eventually terminating within ITC (Livingstone and Hubel, 1988).

More recently, Zeki (1993) has divided the visual system into the two M and P pathways with two subdivisions of each thus creating 4 pathways: a motion pathway, a

colour pathway, and two form pathways. This model is very similar to that proposed by Livingstone and Hubel (1988) and includes an additional subdivision. More specifically, there exists a motion pathway which originates in the parasol (Pα) ganglion cells of the retina and is relayed to the magnocellular layers of the LGN from where it projects to layer 4B of V1 followed by the thick stripes of V2, eventually ending in area V5. The dynamic form pathway also originates in the parasol ganglion cells and passes through the magnocellular division of LGN, projecting to orientation selective cells of layer 4B and from there to area V3, both directly and via the thick stripes of V2. These are both subdivisions of the M pathway. The two subdivisions of the P pathway originate in the midget ganglion cells of the retina and pass through the parvocellular layers of LGN and from layer 4C. One feeds the blobs and the other the interblobs of layers 2 and 3 to create a colour pathway and a form pathway respectively. They relay to area V4 both directly and via the thin stripes and interstripes of area V2. The form subdivision of the P pathway is concerned with form in association with colour.

The idea that the primate visual cortex consists of two separate functional pathways was first suggested by Ungerleider and Mishkin (1982) who described two streams of processing that diverge on exit from V2 with one leading to the visual cortex of the temporal lobe and the other to the visual cortex of the parietal lobe. These streams have different visual capabilities: the temporal system analyses the physical properties of a visual scene and is therefore involved in identification of objects. It is also referred to as the 'what', or the ventral, stream because it is thought to lie more ventrally. The parietal stream is believed to be involved in analysing the spatial relationship of objects in a visual scene and is therefore concerned with the position of an object. It is also referred to as the 'where', or the dorsal stream because it is thought to lie dorsally.

Clinical observations in humans indicate that damage to either the parietal cortex or to the 'where' system through which V1 projects to the parietal lobes, produces deficits in perception of position or movement of objects but does not effect performance on object discrimination tasks (Zihl et al., 1983). On the other hand, damage to either the temporal cortex or to the 'what' system through which V1 projects to the temporal lobes, produces

deficits in perception of discrimination and recognition of objects but not those related to visuospatial tasks (Damasio et al., 1982). Similar results have been obtained in the macaque monkey where studies have shown that lesions of temporal cortex impair visual discrimination of an object regardless of its colour, pattern, or shape. Conversely, lesions of the parietal cortex impair the animal's judgement on detecting the location of an object while object discrimination tasks remain intact (Mishkin et al., 1983). These differences in lesion effects may reflect the fact that certain regions in the parietal and temporal cortices are associated with processing different attributes of vision. The M and P pathways are believed to roughly correspond to the 'what and where' systems. The parietal 'where' system, with its representation of spatial relationships in the visual field seems to correspond with the M pathway, which conveys information about motion, luminance and depth whereas, the temporal 'what' system with its representation of objects seems to correspond with the P pathway, which conveys information about form and colour.

By taking into account the wealth of existing evidence regarding the functional segregation within the visual system, a general picture has emerged which can be broadly summarised as such:

1. Midget (P) retinal ganglion cells ⇒ colour-opponent system or parvocellular pathway ⇒ parvo LGN ⇒ occipital lobe ⇒ layer 4Cβ (V1) ⇒ interblobs of layers 2 and 3 ⇒ pale interstripes (V2) ⇒ V4 ⇒ ITC ⇒ perception of form and shape

2. Midget (P) retinal ganglion cells ⇒ colour-opponent system or parvocellular pathway ⇒ Parvo LGN ⇒ occipital lobe ⇒ layer 4Cβ (V1) ⇒ blobs of layers 2 and 3 (V1) ⇒ thin stripes (V2) ⇒ V4 ⇒ ITC ⇒ perception of colour

3. Parasol (M) retinal ganglion cells ⇒ broad-band system or the magnocellular pathway ⇒ magno LGN ⇒ occipital lobe ⇒ 4Cα (V1) ⇒ layer 4B (V1) ⇒ layer 6 (V1) ⇒ V3 ⇒ V5 (MT) ⇒ perception of movement and stereoscopic depth

3.8 Borders of the visual areas in humans

Although anatomical and physiological studies of the monkey cortex provide sufficient information regarding the cytoarchitecture and pattern of connectivity between the visual areas in primates, they are nevertheless limited in that they tell us very little about the precise location of each area within the visual cortex of man. For reasons that are obvious, much less is known about the organisation of visual areas in humans compared to that from other primates. In terms of their function, it has been shown that at least areas V1 and V2 of man show striking similarities with other primates particularly in cytochrome oxidase patterns, revealing blobs and stripes, retinal projections, and visual field representations (Van Essen et al, 1993). Post-mortem studies have also revealed similarities in the patterns of connectivity between the visual areas of man and other primates (Burkhalter and Bernardo, 1989). It is therefore likely that similarities will be found for other areas. However, the topographical organisation of visual areas differs between humans and other primates whose visual cortical organisation has been studied anatomically in much detail. In man, the most advanced and often non-invasive technique in distinguishing the visual areas is the use of functional imaging modalities and is based on the retinotopical organisation in the visual system. In what follows, a brief summary of such methods will be presented.

3.8.1 Retinotopic mapping

With the technological advancement in functional imaging techniques such as positron emission tomography (PET), and functional magnetic resonance imaging (fMRI), it has become possible to estimate spatially localised activity in the human brain, given our knowledge of the functional interconnectivity and specificity of the visual areas (Zeki et al., 1991; Wandell, 1996). Imaging techniques have been used to determine the position of the retinotopically organised visual areas, which once identified in one brain, can provide a functional co-ordinate frame of the visual areas that is generalisable to other brains irrespective of their physical size and shape.

In the human brain, area V1 is located at the occipital pole occupying roughly 4 to 8 cm of cortex the majority of which lies within the calcarine sulcus (figure). Studies of human cortical lesions have revealed that the receptive field of V1 neurons are retinotopically organised such that visual field representation from posterior to anterior cortex shifts from central retina (fovea) to periphery (Horton and Hoyt, 1991). This retinotopic organisation is referred to as eccentricity. Points on the visual field are inversely related to those in V1 such that those on the upper, middle, and lower visual field are found on the lower, middle, and upper portions of the calcarine sulcus respectively.

Given the knowledge regarding the retinotopic organisation of V1, and the fact that eccentricity is shared by nearby areas V2 and V3, Engel et al. (1994) measured the location of the neural activity using stimuli that comprised of expanding and contracting rings of flickering squares. An expanding ring started at the centre and expanded until it reached beyond the edge of the visual field whereby it was replaced by a new one starting at the centre. Conversely, a contracting ring started at the periphery and reached the centre whereby it was replaced by another ring at the edge of the viewing apparatus. Each ring lasted either 32 or 48 seconds representing one cycle of the stimulus. The moving rings are designed to create a travelling wave of neural activity that spreads from anterior to posterior cortex in accordance with visual eccentricity. In other words, as the stimulus moves from fovea to periphery, activity at cortical locations with peripheral receptive fields is delayed in comparison with cortical locations that have foveal representation.

The boundaries of the visual areas can be revealed using a stimulus comprising of a wedge of contrast-reversing flickering squares that rotates about the fixation point. The angular dimension of retinotopic organisation stretches from the lower to the upper lip of the calcarine sulcus. Meanwhile the visual field representation shifts from one quadrant to another creating a travelling wave of neural activity that itself shifts from the lower to the upper lip of the calcarine fissure. Because the angular representation of each area is different, the travelling wave reverses direction at the border between V1, V2 and V3 thus identifying the cut-off points for each area. The results of these measures are then presented on images of flattened visual cortex (figure 3-8).

Figure 3-7. A flattened cortical representation of the visual cortex based on its retinotopic organisation. From subject KDS (see chapter 5) at the MEG laboratory at Aston.

3.8.2 Functional imaging of the visual areas

Imaging techniques can also identify the location of specialised areas of the brain by measuring responses associated with various attributes of vision such as motion, form, and colour. This provides a vital link between the anatomical studies of the visual areas in primates and their functions in humans. In one of the earliest functional studies, Zeki et al. (1991) have demonstrated cortical specialisation for colour and motion using PET which measures the levels of regional cerebral blood flow (rCBF). When comparing brain activity during colour and grey stimulation, they observed significant change of activity in the lingual and fusiform gyri of the prestriate areas, which they refer to as area V4 in humans. For this stimulus, although both sides were activated, the statistical analysis of the data revealed a lateralisation of function to the left. For motion, a black and white random square pattern was selected with the checks moving randomly and at a constant rate. They observed a significant change of activity at the junction of parietal and occipital cortices and approximately at the junction of the Brodmann areas 19 and 37. They refer to this area as V5, the homologous of MT in the macaque monkey. In all conditions, V1 and V2 were also activated indicating that consistent with studies in the macaque, they act functionally

as segregators since V4 and V5 activations covaried with V1/V2 during the colour and motion studies respectively. Finally, it was concluded that V1/V2 outputs must be in parallel, because V5 was not active in the colour study, nor was V4 in the motion study. These and other studies in imaging the brain activity has gained widespread popularity over the last decade and many more such studies have confirmed the existence of specialised areas. The concept of functional specialisation in the brain can be studied invasively by recording the response properties of single neurons, or it can be studied non-invasively by recording the rhythmic activity of larger neuronal populations using EEG/MEG. These studies provide precise information regarding the spatio-temporal properties of brain regions in response to stimuli of interest.

3.9 Perceptual binding

As described above, functional specificity states that different attributes of an object are recognised by different groups of neurons. Therefore, the question arises as to how these widely distributed processing areas are bound together in order to produce a unified perception of images. Current opinion in neuroscience holds that the recognition of an object is processed through a mechanism that groups together its common features (Engel et al., 1990). As an example, consider the classic Rubin face-vase image shown in figure 3-9. The selection of a different percept relates to the grouping of neuronal assemblies, based upon the spatio-temporal aspect of their response (Engel et al., 1990). Single unit electrophysiological recordings of cortical cells in the visual cortex of cats and the macaque indicate that these neuronal assemblies respond to the common features of an image in a temporally synchronous fashion, correlated on a millisecond time scale (Gray et al., 1989; Singer, 1993; Singer and Gray, 1995). It is thus suggested that such neuronal synchronisation binds neurons into assemblies that create coherent percept of object features (Engel et al., 1990). This suggestion has been confirmed by a number of studies that demonstrate synchronous firing in the visual cortex is stimulus-dependent (Gray and Singer, 1987; Gray et al., 1990; Engel et al., 1990; Fries et al., 1997). These findings have led to the debate surrounding the functional significance of synchronous activity, which is often associated with increased firing in the gamma frequency range of 20-70 Hz (Gray et al., 1989; Engel and Singer, 2001). It has even been suggested that strong neuronal synchrony forms the very basis of consciousness (Llinas et al., 1998; Engel and Singer, 2001).

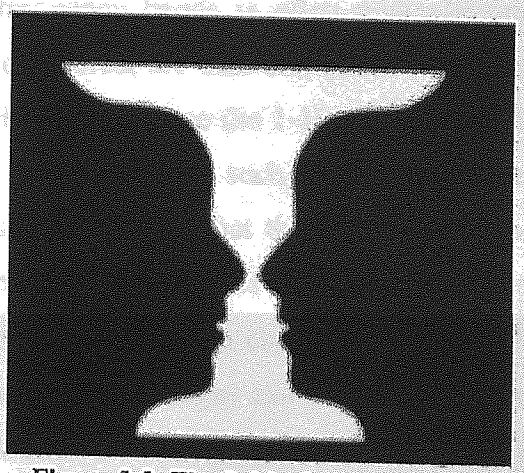

Figure 3-8. The Rubin face-vase figure is perceived as either two faces or a vase.

3.9.1 Oscillatory brain activity

The alpha wave was the first feature recognised in the human EEG (Berger, 1930; cited in Pfurtscheller and Lopes Da Silva, 1990a) although its amplitude and frequency varies between subjects and cannot always be seen in EEG or MEG traces (Basar et al., 1999). Consequently, the frequency of rhythmic activity is very important when speaking in terms of their functional significance. The historical nomenclature of cortical rhythms is given in table 3-2. It is a logarithmic division with narrow bands at lower and wide bands at higher frequencies and although still used widely, it will not be used in the remainder of this thesis when functional data are analysed. It has been shown that for alpha activity the frequencies vary between different individuals (Basar et al., 1999) and studies into functional aspects of cortical rhythms in these frequency bands is often contradictory. Therefore, it will not be assumed that the effects of interest are best defined in frequency bands defined by the classical nomenclature. In this work, we use the 1-100 Hz band with frequency distributions of 10 Hz wide. It must be noted that such a division is not commonly applied, particularly since many studies have shown that the theta, alpha, and beta bands have task-specific responses (for a review see Pfurtscheller and Lopez Da Silve, 1999b). However, the main purpose of the studies in the next two chapters is to identify spatial location of cortical activity, while the spectral power changes can be analysed using frequency spectrograms of the locations of interest. In the following sections a brief review of the literature is given with reference to functional aspects of oscillatory brain activity in the context of the classical EEG frequency bands.

	FREQUENCY
delta (δ)	0.5 - 3 Hz
theta (θ)	4 - 7 Hz
alpha (α)	8 - 13 Hz
beta (β)	14 - 25 Hz
gamma (γ)	> 25 Hz

Table 3-2. The division of cortical rhythms in the classic EEG frequency bands. Note that this classification increases in logarithmic scale, which may not be the same in all individuals.

3.9.2 Event-related changes in cortical dynamics

One important feature of the brain is its ability to alternate between a synchronised and a desynchronised state, reflecting changes in cortical power, that are initiated by external events and represented, in the recorded signals, by high and low amplitude oscillations respectively (Nunez, 1981; Lopes da Silva 1991; Pfurtscheller and Lopes da Silva, 1999a). The potential measured by a scalp electrode is the spatial average of potentials produced by the underlying neuronal concentration. Detection of a large enough amplitude signal requires synchronised activity of a large mass of cortical neurons. This synchronised activity means that the neurons are either excited or inhibited at the same time.

In general, it is believed that two kinds of changes occur in the electrical activity of the brain. One change is characterised by an evoked potential from the relatively synchronous activity of a small area of cortex, and is both time-locked and phase-locked to an external event. It is assumed that such event-related potentials (ERPs) have an almost fixed time-delay to the stimulus, and are post-synaptic responses of the pyramidal neurons (see section 1.1). These can be extracted from the 'noise', created by the ongoing MEG/EEG signals, using a simple linear method such as averaging. Another kind of change in cortical dynamics is characterised by time-locked, but not phase-locked (or induced) responses to an event. Changes in cortical oscillations reflect the response of cortical neurons to the onset of external events, such as the blocking of alpha activity on opening of the eyes (Berger, 1930, cited in Pfurtscheller and Lopes da Silva, 1999a), and various cognitive functions (Engel and Singer, 2001). These must be extracted from the data by some form of non-linear technique such as spectral and frequency analysis. These phenomena occur within specific frequency band of the ongoing EEG/MEG activity and can appear as either a decrease, or an increase, in cortical power. This resonant behaviour results from an increase, or a decrease, in synchronised activity (or power) and are usually referred to as Event-related Synchronisation (ERS) or Event-Related Desynchronisation (ERD) (Pfurtscheller and Lopes da Silva, 1999a). ERS and ERD phenomena can occur

across a whole range of frequencies, including the gamma (~40 Hz), and the slower theta (~4-7 Hz) bands related to memory processes (Burgess and Gruzelier, 2000).

As mentioned above, ERPs are considered by many to be the response of a stationary system to the external stimulus due to synchronous changes in afferent activity of neurons. The ERP is assumed to occur with fixed latency and polarity, independently from the rest of the EEG, which is commonly regarded as noise. More recently, however, Makeig et al. (2002) have offered a radically different perspective by suggesting that the ERP is due to 'phase resetting' of the ongoing EEG activity that results from stimulus presentation. They make the observation that an ERP alone cannot necessarily reveal whether brain modulation is mediated by phase or by amplitude. By looking at spectral characteristics of single trial EEG, it becomes possible to understand whether phase or amplitude is responsible for the ERP. Makeig et al. (2002) found no stimulus-induced increase in the power band of interest indicating that phase modulation is the more likely mechanism that underlies ERPs. According to Makeig and colleagues, by merging the fields of event-related EEG (or MEG) and ERP a much richer picture of brain dynamics in cognition becomes apparent.

According to Pfurtscheller and Lopes Da Silva (1999a, and 1999b), the induced ERD/ERS rhythms reflect functional connectivity within the cortex. These rhythmic activity are conditioned by factors related to neuronal assemblies and include the following (Lopes da Silva, 1991): (i) the intrinsic properties of the neuronal membrane, (ii) the structure of the interconnectivity between network elements and synaptic processes related to the function of feedback and feed-forward (thalamo-cortical and cortico-cortical) loops, and (iii) the modulating effects of the local or general neurotransmitters. Furthermore, these oscillations occur at the macroscopic level of the neuronal mass and their appearance in the MEG/EEG signals depends on the extent of the cortical area where synchronised and desynchronised activity occurs, as well as the topology of this area and its relation to the position of sensors on, or around the periphery, of the scalp.

3.9.3 Frequency specificity of ERD/ERS

Neuronal populations and networks produce oscillations at various frequencies. Lopes da Silva (1970) and Lopes da Silva (1991) have recorded alpha, beta, and gamma activities from the same cortical area in dog whereby the frequency of oscillations depended upon the attentive state of the animal. alpha oscillations are common all over the visual cortex occupying neurons in large cortical areas, while beta and gamma activities are more spatially and temporally variable, occupying smaller cortical areas (Lopes da Silva, 1991). Nunez (1995) has estimated that in order to obtain amplitude of a scalp EEG signal, such as alpha rhythm, the synchronous activity of neurons within a $1cm^2$ cortical surface is required.

In general, an increase in the frequency of brain oscillations coincides with a decrease in amplitude (Pfurtscheller and Lopes da Silva, 1999a). The ERD and ERS phenomena are highly frequency specific, with the former mainly present in the Alpha and Beta bands, while the latter is also found in the Gamma as well as the Alpha and Beta bands (Lopes da Silva, 1991). Certain features are characteristic of both ERD and ERS phenomena, such as latency, magnitude, and spatial localisation. More importantly, ERD and ERS occur at certain frequency bands specific to the event that initiates them. Gray and Singer (1989) have shown that frequency-specific power changes are related to specific function, while more recently, Engel and Singer (2001) suggest that these power changes may reveal the basic mechanisms underlying perceptual binding. Nunez (1995) differentiates between the three types of, global, regional, and local cortical oscillations. Global rhythms are oscillations in specific frequency band that can be recorded all over the scalp, such as alpha, which is often present across the entire cortex. With regional oscillations, these alpha waves are restricted within a cortical boundary such as the occipital cortex; and local oscillations represent specific neuronal activity recorded from spatial patterns of neuronal connectivity, such as the 40Hz waves generated by intra-cortical networks.

In order to analyse alterations in cortical power related to a specific event, the frequency band of interest must be specified, the width of which may depend on certain factors. Sometimes it is appropriate to select bandwidths as narrow as 2 Hz to distinguish between different cortical sources with specific reactivity. Lopes da Silva (1993) showed that during a right index finger movement, activity within the alpha band could be divided into an upper 10-12 Hz and a lower 8-10 Hz band, each with a different spatial spread, depending on the component of a task. Other times, it is possible to select wider frequency bands, such as hand movement that is accompanied with ERD within the 16-21 Hz beta band, or ERS related to foot movement within the post-beta 19-26 Hz band (Pfurtscheller et al. 1997). It has been shown that both the frequency as well as the amplitude of oscillations depends on the size of the activated area (Singer, 1993). In principal, the faster and higher frequency brain rhythms originate from smaller cell assemblies with fewer neurons compared to the slowly oscillating cell assemblies that emanate from a larger cortical area with a larger number of neurons. This may explain the frequency differences found between hand and foot movement in the beta region as mentioned above. The anatomical map of the motor homunculus shows that the hand and foot representations occupy different areas that differ in size with the former occupying a larger area, thus explaining the lower frequency ERDs.

The ERS and ERD phenomena can also occur simultaneously at different locations on the scalp. Since even highly complex tasks involve only a few number of brain regions, spatiotemporal analysis of EEG/MEG data can reveal task-specific spatial patterns of activation that change in fractions of a second. Pfurtscheller et al (1997) demonstrated the occurrence of simultaneous, and contralateral, mu rhythm ERD and occipital alpha rhythm ERS when subjects performed a hand movement task. They also showed that voluntary hand movement could produce ERD in the cortical hand area while the foot area produced simultaneous ERS; the opposite pattern of activity occurred for foot movement. Furthermore, imagination of right hand movement produced contralateral beta ERD and an ipsilateral beta ERS. Regarding the simultaneous and seemingly antagonistic occurrence of ERD and ERS, Pfurtscheller and Lopes Da Silva (1999b) differentiate between three states of processing at the level of cortical networks: a resting state where no specific sensory,

motor, or cognitive processing is evident; an activated state with increased information processing and excitability of cortical neurons; and, a deactivated state without information processing and decreased excitability of cortical neurons. This is a similar concept to the different states of rest, hyperpolarisation, and depolarisation observed at the level of single neurons.

Steriade and Llinas, (1988) suggest that low amplitude desynchronised EEG is caused by increased cellular excitability. ERD is a brief blocking of oscillations in specific frequency bands that occur during or before an event. Pfurtscheller (1992), therefore, has suggested that ERD may be thought of as an electrophysiological correlate of an activated cortical network involved in sensory or cognitive functions, or a neural network preparing to process sensory input or execute a motor command. Conversely, ERS could be thought of as a correlate of a deactivated region of cortical neurons. A strong, or spatially enhanced, ERD could thus be interpreted as involving a large area of highly activated neuronal network. Factors that contribute to the enhancement of the ERD include task complexity and attention to learning of a new task. In such cases, it has been shown that once a task has been learnt and is performed automatically, the ERD is reduced (Zhuang et al., 1997). ERS oscillations in the alpha and lower beta band, therefore, may characterise relatively large deactivated neuronal networks whereas higher frequency oscillations of around 40 Hz may represent small cell assemblies processing sensory and motor action where activities are bound together (Pfurtscheller and Lopes Da Silva, 1999b).

3.9.4 ERS in the Gamma band

Gamma band oscillations occur around 40 Hz and have been reported during cognitive processing, sensorimotor activity, as well as within the visual areas 17 and 18 (Gray and Singer, 1989). It has been shown that sensory stimuli can enhance gamma activity of the brain more than other types of stimuli (Ribary et al., 1991). Recently, gamma band oscillations have been shown to be a prominent feature of neuronal activity within the primary visual cortex (Friedman-Hill et al., 2000; Maldonado, 2000). Visual stimuli often produce activity over a number of cortical locations. It has been suggested that neurons that

respond to common features, exhibit synchronous firing in the visual cortex and are stimulus-dependent (Gray and Viana Di Prisco, 1997). Livingstone (1996) has found that the probability and magnitude of response synchronisation is directly correlated with rhythmic firing in the gamma frequency band, and while the rhythmic firing is not necessary, it is a good predictor of the occurrence of synchronisation. Maldonado (2000) have also suggested the possibility that oscillatory firing might in fact contribute to the generation of cortical synchrony.

It is generally believed that gamma activity mediates feature binding. Induced gamma activity has been shown to increase during complex or attention demanding tasks and in response to static coherent and incoherent stimuli. Tallon-Baudry et al. (1996) measured EEG responses to both coherent and incoherent stimuli and found evoked gamma 100 ms after and induced gamma activity 280ms after onset in response to coherent triangles. Incoherent stimuli only produced the evoked gamma and no induced gamma was followed. The signal was enhanced when spatially distinct features had to be bound together compared to when they were to remain separate. Therefore, it has been suggested that induced gamma activity reflects the spatial binding of the elementary features of the stimulus into a coherent image (Tallon-Baudry et al., 1996; Tallon-Baudry et al., 1997). It is not known what mechanism underlies the occurrence of gamma activity. It has been suggested that they arise from muscular activity (Tallon-Baudry and Bertrand, 1999). However, this is unlikely since muscular activity has a much more variable frequency than the specific 30-60 Hz of gamma. It has even been suggested that gamma maybe an epiphenomenon (harmonic) of other rhythmic cortical activity such as alpha or beta (Jurgens et al. 1995). This is also unlikely to be the case since gamma is highly task-dependent with variations in its topography. A possible involvement of certain pyramidal neurons, called chattering cells cannot be ruled out (Gray and McCormick, 1996)

3.10 Conclusion

The magnocellular and the parvocellular pathways of the visual system are the major conveyors of visual information to the visual cortex. Once the signals arrive in the brain, different attributes of the signal are processed separately in different areas of the visual cortex. All visual areas receive an input from V1 or V2 or both which have within them cells that are selective for all the components of vision such as motion, form, orientation, luminance, and wavelength. Although the segregation of pathways may not be absolute within the visual cortex, current evidence is overwhelmingly in support of two processing streams that play a prominent role in processing of different visual submodalities at all levels. The mechanism responsible in binding the variety of information is thought to be the oscillatory rhythmic activity of the neuronal populations that exhibit synchronised responses on a millisecond time basis, although the precise functional significance of these oscillations remains unclear.

Chapter 4: Cortical Oscillations in Visual Discomfort

4.1 Introduction

Certain visual stimuli are unpleasant to look at due to their inherent physical properties. Wilkins et al. (1984) have described a range of unpleasant somatic and perceptual effects that occur from exposure to repetitive stripe patterns, which they call *visual discomfort*, or more recently *visual stress* (Wilkins 1995). Some patients with epilepsy and migraine are photosensitive and suffer attacks of epilepsy or migraine induced by certain flickering lights or patterns of stripes (Harding and Jeavons, 1994). Such stimuli often consist of light that reaches the eye in a periodic and intermittent fashion examples of which are television, sunlight flashing between roadside trees, and certain geometric patterns. The pattern of stripes in figure 4-1 can cause a number of anomalous perceptual effects such as illusions of colour, shape, and motion. In people without neurological disorders, the pattern is also known to cause eyestrain, nausea, and dizziness (referred to as somatic discomfort), while individuals suffering from photosensitive epilepsy and migraine are advised to avoid looking at the pattern all together in order to avoid an attack. Similar effects are reported by patterns that exist in the real world where stripes are commonly used, such as on items of clothing and many op art paintings (Wade, 1978). More notably, an article in the medical journal, Lancet, reported potential 'injury' caused by escalators with striped metal treads that produced a sensation of 'dazzling glare' (Collins, 1969). The type and severity of the abnormalities experienced is subjective and differs from person to person but almost everyone experiences some degree of discomfort. These range from illusions such as blurring or bending and shimmering of lines in normal observers, to tonic-clonic attacks of epilepsy or migraine attacks in individuals with photosensitivity. Wilkins (personal communication) relates the rare case of a young girl who was sensitive to stripes from radiators, patterned clothing, grills, and so forth, who suffered absence seizures as a result. It has also been found that even simple printed text can have spatial characteristics resembling those of the stressful pattern, and that it can induce anomalous effects, headaches and attacks of epilepsy (Wilkins and Nimmo-Smith, 1984). Irlen (1991) claims that some children experience perceptual distortions resulting from text. This chapter is

thus concerned with such patterns, with which it is attempted to explore the response of the visual cortex using SAM technique described in chapter 3.

Figure 4-1. The pattern in the next page is provocative and can cause a number of severe undesirable effects. Do not look at the pattern if you suffer from epilepsy, recurrent headaches or migraine.

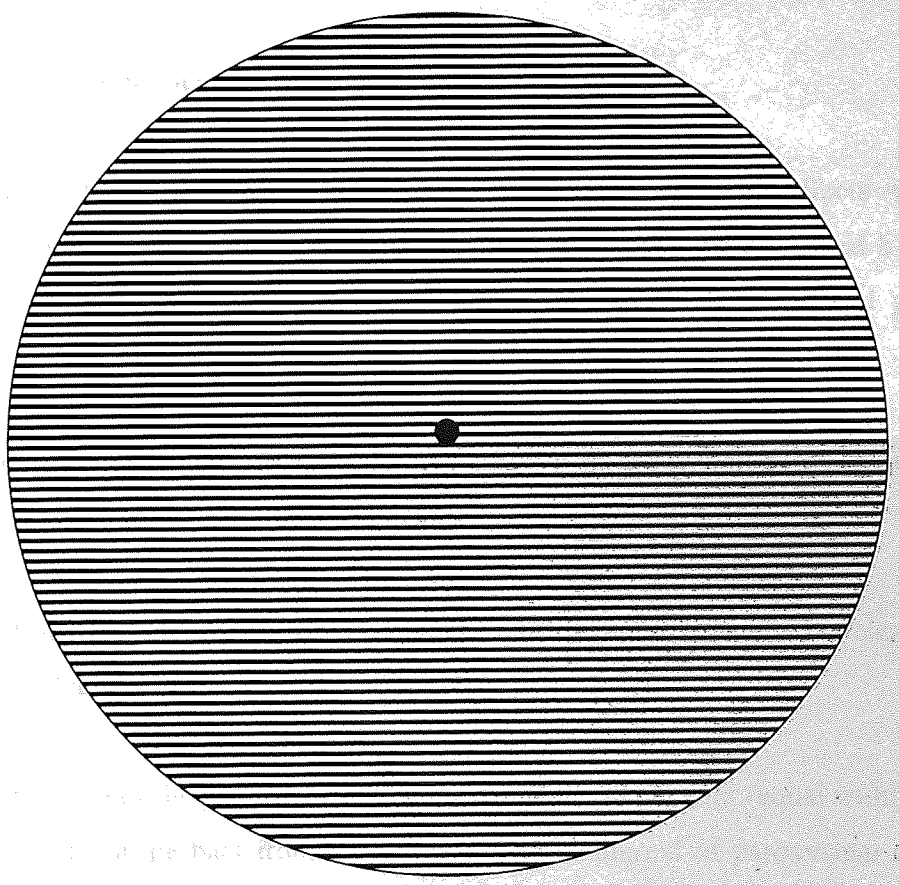

4.2 Parameters of visually stressful gratings

In a series of experiments, Wilkins et al. (1984) have asked normal observers to look at various grating patterns and report the illusions they saw by ticking off items on a checklist. They concluded that in addition to visuo-perceptual distortions, these patterns could cause a range of visual abnormalities such as illusions of shape, colour, and motion, which tend to co-occur. These grating patterns may have dazzling effects, which produce a sensation known as pattern glare (Wilkins and Nimmo-Smith, 1984).

4.2.1 Physical properties

Patterns which are most likely to produce abnormal perceptual effects and illusions have precisely the same parameters as those optimal for inducing paroxysmal EEG activity in patients with photosensitive epilepsy (Wilkins et al., 1979; 1984) and possess the following specific parameters:

1-) Pattern must be striped (as opposed to checker); the longer the stripes the more the likelihood of paroxysmal activity and illusions;

2-) The optimal spatial frequency of the pattern must be approximately 3 cycles per degree (cpd) of visual angle;

3-) The duty cycle of the pattern must be approximately 50 per cent (equal width, and equal separation of the stripe bars from each other). The likelihood of paroxysmal activity and illusions is at a maximum when the spacing and the width are at a ratio of about 1:1;

4-) Pattern must have a high contrast; anomalous activity increases with the Michelson contrast in the range of 5-30 per cent.

5-) Individuals differ with regard to threshold size below which no abnormal activity appears; the larger the pattern the higher the chances of paroxysmal activity and illusions.

6-) Pattern must be viewed binocularly (with both eyes). Monocular presentation of stimuli reduces the likelihood of paroxysmal activity.

The illusions caused by a grating pattern with these properties are associated with discomfort. Wilkins et al. (1984) asked normal observers to rate their preference for several different patterns and found that the pattern, which produced illusions, was significantly less preferred and, after prolonged viewing, many observers reported nausea or headache. Therefore, the pattern can induce epilepsy and migraine in photosensitive individuals, but also it can affect many observers with no neurological disorder. Conversely, people who are susceptible to visual illusions when observing a pattern with these properties tend to suffer more frequent headaches than those who are not. Wilkins et al. (1984) also report a high correlation between number of headaches and number of illusions reported. This correlation was most significant when the spatial frequency of the pattern was 4cpd. For epilepsy and migraine, phase-reversing patterns are more indusive, particularly at certain temporal frequencies.

4.2.2 Preventive measures

There are a number of ways in which the anomalous effects of such patterns can be reduced. Chatrian et al. (1970) and Wilkins et al. (1979; 1984) discovered a significant reduction in the number of illusions reported under monocular, as opposed to binocular, viewing. Furthermore, Jeavons and Harding (1975) found that covering one eye significantly reduced the photoconvulsive response to flicker in 164 of the 244 the patients they studied. Furthermore, people who suffer from migraine tend to choose certain colours for reading text, while avoiding red illumination (Chronicle and Wilkins, 1991). The perceptual distortions of text and reading can also disappear when the text has a particular colour. These findings all suggest that the visual system is greatly involved in bringing about the anomalous phenomena. Wilkins (1995) suggests that the colour of light, which illuminates the pattern, is an important factor involved in evoking the anomalous effects. Therefore, precision tints, selected based on subjective preference, could be used to reduce the phenomena associated with the patterns (Wilkins et al., 2002). Such therapeutic colours

are believed to alter the pattern of excitation in the cortical network, thus avoiding focal hyperexcitability (Wilkins, 1995).

4.3 Variations in spatial frequency of stripes

Wilkins et al., (1984) have shown that patterns, which are most unpleasant to look at are also those that induce the most illusions. Moreover, the illusions induced by striped patterns are related to headaches and migraine in photosensitive cases. The degree to which different individuals experience illusions and discomfort from a grating pattern is subjective but almost everyone experiences some degree of the phenomena. This and the results of numerous behavioural studies indicate that the incidence of visual phenomena is related to the specific and intrinsic physical properties of the grating pattern. It has been found that these unpleasant effects are mostly dependent upon the spatial frequency of the pattern and that the percentage of subjects reporting illusions is a very similar function of spatial frequency. Wilkins et al., (1984) found that gratings with more extreme spatial frequencies were preferred to those with frequencies between 2 and 8 cpd with a peak at around 3-4cpd. Figure 4-2 illustrates the probability of abnormal EEG activity and number of illusions reported as a function of pattern spatial frequency. Wilkins (1994) attributes visual discomfort to the hypersensitivity of some cortical cells that respond to specific spatial frequencies and orientations of square wave grating patterns. Psychophysical studies of Georgeson (1976, 1980) have linked the illusions of spatial frequency, motion, and orientation to the inhibitory interactions at the striate cortex and are specifically due to a release of inhibition, called 'disinhibition' of specific cell groups. More specifically, it was found that adaptation at a specific spatial frequency, results in inhibition of similar spatial frequencies, and the facilitation of spatial frequencies two to three octaves higher and lower than the adapting spatial frequency. Georgeson (1976, 1980) thus suggests that adaptation of specific spatial frequency channels causes the release from inhibition of neighbouring channels. Consequently, the disinhibited channels increase their firing rate, leading to the occurrence of visual illusions.

Figure 4-2, Mean number of paroxysmal activity **(a)**, and of visual illusions **(b)**, as a function of the spatial frequency of square-wave luminance contrast stripes. Note that in both cases, the probability of anomalies occurring is maximal around 3cpd. Redrawn from Wilkins et al., 1984.

4.3.1 Spatial frequency selectivity within the visual system

The responses of the majority of cells within the visual system to a grating pattern are characterised by the physical properties of that pattern. These properties include variations in phase, orientation, luminance, and spatial frequency. For the pattern spatial frequency, these responses will now be briefly described with reference to retinal ganglion cells and the primary visual cortex.

4.3.1.1 Retinal ganglion cells

The responses of most retinal ganglion cells to a grating pattern are dependent upon the spatial frequency of that grating. A ganglion cell would respond with maximum depolarisation to a grating with spatial frequency whereby the light bar coincides with the centre of its receptive field (RF). The adjacent black bars would then coincide with the RF surround causing a decrease in hyperpolarisation, thus producing a large overall depolarisation of the cell. For lower spatial frequencies, the light bar would not only cover the RF centre but it would also cover part of the RF surround of that cell. The overlapping of bright bars on the surround would produce a hyperpolarisation that partially cancels the depolarising effect of centre stimulation from the light bar. Thus the cell exhibits an overall

decrease in its response. Finally, for gratings with too high a spatial frequency, the bright bar would not only cover part of the RF centre but also parts of its surround. Similarly, the rest of the RF centre, as well as surround, would be stimulated equally by dark bars, producing a cancelling depolarisation (DeValois and De Valois, 1990).

4.3.1.2 Visual Cortex

Neurons in the primary visual cortex respond preferentially to stimuli with distinct spatial frequencies. Studies of SF-specific adaptation (Blakemore and Campbell, 1969) indicate that the visual cortex consists of multiple processing channels, each of which is tuned to a specific spatial frequency. This view holds that all spatial frequencies are separately represented across the visual cortex in a graded fashion (Tootell et al., 1981), which explains the characteristic shape of the human contrast sensitivity function. De Valois and De Valois (1990) report the existence of spatial frequency selective cells in the blobs of layers 2 and 3 in V1.

4.3.2 Simple and complex cells of V1

There is some evidence to suggest that the seizures and illusions are more likely to occur when the pattern is at certain orientations (Wilkins, 1995). This implies that the initial trigger could occur focally in the visual cortex, involving a small area whose cells possess the appropriate orientation specificity. Hubel and Wiesel (1962, 1968) studied the physiological properties of cells in the cat and monkey primary visual cortex by inserting electrodes in the cells and recording their on-going electrical discharges in response to various kinds of visual stimuli. They discovered that all cells in V1 had very small receptive fields and that all cells outside layer 4, which predominantly receives direct input from the LGN, were orientation selective. These cells respond optimally when stimulated by lines of certain orientation that must fall within the excitatory part of the cell's receptive field. Different cells had different orientation preferences and an optimal response was obtained when the orientation of the line extended the full length of the cell's receptive field. A line at half-length produced half the response, but a line extended beyond the

borders of the cell's receptive field did not increase the magnitude of the response. Furthermore, when a line of appropriate orientation was presented in any region of the cell's receptive field, it produced an ON response. In contrast, a line presented in a cell's adjacent regions inhibited that cell and produced an OFF response as a result of the inhibition when the stimulus was withdrawn. Hubel and Wiesel called these simple cells as opposed to complex cells, which were also orientation selective but had larger receptive fields. In addition, instead of having particular areas that produced ON and OFF responses, any region of a complex cell's receptive field could generate ON and OFF responses. It was therefore concluded that one complex cell is excited by several simple cells in a hierarchical, building block, fashion.

4.4 Mechanism of visual illusions and discomfort

The mechanism that is responsible for the occurrence of visual illusions and discomfort is far from understood and the reasons for the phenomena remain largely unknown. In the following sections, some of the more prominent theories and suggestions regarding the occurrence of the abnormalities are described.

4.4.1 Cortical basis of visual abnormalities

Wilkins et al. (1984) have shown that the mean number of visual illusions has a function very similar to that for the probability of paroxysmal activity and patterns that trigger seizures in patients with photosensitive epilepsy provoke illusions and feelings of visual discomfort in others. Since the parameters of patterns optimal for evoking paroxysmal EEG activity is also precisely the same as those that induce visual illusions, it has been suggested that the underlying neuronal mechanism for both abnormalities are, at least to some extent, the same (Wilkins et al., 1979; Wilkins et al., 1984). Studies of photoconvulsive responses to different pattern stimuli indicate that epileptogenicity of patterns is determined at the cortical level. For instance, patterns presented binocularly and to the centre of the field of vision are more epileptogenic than those presented monocularly, or those presented in different parts of the visual field (Wilkins et al., 1979; 1980). Furthermore, the probability of paroxysmal activity, as well as visual illusions, is critically dependent upon the size of the pattern, i.e. they increase in frequency with an increase in the radius of the pattern (Wilkins et al., 1979). Moreover, the triggering mechanism for either the seizure or the illusions maybe lateralised, since it has been shown that the hemispheres are independent in their initiation of hyperexcitability. Wilkins et al. (1981) have shown that stimulation of one lateral hemifield with the pattern was more epileptogenic than the stimulation of lower and upper fields. Either hemisphere alone, thus, can cause an attack but the degree of the abnormality of the response is various, while full visual field stimulation significantly increases the frequency of anomalous effects (Meldrum and Wilkins, 1984). For these reasons, a primarily cortical basis for the occurrence of these phenomena has been sought. However, despite the striking similarities

between patterns that cause epileptiform EEG responses and those that produce abnormal visual phenomena, there is a difference between neuronal responses in illusions and visual discomfort on the one hand and epileptiform EEG responses on the other. In the case of the latter, the abnormal excitation of neurons spreads to neighbouring cells, often extending to the adjacent hemisphere, while in the case of illusions and discomfort, the excitation is focal, and does not spread to other cortical regions (Wilkins, 1995).

4.4.2 The GABAergic hypothesis

Photosensitive epileptiform abnormalities have been attributed to a GABAergic minimum diffuse failure of cortical inhibition in man and the photosensitive baboon, *Papio papio* (Meldrum and Wilkins, 1984). The theory is based on the pharmacological evidence that drugs, which antagonise the postsynaptic inhibitory effects of GABA and its postsynaptic depolarising action, can facilitate the induction of a photoparoxysmal response (Meldrum, 1979, Meldrum and Wilkins, 1984). Drugs such as barbiturates and benzodiazepines that enhance the GABA-mediated inhibition of cortical neurons are thus used against photically induced seizures. Any stimulus that intensely excites the cortex may cause the collapse of inhibitory mechanisms that could either spread or remain localised. The stimuli that bring this mechanism into action consist of the appropriate intermittent light or patterned visual inputs. If the excitation is strong enough to exceed a 'critical mass', it will spread to other locations of the cortex and produce abnormal EEG discharges, which may ultimately cause a clinical seizure. If, on the other hand, the discharge remains localised within the visual cortex, the cells maybe inappropriately excited to produce abnormal visual effects without any electrical disturbances measurable at the scalp (Meldrum and Wilkins, 1984). Therefore, in people with no history of photosensitivity or epilepsy, the same mechanism is involved in production of visual illusions and discomfort.

4.4.3 The role of the Magnocellular and Parvocellular pathways

As described in chapter 3, the M and P pathways have different functional characteristics and are responsible for separate but interconnected streams of information.

The parvocellular system is coded for colour where the majority of neurons are colour-opponent. The magnocellualr cells are colour blind but respond to light of all visible wavelengths. They have a low spatial resolution, larger receptive fields, are sensitive to direction of motion, and respond faster and more transiently than parvocellular cells (see figure 3-3). Wilkins (1994) has speculated that because of their properties, the Magnocellular system is somehow related to the patterns that cause the anomalous effects. The reasons for this conjecture are outlined below:

- Patterns of stripes that differ in contrast (i.e. luminance gratings that are black and white) are epileptogenic, while those that differ in colour contrast are not.

- The fact that pattern motion has been shown to facilitate seizure induction is further indication of the involvement of the M pathway because the cells in this pathway are direction sensitive.

- The fact that visual discomfort occurs at lower spatial frequencies is consistent with the low spatial resolution of cells in the M pathway.

- The high temporal resolution of M cells would be consistent with the effects of flicker in photosensitive epilepsy.

These suggestions, however, are based merely upon the similarity between the response properties of the pathways and the characteristics of the pattern, and there is as yet no conclusive evidence to support a link between the M pathway and the visual discomfort associated with the pattern.

4.5 The purpose of this study

The aim of this study is to conduct a thorough investigation of the visual cortical responses to stripe patterns that have been shown to cause visual discomfort and visual illusions. In the results that are presented, the responses of neurons in the visual cortex are of particular interest due to their involvement in visual discomfort (Meldrum, 1979, Meldrum and Wilkins, 1984; see section 3.5.1). Of particular interest is response of the primary visual cortex due to specific responses of cells to such stimuli. It is not known how the response of V1 is modified by changes in the spatial frequency of the stripes during studies of visual discomfort. Tuning curves are obtained reflecting V1 responses to different conditions (spatial frequency) of the stripes. Therefore, tuning in this context refers to the spatial frequency at which populations of neurons respond optimally.

As described earlier, the effects of the grating patterns have been studied using subjective reports of the incidence of the abnormal visual phenomena. There have been no imaging studies that measure the responses of visual cortex to this stimulus and determine the precise location of cortical responses. The traditional EEG is still the only available method for diagnosis of photosensitive epilepsy and is used to detect photoparoxysmal responses and occipital spikes particularly since the latter are phase-locked to intermittent photic stimulation or to the frequency of phase reversing gratings. However, the traditional EEG cannot be used for localising the precise origin of these abnormal responses. To understand the cortical events that underlie the occurrence of abnormal effects in normal individuals, information is required regarding the precise location of cortical activations. More importantly, we require information regarding the induced changes in the ongoing brain activity brought about by viewing of the stimuli. Due to its poor spatial resolution, the traditional EEG is even less suitable for studying the effects of patterns in terms of changes in the ongoing brain activity. On the other hand, the MEG analysis method of SAM (see section 1.6) is ideal for studying the effect of the stimuli on the ongoing activity of the brain. Firstly, SAM does not require averaging of hundreds of epochs each phase-locked to short presentations of a stimulus, but in fact the duration of stimulus presentation can be many seconds long. In this respect, SAM provides precise information regarding changes in

terms of frequency-specific increases, or decreases, in cortical power, which are perfectly correlated with external events. Finally, with SAM, it is possible to investigate temporal sequencing of cortical synchronisation by using time-frequency spectrograms, which allow the time-series of each voxel to be examined on a millisecond time resolution. Individual as well as group SAM data are employed with parametric, and non-parametric, group statistical analyses in an attempt to identify cortical locations where the most significant responses occur. The methods and tools employed to answer the questions in this study are now described.

4.6 Methods

Stimuli

The stimuli used in this study are those that elicit the perception of pattern glare. They consist of black and white (BW) stripes, of 80% Michelson contrast, square-wave in luminance profile, and a duty cycle of 50 percent. The parameters of these gratings are therefore identical to those described in section 4.2. The Delphi programming language was used to define the grating stimuli and generated with the Cambridge Research Systems VSG 2/3 computer graphics system and displayed on an Eizo Flexscan T560i, gamma-corrected, colour monitor with 14-bit luminance resolution, at a frame rate of 100Hz.

The gratings were presented horizontally for 5 seconds and replaced by a homogenous grey background of the same mean hue and luminance. The gratings subtended 12 degrees horizontally by 8 degrees vertically and were projected on to a mirror through a window in the wall of the shielded room (figure 1-9) at a total distance of 2.10 metres. To ensure maximum effects, full visual field stimulation of static patterns was preferred to unilateral, hemifield, or drifting gratings since it has been shown that full field static gratings are significantly more likely to produce the abnormal effects (Wilkins et al., 1981; Meldrum and Wilkins, 1984). All stimuli were viewed binocularly, and subjects were instructed to maintain fixation on a small circle in the centre of all the stimuli throughout the whole of the session.

The sequence of stimulus presentation

The sequence of stimulus presentation is shown in figure 4-3. The first and second epochs comprise of a homogeneous yellow screen and isoluminant chromatic gratings. The main reason for incorporating another stimulus in the design of this study is to compensate for the undesirable effects of the stimuli and is preferred to one in which subjects are continuously subjected to stripes that are a potential cause of eyestrain and headache. The data relating to the first and second epochs are the analysed separately for the purpose of another investigation into the visual system, details of which are given in chapter 5. For the purpose of this study, SAM comparisons are made between the third and the fourth epochs, comparing the black/white and the homogenous grey pattern. The independent variable in this study was the spatial frequency of the grating pattern with 7 levels, varying from 0.5 to 6cpd. Each condition of the stimulus was presented at random to each subject such that a grating of 2cpd did not necessarily follow a grating of 1cpd. Throughout the data collection the inside and the outside of the recording room was darkened as far as possible in order to eliminate source of luminance.

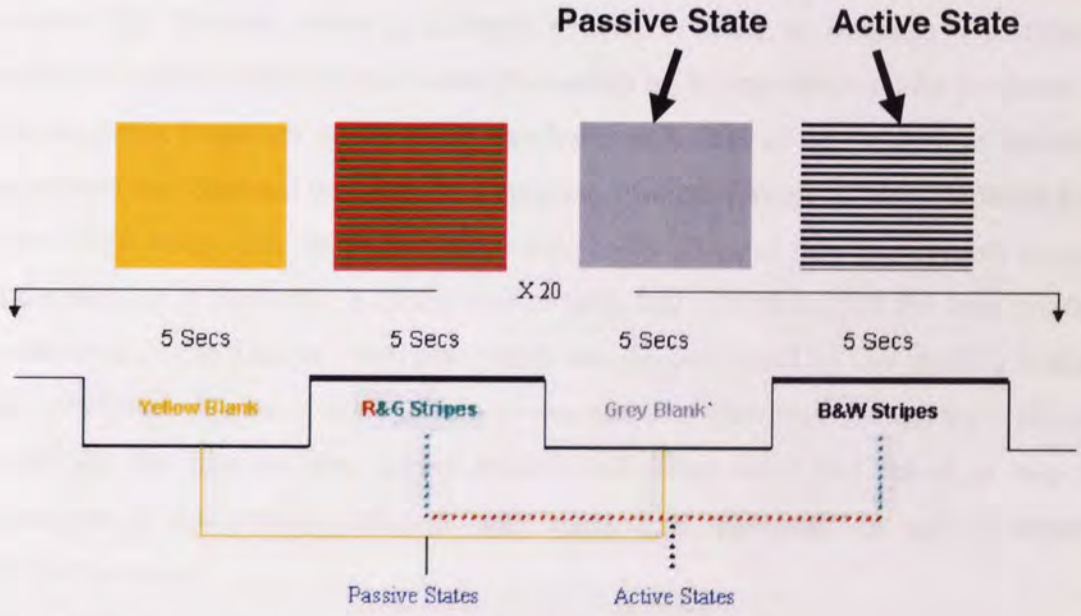

Figure 4-3. The sequence of stimulus presentation. The first and second epochs are described in the next chapter and their inclusion in the design of this study was to provide relief from potentially undesirable effects to the subjects. The third and fourth epochs are of interest in this study, which are presented at different spatial frequencies. Each epoch remained on the screen for 5 seconds and the sequence was repeated 20 times.

Subjects

7 individuals (3 males, 4 females, 35 ±12 years) consented to participate in the study. All had normal visual fields and colour vision and normal, or corrected-to-normal, snellen acuity of 6/6. They were all selected from the population of student and staff members of Aston University Neuroscience Research Institute. Subjects were advised to inform the examiner if they wished to discontinue the task and if any discomfort occurred.

MEG data were collected using a 151-channel CTF Omega System (CTF Systems Inc., Port Coquitlam, Canada) described in section 1.4. Data was sampled at a rate of 1250 Hz and analysed in the frequency range of 1-100 and in bands of 10 Hz wide.

The incidence of visual discomfort

As described earlier, the illusions and discomfort associated with the gratings are subjective and although most people experience the phenomena, the degree of the discomfort and illusions varies in different people. In order to establish a correlation between the incidence of abnormal visual phenomena on the one hand and the properties of the visual cortex responses on the other, psychophysical data of the incident of abnormal visual effects was obtained post hoc for 3 subjects. 2 of the 7 subjects were excluded from this part of the study, because by the time this data was collected they had become familiar with the purpose of the study. A further two subjects had moved away at the time this data was collected. A checklist of visual discomfort was devised based on that used by Wilkins et al., (1984) (see Appendix A). The subject was asked to view each pattern for 5 seconds and tick off the illusions that he/she experienced. They were also asked to rate the pleasantness of the pattern. Subjects were advised to relinquish the task if somatic discomfort occurred.

Measuring the responses from the primary visual cortex

Activation of the primary visual cortex is of particular interest in studies of the visual cortex described throughout the rest of this work. This is because area V1 is the first site of entry for the incoming information to the visual cortex. It is therefore necessary to isolate this area from the rest of the visual cortex and measure its involvement in cortical responses independently. We use mri3dX (http://www.aston.ac.uk/~singhkd/mri3dX), an integrated tool for visualization and analysis of structural, and functional magnetic resonance images. With mri3dX, it is possible to calculate activity within any region of interest (ROI) by applying a 'shade' in order to isolate the ROI. The identification of the primary visual cortex is based on the calcarine fissure. This can be done for each individual MRI, for the purpose of analysing individual data, and for a normalised template brain which is used to calculate group SAM images (see section 1.6). Subsequently, each SAM functional volume is superimposed on this shaded brain and the average activity generated within the voxels of ROI is obtained. It must be noted here that it is difficult to distinguish between V1 and V2 due to the proximity of these areas and the nature of MRI scans. In any case, this is not a major problem since V2 receives direct projections from V1 (see also section 3.7) and the cells in this area have very similar response properties to those found in V1.

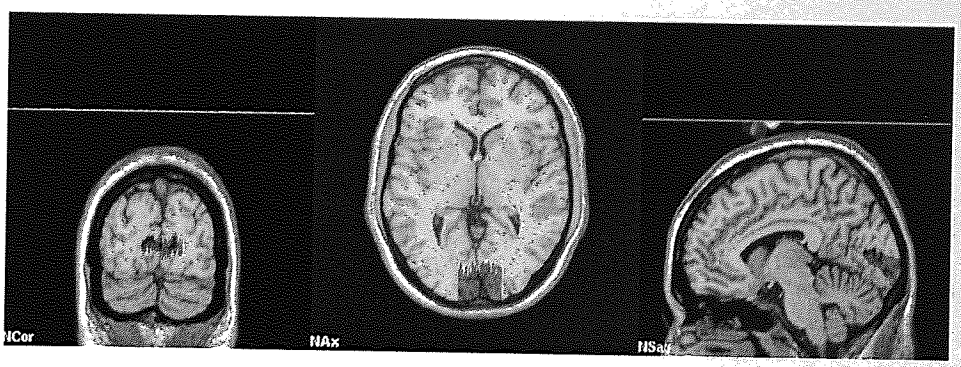

Figure 4-4. The shaded region of visual cortex corresponding to area V1 shown in the three views. For each subject's MRI V1 was shaded and the activity within it was calculated for each frequency bandwidth and each spatial frequency of the pattern. For group SAM images shading was applied to a template brain.

Time-frequency spectrograms

As described earlier, the brain produces different patterns of synchronised activity characterised by either low (ERD) or high (ERS) amplitude signals (see section 3.9.1), which can be described by both their spatiotemporal pattern and their frequency specificity. The spatiotemporal pattern of ERD/ERS seen in functional volumes of SAM represents the average activation generated in a specific cortical location for the duration of stimulus presentation and for the specific frequency band in which they were analysed. Therefore, it is desirable to examine the timeseries of each voxel that shows significant stimulus-related power change. This is done by using a moving window Fourier transform to generate a time-frequency spectrogram (Singh et al., 2002). Spectrograms define ERD/ERS in terms of the proportional power increase or power decrease in the active state in relation to an average of silent trials, usually placed some seconds before the active state. This technique allows temporal sequencing of cortical synchronisation to be investigated with millisecond resolution. In this study we use arbitrary frequency bands with widths of 10Hz. Another advantage of using time-frequency spectrograms is that it provides the precise frequencies at which ERD/ERS occur in the selected voxels. This information can then be used to construct SAM images in smaller frequency bands rather than those initially used in order to increase the signal-to-noise ratio of the SAM analysis (Singh et al., 2002).

4.7 Results

The main aim of this study was to investigate the spatiotemporal aspects of visual cortex responses to stripe patterns that have been implicated in the onset of visual abnormalities, visual discomfort, photosensitive migraine, and photosensitive epilepsy. Of particular interest were the responses of the primary visual cortex to the different conditions (spatial frequencies) of the stripes. Individual and group SAM results are now presented.

Individual SAM responses

The cortical pattern of activation in response to all conditions of the stimulus followed a specific tendency for all 7 subjects. In the alpha and the beta bands (1-10 Hz and 10-20 Hz) the most pronounced oscillations for all conditions of the stimulus occurred predominantly as ERDs, with the majority occurring within the boundaries of the visual cortex. Figure 4-5 A to F illustrates examples of some typical responses of the brain to the contrast gratings. In each image, the t value represents the most pronounced cluster resulting from the comparison of the active and passive states. For only a few conditions, the patterns produced ERDs in the frontal and temporal areas with no consistency among subjects. Nonetheless, where there was simultaneous activation of the visual cortex, it was generally manifest as ERD. On the other hand, in the gamma frequency range of 20-70 Hz, the vast majority of the most pronounced activations occurred as ERS, which were confined within the boundaries of the visual cortex. The magnitude of this response was variable for different frequency distributions of gamma but for most subjects this ERS was generally more pronounced in the 30-40 and 40-50 Hz. At the same time, the magnitude of this ERS in the gamma bands was influenced by the spatial frequency of the stripes, such that in most subjects the highest t values occurred in response to patterns of 2 to 4 cpd. Furthermore, the precise location of the synchronised responses within the visual cortex was various. In all the distributions of gamma, the calcarine fissure (area V1) was heavily activated. ERS in the extrastriate areas was also commonly observed in the much of the gamma bands.

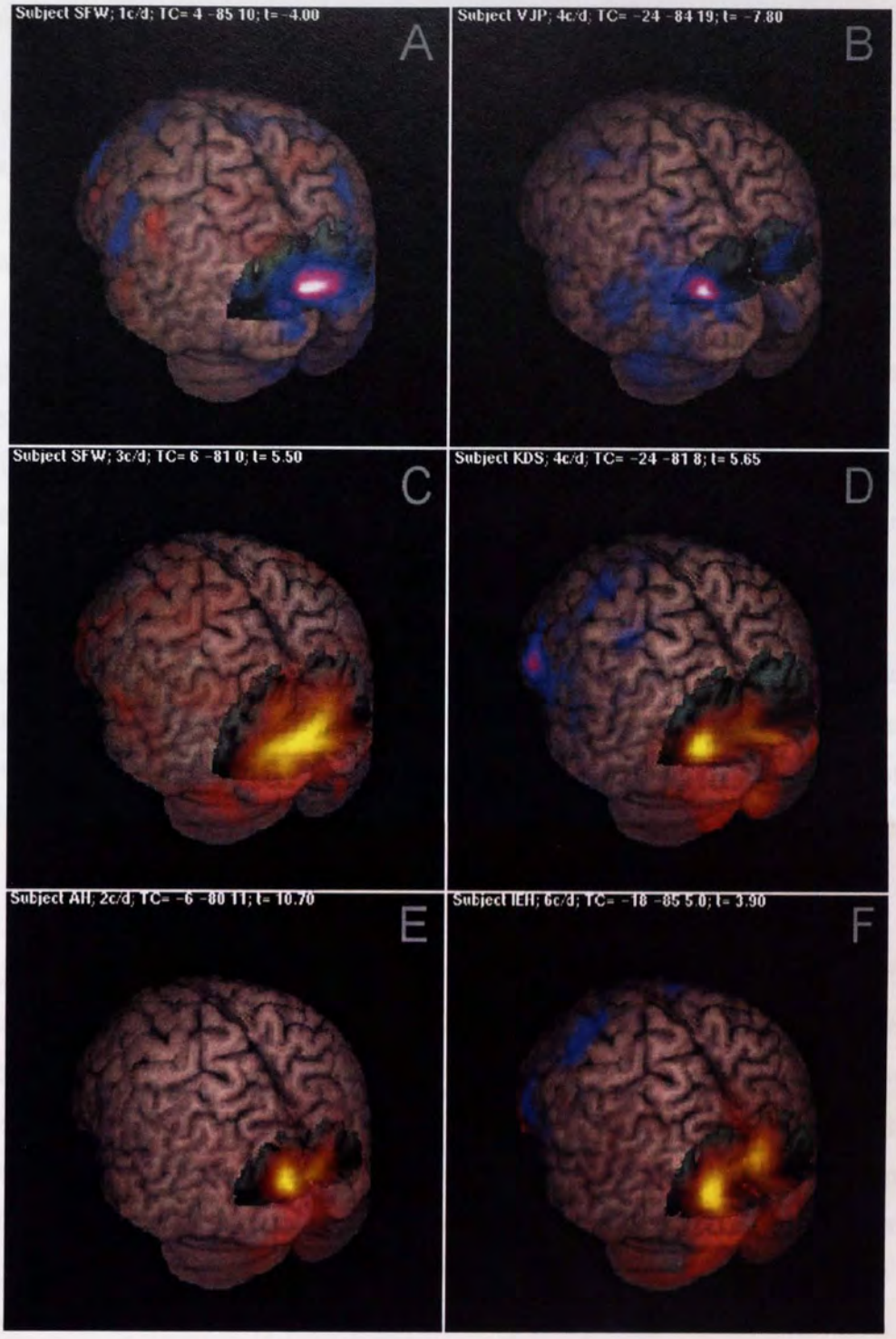

Figure 4-5. An example of individual responses to the black and white stripes. The pseudo t values and Talairach co-ordinates are given inset. **A** and **B** show typical responses of the visual cortex in the 1-10 Hz and 10-20 Hz respectively. **C** shows the spread of ERS in the 20-30 Hz band. **D** shows ERS in the 30-40 Hz band, where the focus of the peak activity is in the extrastriate cortex. **E** shows ERS in the 40-50 Hz band; note the magnitude of t value for this SAM comparison. **F** is the response of visual cortex in the 50-60 Hz band. Note that in all cases most pronounced activation arises from the primary visual cortex.

Grouped SAM responses

For the group SAM data, the pseudo t values are calculated by obtaining the average of individual t values. These are shown in table 4-1. Figure 4-6 depicts the cortical location and spatial spread of the most heightened responses produced by all the conditions of the stimulus. The grouped data can be summarised as follows:

- Spatial frequency responses: the highest magnitude of cortical activations, as reflected by the t values, occur in response to middle spatial frequencies of 2 to 4 cpd of the stimulus. The lowest and highest spatial frequency gratings elicit weaker responses in the visual cortex. The highest statistical difference occurred for the grating pattern that extends 3 cpd of visual angle (pseudo t = 14.02)

- Temporal frequency responses: The highest responses are in the gamma frequency range (20-60 Hz). Subsequently, there is a decrease in cortical power within the highest and the lowest frequency distributions. These activations are exclusively in the form of ERS. At the two lowest frequency bands (1-10 Hz and 10-20 Hz), the data is dominated by ERDs.

- The location of activations: The strongest activations occur in the region of the primary visual cortex. These pronounced V1 activations almost certainly involve V2 but we cannot be sure because of the difficulty in identifying the borders between the two areas and the smoothness of SAM functional volumes. At the lowest and highest frequency bandwidths, cortical responses are weaker and more sporadic with the visual cortex becoming less involved as shown in figure 4-6, rows 1, 2, 7, 8, 9, and 10. These images are scaled relative to one another ($|t|<3$), so that they clearly demonstrate the differences between stimulus conditions.

There is thus a 3-way relationship apparent in the group SAM data between the spatial frequency of the stripes, the temporal frequency of the brain, and the regions of heightened cortical activity. Cortical responses become intensified for stripes of 2-4 cpd, coinciding with the gamma frequency range of 20-60 Hz, covering a vast area of the visual

cortex, particularly the primary visual cortex. For stripes of 2-4 cpd weak desynchronisation of prestriate areas occur in the alpha and beta bands, while no discernible differences are apparent when data is analysed in frequency distributions above 70 Hz. For these higher frequency bands the t values are often less than the cut-off point of $|t|<3$.

	Spatial Frequency of the squre-wave grating						
Frequency Band	***0.5***	***1***	***2***	***3***	***4***	***5***	***6***
1-10 Hz	3.13	-3.83	-4.25	-3.77	-3.60	-3.40	4.72
10-20 Hz	3.36	-4.10	-3.04	-3.65	-4.56	-4.00	-3.65
20-30 Hz	7.00	6.37	7.20	7.65	5.51	4.47	5.25
30-40 Hz	6.96	10.51	11.13	10.42	10.66	4.40	3.74
40-50 Hz	5.42	8.53	11.84	14.02	13.16	4.93	5.17
50-60 Hz	4.37	6.08	8.07	8.45	7.53	5.00	4.06
60-70 Hz	-3.62	2.96	3.16	3.23	3.38	3.80	2.28
70-80 Hz	-4.01	3.29	-2.28	2.06	3.48	-1.90	-2.19
80-90 Hz	-3.23	2.32	-2.32	1.42	3.25	3.85	-2.22
90-100 Hz	-4.34	2.93	-2.71	1.87	3.20	-3.67	-2.76

Table 4-1. *Pseudo t* statistics calculated for the group SAM activations (N=7) between the passive and active states that represent a simple average of *pseudo t* values for the 7 subjects. Note: these values correspond to the peaks of activated locations shown in figure 4-6, below.

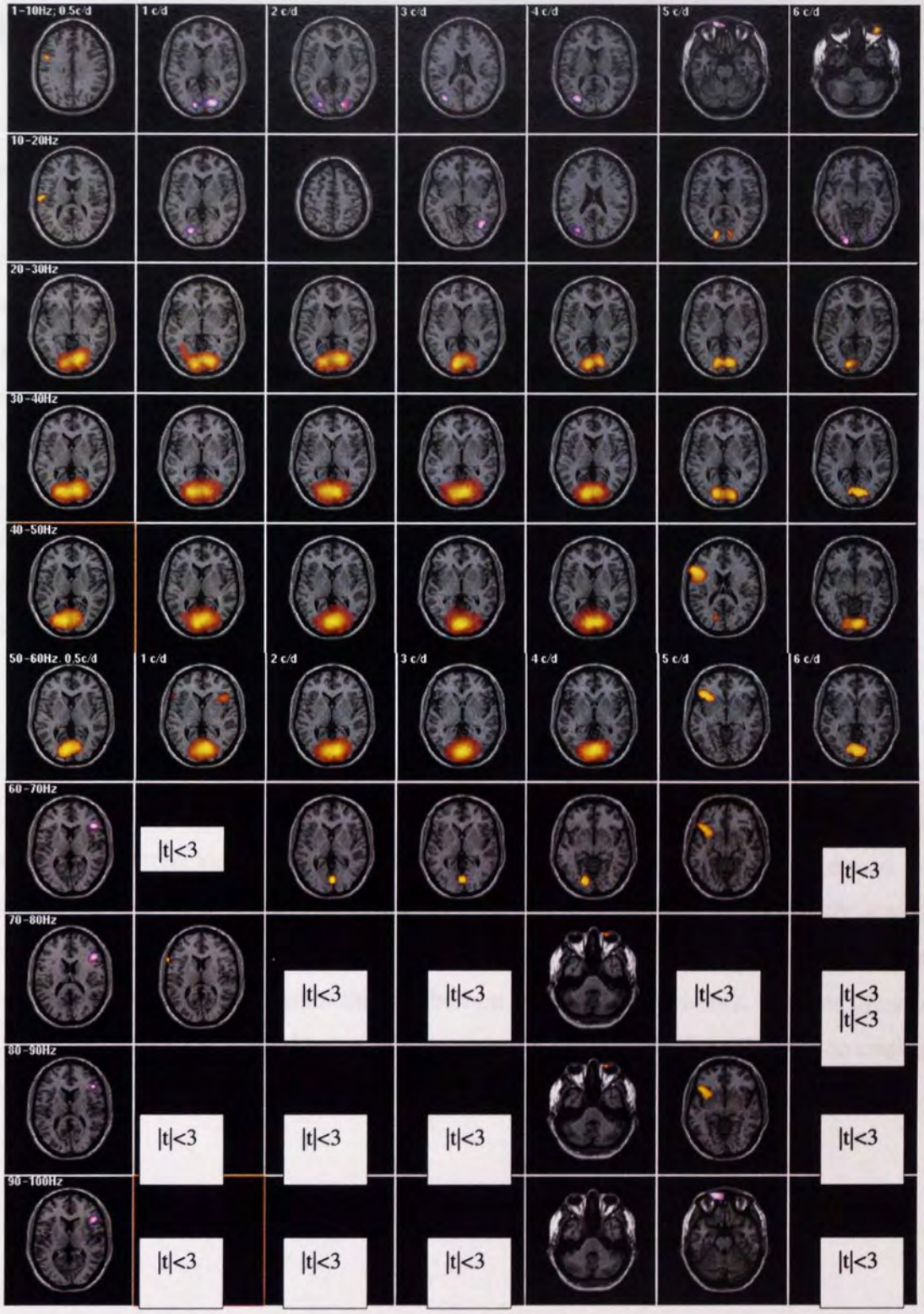

Figure 4-6. Group SAM images showing the location of activated cortex for each spatial frequency of the pattern (columns) and analysed in the specified frequency bands (rows). Pronounced ERS in the visual cortex occurs in the gamma range in response to all conditions of the stimulus. ERD dominates the 1-10 Hz and 10-20 Hz bands. In the highest frequency bands visual cortex activations disappear. Note: all images are scaled such that $|t|<3$ are not shown.

Non-parametric statistical analysis

As described in section 1.6.1, group SAM data using a fixed effects model can be misleading since it uses intra-subject variances to calculate significance, and assumes that the data is normally distributed for all subject. However, ERD and ERS can be highly variable between subjects, and for relatively low number of subjects in particular, the assumption of normality could be violated (Singh et al., in press). As a result, group images using fixed effects could be dominated by a strong response from a single subject, possibly obscuring significant activations in other subjects. Therefore, in order to correct for multiple comparisons, voxel-level analysis was performed using a non-parametric test that does not assume normality or the spatial spread of the activations. This method looks for voxels that are significantly activated at the $p<0.05$ level, producing a voxel-based t image using inter-subject variances (Singh et al., in press). This procedure was carried out for all the SAM comparisons in the study.

Only one group SAM functional volume, namely that in response to a 3c/d pattern and in the 40-50 Hz frequency distribution, showed significant inter-subject clusters. The results of this SnPM analysis are shown in figure 4-7, displaying images of the significant cluster in 3 different views. No significant power decreases (i.e. ERD) was found when comparing the passive to the active phase, only ERS. The most significant cluster occurs in the visual cortex of the left hemisphere and is evident in the three views. The other clusters reveal significant activation within the cerebellum of both hemispheres. It is not clear why this cerebellar activation should occur in response to a visual stimulus. The TC co-ordinates of these clusters are given in the subsequent table and shown more clearly in mri3dX.

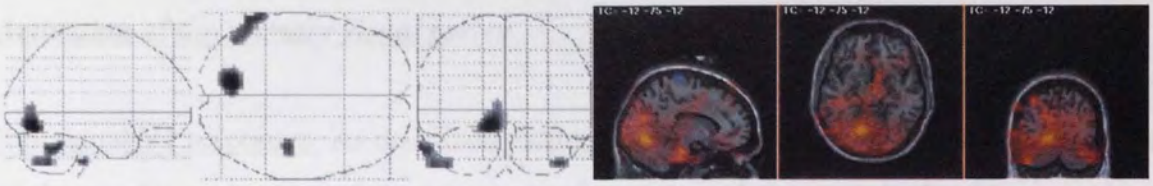

region	size (k)	Pseudo-$R(T_{max} >= u)$		(x,y,z) mm		
1	229	7.18	0.008	-12	-75	-12
2	157	6.58	0.023	-63	-54	-33
		6.44	0.031	-57	-60	-48
		6.31	0.031	-45	-69	-48
3	34	6.43	0.031	42	-27	-45

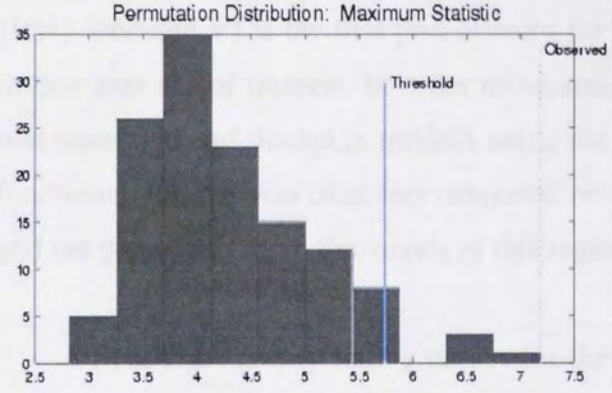

Figure 4-7. SnPM Group SAM results showing ERS effects in the 40-50 Hz range. In the upper left 'glass-brain' format, activation is shown for the only active-passive comparison that produced significant voxel-based clusters at the P<0.05 level. Dark regions signify highly significant ERS, or positive, clusters of voxels. The corresponding random effects images are shown above in mri3dX. The table below details each clustered region and the Tailarach co-ordinates for each in the normalised space. The histogram on the bottom of the figure shows the probability distribution for the maximum pseudo T-statistic. The critical threshold was calculated to be 5.8 indicating that the voxels which are significantly activated at the P<0.05 level have a pseudo-T statistic greater than 5.8.

Activation of the primary visual cortex

Individual V1 responses: As described earlier, the activation of the visual cortex in majority of the conditions involves the primary visual cortex, and the magnitude of this response is dependent upon the spatial frequency of the patterns. The abnormal visual effects have been attributed to excessive processing of the stimuli by neurons in the visual cortex mainly due to the prolonged exposure to the grating patterns (Meldrum, 1979, Meldrum and Wilkins, 1984). Because V1 is the first port of entry for visual information, the responses of neurons in this area are of interest. In order to measure the activation of V1, the calcarine fissure was identified and shaded in mri3dX using the procedure described in methods. Each SAM functional volume was then superimposed on the ROI similar to that shown in figure 4-4 and the mean activity in the voxels of this region was calculated.

Spatial frequency tuning curves for the 7 subjects are shown in figures 4-8 to 4-14. These curves represent the relationship between spatial frequency of the pattern and the brain responses in which area V1 is most intensely activated. They represent increases and decreases in the magnitude of synchronised neural activity between the active and passive epochs. Since ERS and ERD demonstrate high or low amplitude synchronised responses, they can be regarded as reflecting the oscillatory power of neuronal assemblies. For each subject, the activation of V1 is clearly dependent upon the spatial frequency of the grating patterns with the middle frequencies of 1-4cpd producing the highest increases in magnitude of ERS. The responses of V1 attenuate for gratings of 5 and 6cpd. These increases in power are only produced within the middle gamma distributions of 30-50 Hz, while the highest (70-100 Hz) and lowest frequency ranges (1-20 Hz) produce no discernible differences. In general, these results indicate that V1 responses are dependent upon the spatial frequency of the grating patterns, occurring most visibly in the 30-60 Hz gamma frequency range. In general, the variations in the magnitude of cortical activity, observed in the individual as well as group SAM data, are accurately reflected in the activation of the primary visual cortex in the gamma band. This excitatory gamma activity in response to provocative stimuli may be considered as paroxysmal response of an intact cortical mechanism in these subjects. Hence they do not spread to other cortical regions.

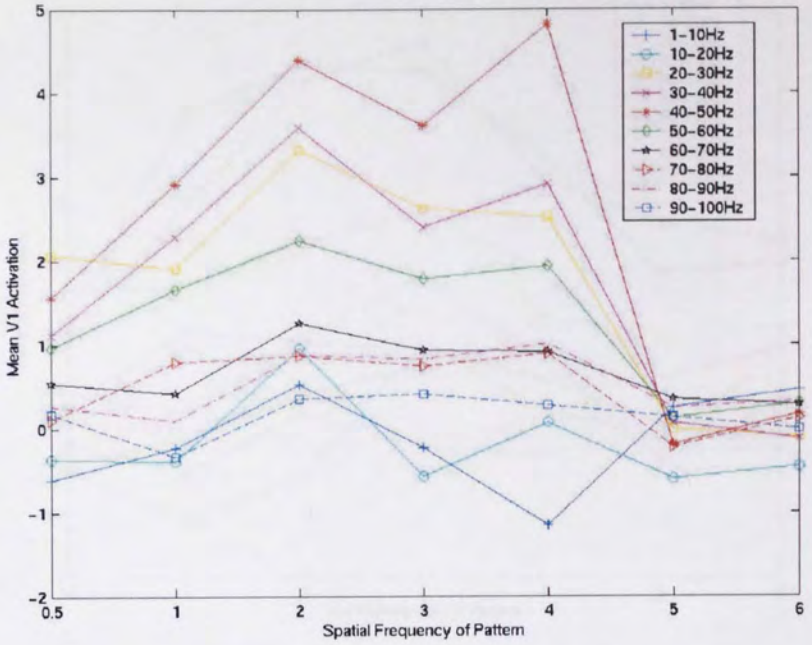

Figure 4-8. V1 tuning for subject AH. ERS mainly occurs for patterns of 0.5 to 4 cpd in the 20-80 Hz range. Patterns of 5 and 6cpd consistently produce weak ERDs. The most pronounced ERS occurs in the 40-50 Hz frequency distribution.

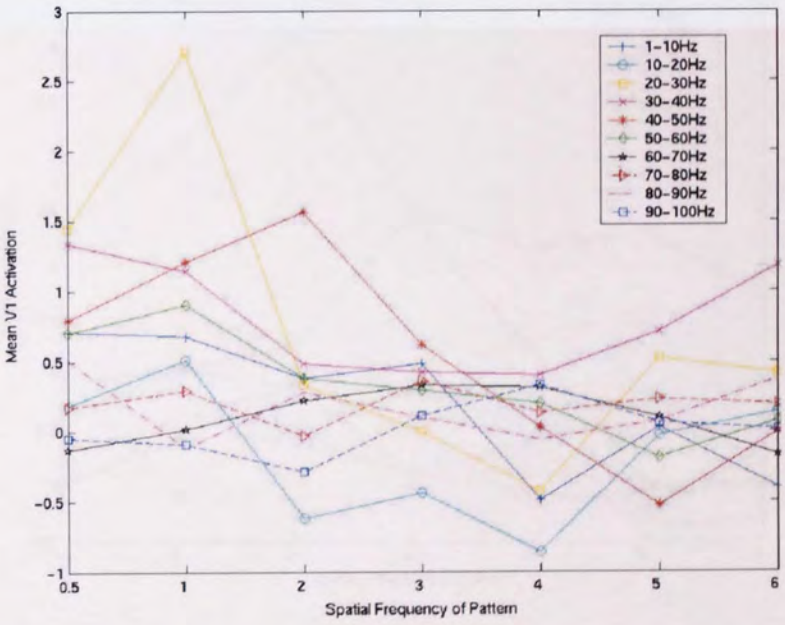

Figure 4-9. V1 tuning for subject ELS. The stripes produce rather weak responses for all pattern spatial frequencies and in all frequency distributions. Middle spatial frequencies generally produce low amplitude oscillations. ERDs also occur in the middle spatial frequencies. The most pronounced response occurs in the 20-30 Hz frequency distribution.

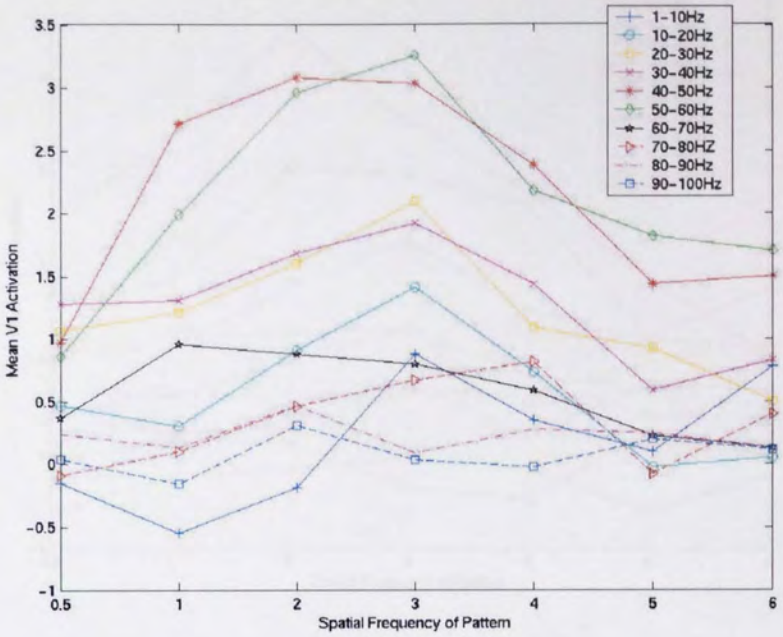

Figure 4-10. V1 tuning for subject FAM. Strong ERS occurs in the 40-50 Hz and 50-60 Hz frequency bands and for stripes of 2 and 3cpd. Weak ERS is seen in other gamma frequency bands (20-30 Hz, 30-40 Hz and 60-70 Hz).

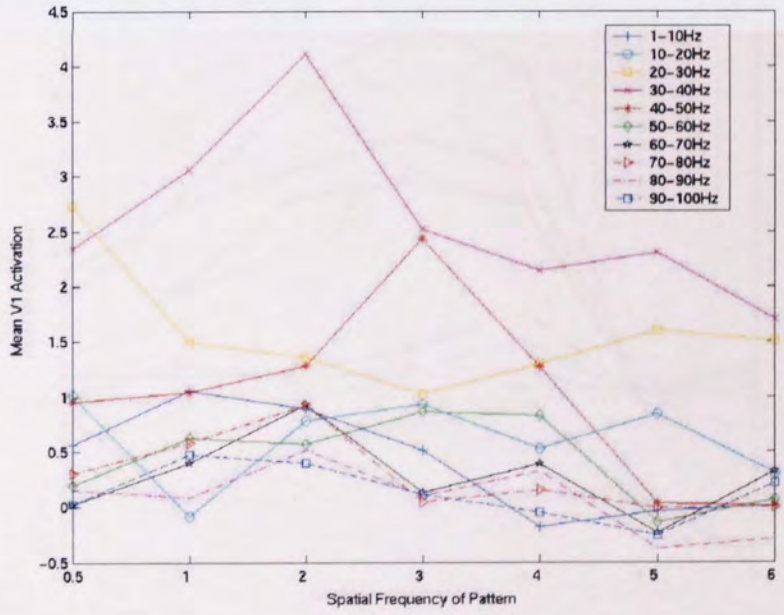

Figure 4-11. V1 tuning for subject IEH. The strongest ERS occurs in the 30-40 Hz band and in response to a pattern of 2cpd. Weaker ERS is seen in other frequency bands, particularly those in the gamma range.

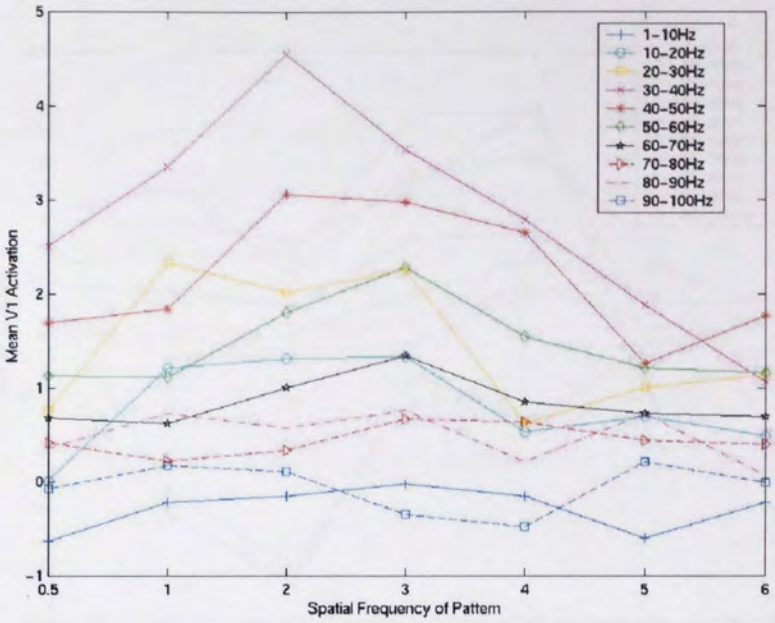

Figure 4-12. V1 tuning for subject KDS. The most pronounced ERS occurs for a pattern of at 2cpd in the gamma 30-40 Hz. Again, the middle spatial frequencies produce ERS responses in the gamma bands. The highest (70-100 Hz) and lowest (1-20 Hz) frequency distributions produce little discernible response to variations in spatial frequency.

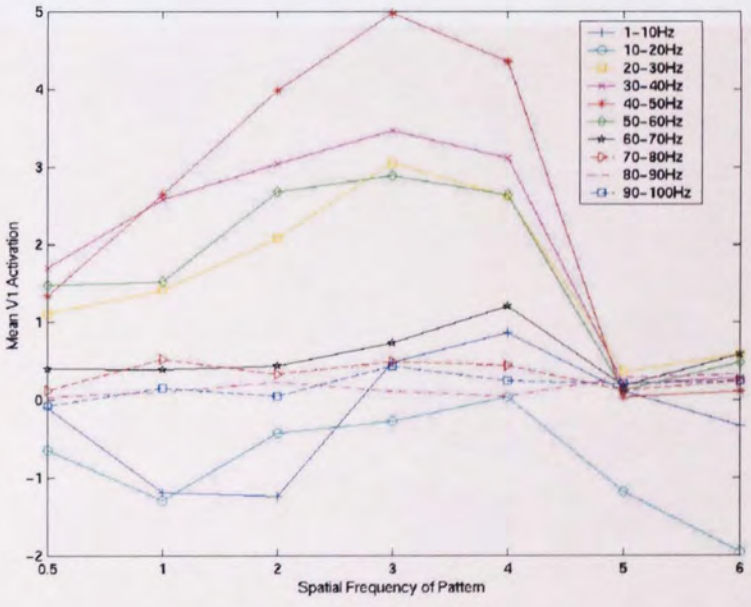

Figure 4-13. V1 tuning for subject SFW. The most pronounced ERS response occurs in the 40-50 Hz gamma band for the pattern of 3cpd. The gamma range of 20-60 Hz produce the most visible responses to variations in spatial frequency. The 70-100 Hz range produce no discernible responses to spatial frequency.

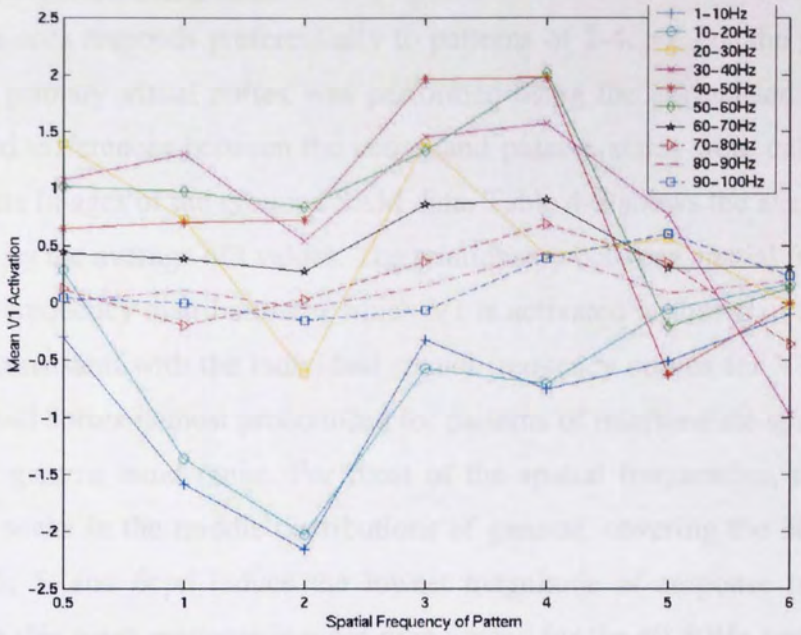

Figure 4-14. V1 tuning for subject VJP. In this subject ERS is less pronounced in the gamma range compared to those found in the rest of the subjects. Patterns of 3 and 4cpd show increased ERS in the 40-60 Hz range. On the other hand, the magnitude of ERD in the lower frequency distributions is most pronounced from all the subjects.

V1 responses for group data: Individual curves for area V1 indicate that in almost all subjects this area responds preferentially to patterns of 2-4cpd. For the group data, the shading of the primary visual cortex was performed using the normalised template brain (figure 4.4), and differences between the active and passive states were calculated for the simplified effects images of the grouped SAM data. Table 4-2 shows the average activity in V1 as reflected by the average of t values. The relationship between spatial frequency of the pattern and the frequency distribution in which V1 is activated is shown in figure 4-15. As expected, and consistent with the individual spatial frequency curves for V1, activation of the primary visual cortex is most pronounced for patterns of intermediate spatial frequency, and within the gamma band range. For most of the spatial frequencies, this increase in cortical power peaks in the middle distributions of gamma, covering the 30-60 Hz range. Gratings of 0.5, 5, and 6cpd induce the lowest magnitude of response from the visual cortex, yet even this weak response is more pronounced for the 40-50Hz band. It is evident from the averaged V1 responses for the 7 subjects (table 4-2, figure 4-15) that a 3-way relationship exists in the way V1 neurons respond to high contrast gratings. As the spatial frequency of the pattern increases, there is heightened activity in the middle frequency distribution. Cortical power then subsides with increasing spatial frequency coinciding with higher frequency bands.

Therefore, the neuronal populations in V1 are most sensitive to contrast gratings of 2-4cpd, responding maximally in the middle gamma ranges of 30-60 Hz. Furthermore, these responses are modulated by the changing spatial frequency of the gratings.

	Spatial Frequency of the square-wave grating						
Frequency Band	***0.5***	***1***	***2***	***3***	***4***	***5***	***6***
1-10 Hz	-0.57	-2.11	-1.67	-0.02	-0.31	-0.27	0.32
10-20 Hz	0.47	-1.00	0.63	0.23	0.25	-0.94	-0.86
20-30 Hz	4.33	4.21	4.50	4.53	3.36	2.04	1.56
30-40 Hz	4.66	6.11	7.30	6.90	6.51	2.62	2.21
40-50 Hz	3.41	5.47	7.81	8.60	8.10	3.00	3.10
50-60 Hz	2.73	3.91	5.25	5.50	4.93	2.60	2.70
60-70 Hz	0.95	1.41	2.23	2.20	2.20	1.20	1.01
70-80 Hz	0.60	1.00	1.35	1.41	1.60	0.35	0.74
80-90 Hz	0.56	0.46	1.20	0.84	0.94	1.11	0.44
90-100 Hz	0	0.06	0.50	0.24	0.15	-0.14	0.40

Table 4-2. Average activations calculated for area V1 for the group SAM data. Note: these values are not necessarily proportional to group SAM activations shown in table 4-1.

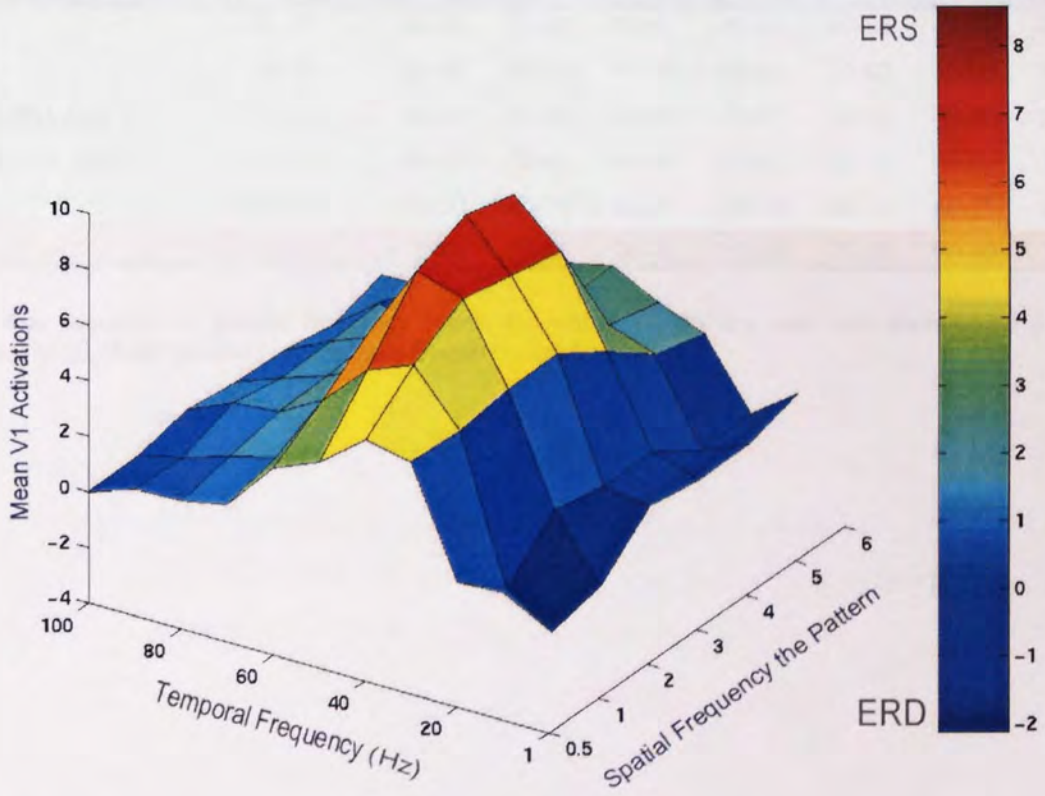

Figure 4-15. 3D representation of V1 activity as a function of spatial frequency and temporal frequency. Square wave patterns of varying spatial frequency produce strong activity within the striate cortex as shown here. This activity occurs within the gamma band (20-60 Hz) and is particularly pronounced when the pattern extends 3cpd of visual angle. Note that the magnitude of V1 activity is dependent upon the spatial frequency of gratings.

The sequence of gamma frequency distributions

Because the gamma frequency covers a broad range of frequencies extending from 20-80 Hz, it was desirable to identify the frequency distributions in which the most pronounced ERS occurred for area V1. Table 4-3 depicts the frequency bands in which V1 activations were most pronounced for each subject in the study. The ERS observed in the data occur most commonly in the 40-50 Hz and 30-40 Hz frequency bands. Subject ELS is an exception to this norm as the most pronounced ERS occurred in the higher frequency distribution of 50-60 Hz.

	GROUP SAM	*AH*	*ELS*	*FAM*	*IEH*	*KDS*	*SW*	*VJP*
	40-50	40-50	50-60	30-40	30-40	40-50	40-50	40-50
	30-40	30-40	40-50	40-50	40-50	30-40	50-60	30-40
FREQUENCY	20-30	20-30	20-30	20-30	20-30	50-60	30-40	50-60
BAND (HZ)	50-60	50-60	30-40	50-60	50-60	20-30	20-30	20-30
	60-70	60-70	60-70	60-70	60-70	60-70	60-70	60-70
	70-80	70-80	70-80	70-80	70-80	70-80	70-80	70-80

Table 4-3. Sequence of gamma frequency bands, for which V1 activity was most pronounced for each subject. The 30-50 Hz gamma range is most frequently implicated.

The incidence of visual discomfort

In an attempt to establish a relationship between visual illusions and discomfort on the one hand and the heightened responses of visual cortex in the gamma range on the other, it is necessary to show that the same patterns of stripes are indeed responsible for both phenomena. The individual response curves of V1 (figures 4-8to 4-14) showed that patterns of 2-4 cpd produce the most pronounced responses. Behavioural data regarding the incidence of abnormal visual effects is necessary in order to establish or reject a link between the physiological responses and behavioural phenomena.

Figures 4-16 to 4-18 depict the reported incidence of abnormal visual phenomena (solid black line) relative to each subject's V1 activation in the selected frequency bands. In subjects AH and FAM, the abnormal visual phenomena increase with spatial frequency of the stripes and decrease with the higher spatial frequencies. From the three individuals tested, AH shows least sensitivity to the gratings. Subject SFW reported the most number of illusions, particularly for patterns of 3 and 4 cpd. In most cases, the illusions were those of colour, blurring, and shimmering of the lines while none of the subjects reported incidents of nausea, dizziness, headache, or eye-strain. In these subjects, therefore, the incidents of visual illusions are coincident with V1 activation in the gamma bands. These data provide an excellent example of a link between conscious experience and specific brain activity. However, the incidence of visual illusions and discomfort is not proportional to the magnitude of V1 responses in this group of subjects. It must also be noted that although clearly there is a relationship between the reported incidence of abnormal visual experiences and increase in the gamma oscillations, the results do not indicate a statistically significant correlation between the two types of response.

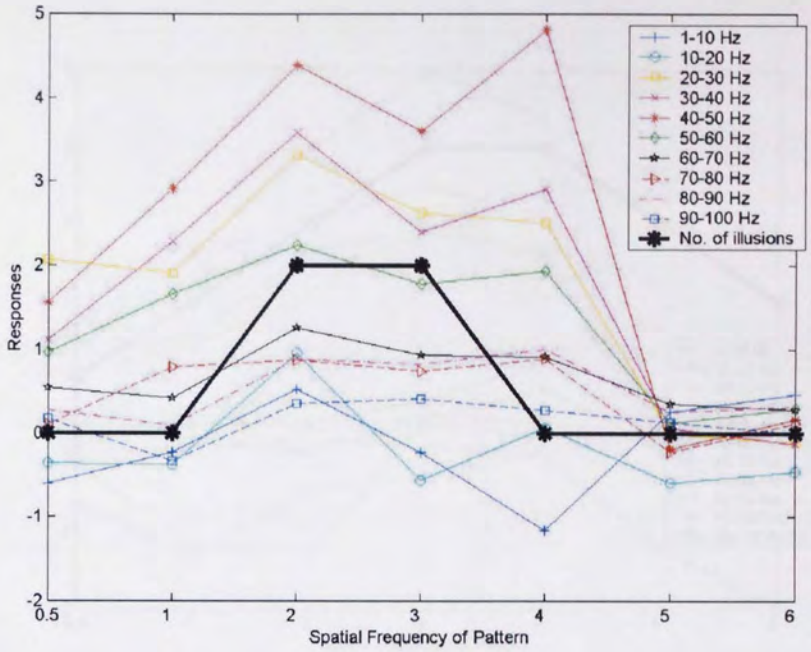

Figure 4-16. Subject AH. This subject reported illusions of colour (red and green) while viewing patterns of 2 and 3 cpd. He also rated all patterns as 'mildly unpleasant'.

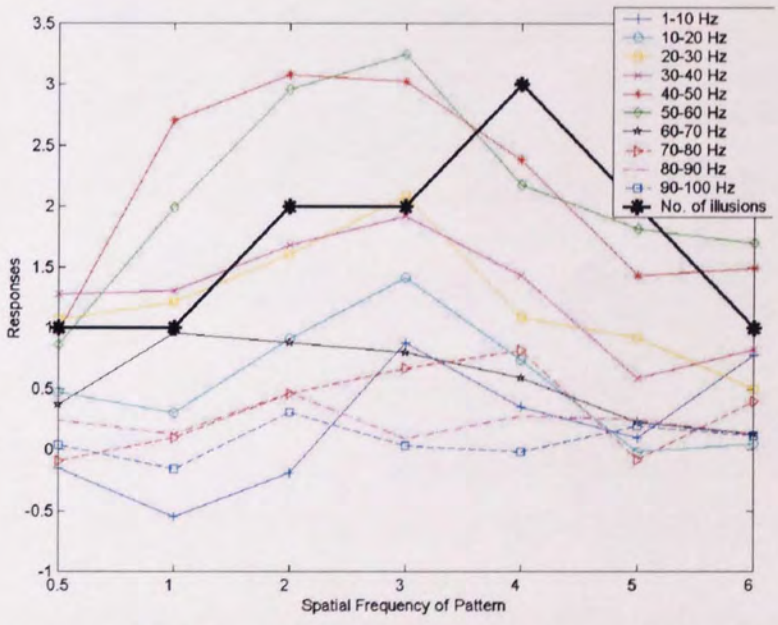

Figure 4-17. Subject FAM. This subject reported mainly illusions of 'shadowy shapes amongst the lines, shimmering of the lines, blurring, and colour. The incident of illusions increased for a pattern of 4 cpd, which the subject rated as 'uncomfortable to look at'.

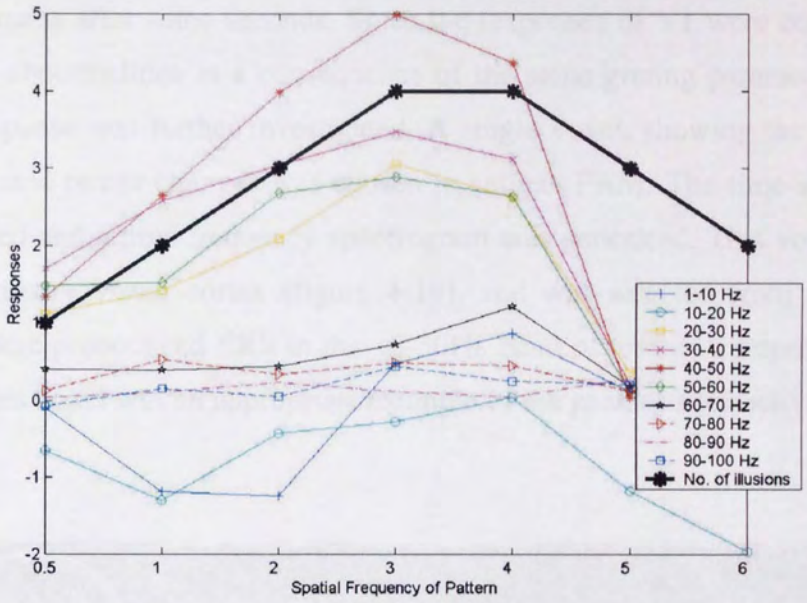

Figure 4-18. Subject SFW. This subject rated all patterns of 2 –6 cpd as uncomfortable to look at. She experienced many illusions, particularly those of colour, blurring, and shimmering of lines. Again the incidence of illusions peaks for the stripes of 3 and 4 cpd, which is most consistent with the increase in V1 activity in the 40-50 Hz band.

Power spectrum analysis

It has been shown that the undesirable effects of a stripe pattern are induced and due to prolonged viewing (Wilkins, 1994), and many subjects who are not photosensitive experience the phenomena after some seconds. Since the responses of V1 were correlated with the incidence of abnormalities as a consequence of the same grating parameters, the time-series of this response was further investigated. A single voxel, showing the highest magnitude of task related power changes was chosen in subject FAM. The time-series of this voxel was analysed and a time-frequency spectrogram was generated. This voxel was located within the primary visual cortex (figure 4-19), and was selected from a SAM functional volume where pronounced ERS in the 40-50Hz band occurred in response to a 3cpd pattern. Hence this voxel was an appropriate example of the peak of ERS activity seen in most subjects.

Figure 4-19. The location of the voxel on which the spectrogram was computed (green dot) for a pattern of 3cpd. Image from an individual SAM file (t=6.67) from subject FM, from a pattern of 3 cpd at frequency bandwidth of 40-50 Hz, producing highest activation for this subject.

The frequency spectrogram is shown in figures 4-20a, averaged for the two active and passive time windows each lasting 5 s. It can be seen from top panel in 4-20a that synchronised response occurs in the 50-70 Hz range with the onset of the active state. Simultaneously, ERD occurs in the 10-20 Hz band. The bottom panel in figure 4-20a depicts the change in power in the selected voxel over the 10 seconds of interest in the 0-100 Hz range. Note that there is heightened ERS between 2-4 seconds occurring around 40 Hz. This effect is shown more clearly in figure 4-20b (top), which shows the activity in the narrower 30-60 Hz range. Note again the ERS in the 50-60 Hz appearing shortly after the

onset of the grating pattern. It can also be seen that around 40 Hz there is an increase in response between 2-3 seconds. The bottom panel in 4-20b shows the sudden increase in power from passive to active state for the 30-60 Hz band.

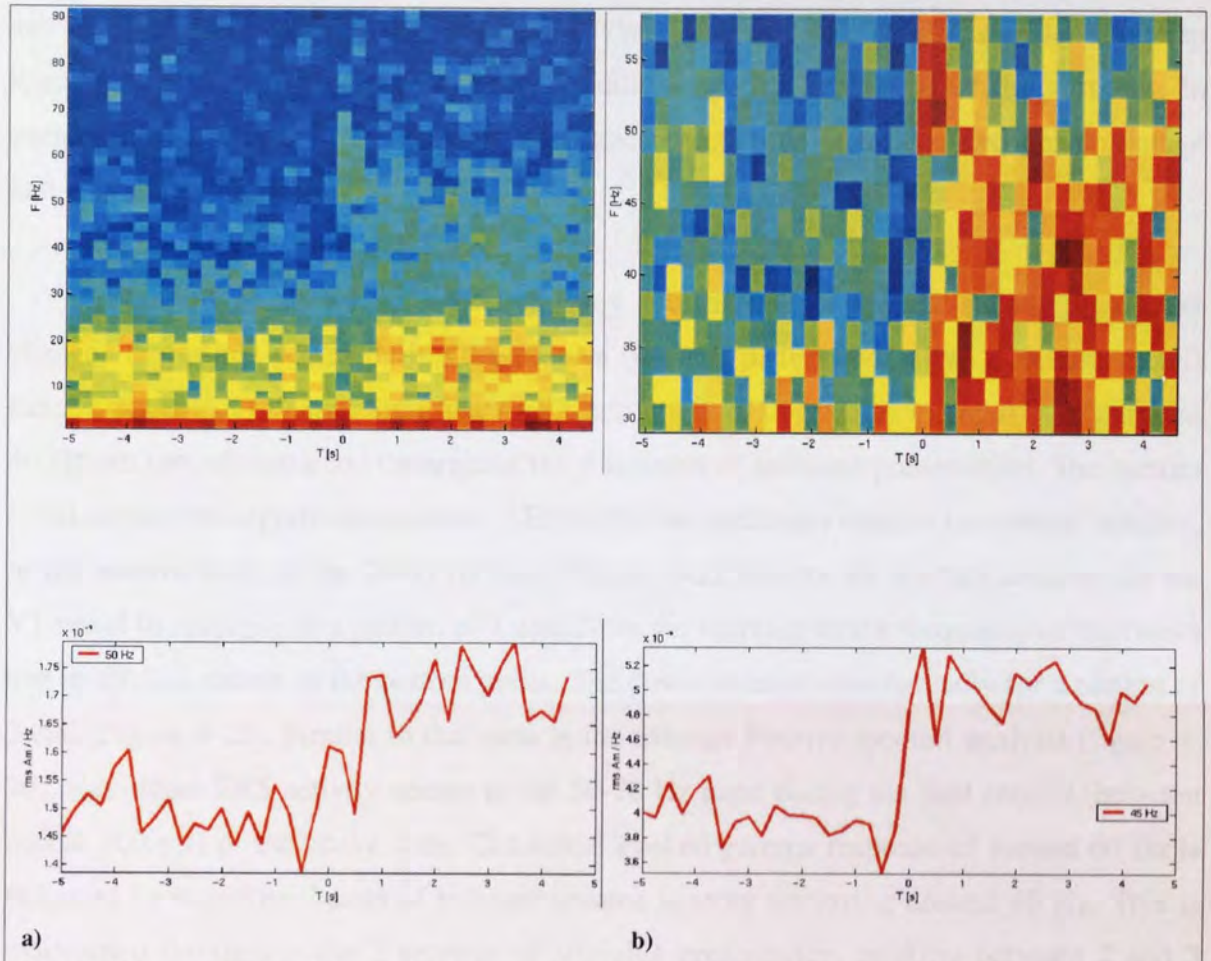

a) b)

Figure 4-20a and b. Frequency spectrograms of single voxel, single subject MEG data, as a function of time. The time-windows used to calculate the spectrogram were the averaged passive and active states totalling 10 seconds. Note the sudden increase in ERS with the onset of a 3cpd square-wave grating pattern **(a)**, which occurs in the 50-60 Hz band **(b)**. Also note that after the onset of the active state, increase in power occurs around 2.5 seconds around 40 Hz.

These frequency spectrograms, however, show task-related power changes in the selected virtual electrode due to the onset of the stimulus but do not provide a precise measure of statistical significance of the power change (ERS/ERD) due to the passive and active states. Moreover, the spectrogram in figure 4-20 is calculated using the conventional Fourier transform, which assumes stationarity of the processed signal epoch and estimates the average of different frequency components in the entire epoch. But MEG/EEG data are

transient and non-stationary. Therefore, the duration of a certain frequency component within a certain frequency band in the time series, as well as the phase and amplitude of the data must be assessed. The wavelet transform in conjunction with the Bootstrap method suitably answer these questions. Bootstrapping provides the proportion of significant ERD and ERS in each state relative to a baseline. Using one subject's results, wavelet bootstrap spectrograms were performed for each condition (spatial frequency) of the stimulus. In each case, the selected voxel showed the highest magnitude of task-related power change and was situated in V1.

Figure 4-21 shows the time-frequency spectrogram of the statistically significant changes in cortical power during the passive (top left panel) and active (top right panel) states a pattern of 0.5 cpd. Significant ERS activity ($p<0.05$) occurs in small bursts around 40 Hz but are not sustained throughout the 5 seconds of stimulus presentation. The bottom panel depicts the significant amount of ERD/ERS in each state relative to average baseline, or the passive state, in the 20-60 Hz band. Figure 4-22 depicts the spectral analysis for the V1 voxel in response to a pattern of 1 cpd. Note the increase in the frequency of the bursts and in ERS as shown in the bottom panel. The power changes dramatically for a pattern of 3 cpd (Figure 4-23). Similar to that seen in the average Fourier spectral analysis (figure 4-20), significant ERS activity occurs in the 50-70 Hz band during the first second (between 200 to 700 ms) of the active state. The initial evoked gamma response of around 60 Hz is followed by repetitive bursts of induced gamma activity occurring around 40 Hz. This is maintained throughout the 5 seconds of stimulus presentation, peaking between 2 and 3 seconds. Conversely, little significant ERD or ERS occurs during the passive state. The bottom panel of figure 4-23 shows the mean percentage of statistically significant ERD/ERS occurring in the 20-60 Hz range for the active and passive states. These bursts diminish gradually for voxels of V1 in response to patterns of 4 and 5 cpd such that for a pattern of 6 cpd there is little activity (Figure 4-24) and the power in the active state is dramatically reduced (bottom panel, figure 4-24). Therefore, the stimulus that induces the most pronounced bursts of V1 gamma-band activity is a square-wave pattern of 3 cpd. These phenomena were observed in spectral analysis performed for V1 voxels in most other subjects.

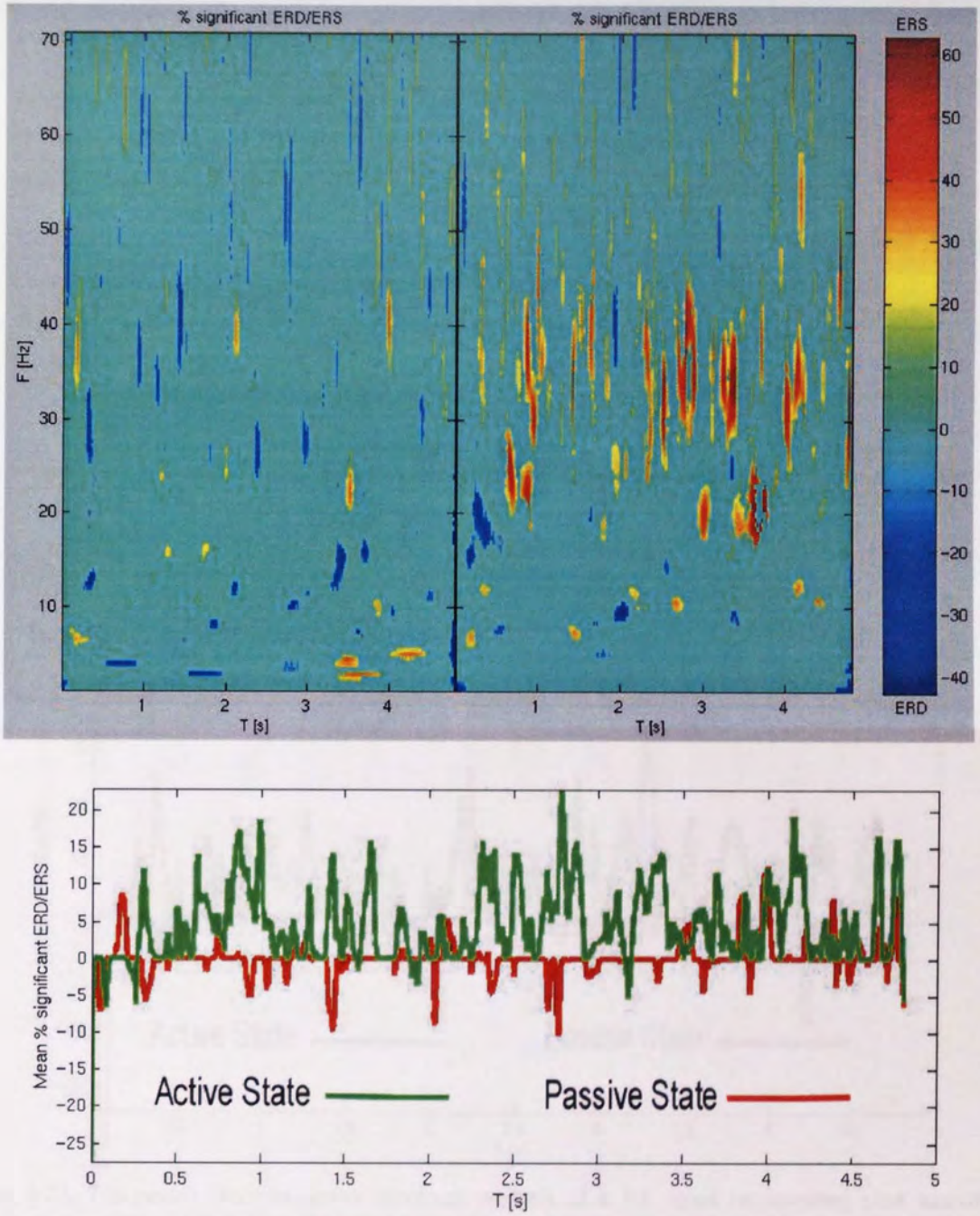

Figure 4-21. *Top Panel:* wavelet power spectrum analysis using the bootstrap method for a voxel in V1 representing peak response to a pattern of 0.5 cpd. Note the brief bursts of gamma activity most visible in the 30-40 Hz band. *Bottom panel:* mean percentage of significant ($p<0.05$) ERD/ERS activity in the 20-60 Hz for each epoch in comparison to the baseline.

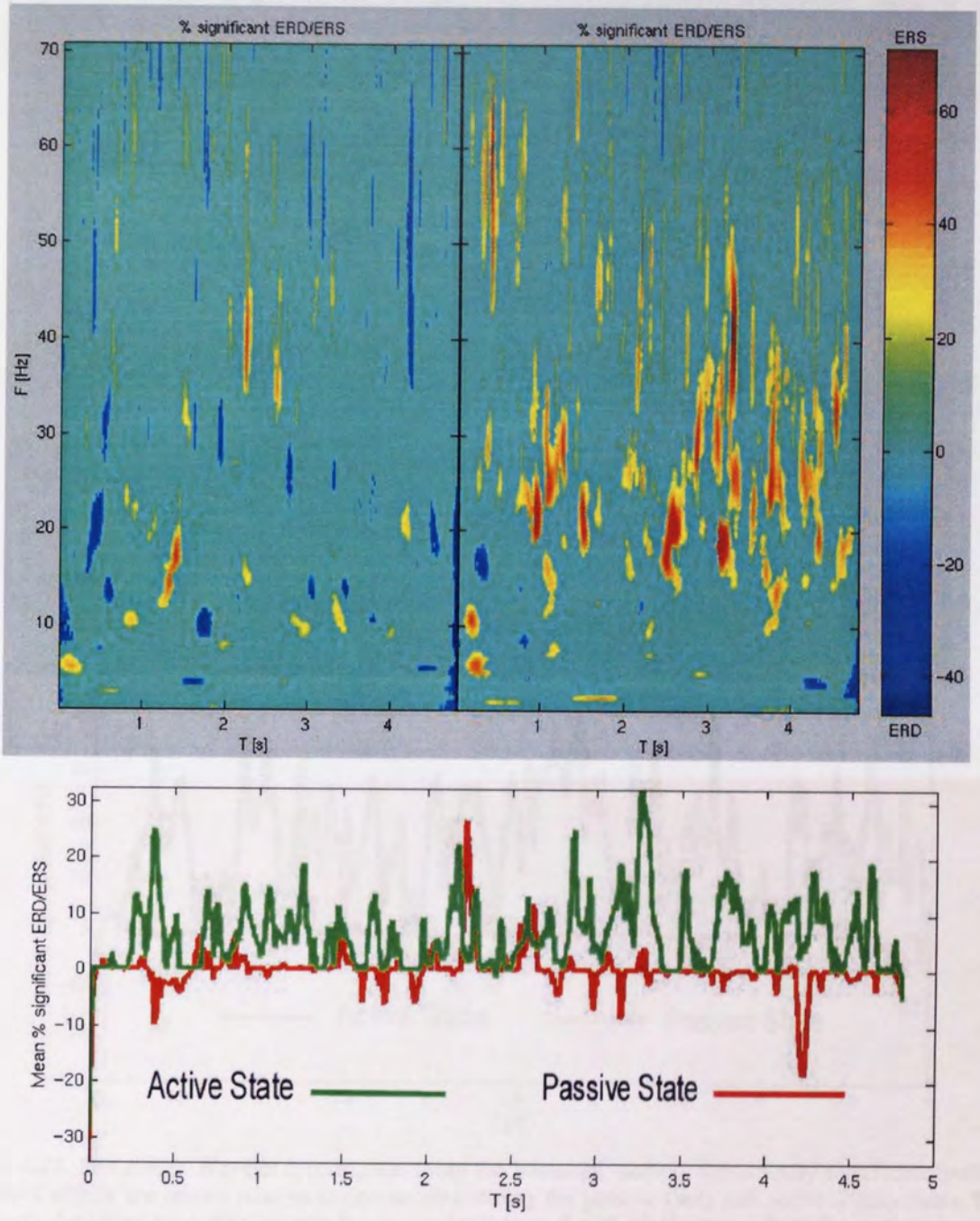

Figure 4-22. *Top panel*: Wavelet power spectrum analysis of a V1 voxel representing peak activity in response to a pattern of 1 cpd. Note the initial burst of evoked gamma (around 60 Hz) within the first second. With prolonged viewing of the stimulus, the bursts increase in frequency and occur most often in the 20-30 Hz band. *Bottom panel:* mean percentage of significant ($p<0.05$) ERD/ERS activity in the 20-60 Hz band. Note the increase in average power in the active state in the gamma band.

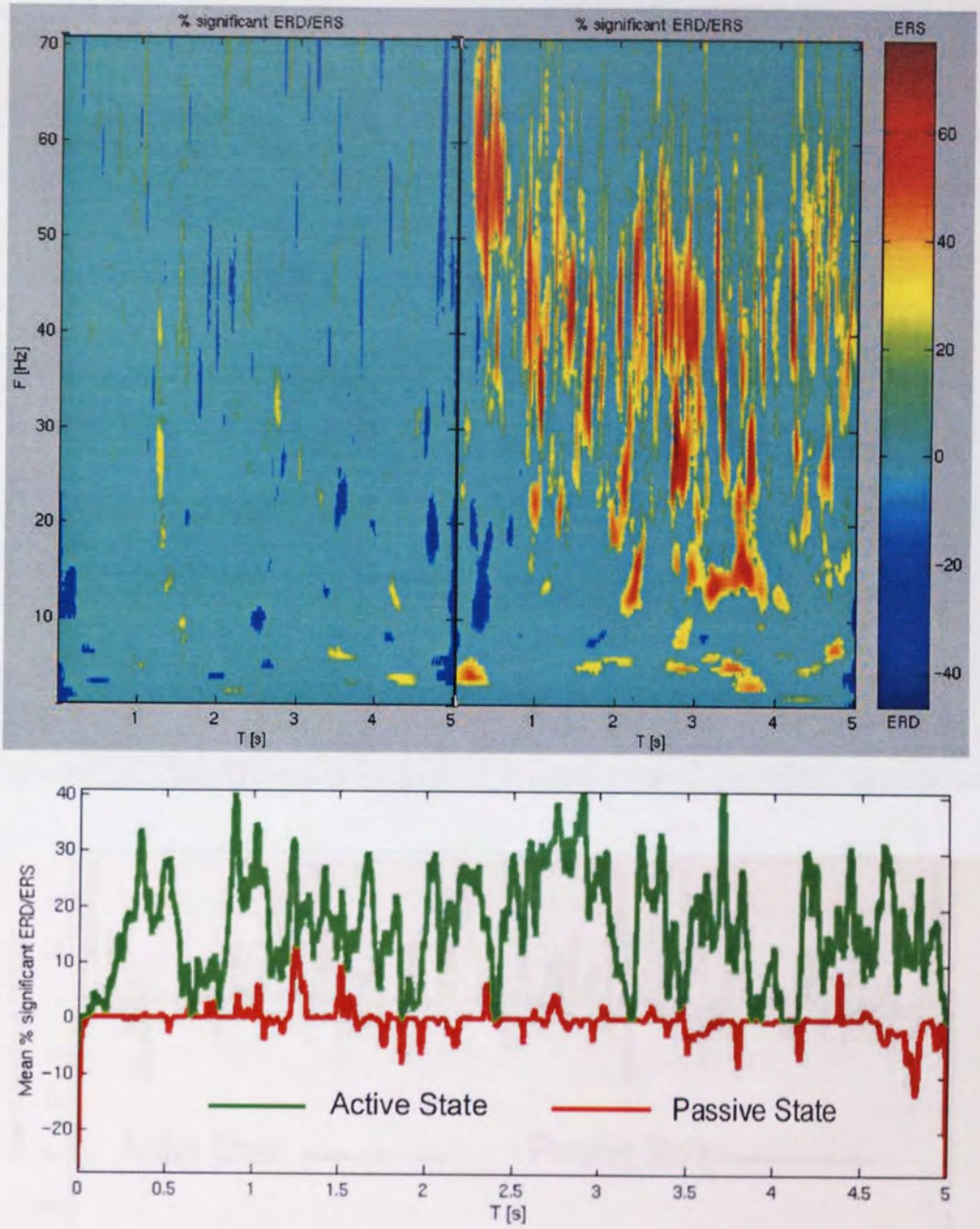

Figure 4-23. *Top panel:* Wavelet spectrogram using the bootstrap method. Statistically significant ($p<0.05$) ERD/ERS effects are shown relative to one another during the passive (left) and active (right) states. ERS dominates the active state, occurring in bursts, particularly in the 30-60 Hz range. Note the evoked response with the onset of the active state (around 5 Hz). Also note the sustained ERS that occurs in the first second and then again after 2.5 seconds. On the other hand little significant ERD or ERS occurs during the passive state compared to the baseline. *Bottom panel:* The mean percentage of the significant ERD/ERS occurring in the 20-60 Hz range during each state.

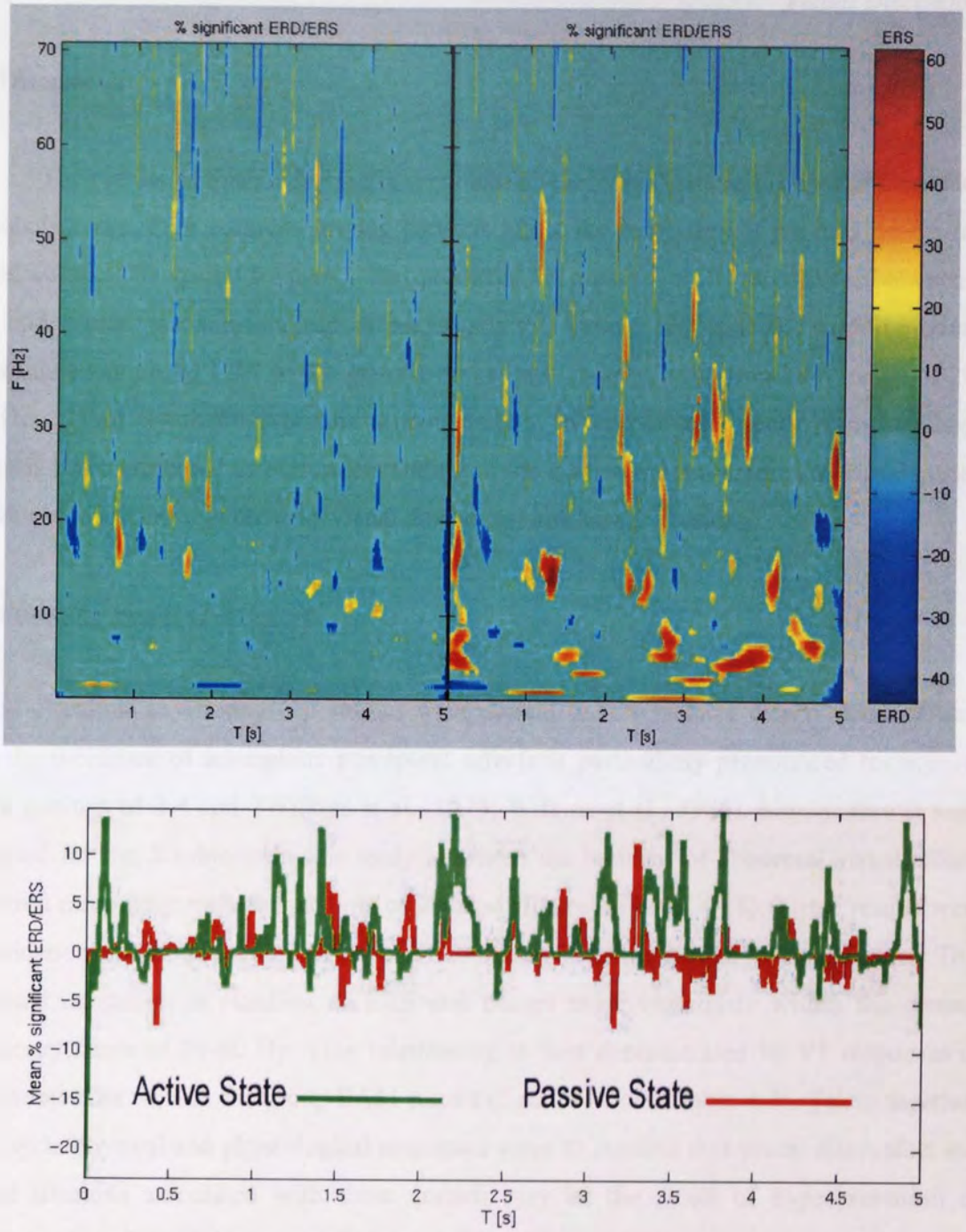

Figure 2-24. *Top panel:* Wavelet analysis of power spectrum for the most active voxel in V1 in response to a pattern of 6 cpd. There is little effect of the stimulus in the activity of V1 as evident by the similarity between activities in each state. The bursts of gamma that dominate the responses of the corresponding voxel to a pattern of 3 cpd are most notably absent. *Bottom panel:* mean percentage of significant (<0.05) ERD/ERS in the 20-60 Hz band. Note the dramatic decrease in power within the active state in comparison to the voxel responding to a pattern of 3cpd.

4.8 Discussion

The results of this study clearly demonstrate that variations in the spatial frequency of square-wave, high contrast, grating patterns affect the responses of neurons within the visual cortex. The spatial frequency that produces the most vigorous response is between 2 to 4 cpd, while most subjects respond maximally to a pattern of 3 cpd. The stimuli produce clear and pronounced ERS in the gamma range, particularly in the frequency range of 20-60 Hz. Using Synthetic Aperture Magnetometry in combination with time-frequency analysis has contributed to our understanding of the spatiotemporal aspects of visual cortex responses to stimuli that provoke visual discomfort and visual illusions.

Illusions and visual discomfort

Previous psychophysical studies with normal observers have clearly demonstrated that the incidence of anomalous perceptual effects is particularly pronounced for square-wave gratings of 2-4 cpd. (Wilkins et al., 1979; Wilkins et al., 1984). Similar results were obtained for the 3 subjects in this study in whom the incident of abnormal visual effects occurred more frequently for patterns of 2-4 cpd (figures 4-16 to 4-18). These results were coincident with pronounced gamma band oscillations in the primary visual cortex. This neuronal excitation is manifest as ERS and occurs more vigorously within the gamma frequency range of 30-60 Hz. This relationship is best demonstrated by V1 responses of each subject as well as the group SAM results (figure 4-15 and table 4-2). Taken together, the psychophysical and physiological responses seem to confirm that visual discomfort and visual illusions associated with these stimuli may be the result of hyperexcitation of neurons within V1 (Meldrum and Wilkins, 1984; Wilkins, 1995).

The frequency spectrograms are also consistent with the results of psychophysical studies with normal observers in whom the incidence of visual discomfort and anomalous effects increases with prolonged viewing of the grating pattern (Wilkins, 1984). Figures 4-20a and 4-20b demonstrate an initially sudden onset of neuronal excitation with the onset of a 3 cpd grating, which increases with time and peaks after 3.5 seconds of viewing. The

sudden onset of excitation is most pronounced in the 30-60 Hz band (figure 4-20c and 4-20d). Meldrum and Wilkins (1984) suggest that abnormalities in EEG discharges occur when the normal physiological excitation resulting from pattern stimulation exceeds a critical amount, causing an epileptic attack that spreads to other cortical regions. Moreover, Wilkins et al. (1984) have suggested that the neural processes involved in visual illusions are likely to be localised, as opposed to those that spread and sustain epileptogenic disturbances. The gamma responses in discomfort and illusions seen here reflect localised and focal activity pertaining to a specific location in the visual cortex. It is therefore possible to assume that increased susceptibility to experiencing visual illusions and discomfort is coincidental with increased excitatory activity of neurons within small areas of the primary visual cortex. A number of single unit recording studies have shown that the incidence and magnitude of synchronous firing decreases with spatial separation between cells or groups of cells (Engel et al., 1989). This would also be consistent with the reported increase in the incidents of anomalous visual effects for patterns of 2-4 cpd.

In figures 4-8 to 4-15 it has been shown that the strength of oscillatory activity within the visual cortex is dependent upon spatial frequency of the patterns, such that at the extreme lower and higher spatial frequencies the neurons exhibit weaker oscillatory responses, while the middle spatial frequencies of 2-4 cpd, and the pattern of 3 cpd in particular, produce the most vigorous oscillations. These results are consistent with single unit and multiple unit recordings of macaque V1, which indicate stimulus-dependence of oscillatory activity in V1 (Gray and Singer, 1997; Friedman-Hill et al., 2000). If the rhythmic activity were independent of changes in spatial frequency, one would expect to find equal patterns of neuronal activation from all gratings that evoke a response. Conversely, if the rhythmic neuronal activation reflects spatial frequency preferences, then the optimal stimulus could be defined as that which produces the highest magnitude of oscillatory activity as opposed to the non-optimal stimulus.

The data presented here do not provide sufficient evidence for the preferential involvement of either M or P pathways in relation to these patterns. Therefore, it is not possible to confirm, or reject, the speculation by Wilkins (1995), that the M pathway is

preferentially involved in conveying the information from these patterns to the visual cortex and is thus involved in the abnormal perceptual effects.

The occurrence of gamma oscillations

One important finding of this study was the occurrence of enhanced ERS in the gamma frequency band, which is most pronounced in the 30-60 Hz distributions of gamma (table 4-3). Oscillations around 40 Hz are found in enhanced processing of sensory or cognitive information. Visual stimuli of different characteristics have been known to generate synchronised neuronal activity on the millisecond time scale (Fries et al., 1997; Gray and Di Prisco, 1997). The visual system is thought to recognise images by a process called 'perceptual binding', which is believed to segment scenes into their constituent features. Consequently, these features must be represented separately in the visual cortex, and it has been suggested (Singer and Gray, 1995) that they are represented by networks of neuronal populations, which themselves exhibit synchronised activity on a millisecond time scale.

It has indeed been demonstrated that synchronised activity is characteristic of neuronal response to visual stimuli, but that the response properties are stimulus-dependent (Gray and McCormick, 2000; Friedman-Hill, 2000). Gray et al. (1990) reported that oscillations in area V1 of cats are unlikely to occur to stationary stimuli. But more recently, Friedman-Hill et al. (2000) have found that many cells in the macaque area 17 exhibited significant oscillations in response to static stimuli. These evoked oscillations were often lower in frequency (mean = 36 ± 6 Hz) than those evoked by drifting stimuli (mean = 47 ± 8 Hz), nevertheless the two types of stimuli evoked equally strong rhythmic responses. Neither the orientation nor the direction of motion of the stimulus was related to the frequency of oscillations. Recently, it has been shown that in response to visual stimulation, many neurons in the visual cortex of cats and monkey display synchronised rhythmic discharge in the gamma frequency band (Frien et al., 1994). It has been suggested that these cells originate in the different functional columns of the striate cortex (Livingstone, 1996), thus implying a functional link between oscillations of the gamma frequency band and the

response synchronisation. Gray and McCormick (1996) have described a new subset of superficial pyramidal neurons in the striate and prestriate cortex, which they refer to as chattering cells (CH), found in layers 2 and 3, which have distinct biophysical properties. These cells are excitatory, have simple receptive field properties, and exhibit synchronous rhythmic oscillations in the gamma frequency band (20-80 Hz). Using intracellular recording and staining of single cells from the striate cortex of cats in vivo, Gray and McCormick (1996) studied the intrinsic membrane properties of all cells in this region. They describe four distinct classes of pyramidal cells based on their response properties following injection of depolarising or hyperpolarising current pulses. Regular spiking (RS) cells displayed repetitive action potentials lasting on average 0.62 ms. Intrinsic bursting (IB) cells generated bursts of two to six spikes on a depolarising potential followed by hyperpolarisation, and tonic firing. Their action potentials lasted on average 0.57 ms. Fast spiking (FS) cells produced tonic firing at rates of 800 Hz and their action potentials lasted on average 0.48 ms. These three classes of cells had been previously described in other studies (McCormick et al., 1985). The new subset of cells, or CH cells, however, produced markedly different firing properties, such that in response to a depolarising current pulse, they produced repetitive discharges of two to five spikes per burst with an intraburst firing rate as high as 800 spikes per second. Another distinguishing property of these cells was their response to visual stimulation and their tendency to fire in repetitive bursts of action potentials at a rate of 30-60 Hz when presented with the optimal stimulus. The stimuli consisted of moving, as well as stationary, square wave and sine wave gratings. The membrane potential of these cells was also dominated by frequencies in the 30-60 Hz band during visual response and the rhythmic fluctuations were not time-locked to the onset of the stimulus meaning that gamma oscillations were absent when visual stimuli were withdrawn and during periods of spontaneous activity. Gray and McCormick suggest that this characteristic response might be the pacemaker for the widespread gamma oscillations, because rapid bursts of action potentials are far more likely to cause other neurons to fire than are single pulses. If these cells are the source of oscillations, the gamma frequency should be an intrinsic property of these cells and not the consequence of other oscillating neurons. They found that this chattering occurred in response to square wave gratings as well as to hyperpolarising and depolarising current pulses. This seemed to suggest that the

rhythmic bursting is an intrinsic behaviour of these cells. In a subsequent study in visual cortex of alert cats, Grey and Viana Di Prisco (1997) showed that these cells were indeed prominent within area V1. More recently, these results have been confirmed in the visual cortex of the macaque monkey by Friedman-Hill (2000) and Maldonado (2000) who demonstrated that cells producing gamma-band oscillations also tended to fire in high-frequency bursts. Interestingly, the results of our bootstrap analysis (figure 4-21) revealed a remarkably similar pattern of activation in the selected voxel in V1. We discovered that high-frequency bursts of synchronised activity is a feature of cortical responses to gratings that are similar to those used by Gray and McCormick (1996). These bursts of synchronised activity lasted a few hundred milliseconds, between which no significant activity occurred. Subsequently, similar analyses were performed in other subjects with almost identical results where bursts of synchronised activity were most frequent in the 30-60 Hz frequency range.

In their recordings of CH cells in the macaque V1, Friedman-Hill et al. (2000) found that the oscillatory activity evoked by the gratings was most prominent in the 40-50 Hz frequency range with a mean of 48 Hz. They conclude that the most robust oscillations correspond to gamma activity in the 30-60 Hz range, producing significant amplitude of oscillations. On the other hand, CH cell responses in the more extreme distributions of the gamma band, i.e. 20-30 Hz and 60-80 Hz, tended to be lower in amplitude. Figure 4-8 to 4-14 show that for each subject in this study the gamma frequency range of 20-70 Hz produce higher responses than the 1-20 Hz and 70-100 Hz ranges, in which the oscillatory responses of V1 cells do not alter significantly as a function of changes in spatial frequency. It is therefore likely that the gamma band activity seen in this study are produced by a particular subset of neuronal assemblies, i.e. those that have the same response characteristics to the CH cells in cats and the macaque monkey. Furthermore, in all but one subject, the highest V1 responses were within the 30-50 Hz distributions of the gamma frequency range (Table 4-3). The findings in this study indicate that consistent with results of single unit recordings from the macaque visual cortex, in man too, there is strong V1 oscillatory activity in the gamma frequency range in response to static stimuli. Therefore, as with the macaque studies, in man too, the magnitude of neuronal synchronisation is dependent upon the

features of the stimulus, which in this case is the spatial frequency of the grating pattern. These cells thus become the most likely source of the ERS seen in V1 of human subjects. These findings strongly suggest the possibility that chattering cells are also prominent within the human visual cortex. This possibility becomes even more likely since CH cells are superficial pyramidal cortical neurons that produce the tangential sources to which MEG is most sensitive. It is however difficult to assess the population density and the percentage of CH cells compared to other cell types. In single unit recordings, this is mainly due to the sampling bias that occurs in electrophysiological recordings, but they are likely to be widespread and ubiquitous (Gray, personal communication).

4.9 A causal hypothesis for visual illusions and photosensitive epilepsy

In the light of the findings presented in this chapter, it is now possible to propose a mechanism for visual discomfort. The increased synchronised oscillations in the gamma band occur in response to the same stimulus properties that generate the abnormal visual phenomena and therefore they maybe paroxysmal. The excess excitation causes the neurons of V1 to fire more vigorously, which in the light of what is known of their properties, may lead to illusions of shape, motion, colour, etc. Because of intact controlling mechanisms, this increase in synchronised activity remains within safe limits in normal observers, causing visual discomfort or 'visual stress' (Wilkins, 1995). This neuronal hyperexcitability might be the precursor for attacks of photosensitive epilepsy. Indeed, gamma oscillations have been reported at the onset of different subtypes of epileptic seizures using intracranial recording (Traub et al., 2001). Gamma oscillations are local, and required for brain function in terms of binding the elementary features of an image into a coherent percept (Gray et al., 1989; Tallon-Baudry and Bertrand, 1999). A photoparoxysmal response (PPR) occurs when the hypothetical controlling mechanisms of the brain fail to keep the increased synchrony within required limits, thus spreading to other cortical regions. In order for this high degree of synchrony to be detected by MEG/EEG, some large population of cells that create a network of feed-forward or feed-back loops is necessary. It is not clear what mechanism is responsible for this excitatory gamma activity but the intrinsic properties of CH cells may provide a significant contribution to their generation.

4.10 Conclusion and recommendations

The results presented in this study provide an indication of the link between consciousness and specific oscillatory responses of cortical neurons. It has been demonstrated that stimuli, which exert certain behavioural responses, such as visual discomfort and visual illusions, also exert pronounced synchronised cortical activity in the gamma range of 30-60 Hz. Although the results of this study shed little light on the precise mechanism responsible for the illusions, we can conclude that visual illusions and discomfort are clearly associated with synchronized firing of excitatory neurons in V1. Synchronised activity in the gamma frequency range is a prevalent characteristic of visual cortex responses, the magnitude of which is dependent upon the characteristics of the stimulus, and in this case the spatial frequency of the patterns. These findings are consistent with those from single unit recordings of the cat and macaque visual cortices where a specific category of cells produce high frequency oscillations in the gamma range in response to stationary and moving grating patterns. The results of SAM comparisons from this study demonstrate that gamma band oscillations are a characteristic of neuronal activity in the human striate cortex, and indicate that the chattering cells that generate them are not a unique feature of the macaque and the cat visual cortices, but are densely present within the mammalian visual cortex.

The physical properties of the gratings, which activated the visual cortex optimally were precisely those implicated in generating visual discomfort and attacks of migraine and epilepsy in photosensitivity. The reports of psychophysical data have identified specific physical properties of stripes necessary to induce the highest incidence of visual illusions and visual discomfort. These are a square-wave luminance profile, maximum contrast between the light and dark bars, and spatial frequencies of 2-4cpd. It has been shown that altering any one of these parameters results in significant reduction of the undesirable visual effects. We do not know if alterations in these parameters would also lead to a proportional decrease in the responses of the visual cortex. Therefore, future work should establish the magnitude and response properties of visual cortex neurons when other parameters of the stimulus, apart from its spatial frequency, are changed. For instance, if

decreases in cortical power coincide with reduction of visual abnormalities, they would provide valuable clues in the understanding of both phenomena. If changes in the parameters of the stimuli were found to equally affect cortical responses as well as the abnormal visual effects, it would then be possible to suggest a prominent role for chattering cells in mediating the anomalous effects observed in visual stress and perhaps establish their role in the onset of photoparoxysmal responses in photosensitive epilepsy.

Incorporating a time-frequency analysis was particularly revealing in this study since the results uncovered changes in cortical power at specific times. In future studies these fluctuations in cortical power can be correlated with precise psychophysical data regarding the temporal aspects at which maximum discomfort occurs. Inferences can then be made regarding the effects of the gratings as a function of time with implications for prevention of visual discomfort.

Chapter 5: Visual Cortical Oscillatory Responses to Colour Stimuli Using Synthetic Aperture Magnetometry

5.1 Introduction

Colour is an attribute of a visual scene that has generated much debate regarding its processing throughout the visual system. Early processing of colour in the eye begins with the cones, which are sensitive to variations in wavelength of the incoming light (chapter 3). Further processing is then taken up by the colour-opponent system, and is conveyed to the higher cortical areas through the parvocellular layers of the LGN. There has been much debate as to the fate of this pathway and the final cortical destination of colour inputs. Following the demonstration of functional specialisation in the visual cortex of the macaque brain, the question of a region specialised solely for the purpose of colour vision was investigated using a variety of techniques.

This chapter begins by a brief history of the debate regarding the existence of a colour centre in the visual cortex. The colour pathways and area V4 are then briefly described. Finally, the results of a thorough investigation into the responses of visual cortex to colour stimuli using the novel MEG analytical technique of SAM is then presented.

5.2 A historical perspective on cortical colour specialisation

The debate surrounding colour specialisation in the visual cortex is dated back to early in the 19^{th} century when there was considerable disagreement among scientists regarding the existence of a cortical centre solely responsible for colour processing. Zeki (1990), who is a proponent of the existence of colour centre in the visual cortex, provides a comprehensive account of that controversy some of which is recounted below. The aim of the following sections, however, is to provide a more balanced and less biased account of the history of colour localisation in the visual cortex.

5.2.1 Cerebral achromatopsia

Cerebral achromatopsia refers to the inability to see colours after damage to a specific region of the cortex. The first description of pure achromatopsia in the clinical literature is that of Steffan (1881, cited in Zeki, 1990) who described a patient with total bilateral achromatopsia as a result of a stroke with seemingly no accompanying defects such as scotoma, amblyopia, or reduction in visual acuity. Steffan believed that this phenomenon was evidence for 'the existence of pathological colour blindness', and that there must be a special cortical centre for colour vision. A more accurate account of cerebral achromatopsia was given by Verrey (1888; cited in Zeki, 1990), who following a postmortem examination of his patient concluded that the colour centre is situated in the fusiform and lingual gyri, which are situated next to each other. Some years later, following postmortem investigations of a patient, MacKay and Dunlop (1899; cited in Zeki, 1990) also provided evidence for the existence of a specialised centre for colour vision situated in 'the grey matter of the fusiform convolution'. At the time of these reports, however, the precise boundaries of the primary visual cortex were not established and its topographical organisation was still a source of much controversy. Moreover, visual disturbances such as achromatopsia and other agnosias were often accompanied by scotomas since the lesions very often covered a large area or scattered areas of cortex. The combination of these factors lent weight to the case of those such as Henschen (1893; cited in Zeki, 1990) and later Lashley (1948) who argued against the existence of a cortical centre solely devoted to the processing of colour. However, it was also noticed that for the scotomas, the defect always involved peripheral vision while for colour defects it always involved the central fields. Despite the central nature of the achromatopsic defect, the presence of scotoma or hemianopia was the chief reason for rejecting the existence of a colour centre in the visual cortex.

Today, it is established that there is a close spatial relationship between the fusiform and lingual gyri on the one hand and the calcarine or striate cortex on the other such that the lower border of striate cortex, which represents the upper field of view, overlaps part of the lingual gyrus. We also know that in the macaque V4, which is involved in colour vision,

central fields are heavily represented at the expense of peripheral fields (Zeki, 1977). Although this may not necessarily be the case in humans, other similarities between the macaque and human visual cortex favour that some parallels must exist. Moreover, research has established that the input to area V4 is from that region of V1 with foveal representation, which is heavily implicated in day vision, and contains an abundance of colour processing cones.

Indeed, it is a fact that scotoma accompanies the majority of achromatopsic cases (Meadows, 1974) indicating that the primary visual receptive area must be involved in the processing of colour, and has been used as an argument against the existence of a separate colour centre. However, as long as the lingual and fusiform gyri are only among several damaged cortical areas, it is hard to assess their role in visual function, and other defects such as scotoma will surely be present. Equally as important was the observation that in the majority of reported cases of cerebral achromatopsia with accompanying scotoma, the upper visual fields were uniquely involved with no disruption of the lower visual fields alone. This can be explained by the anatomical location of the lingual and fusiform gyri, which are situated ventrally and border the inferior bank of the calcarine cortex where the upper fields are represented. It thus follows that any damage to the lingual and fusiform gyri is likely to also damage the lower part of the calcarine sulcus.

Other visual defects too are often observed in cases of achromatopsia, including alexia and prosopagnosia. The latter is characterised by the inability to recognise faces, and is particularly implicated throughout the literature (Meadows, 1974). However, the converse is also true in that there are many cases of visual defects such as prosopagnosia where colour vision remains intact. There are also reports of postmortem examinations such as that by Lenz (1921; cited in Zeki, 1990), whose patient suffered from central achromatopsia following a stroke, where damage was confined to the optic radiation and the region of fusiform gyrus.

Early in the last century, the nearest scientists came to accepting some degree of functional specialisation was the supposition that different layers of V1 had different

functional mechanisms. Henschen's supposition that all visual processing occurred in the striate cortex meant that at least a part of this cortex itself must be specialised for colour vision. Following postmortem examination of a patient, Poppelreuter (1923, cited in Zeki, 1990) concluded that the calcarine cortex consists of multiple systems, which are individually concerned with luminance, motion, colour, orientation, and form in such a way that they can be selectively disturbed. As for a cortical colour centre, Halpern and Hoff (1929, cited in Zeki, 1990) proposed that it is localised to layers 2 and 3 of the striate cortex. It was not until the latter part of the last century that based on physiological and anatomical investigations of the monkey cortex the concept of striate cortex acting as a functional segregator became established. In the meantime, Henschen became aware of the properties of cells within the lateral geniculate nucleus and proposed the 'principle of the size of cells'. He found that the upper 4 layers of LGN have smaller cells whereas the lower two have larger cells. Based on this he proposed that this organisation meant that the larger cells were concerned with peripheral vision and therefore with the 'light' sense, while the smaller cells were concerned with macular vision or the colour 'impressions'. His theory of colour perception was therefore based on cell size throughout the visual system such that all small cells were concerned with colour and all large cells dealt with light. As for the striate cortex, he pointed to the small cells of layer 4 and postulated that in all cases, the colour centre is within the calcarine cortex.

Traditional view has held that functional differences in the cerebral cortex are reflected in architectonic differences, and that an area of uniform architecture is one of uniform function. This view is correct insofar as the method of cytoarchitectonics must be adequate to reveal anatomical differences between each area. However, this has not always been the case, and initially, using the cytoarchitectonic technique no one was able to distinguish a distinct area in the fusiform and lingual gyri. As a result, and based on architectonic uniformity, the evidence for functional specialisation within the macaque monkey striate cortex was dismissed, most notoriously by Hubel and Wiesel (1977), who reported all cells outside layer 4C of V1 to be orientation selective. On the other hand, physiological evidence had shown that many cells of V1 are wavelength selective with no orientation selectivity (Dow and Gouras, 1973). It also contradicted the theory of functional

specialisation, which suggested that there must be some degree of functional segregation within the primary visual cortex since the prestriate visual areas are fed their input from the striate cortex. The search for a colour pathway within the visual cortex began with the discovery of anatomical non-uniformity of V1 and in particular, it began with the discovery of blob and the interblob regions of layers 2 and 3 (Livingstone and Hubel, 1984). Over half a century after the suggestion by Poppelreuter that the striate cortex contains different functional systems, Livingstone and Hubel (1984) showed that indeed cells inside the blobs are mainly wavelength selective. This finding, coupled with the discovery of motion responsive cells in layer 4B (Lund et al., 1975), as well as the demonstration of multiple visual areas in the prestriate cortex, changed the concept of the organisation and function of visual system as being a dual process.

As described in chapter 3, the first area to be functionally characterised was V5 where the optimal response of cells was to direction of stimuli (Zeki, 1974b). This was followed by the demonstration that in the macaque monkey colour and wavelength selectivity is characteristic of cells in area V4 (Zeki, 1977), and that cells of area V3 are orientation selective. Anatomical evidence also indicated that prestriate visual areas are not connected serially, but that each part of V1 sends separate, independent, yet parallel outputs to different prestriate areas. This was the beginning of the theory of functional specialisation.

5.3 The colour pathways in the cerebral cortex

The demonstration of colour selective cells in area V4 of the macaque monkey suggested that such specialisation is equally plausible in man and was compatible with cases of achromatopsia that had been described by Verrey and others. In man, the lingual and fusiform gyri are the analogue of area V4 in the macaque monkey (Zeki, 1990). As described in chapter 2, separation of visual pathways starts at the retina with the ganglion cells. For colour, the midget (or Pβ) ganglion cells are wavelength selective and have colour-opponent properties in that they receive opponent input from different cone mechanisms. These project to the parvocellular layers of the LGN and from there, to blobs and interblobs of layers 2 and 3 where wavelength selectivity is confined to the blobs and orientation selectivity to the interblobs. The thin stripes of V2 are the next recipients along the colour pathway, but V1 also projects directly to areas V3, V5, and V4 with the latter area receiving mostly projections from the foveal V1. V2 also sends projections to V4, which are predominantly from the thin stripes and the interstripes (DeYeo and Van Essen, 1985; Shipp and Zeki, 1985).

The blobs of V1 contain colour-opponent and double colour-opponent cells, and there is segregation in the different forms of colour opponency in that a neuron will be either red/green opponent or blue/yellow opponent. This means that an individual blob is responsible for processing of one colour opponency system. Moreover, the unequal proportion of different colour blobs reflects that found in the retina where red/green ganglion cells outnumber the blue/yellow ganglion cells; in V1, too, red/green blobs outnumber the yellow/blue blobs.

5.3.1 Area V4

The human homologue of V4 of the macaque is located in the fusiform and lingual gyri (Zeki, 1993). In the macaque, area V4 has been further subdivided in a posterior part, simply referred to as V4, receiving input from V2, and an anterior part, referred to as V4A, which receives its input from V4 (Zeki, 1977). Retinotopic specificity decreases

significantly in V4, a fact reflected by the size of receptive fields that are 30 times larger than those found in V1 and V2 (Van Essen and Zeki, 1978). V4 is almost exclusively concerned with the central 30 degrees of vision; physiologically it has also been shown that many V4 cells lack colour selectivity and are more concerned with spatial frequency and orientation selectivity (Desimone et al., 1985). Nevertheless, it mainly contains wavelength selective cells and even the many orientation selective cells within it exhibit some degree of wavelength selectivity. Zeki and Shipp (1989) have suggested some extent of compartmentalisation within V4 whereby one compartment consists of mainly orientation selective cells that receive inputs from interstripes of V2, while the other consists mainly of wavelength selective cells that receive inputs from the stripes of V2. Since the majority of interstripe cells are not wavelength selective, Zeki and Shipp (1989) suggest the possibility of intrinsic connections within V4. As described in chapter 3, the colour and form pathways seem to be closely linked. Both pathways terminate in the inferotemporal cortex where colour and orientation selective cells have been found in both its anterior and posterior parts (Desimone et al., 1984). Moreover, lesions of the inferotemporal cortex cause deficits in discrimination of pattern, shape, and size (Gross et al., 1972).

5.3.2 Evidence against a colour centre

Despite the evidence regarding colour specialisation in V4, there is some line of evidence that suggest area V4 is involved in other aspects of vision and that colour perception is not confined to a specialised area. Following bilateral ablation of V4 in monkeys, Schiller (1995) did not find deficits as those described in achromatopsia but only moderate deficits in colour discrimination. Schiller (1993) also found only mild deficits in colour detection and discrimination in monkeys with selective lesions of V4. Schoppig et al. (1999) studied colour discrimination, colour short-term memory and colour constancy in patients with focal lesions limited to area V4 and found that this area plays an important role in colour constancy (Clarke et al. 1998) and colour short-term memory, but not in simple colour discrimination. Therefore, it may be that while V4 plays a role in analysis of colour information, it is not as specialized, or as important, a centre for colour processing as is thought to be by some.

5.4 Representation of colour in the visual cortex of man

In the monkey, evidence for colour selectivity is mainly derived from single cell physiological studies and from the many works of Zeki (1973, 1983a, 1983b). In man, there is no direct anatomical or cell physiological evidence for colour selectivity of area V4. Recent evidence regarding the specialisation of V4 for colour processing is derived from functional imaging studies. Using PET and fMRI, a number of studies have successfully revealed an area in the fusiform gyrus in response to colour stimuli, which will be briefly reviewed below. On the other hand, there have been very few MEG studies in colour processing in the visual cortex. These studies are briefly described below.

5.4.1 fMRI and PET studies

Lueck et al., (1989) claim to be the first to demonstrate the existence of a specialised colour centre in the visual cortex of man using positron emission tomography, which measures changes in regional blood flow. To maximise activation of colour-responsive areas, they used a Land Colour Mondrian for experimental trials, which consists of abstract display of coloured squares and rectangles. For control trials, they used an identical display but in this case the squares and rectangles were different shades of grey (i.e. achromatic Mondrian which contained luminance contrast). They found two cortical regions of heightened activity resulting from their experimental trials, one situated in the striate cortex, and the other in the lingual and fusiform gyri. The authors were not certain as to whether striate cortex activation included simultaneous activation of V2 since the low resolution of the technique did not allow for a clear distinction of the two areas. On the other hand, when the achromatic Mondrian containing luminance contrast was presented, activity in the fusiform and lingual gyri decreased significantly while activity in V1 remained the same. McKeefry and Zeki (1997) suggest that the human colour centre in the fusiform gyrus is one part of a greater cortical system for processing of colour. This system extends from V1 through to area V2 to V4, extending further beyond the inferior temporal cortex. More recently, Bartels and Zeki (2000) have identified a multiple regions that are activated by colour stimuli. They distinguish between two subdivisions of V4 that consists

of a posterior part, simply referred to as V4, and an anterior part, which they call V4α.The main difference between the two areas, is that the posterior area (V4) is retinotopically organised while the anterior area (V4α) is not. Together, these make up an area they refer to as the V4-complex, both parts of which are strongly implicated in colour processing. A specialised centre for colour in the fusiform gyrus has also been implicated by other studies (Corbetta et al., 1991; Zeki et al., 1991; Hadjikhani et al., 1998).

5.4.2 MEG studies

Until very recently there have been no MEG studies into the responses of visual cortex to chromatic stimuli. Regan and He (1996) were the first to measure magnetic brain responses to chromatic and achromatic stimuli in humans and have reported differences in response amplitude and latency. At low spatial frequencies, the amplitude of the response to isoluminant red-green gratings was considerably greater than the responses to its red and green components presented alone. Furthermore, responses to isoluminant red-green gratings were low-pass with respect to spatial frequency, whereas responses to luminance gratings were bandpass. Finally, responses to an isoluminant red-green grating attenuated more steeply with increasing spatial frequency above 2cpd than those in response to a monochromatic luminance grating, which fell to noise level at lower spatial frequencies. Regan and He (1996) made no attempt to determine the precise cortical area generating the evoked responses. In another MEG study, Fylan et al. (1997) also studied the response properties of the visual cortex to chromatic stimuli by recording evoked responses to isoluminant red-green gratings of a range of spatial frequencies. For each condition, the response was dominated by a single major component originating from area V1 as modelled by an equivalent current dipole. Moreover, Fylan et al. (1997) calculated the maximum global field power as a function of spatial frequency and found that the spatial frequency tuning function peaked at 1-2cpd, with some attenuation occurring in field power at lower spatial frequencies. They too conclude that chromatic evoked responses are low pass with respect to spatial frequency. However, this study failed to implicate an area in the extrastriate cortex that is activated in response to the chromatic stimuli.

5.4.3 Anatomical location of area V4 in the visual cortex of man

As described in section 5.4.1, a number of neuroimaging studies using PET and fMRI have consistently revealed bilateral activity in an area covering the fusiform gyrus and parts of lingual gyrus in response to colour stimulation. The location and spatial spread of V4 colour centre in man is typically expressed in terms of its Tailarach co-ordinates (e.g. Lueck et al., 1989; McKeefry and Zeki, 1997; Bartels and Zeki, 2000). These co-ordinates for the human homologue of area V4 as identified in PET and fMRI studies are given in Table 6-1.

	V4			
	x	**y**	**z**	**Z-Score**
Lueck et al. 1989 (PET, *n*=3)				
Left	-27	-56	-4	-
Right	24	-58	-7	-
Zeki et al. 1991 (PET, *n*=6)				
Left	-26	-68	-7	-
Right	20	-66	-4	-
McKeefry et al. 1997 (fMRI, *n*=12)				
Left	-26	-80	-14	7.99
Right	30	-78	-18	8.05
Bartels and Zeki, 2000 (fMRI, *n*=6)				
Left (posterior)	-34	-68	-18	7.25
	-19	-76	-16	6.97
	-28	-76	-16	4.84
Left (anterior)	-28	-56	-20	4.71
	-28	-54	-18	5.39
	-38	-56	-22	6.03
Right (posterior)	34	-74	-14	6.90
	32	-74	-14	4.34
Right (anterior)	38	-54	-24	5.14
	28	-50	-16	7.18

Table 5-1. Talairach co-ordinates from colour selective regions identified in the fusiform gyrus from some previous studies. Earlier studies did not distinguish between areas V4 (posterior) and V4α (anterior). *n*, number of subjects in the study.

5.5 The purpose of this study

Whether there exists a specialised centre in the visual cortex for processing of colour alone has been the cause of much debate and controversy. Since the advance of functional neuroimaging techniques, a number of studies have shown activation of fusiform and lingual gyri (the human homologue of V4) in response to a variety of colour stimuli using fMRI and PET (Lueck et al., 1989; Corbetta et al., 1991; McKeefry and Zeki, 1997; Zeki and Marini, 1998; Bartels and Zeki, 2000). This in addition to clinical evidence in the last century as well as single cell recordings in the macaque lends support to the existence of an area beyond V1 where colour is preferentially processed.

Whereas fMRI and PET studies have implicated an area in the extrastriate cortex to be specialised for colour processing, traditional MEG methods that use equivalent current dipoles have failed to show activity in response to colour stimuli beyond V1 (Fylan et al., 1998). Since V1 is the first port of entry to the visual cortex for the visual pathways, a transient evoked response occurs to all kinds of visual stimulation regardless of their finer characteristics. Unlike sensory stimuli that evoke a clear response from the cortex in the millisecond time scale, localisation of a specific aspect of a stimulus, such as its colour, requires that the presentation of stimuli be sustained rather than one that merely evokes a brief and transient response. An evoked response and the dipole fitting procedures are therefore inadequate in providing information regarding higher cognitive processes such as colour. Hence it is very likely that one reason for the failure of dipole fitting procedures in localising colour beyond V1 is that colour as a distinct feature of visual stimuli requires longer processing than is allowed by a mere evoked response. Furthermore, it is also likely that any extrastriate activity is obscured by strong signals emanating from V1. For these reasons, SAM is a far more suitable technique for measuring the spatiotemporal responses of the brain to specific aspects of stimuli. Much like fMRI and PET, it is possible to study cortical responses to non-phase-locked stimuli. Using SAM, the purpose of this study is to conduct a thorough investigation of the visual cortex responses to chromatic gratings as a function of spatial frequency. SAM provides information regarding the precise location of the most active regions of the brain averaged for the duration of stimulus presentation, and

measures changes in the ongoing brain activity by revealing increases and decreases in synchronised neuronal activity (ERD/ERS) in any activated region of the brain. An added advantage of SAM over those of fMRI and PET is that it provides information regarding time-frequency responses of the cortical regions most active during stimulus presentation. We therefore aim to answer the following general questions: What are the most active regions of the brain in response to the chromatic stimuli? Are these regions the same as those that have been implicated in studies with fMRI and PET (i.e. human homologue of area V4)? How is the magnitude of cortical responses affected by changes in the spatial frequency of the grating patterns? Individual as well as group SAM results are employed to provide answers to these questions. Of particular interest are the responses emanating from the primary visual cortex and from area V4. Therefore, for each subject, these areas are independently isolated and their responses to different conditions of the stimulus are measured. We use a number of techniques such as time-frequency spectrograms described in chapter 4 and a combination of other techniques, which are described below together with the methods employed in this study.

5.6 Methods

Stimuli

The chromatic stimuli were square wave gratings generated using a Cambridge Research Systems VSG2/3 computer graphics system and displayed on an Eizo Flexscan T560i, gamma-corrected, colour monitor with 14-bit luminance resolution, at a frame rate of 100Hz. The chromaticity co-ordinates of the three phosphors were r_x=0.625, r_y= 0.340, g_x=0.280, g_y=0.595, b_x=0.155, b_y=0.070. Luminance was measured with a Minolta photometer and the display was gamma corrected. Red and green gratings were generated and modulated independently for physical luminance. They were then combined 180 degrees out of phase to produce physically isoluminant red/green gratings. They were presented horizontally for 5 seconds and then replaced by a homogenous yellow background of the same mean hue and luminance with no inter-stimulus interval. The homogenous background resembled a uniform yellow screen when presented on the monitor and was used as the passive state, or epoch, for the purpose of SAM analysis. All stimuli subtended 12 degrees horizontally by 8 degrees vertically and were viewed at a distance of 2.10 metres projected on to a mirror through a window in the wall of the shielded room (figure 1-8). They were viewed binocularly, and subjects were instructed to maintain fixation on a small circle in the centre of all the stimuli throughout the whole of the session. Throughout the data collection the inside and the outside of the recording room was darkened as far as possible in order to eliminate source of luminance.

The sequence of data presentation is the same as that shown in figure 4-3. The two epochs of interest in this study are the first and second time windows (shown by the arrows in figure 6.1) where SAM comparisons are made between the yellow blank screen and the coloured grating, or the passive and active states respectively. This sequence was repeated 20 times after which the spatial frequency of the grating was changed and MEG recording was made for the new condition. This procedure was repeated 7 times for spatial frequencies of 0.5 to 6cpd. Each condition of the stimulus was presented randomly to each subject such that a stripe of 2cpd did not necessarily follow that of 1cpd.

Subjects

Data from all 7 individuals (3 males, 4 females, 35 ±12 years) who also participated in the previous study was analysed. All had normal visual fields and colour vision and normal, or corrected-to-normal, snellen acuity of 6/6. They were all selected from the population of student and staff members of Aston University Neuroscience Research Institute. Subjects were given particular instruction regarding the chromatic stripes. Corbetta et al. (1991) have demonstrated that attention to colour as a means of enhancing its perception is correlated with increased activity in the colour centres. Subjects were therefore requested to attend to the colour of the stimuli to maximise their cortical effects.

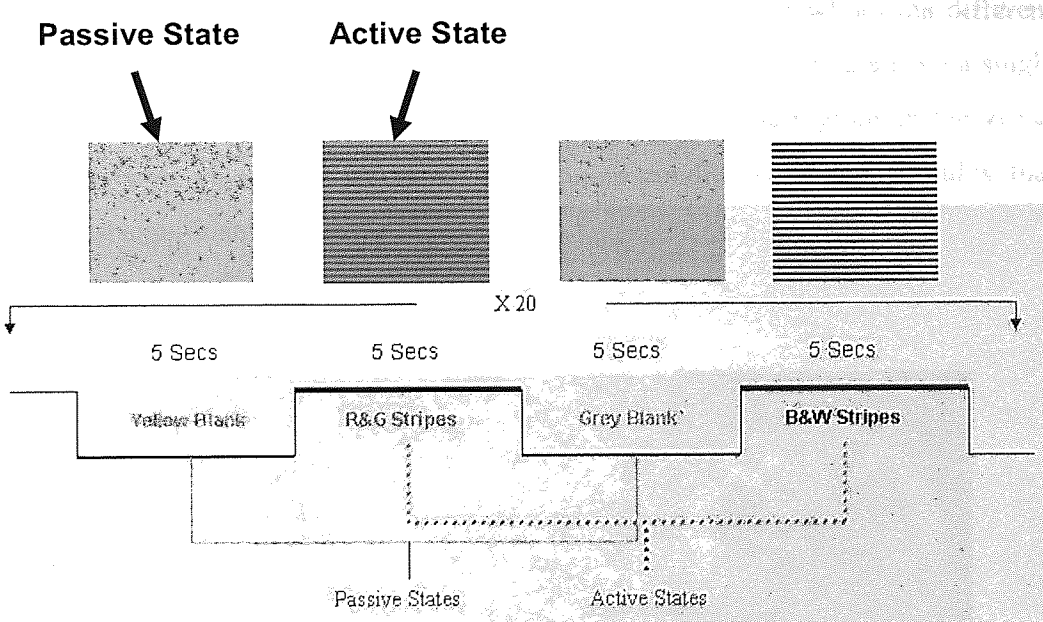

Figure 5-1. The sequence of stimulus presentation for the purpose of SAM analysis. The two epochs of interest in this study are the yellow blank and the isoluminant coloured stripes as shown by the arrows. Each epoch remained on the screen for 5 seconds and repeated 20 times.

MEG data were collected using a 151-channel CTF Omega System (CTF Systems Inc., Port Coquitlam, Canada) described in section 1.4. Data was sampled at a rate of 1250 kHz and analysed in the frequency range of 1-100 with bandwidths of 10 Hz wide.

Calculation of activity within the visual areas

In studies of visual cortex, it is often desirable to identify the activated regions in terms of the visual areas. If as suggested, the P pathway were the principal channel for conveyance of colour information to the visual cortex, and if V4 is specialised for processing of this information, it would be expected that the activity in this area (to which the P pathway sends heavy projections via V1) be more pronounced relative to other areas. Ideally we need information regarding the retinotopic organisation of the visual cortex for each subject, from which a flatmap of the visual areas can be constructed. Once the visual areas are identified they are isolated by applying the 'shading' procedure. Subsequently, the SAM functional volumes are superimposed onto the shaded MRI volume for each subject and the activity in each of the visual areas is calculated. However, of the 7 subjects in the study, this information was only available for one subject (KDS) for whom the different visual areas are shown in different colours in figure 5-2. By mapping the data from a single subject on a retinotopic flatmap, an attempt is made to discover the regions in the visual cortex that are more vigorously activated in response conditions of the stimulus that produce the most significant response.

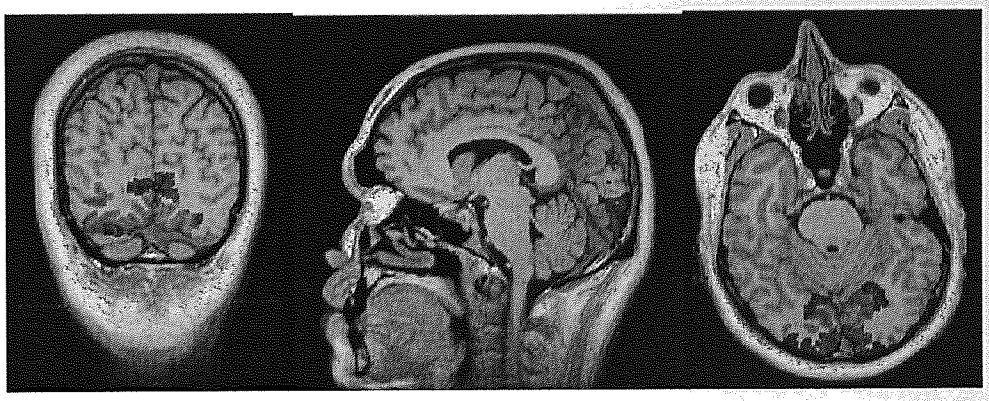

Figure 5-2. The shaded visual cortex for the MRI of subject KDS based on identifying its retinotopic organisation. Each colour represents a different visual area.

Identification and segregation of area V4

As just mentioned, precise retinotopic information regarding the organisation of the visual areas is not available for each subject used in this study. Therefore, we need some way of identifying the fusiform and lingual gyri, which comprise the human homologue of V4. The identification of V4 was therefore based on the Talairach co-ordinates for colour centres as derived from fMRI and PET studies (see section 5.4.2; table 5-1). From the set of co-ordinates given in table 5-1, the minimum and the maximum for the left and right hemispheres were used to isolate the ROI. These co-ordinates are given in table 5-2 and their location is shown in figure 5-3. This specified area is referred to as area V4 throughout the rest of this chapter.

	x		y		z	
	Min	*Max*	*Min*	*Max*	*Min*	*Max*
Left	-38	-19	-78	-48	-22	-4
Right	20	38	-80	-50	-24	-4

Table 5-2. Talairach co-ordinates used to define area V4. They are obtained from the results of PET and fMRI studies where the cortical area implicated in the perception of colour has been defined using its Talairach co-ordinates.

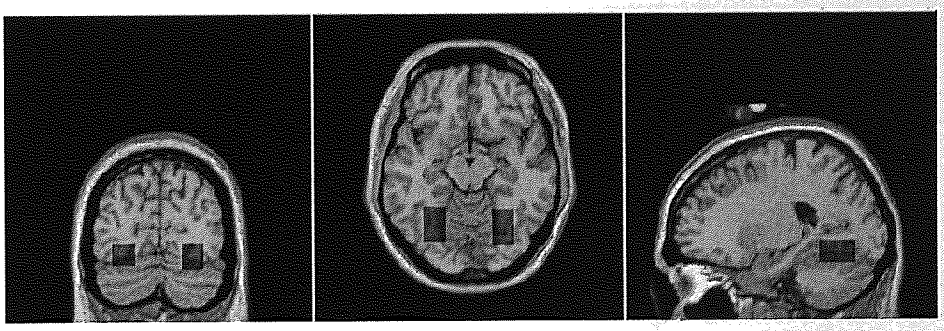

Figure 5-3. The box-shaded bilateral regions of the visual cortex corresponding to area V4 as defined by the co-ordinates in table 6-1.

. All individual data was normalised and displayed on a normalised template brain. Hence all activations of V4 were calculated in the same co-ordinate space. Activations generated in each ROI are plotted as a function of the spatial frequency. The spatial

frequency tuning curves represent alterations in cortical power in terms of synchronised and desynchronised activity in the regions of interest. As in the previous chapter, 'tuning' refers to the spatial frequency at which the response of neuronal assemblies is more pronounced. The activity in V4 in response to chromatic stimuli is then compared to that in response to the non-chromatic stimuli. The purpose of this exercise is to provide a control stimulus to which V4 activity can be compared. The control stimulus was the luminance contrast stripes used in the previous chapter and comprised of the same luminance. If as suggested, area V4 is the centre for colour processing, it is expected that this area be more activated in response to the colour, and not the luminance, stripes.

5.7 Results

The primary aim of this study was to identify the cortical sites most active in response to coloured stimuli using SAM and to determine if these correspond with regions implicated in fMRI studies to process colour. We also aimed to obtain tuning functions for the responses of V1 and V4 to spatial frequencies of the isoluminant colour patterns.

Individual SAM data

In all 7 subjects, the most pronounced activations were circumscribed within the boundaries of the visual cortex for all conditions of the stimulus, but only in the 10-20 Hz frequency band. In all other frequency distributions, peak of the SAM responses were as frequently occurring outside the boundaries of the visual cortex as inside. Moreover, the responses in the 10-20 Hz band were manifest almost exclusively in ERD. The activations shown in figure 5-4 A to D are examples of the peak cortical responses that occurred in the visual cortex in the 10-20 Hz band. On the other hand, in the higher frequency bands (the gamma range of 20-60 Hz), the peak activations were less frequent in the visual cortex and were manifest primarily as ERS. Figures 5-4 E and F are examples of the ERS in the higher frequency ranges. This pattern of cortical activation in response to the isoluminant colour stimuli was consistent across all conditions of the stimulus and for all the subjects. For most conditions, the activation of the visual cortex included the area surrounding the calcarine fissure, or area V1, and extended laterally to the extrastriate areas. However, none of the peak activations occurred inside the boundaries of region identified as the human homologue of area V4. Furthermore, in all cortical activations, it seemed that the responses were lateralised more strongly to one hemisphere. This tendency of visual cortex activations to appear lateralised occurred more frequently in the left hemisphere.

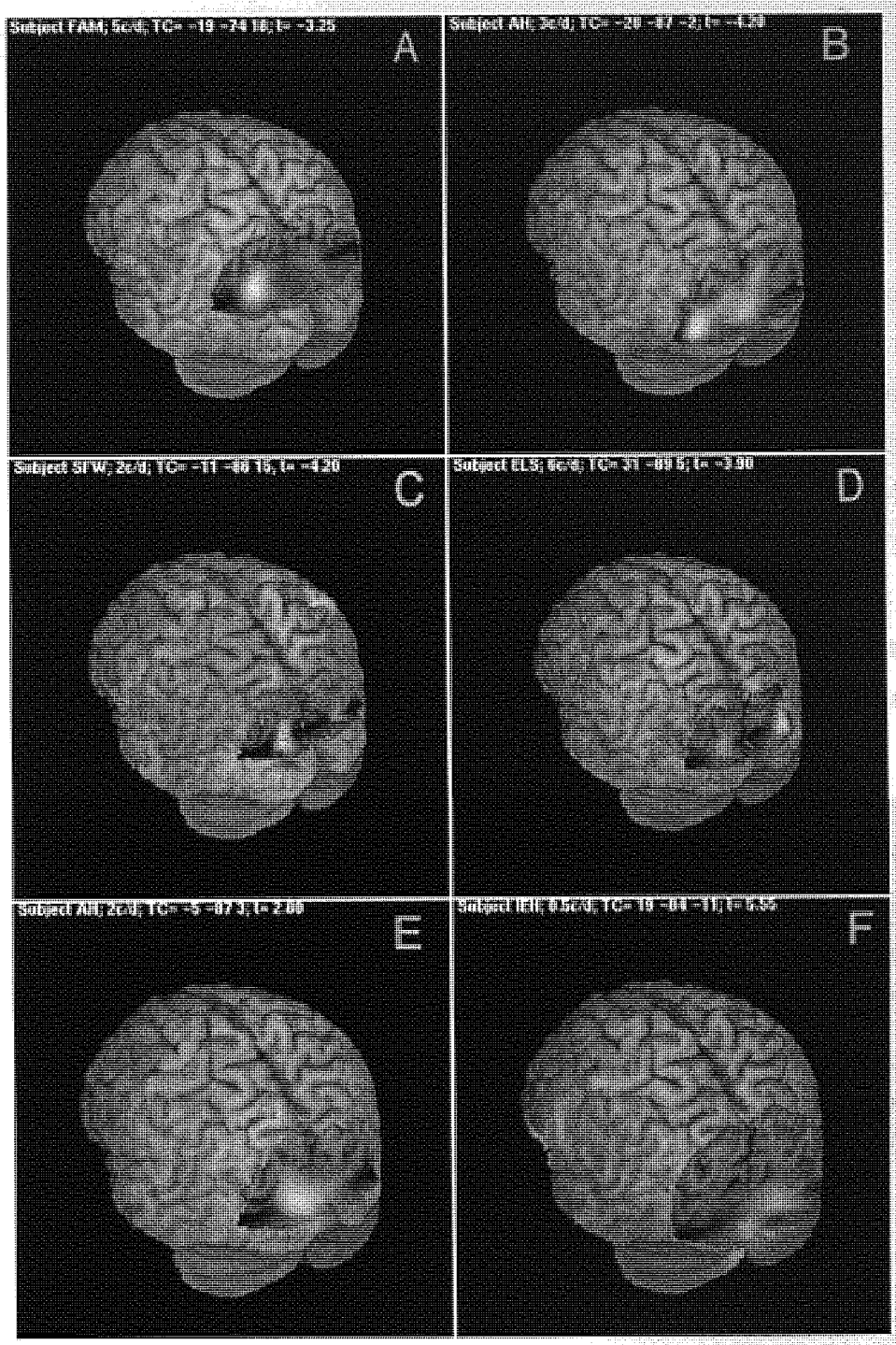

Figure 5-4. Six images that are typical of the major activation patterns confined to the visual cortex, revealed by the comparison of the isoluminant colour stripes and the control stimulus of the same mean luminance. **(A B C D)** ERDs occur in the 10-20 Hz band and are more strongly manifest in one hemisphere although both hemispheres respond to the stimulus. **(E and F)** ERS in the gamma frequency bands of 30-40 and 40-50 Hz respectively. In **E**, the peak of ERS is located within the visual cortex, while in **F** the peak response occurs in the frontal lobe. Talairach co-ordinates of the peak activations and the spatial frequency of the grating pattern are given inset. Note that none of the peak activations correspond to the area defined as human homologue of area V4.

Group SAM data

The results of the group SAM data using the simplified effects images are given in table 5-3. These values represent pronounced differences in cortical power between the active and the passive epochs generated by the coloured gratings and averaged across the 7 subjects. The corresponding average activation maps are shown in figure 5-5. These are all scaled equally at $|t|>2$ such that any comparison of the active with the passive state that produced a t value bigger than -2 and smaller than 2 is not shown. The group activations, closely resemblance the responses observed in the individual subjects (figure 5-4). There are two main trends in the pattern of activation in the visual cortex as shown in figure 5-5:

- In the 10-20 Hz frequency band, peak activations are confined within the boundaries of the visual cortex. These responses are dominated by bilateral ERDs, the peaks of which occur in the prestriate cortex, and cover the area surrounding the calcarine fissure.

- Conversely, in the gamma frequency distributions, visual cortex activations are manifest almost entirely in ERS, but they are not the most pronounced activations generated in the brain. In other words, in the gamma range, isoluminant colour gratings produce peak responses in other areas of the brain (typically in the frontal lobe), although enhanced ERS is also found in the visual cortex.

The pseudo t values representing the most pronounced activations arising from the comparison of passive and active states, shown in table 5-3, illustrate that the greatest overall magnitude of cortical responses is manifest in the form of ERD, occurring in the 10-20 Hz frequency band. Note that the ERS in the gamma range, seen in the visual cortex, are much less pronounced in comparison to those observed in response to the luminance contrast gratings (figure 4-6). In the highest frequency bands, no visual cortex activations were observed.

	Spatial Frequency of the Coloured Pattern						
FREQUENCY BAND	***0.5***	***1***	***2***	***3***	***4***	***5***	***6***
1-10 Hz	3.67	-4.33	-5.63	-5.25	-6.45	-3.43	2.91
10-20 Hz	5.74	-7.82	-8.38	-6.54	-7.08	-4.32	-3.27
20-30 Hz	5.49	4.72	-2.78	3.50	-4.80	3.67	3.72
30-40 Hz	3.29	3.29	-2.92	2.30	-2.30	3.82	3.40
40-50 Hz	2.86	4.58	4.32	2.31	2.46	6.79	6.67
50-60 Hz	3.31	3.47	2.95	2.34	2.89	3.55	3.04
60-70 Hz	-1.73	3.66	-3.18	1.93	2.81	-3.90	1.72
70-80 Hz	-1.88	2.30	-2.99	1.94	3.75	-3.03	1.58
80-90 Hz	-1.43	3.87	-3.10	2.28	2.94	-4.30	1.24
90-100 Hz	-1.69	3.18	-2.05	1.48	3.36	3.42	2.00

Table 5.3. *Pseudo t* statistics, representing the total increases or decreases in cortical power between the passive and active states, calculated for the group SAM data. Note the ERD in the lower frequency bands, and the ERS in the gamma range.

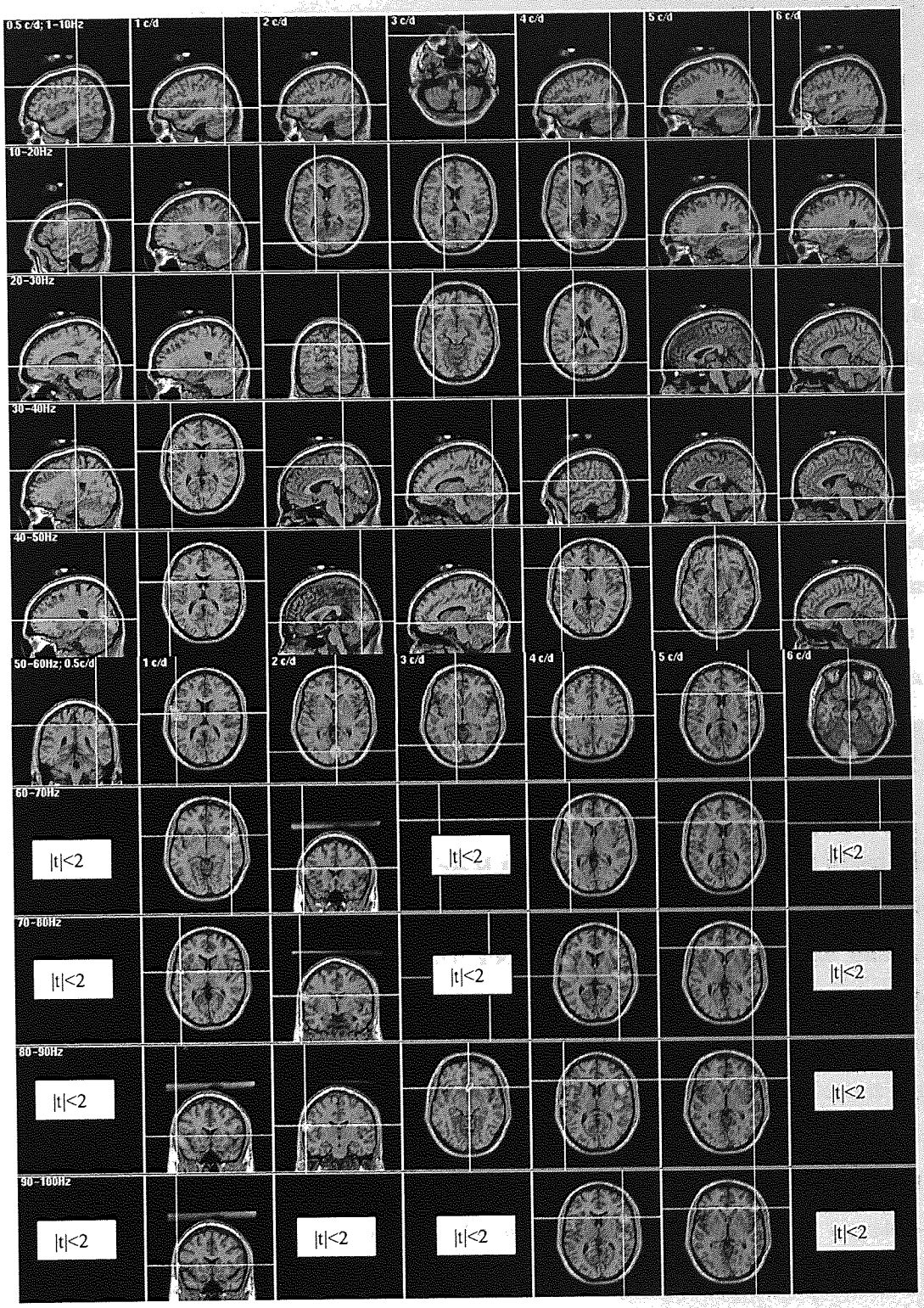

Figure 5-5. Simplified effects of group SAM responses, showing the location of activation in the specified frequency bands (rows) as a function of the spatial frequency of the pattern (columns). Note: the images are scaled for $|t|>2$ meaning that only SAM comparisons producing an absolute pseudo t value of 2 are represented; and the intersection of the crosshairs correspond to peak activations generated by the stimulus.

Cortical peaks of group SAM responses

One aim of this study was to determine the cortical locations that respond most actively to the chromatic stimuli and to see if these are consistent with those identified in fMRI studies. In order to do this, precise information regarding the organisation of the visual cortex is required for each subject. This information is not available for 6 out of 7 subjects in this study. Instead, Talairach co-ordinates for the group SAM data and for all peak activations in this study are presented in table 5-4. Clearly, none of the co-ordinates fall within the pre-defined boundaries of the V4 colour centre (table 5-2). Therefore, the chromatic stimuli do not evoked peak activations from this area, but in most cases they are well circumscribed within the borders of the visual cortex and emanate from the prestriate areas. As with the cortical responses to the luminance gratings described in the previous chapter, colour gratings too produce excitatory oscillations and ERS activity in the gamma frequency range (figure 5-5, rows 3 to 5). However, the magnitude of this response (table 5-3) and the spatial spread of cortical activations (figure 5-4) in response to the colour stimuli are smaller than those in response to contrast luminance stripes (table 5-1 and figure 5-4).

Non-Parametric statistics

As described in section 1.6.1, group SAM results using fixed effects are based upon the assumption that the responses from all subjects are normally distributed such that ERS and ERD occur with relatively similar spatial and temporal spread. Because of this, it is possible that the group image could be dominated by heightened activation of an area by a single subject resulting in failure to detect significant group effects. Therefore, a non-parametric statistical analysis was performed using SnPM, which takes into account inter-subject variances and makes no assumptions regarding the normality of data. A total of nine group-SAM comparisons, which revealed the most pronounced activations were submitted to the non-parametric statistical analysis. The results failed to reveal any statistically significant activation of the grouped data. This indicates that none of the individual data produced sufficiently high activations in response to the chromatic stimuli.

Frequency Band (Hz)	***Tailarach Co-ordinates***																			
	x	*y*	*z*	*x*	*y*	*z*	*x*	*y*	*z*	*x*	*y*	*z*	*x*	*y*	*z*	*x*	*y*	*z*	*x*	*y*	*z*
1-10	42	-40	50	-39	-74	3	-39	-74	4	25	67	-47	-39	-75	1	24	-98	-4	39	56	-48
10-20	-54	-13	36	-22	-80	27	-23	-87	13	-21	-87	15	-25	-86	6	29	-93	-4	28	-89	4
20-30	12	-77	20	21	-84	-6	22	-67	41	-45	42	-11	-21	-77	19	3	-96	-18	9	-98	17
30-40	24	-25	51	-58	13	9	5	-45	53	-10	-88	-5	54	18	18	-1	-95	-10	4	-104	-21
40-50	-18	-76	11	-66	10	15	1	-77	-1	-9	-85	-5	-52	27	9	-1	-100	-4	10	-99	-7
50-60	42	-38	50	-54	-3	15	6	-80	1	-10	-70	-3	-52	30	7	56	25	12	-1	-103	22
60-70		--		51	13	-5	-63	20	19		--		-46	37	4	60	27	12		--	
70-80		--		-53	-1	6	-70	-4	22		--		49	-18	10	59	37	3		--	
80-90		--		-65	16	6	-64	-15	22	5	21	-8	-63	31	13	57	34	0		--	
90-100		--		-66	15	6		--			--		51	16	11	57	32	-1		--	

Figure 5-4. Talairach co-ordinates for the peak SAM activations from the comparison of the active and passive states using the fixed effects model for grouping of SAM data. The corresponding images are shown in figure 5-5. Those comparisons that produced small t values ($|t|<2$) are not shown. Note that none of the co-ordinates listed above are circumscribed within the area defined as human homologue of V4 (table 5-2).

Activation of the visual areas on a flattened map of the visual cortex

For one subject in the study (KDS), information regarding the organisation of visual areas was made available. In order to determine the area in the visual cortex, which is most active in response to the chromatic stimuli, the average amount of activations in the voxels of each visual area was calculated for each of the spatial frequencies of the isoluminant colour gratings. The results are illustrated in figures 5-6 to 5-12. The activity in each visual area is shown by right and left directional arrows depicting the activity of the right and left hemispheres respectively. It can be seen from these plots that for all conditions, areas V2 and V3 are most vigorously activated while the least amount of activity consistently emanates from V4. The ERS is most prominent in the gamma range of 20-60 Hz. ERD is consistently observed in the 1-10 Hz and 10-20 Hz frequency distributions for V2 and V3. Note that for each visual area, the two hemispheres respond in very similar fashion although the activity is seemingly lateralised in some cases. There is also an effect of spatial frequency, such that, in general, the patterns of 2 and 3cpd elicit the most pronounced responses from all visual areas regardless of whether the activity is manifest as ERD or ERS. Visual cortex activations decrease dramatically in response to patterns of 5 and 6cpd.

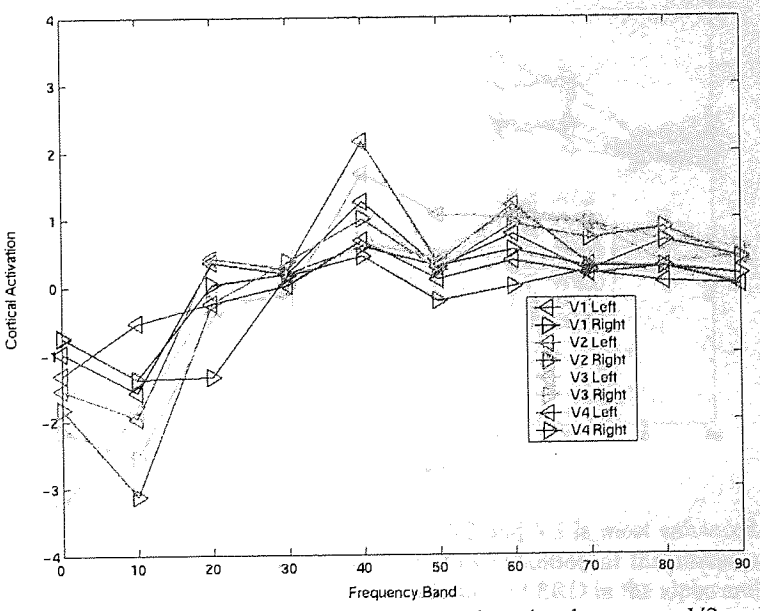

Figure 5-6. Isoluminant colour grating of 0.5cpd. The most active visual areas are V2 and V3. V4 responses are relatively minimal. ERD occurs in the 1-20 Hz range while ERS is most pronounced around 40 Hz.

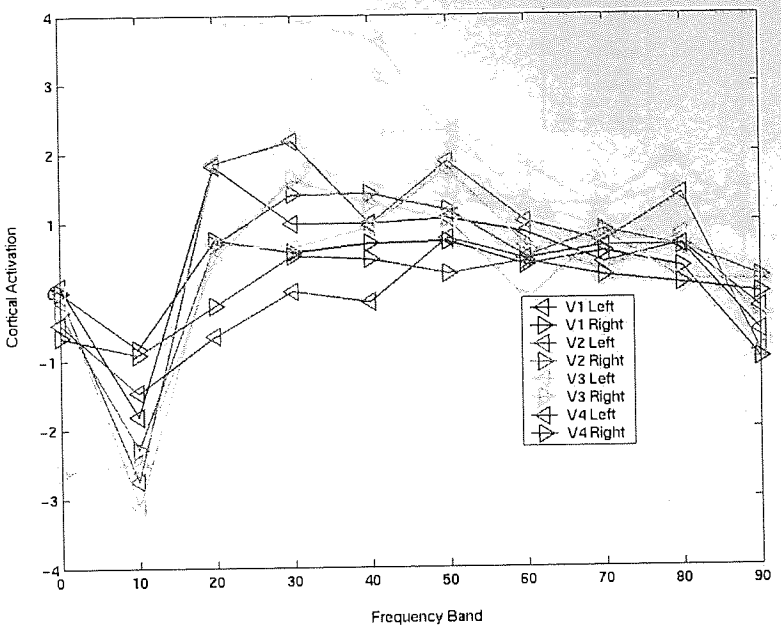

Figure 5-7. Isoluminant colour grating of 1cpd. V2 and V3 respond more vigorously to this condition of the stimulus, while V4 is relatively silent. Once again, note the pronounced ERD in the 10-20 Hz band and the ERS in the gamma range.

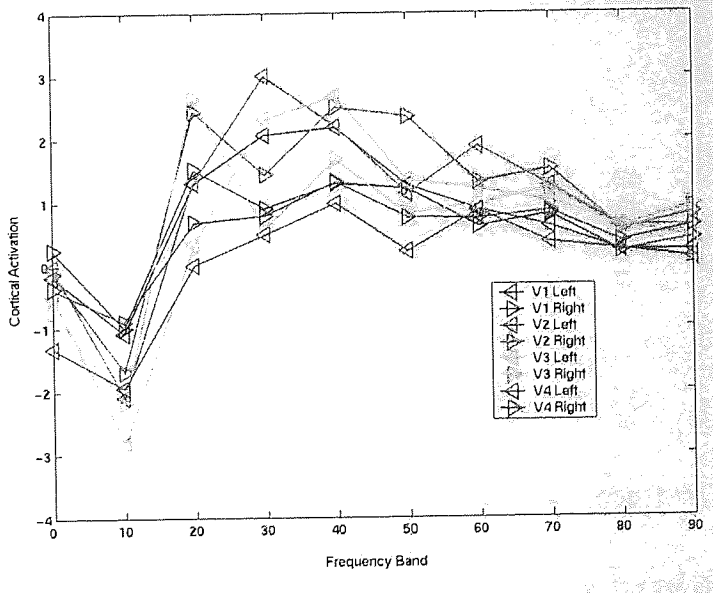

Figure 5-8. Isoluminant colour grating of 2cpd. Activity in V2 and V3 is most enhanced. Most pronounced response of V4 is the ERD that occurs in the 10-20 Hz to this condition of the stimulus. The responses of visual areas to this pattern again demonstrate ERS in the gamma, and ERD in the alpha and beta bands.

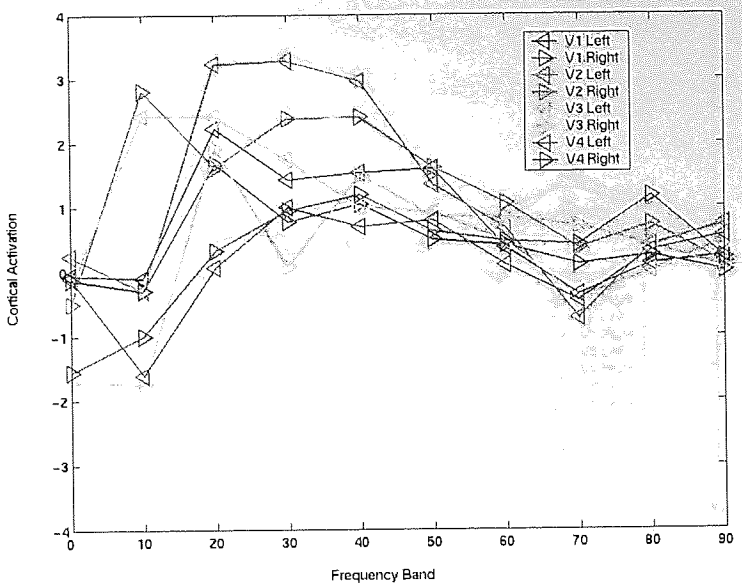

Figure 5-9. Isoluminant colour grating of 3cpd. V2 and V3 are once again the most activated of the visual areas. Note the same trend in ERD/ERS as that in response to a pattern of 2cpd.

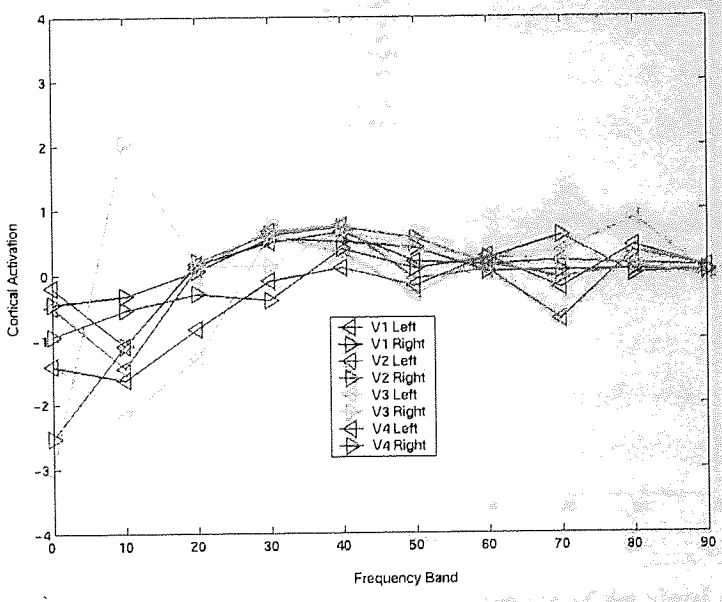

Figure 5-10. Isoluminant colour grating of 4cpd. The overall responses of the visual areas to an isoluminant colour grating of 4cpd are reduced compared to the lower spatial frequencies.

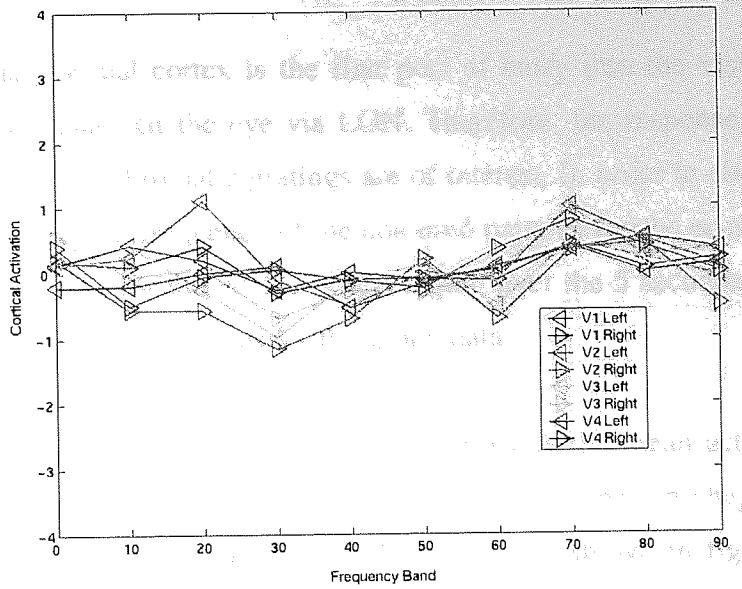

Figure 5-11. Isoluminant colour grating of 5cpd. The response of all visual areas is further reduced in response to this grating compared to the lower spatial frequencies.

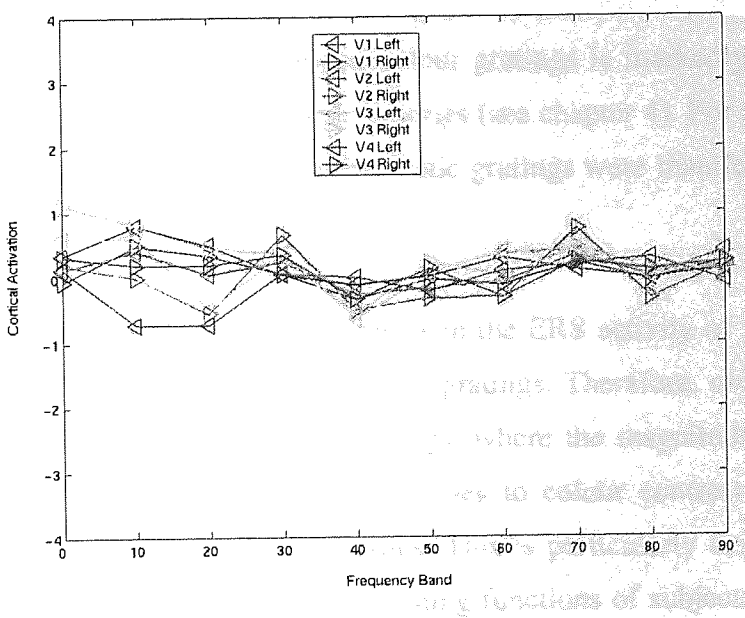

Figure 5-12. Isoluminant colour grating of 6cpd. The overall response of the visual areas is dramatically reduced in response to this condition of the stimulus.

Activations of the primary visual cortex

The primary visual cortex is the first port of entry into the visual cortex for the incoming pathways that exit the eye via LGN. Therefore, the response characteristics of this area to the different chromatic gratings are of interest. In order to obtain tuning curves as a function of the spatial frequency of the coloured patterns for the primary visual cortex, the amount of activation for the voxels of this region over the 5 seconds of activation was calculated for each subject as well as for the group data.

Individual responses of V1: For each subject in the study the mean activation within the voxels of area V1 was calculated using the procedure described in chapter 5. The tuning functions of V1 in response to the coloured gratings are shown in figure 5-13 for each subject. Similar to responses of V1 to the luminance contrast gratings (figures 4-8 to 4-14), the ERS activity in response to the coloured gratings also occurred most frequently in the gamma band of 20-60 Hz. This finding is not surprising since it has been shown that visual stimuli of various kinds produce activity in the gamma band in the visual cortex (Lopes Da Silva et al. 1970; Gray et al. 1988; Gray and Singer, 1989). However, the magnitude of the ERS activity in response to the isoluminant colour gratings is markedly less pronounced than those in response to contrast luminance gratings (see chapter 4). For most subjects, the most pronounced overall responses to the chromatic gratings were manifest as ERD, which occurred in the 10-20 Hz band.

There is little consistency among subjects in the ERS activity of V1 in response to the spatial frequency of the isoluminant coloured gratings. Therefore, unlike the responses of the same region to luminance contrast gratings, where the magnitude of synchronised activity is clearly stimulus-dependent, V1 responses to colour contrast gratings are less likely to be dependent upon stimulus properties. This is particularly evident for the ERS responses in the gamma range. However, the tuning functions of subjects AH, FAM, IEH, SFW, and VJP suggest that the ERD in the 10-20 Hz band is most pronounced in response to a grating of 1, 2, and 3cpd, which often attenuate at the lowest and highest spatial frequencies.

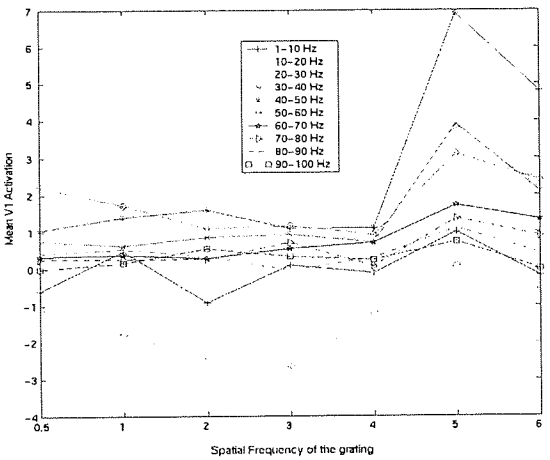

Subject AH

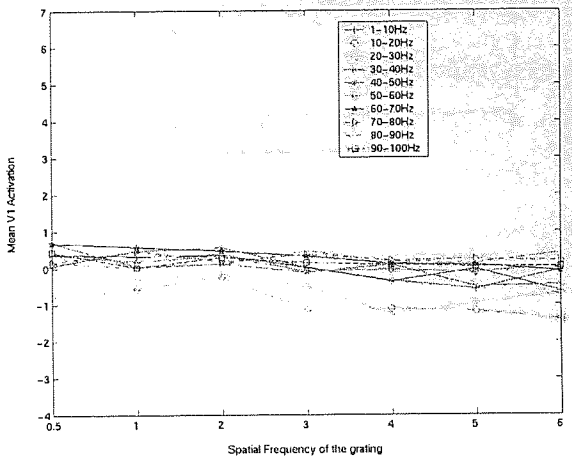

Subject ELS.

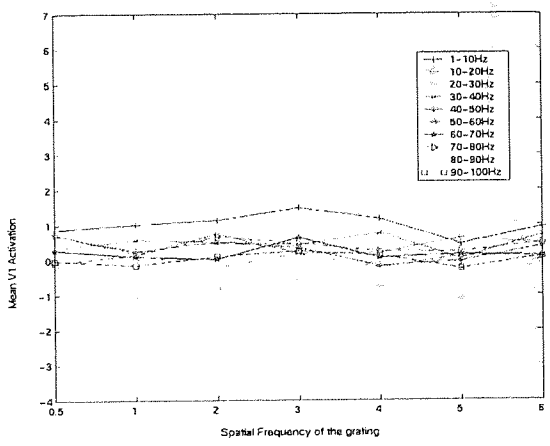

Subject IEH

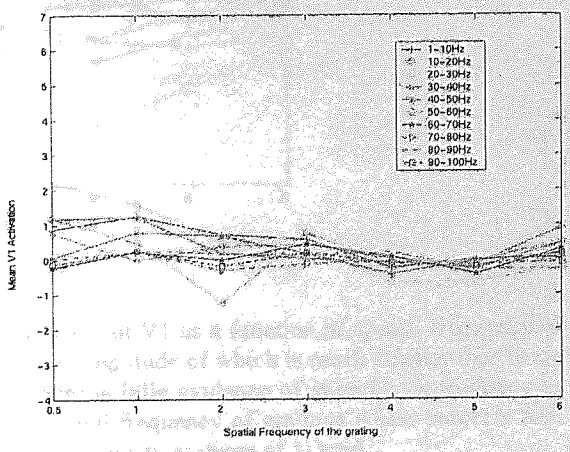

Subject FAM

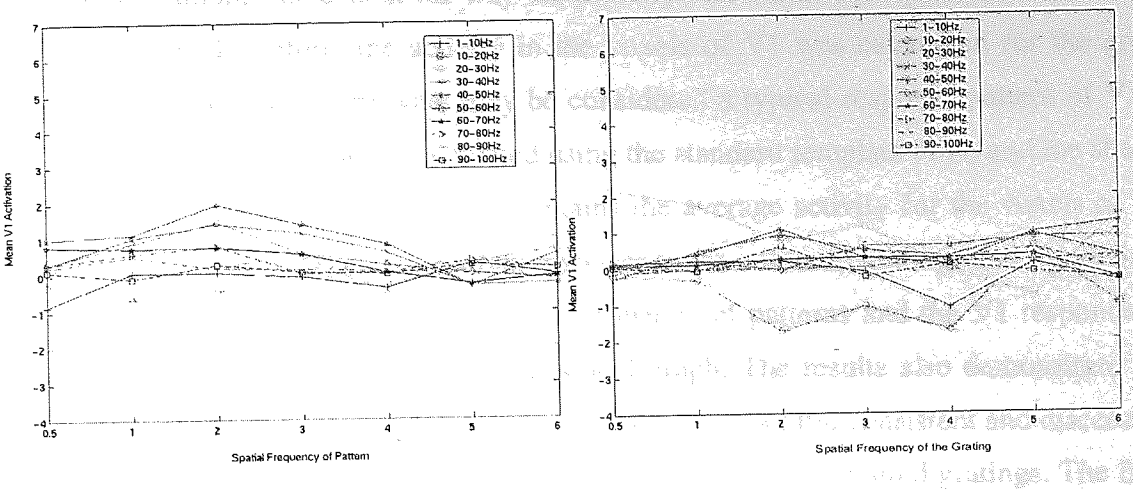

Subject KDS. **Subject SFW.**

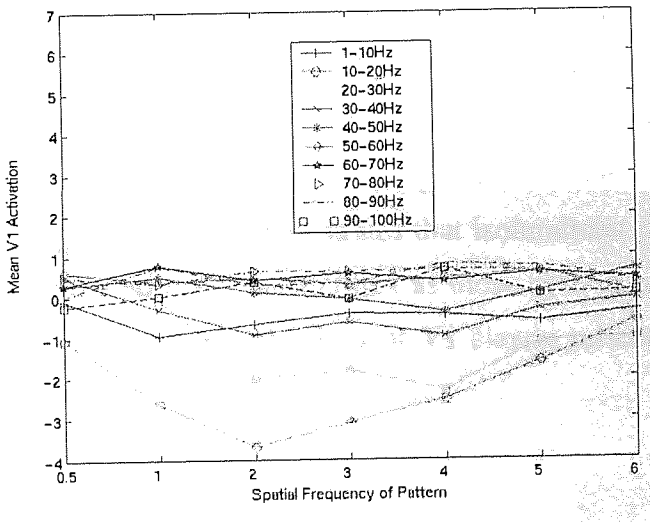

Subject VJP.

Figure 5-13. The individual tuning curves showing the responses of V1 as a function of spatial frequency of isoluminant colour gratings. There is some gamma activity the magnitude of which is much smaller than those observed in response to the luminance contrast gratings. There is little evidence of stimulus-dependency of V1 responses to the chromatic gratings. Note the effect of spatial frequency of gratings where subjects AH, FAM, IEH, SFW, and VJP show stronger ERD in the 10-20 Hz range to gratings of 1-3cpd.

Group responses of V1: The results of individual tuning functions demonstrate some degree of variability among subjects in the way the primary visual cortex responds to isoluminant colour gratings. Therefore, the activity in the voxels of V1 was calculated for the group SAM data in order to discern what may be considered a typical response pattern of V1 to the stimuli. The responses were calculated using the standard template brain and the shaded ROI as shown in figure 4-4. Table 5-5 contains the average activity for the voxels of this region over the 5 seconds of activation in response to the coloured gratings and figure 5-14, depicts the relationship between the spatial frequency of patterns and the V1 responses in the selected frequency bands in a 3 dimensional graph. The results also demonstrate that unlike group SAM responses to luminance gratings, there is little consistent and discernible effect of spatial frequency on the V1 responses to isoluminant coloured gratings. The ERD in the 10-20 Hz frequency band occurs in response to all conditions of the stimulus and is most pronounced for the grating of 2cpd. This ERD was also observed in response to viewing of the luminance stripes but the magnitude of this desynchronisation in response to colour is greater. In the higher frequency distributions, and particularly within the gamma range (20-70 Hz), V1 responses are manifest entirely in ERS. This response was also observed for luminance patterns although the magnitude of the ERS was much more pronounced. This finding once again demonstrates that isoluminant colour gratings do not exert the same effect on the primary visual cortex as those seen in response to luminance contrast gratings. Overall, the group activations of V1 clearly reflect those obtained from each individual.

	Spatial Frequency of the Coloured Pattern						
FREQUENCY BAND	***0.5***	***1***	***2***	***3***	***4***	***5***	***6***
1-10 Hz	0.10	0.90	0.35	0.61	-0.55	0.76	-0.50
10-20 Hz	-1.10	-2.85	-4.00	-2.95	-3.00	-1.05	-1.10
20-30 Hz	3.00	2.30	0	0.11	-1.63	1.10	1.25
30-40 Hz	1.00	1.40	1.20	0.80	0.55	1.55	1.30
40-50 Hz	1.30	1.90	2.45	1.23	0.13	2.80	2.55
50-60 Hz	1.95	1.30	1.70	1.20	0.92	1.77	1.51
60-70 Hz	0.90	1.10	0.85	1.30	0.65	0.67	0.50
70-80 Hz	0.50	0.77	0.95	1.00	0.52	0.90	0.80
80-90 Hz	0.80	0.85	0.35	0.47	0.62	0.65	0.15
90-100 Hz	0.20	0.05	0.55	0.30	0.41	0.20	0.10

Table 5-5. The magnitude of cortical responses calculated for the group SAM data generated in area V1 indicating the differences between the active and the passive states. Note that the most pronounced power in V1 occurs as ERD in the frequency distribution of 10-20 Hz, while ERS occurs in the gamma range. Both ERS and ERD are more pronounced for the middle spatial frequencies (1-4).

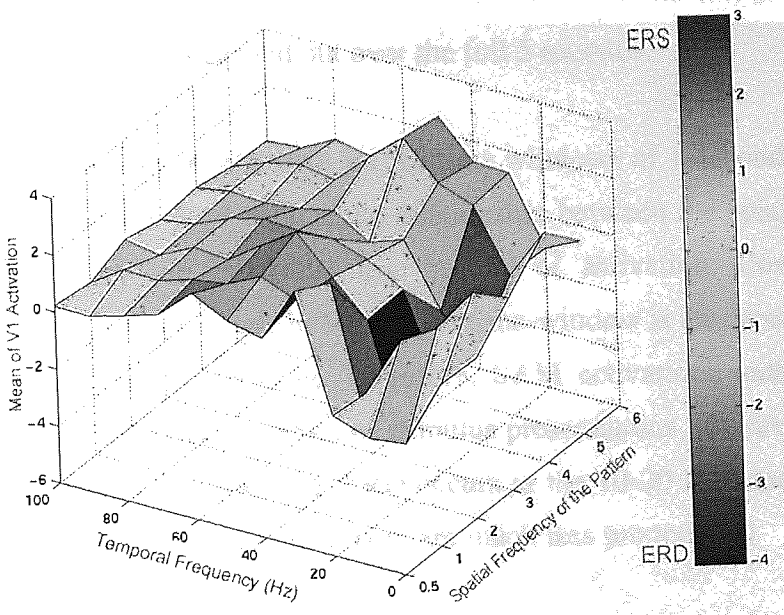

Figure 5-14. A 3D illustration of V1 activity within the specified frequency bands as a function of the spatial frequency of the coloured stripes for 5 seconds of viewing. Pronounced ERDs occur in the 10-20 Hz frequency band. Gamma range activity occurs to the colour stimuli although the magnitude of this response is weak. Note that there is no apparent or consistent effect of spatial frequency on V1 responses for isoluminant colour stripes.

Unlike the contrast luminance gratings that activated large proportions of the primary visual cortex, isoluminant coloured gratings elicited no peak activations from area V1. This is best illustrated by comparing the activations found in area V1 (table 5-4) with that found for the group SAM data (table 5-3). It is clear that the activity emanating from area V1 is considerably less than that found for the general group SAM responses over the 5 seconds of viewing. Some proportion of the group SAM activations include area V1, although the peak of these activations are in the extrastriate cortex. This finding is somewhat surprising since V1 is shown to be the first port of entry in the visual cortex for the sensory afferents (the M and P pathways) that leave the eye. From there, V1 and to some extent V2, act as segregator of the incoming information that feeds the specialised areas where the specific visual attributes, such as colour, motion, and form are rendered for more detailed processing (Livingstone and Hubel, 1987b; 1988; also see section 3.6.2). If this hypothesis is indeed true, it is expected that activity in V1 be more pronounced for the initial phase of the passive viewing. This possibility was assessed by changing the application of time-windows over which the data is analysed and calculating the SAM activations over the first second of each epoch. It was expected that the magnitude of responses, in terms of ERS and ERD, be more pronounced for the initial 1 second of viewing than when the analysis is carried out over the full 5 seconds.

The average activations of voxels in V1 for time windows of 1-second duration are shown in table 5-6, and figure 5-15 depicts the relationship between the spatial frequency of stripes and V1 activity for the initial first second of activation. Contrary to the expectation, the mean activity of voxels in V1 for this time-window is less pronounced than that found for the 5 seconds of viewing. Therefore, SAM activations indicate that V1 activity is best measured for longer duration of stimulus presentations. However, similar to the results found for 5 seconds of viewing, ERD occurs in the 10-20 Hz band and ERS in the gamma range, although the magnitude of both are much less pronounced

	Spatial Frequency of the Coloured Pattern						
FREQUENCY BAND	***0.5***	***1***	***2***	***3***	***4***	***5***	***6***
1-10 Hz	1.15	0.76	0.55	0.50	1.05	0.45	0.55
10-20 Hz	-0.80	-0.70	-0.90	-2.65	-1.10	-0.15	-0.75
20-30 Hz	0	-0.20	-0.65	-1.20	-0.35	0.45	-0.30
30-40 Hz	0.30	0.90	-0.15	-0.45	0	0.90	-0.45
40-50 Hz	0.70	0.45	0.65	0.30	-0.30	0.90	0.55
50-60 Hz	1.40	1.50	0.95	0.50	0.70	0.95	0.70
60-70 Hz	1.10	0.55	1.45	0.35	0.45	0.35	0.10
70-80 Hz	0.90	1.25	0.85	0.65	0.50	1.00	-0.25
80-90 Hz	0.85	0.55	0.77	0.85	0	0.85	0.40
90-100 Hz	-0.45	0.10	0.15	0.30	0.70	0.45	0

Table 5-6. Mean activity calculated for voxels of V1 over the first 1 second of passive viewing of chromatic stripes. Compared to the activation calculated for the entire course of a stimulus presentation, these activations are consistently less pronounced.

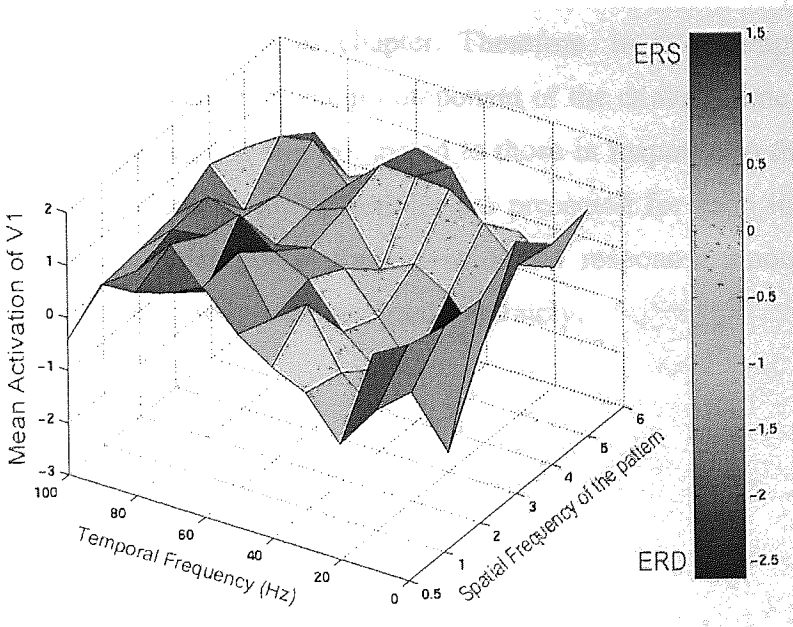

Figure 5-15. A 3D representation of the relationship between the spatial frequency of stripes and mean activity for V1 within the selected frequency bands for 1-second of activation. Note that the ERD occurring in the 10-20 Hz band and the ERS in the 20-80 Hz gamma range.

The involvement of area V4 in colour processing

Although none of the peak activities that resulted from the viewing of colour patterns occurred within the area V4, it is demonstrated in figure 5-4 that visual cortex activations in a number of SAM comparisons extend beyond the areas of peak activation, and in some cases cover a large part of the visual cortex. Therefore, in an attempt to quantify the amount of activity emanating from area V4 in response to the chromatic gratings, the activity within the bilateral regions was calculated as a function of the spatial frequency of the patterns. However, activations confined to area V4 in response to the colour gratings tell us little about the amount of cortical power that is uniquely generated in response to the colour component of the gratings. Precise evaluation of the responses generated in V4 by the colour gratings requires that they be compared to the activation of the same regions in response to a control stimulus. If as suggested, V4 is indeed a colour processing area, it is expected that it exhibits higher magnitude of ERD/ERS in response to the colour but not the control stimuli. Conversely, if the activity in these regions is not different from each other, we can conclude that the proposed region of V4 is not a specialised cortical area for colour processing. This control stimulus was provided by the contrast gratings used in the previous chapter. Therefore, in an attempt to assess the involvement of V4 in processing the colour component of the stimuli alone, the amount of activity in the bilateral V4 regions was compared to those in response to the high contrast black and white gratings. Results of V4 activity are presented for each individual in the study in order to assess variability in the extent of V4 responses among the sampled population and the group data were also analysed separately.

Individual activations of V4: For each subject in the study, the data was normalised and displayed on a template brain, also normalised in the Talairach space, and hence the ROI used was the same for each set of data from the 7 subjects. Figures 5-16 to 5-22 depict the relationship between responses to the chromatic (red lines) and the control (black lines) stimuli, reflecting the average amount of activation in the voxels of bilateral V4 regions. For the colour condition, more pronounced ERD responses dominate the frequency distribution of 10-20 Hz. Therefore, this response is more likely as a consequence of processing the colour component of the stimuli. As also shown in the group SAM images (figure 5-5), ERD responses to colour gratings are pronounced within the visual cortex and dominate the lower frequency bands. Therefore, although this desynchronised activity may not originate from area V4, it dominates the visual cortex in general, evoking similar responses that vary in magnitude.

Another consistent feature of V4 response in almost all subjects is the occurrence of ERS in the gamma range (20-70 Hz) in response to both types of stimuli. However, as with the individual data for area V1 this ERS is more pronounced as a consequence of the achromatic luminance stripes. On the other hand, gamma frequency ERD is also seen in response to the chromatic stripes in some subjects. Gamma frequency ERS in neuronal populations in the visual cortex have been widely reported in response to a variety of visual stimuli (Gray and Singer, 1989). For most subjects, SAM measurements indicate no apparent and consistent effect on responses of V4 as a consequence of changing the spatial frequency of the isoluminant colour stripes. However, there are some consistent changes in ERS as a function of spatial frequency of the contrast stripes where the patterns of 1-4cpd produce more pronounced ERS in the gamma range. This pattern of V4 activation resembles the responses of V1 to the same stimulus.

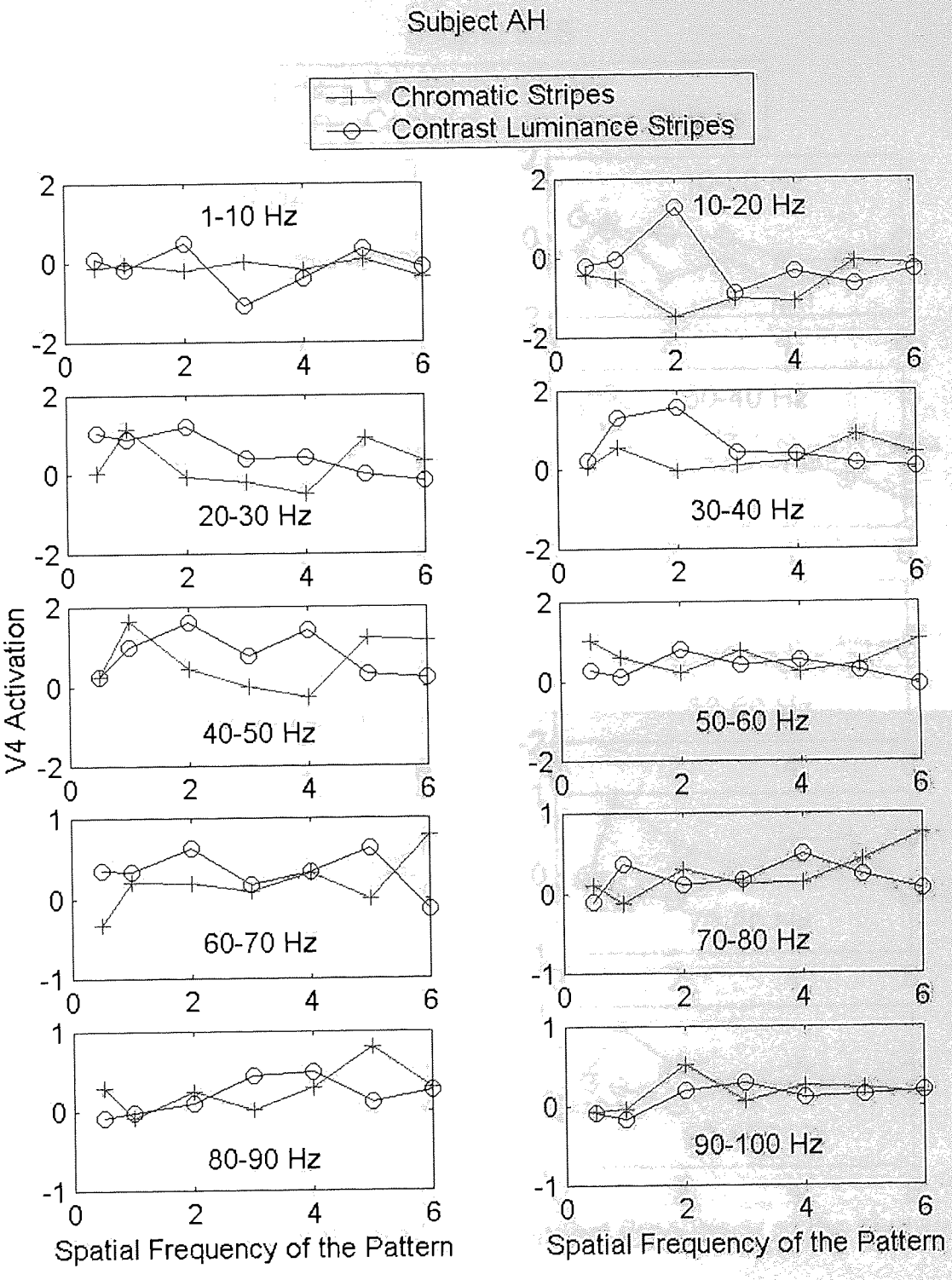

Figure 5-16. In the 10-20 Hz frequency band, pronounced ERD and ERS occur in response to the chromatic and achromatic stripes of 2cpd respectively. In comparison to the colour stimuli, the luminance patterns produce more pronounced ERS in the gamma range (20-70 Hz).

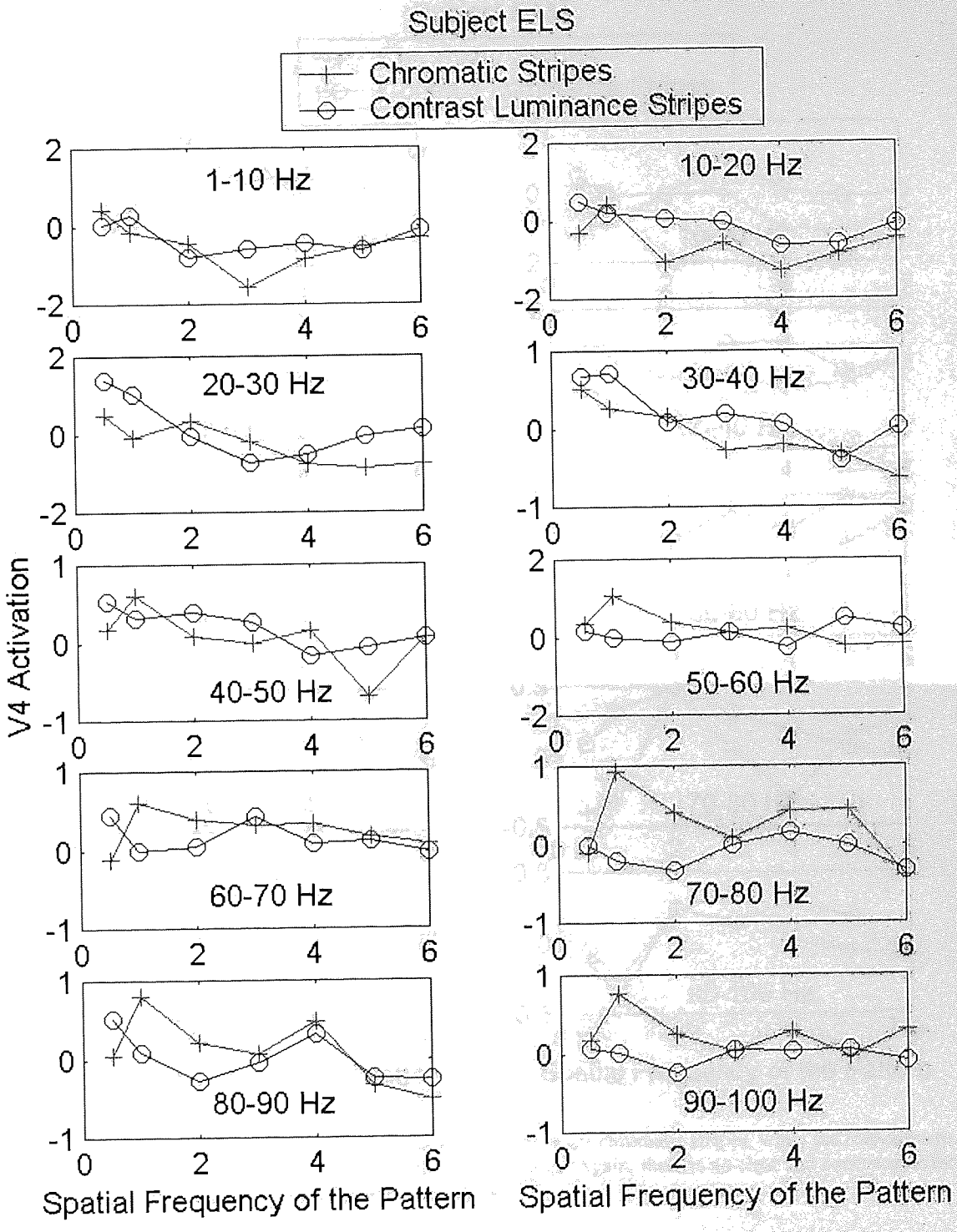

Figure 5-17. The 10-20 Hz frequency distribution produces the strongest ERD for the colour stimuli, while it seems that for this subject, both conditions of the stimulus produce equally pronounced ERS in the gamma band.

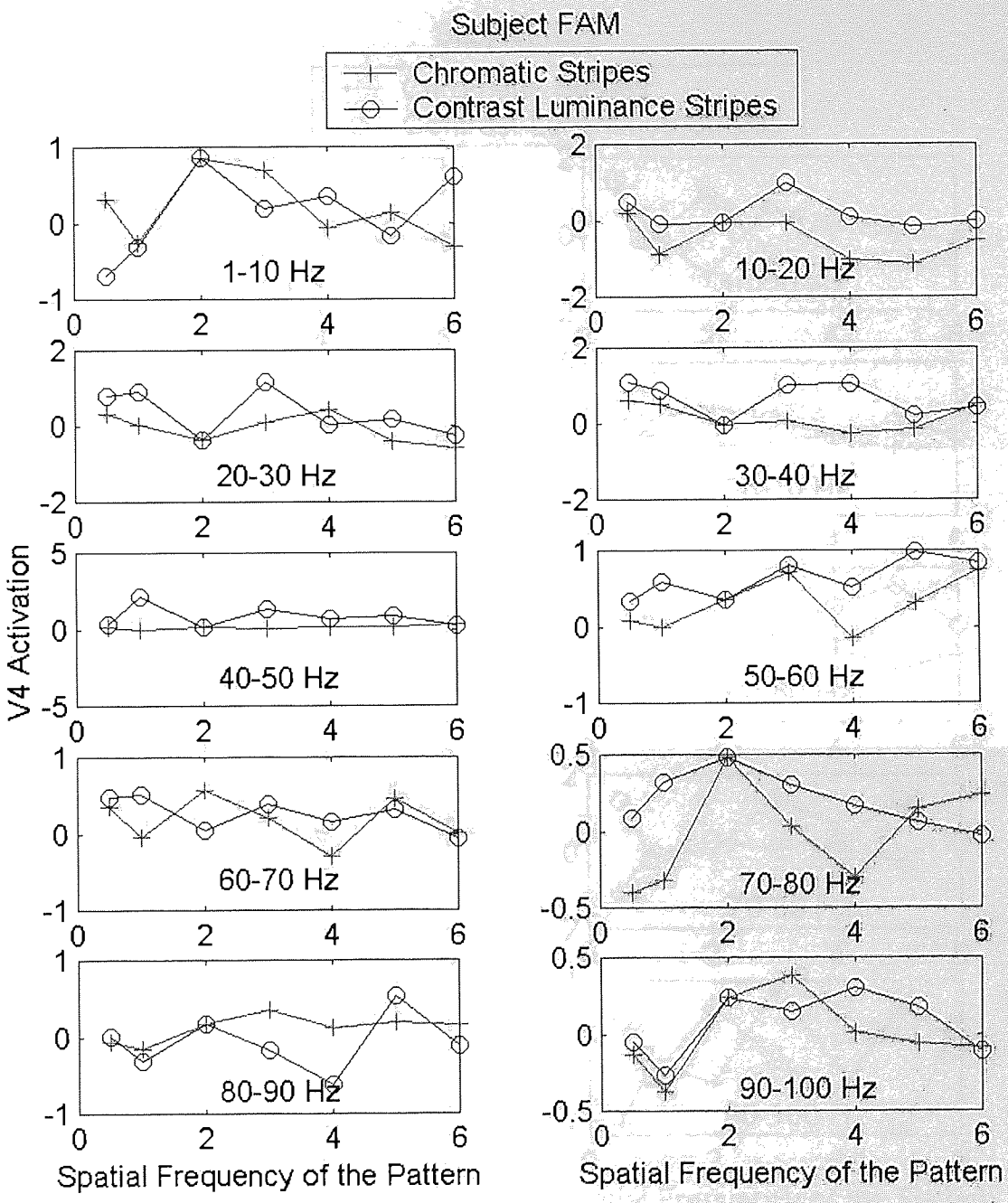

Figure 5-18. ERDs dominate the lowest frequency distributions for chromatic stripes, while the responses to the achromatic stimuli are most pronounced in the gamma range. Again, there is no clear and consistent effect of spatial frequency of the stripes on the responses of V4.

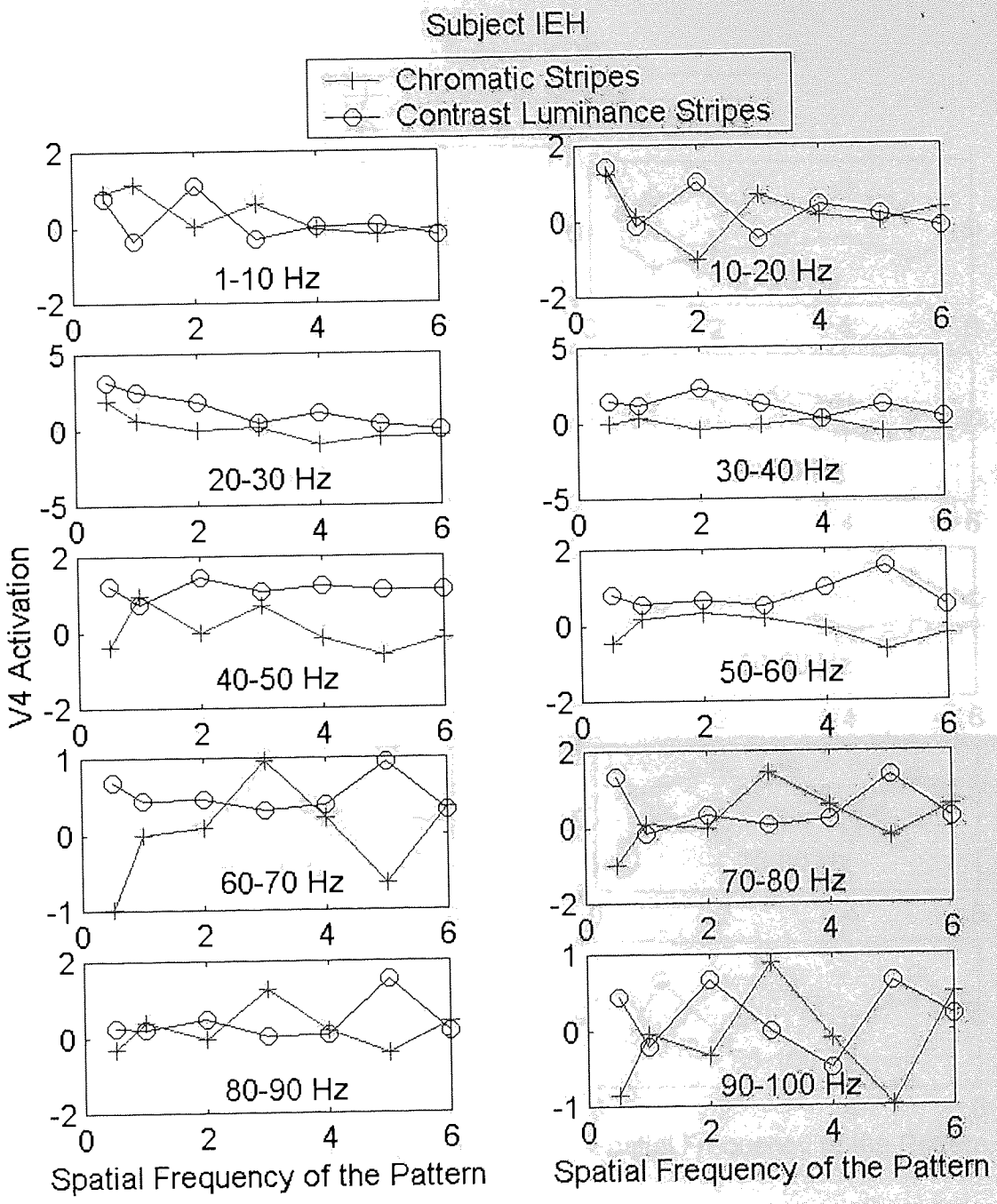

Figure 5-19. In the gamma range the most pronounced responses occur in the 40-50 Hz for the achromatic stimuli. For the chromatic condition, stripes of 3 cpd produce the largest magnitude of ERS. The strongest ERD occurs in the 10-20 Hz.

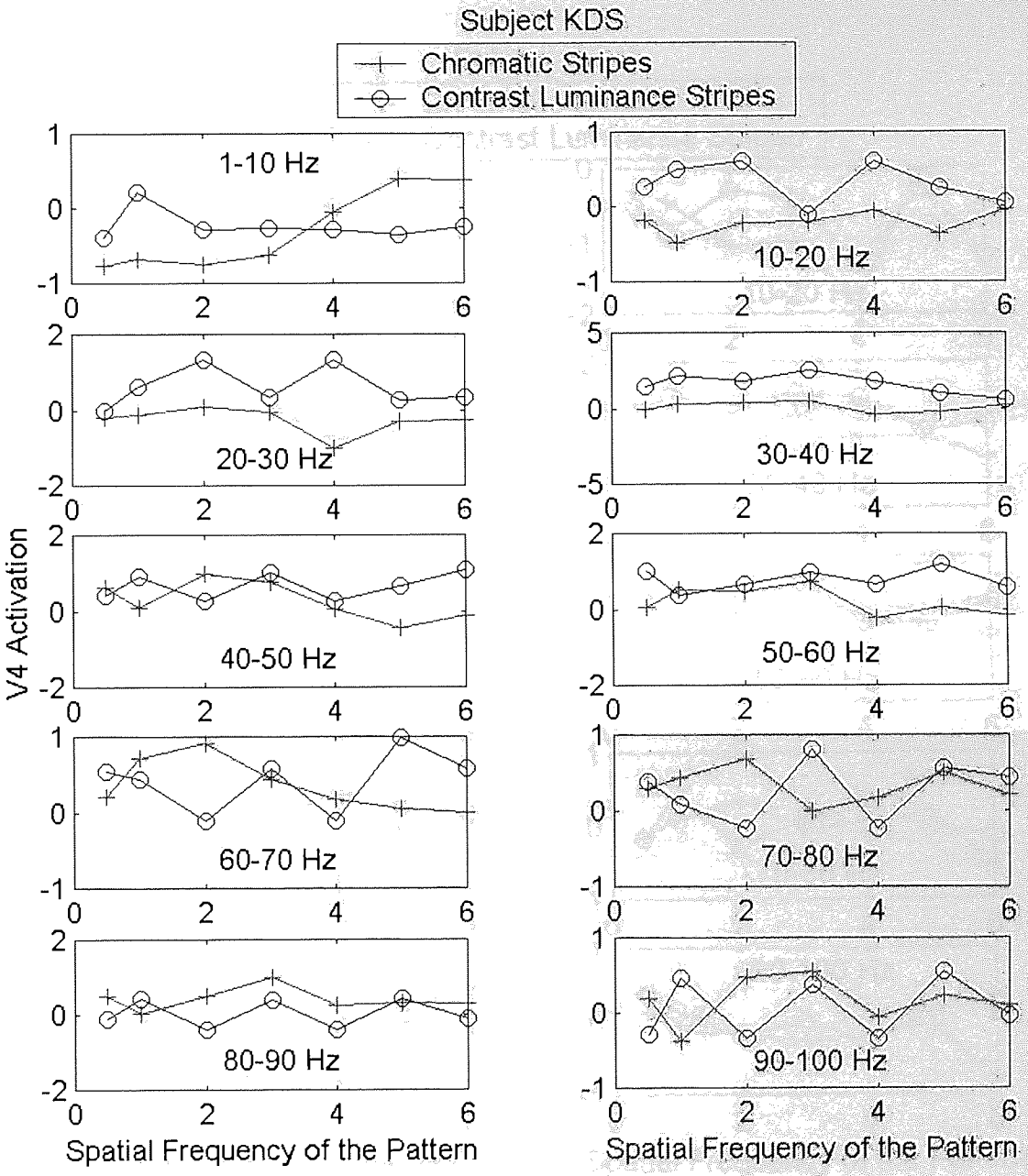

Figure 5-20. ERD is prevalent in the 10-20 Hz band for the colour stripes. For the achromatic stripes, the gamma band of 20-30 Hz produces the largest magnitude of ERS. There is again no apparent difference between the spatial frequencies of the stripe patterns in the responses they generate in area V4.

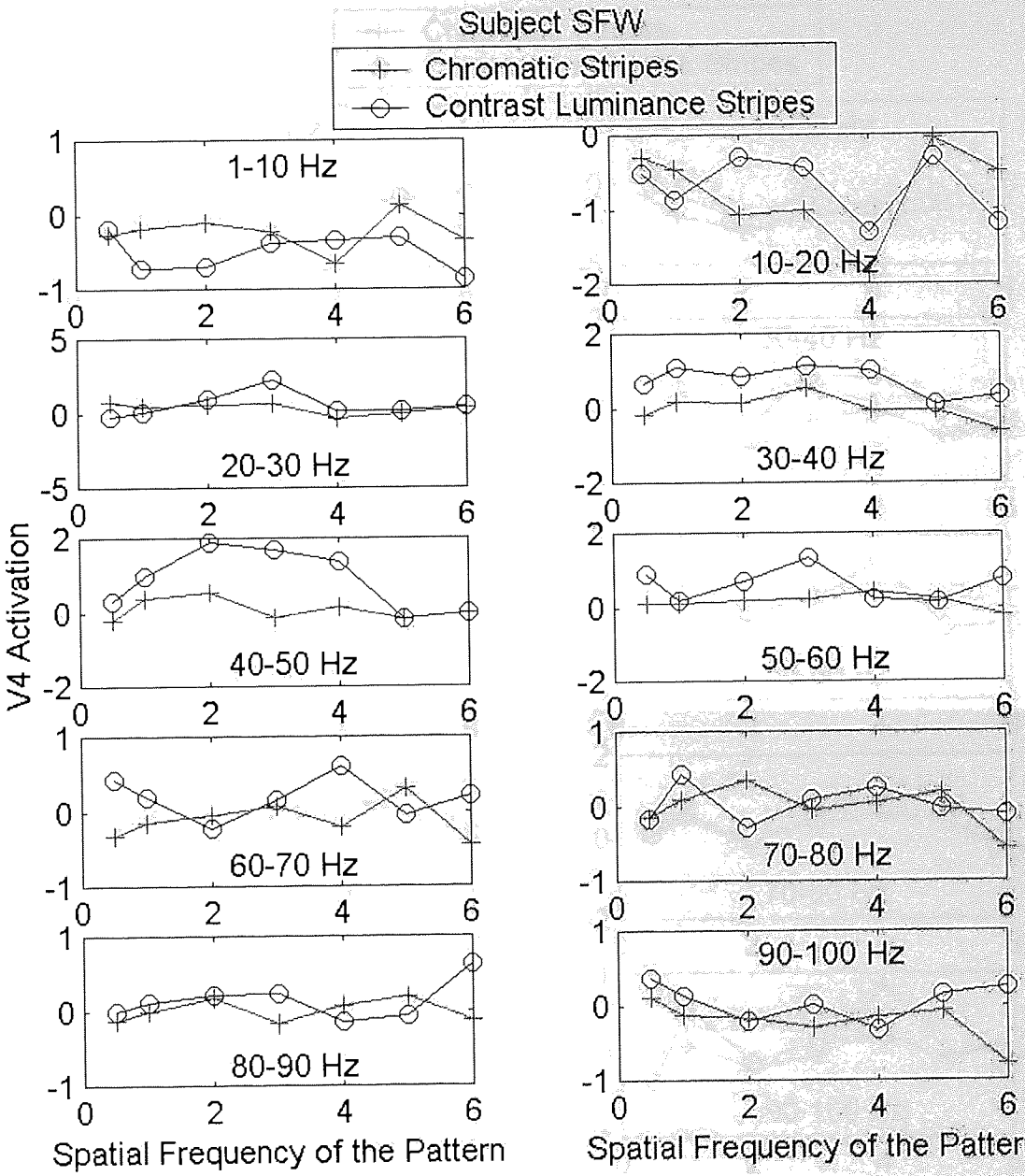

Figure 5-21. The strongest response to the colour stripes occurs in the 10-20 Hz band. In the gamma range, the colour stripes produce little deviation from zero. For the contrast luminance patterns, there is an increase in the magnitude of ERS in the gamma range that coincides with the middle spatial frequencies of the stripes (2-4 cpd).

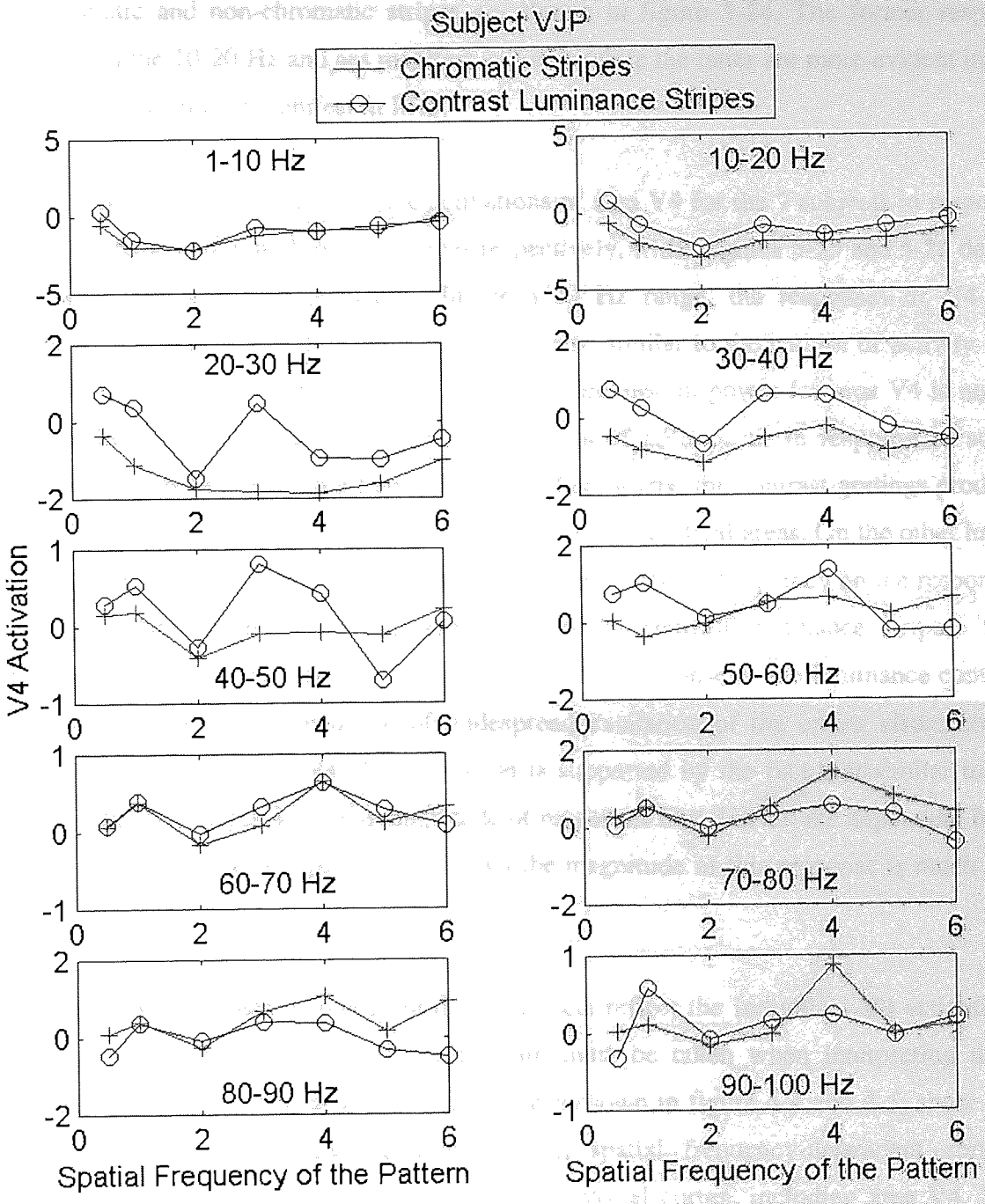

Figure 5-22. In this subject, isoluminant colour stripes produce ERDs in many of the frequency bands, including gamma. The non-chromatic stripes produce ERS in the gamma range.

Group averages of activations in V4: For the group SAM data, the response curves of V4 to the chromatic and non-chromatic stripes are shown in figure 5-24. The former respond optimally in the 10-20 Hz and are manifest in ERD, while the latter are more evident in the 20-60 Hz range and are manifest in ERS.

Tables 5-7 and 5-8 contain the activations of area V4 for the 7 subjects in response to the chromatic and non-chromatic stripes respectively, while figures 5-25 and 5-26 depict the 3-way relationship more clearly. In the 1-20 Hz range, the responses of V4 are dominated by ERDs for both conditions. This is also similar to the pattern of activity that emanates from V1, although the magnitude of the decrease in power for area V4 is not as great as that found for area V1. Small magnitudes of ERS occur in response to some coloured gratings in the gamma frequency range, but clearly, the contrast gratings produce relatively much higher synchronisation in the same visual cortical areas. On the other hand, there is no apparent and consistent effect of the patterns' spatial frequency on the responses of V4 to either isoluminant colour stripes or to the contrast luminance stripes. This consistent pattern of high frequency synchronisation in response to the luminance contrast stripes is perhaps the consequence of widespread excitation of the entire visual cortex (figure 4-5) including area V4. This assertion is supported by the fact that similar to the responses of V1 (figures 4-15) the magnitude of responses found in V4 are dependent upon the spatial frequency of the patterns, although the magnitude of this response is much less pronounced.

The averaged activations from the 7 subjects reflect the individual V4 activations shown in figures 5-22 to 5-28. However, care must be taken when interpreting these findings. Individual as well as group SAM images shown in figure 4-4 and 4-5, show that the contrast luminance stripes generate strong, spatial frequency-dependent cortical synchronisations that spread throughout the entire visual cortex, including area V4. It is likely that rather than reflecting the activation of V4 due to the stimulus, these activations are the results of the smoothness of SAM images.

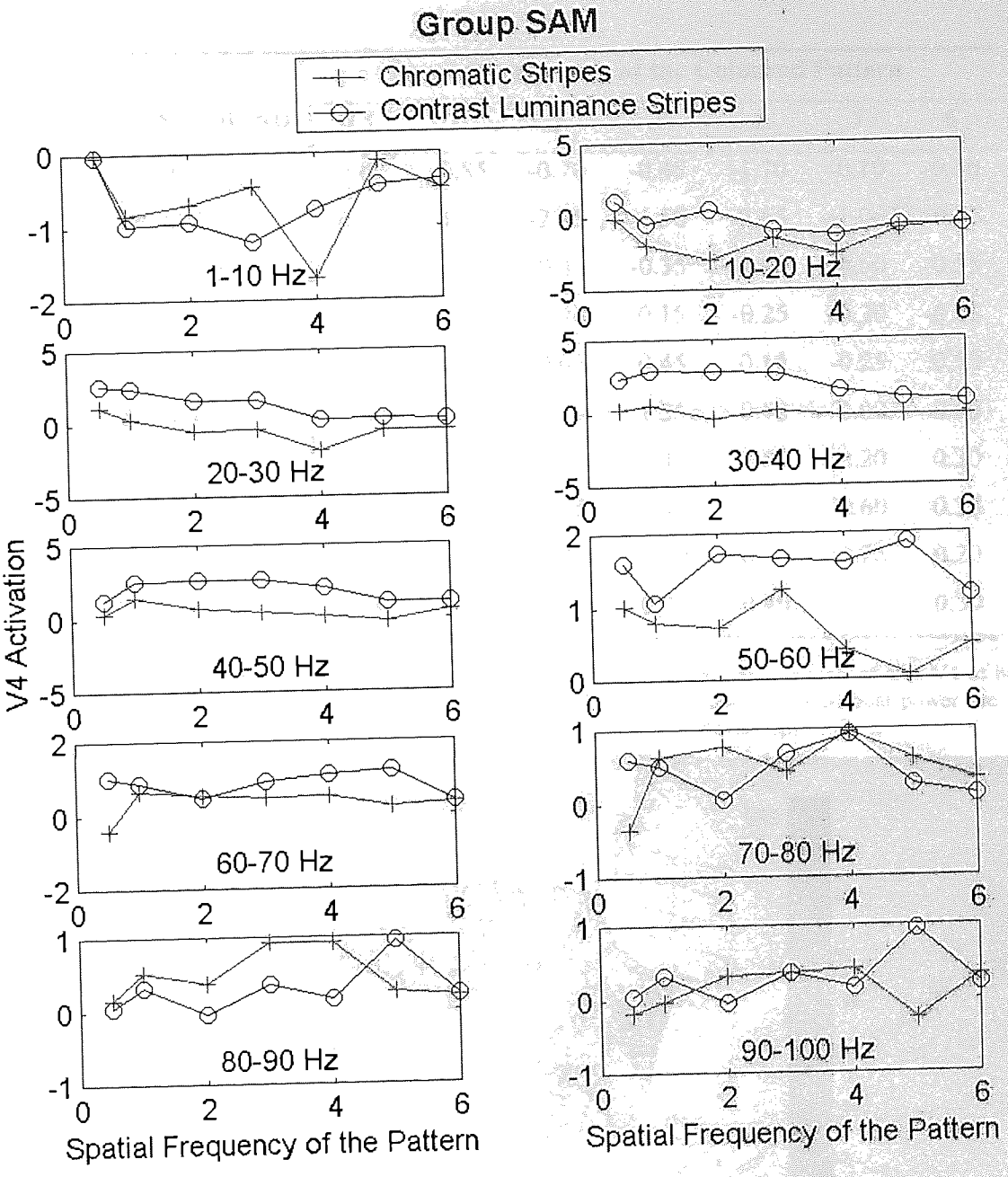

Figure 5-23. Group SAM activations of V4 reflecting the average of the individual responses. In the 10-20 Hz band, the magnitude of ERD in response to the coloured stripes is most pronounced compared to the luminance gratings. On the other hand, strong ERS occurs in the 20-60 Hz gamma range in response to the non-chromatic, but not to the chromatic stimuli.

	Spatial Frequency of the Coloured Pattern						
FREQUENCY BAND	***0.5***	***1***	***2***	***3***	***4***	***5***	***6***
1-10 Hz	0.00	-0.85	-0.70	-0.45	-1.70	-0.10	-0.50
10-20 Hz	0.10	-1.95	-2.95	-1.50	-2.65	-1.00	-0.55
20-30 Hz	1.10	0.35	-0.45	-0.35	-1.90	-0.50	-0.55
30-40 Hz	0.20	0.50	-0.40	0.15	-0.25	-0.20	-0.25
40-50 Hz	0.30	1.45	0.65	0.45	0.15	-0.25	0.50
50-60 Hz	1.00	0.80	0.70	1.25	0.40	0.00	0.50
60-70 Hz	-0.40	0.65	0.55	0.45	0.50	0.20	0.30
70-80 Hz	-0.35	0.65	0.75	0.45	0.95	0.60	0.35
80-90 Hz	0.15	0.50	0.40	0.90	0.90	0.25	0.20
90-100 Hz	-0.20	0.00	0.30	0.35	0.40	-0.25	0.30

Table 5-7. Average activity calculated for the responses to colour gratings in voxels of area V4 of both hemispheres using simple effects group SAM images. Overall, the changes in cortical power are not pronounced and there is little consistent effect of spatial frequency of the pattern.

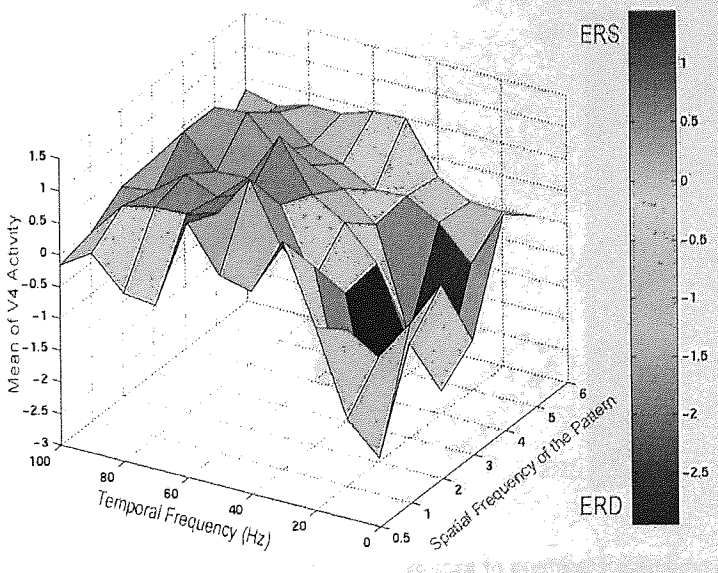

Figure 5-24. A 3D representation of bilateral V4 activity in response to colour stripe patterns for the group data, representing V4 activity as a function of spatial frequency of the stripes. As with the individual response curves, decreases in cortical power are most evident in the lower frequency ranges of 1-20 Hz, while higher frequency bands produce small magnitudes of ERS.

	Spatial Frequency of the Contrast Grating						
FREQUENCY BAND	***0.5***	***1***	***2***	***3***	***4***	***5***	***6***
1-10 Hz	0.00	-1.00	-0.95	-1.20	-0.75	-0.45	-0.35
10-20 Hz	1.00	-0.45	0.40	-1.00	-1.35	-0.65	-0.70
20-30 Hz	2.60	2.40	1.60	1.60	0.20	0.35	0.20
30-40 Hz	2.40	2.90	2.80	2.75	1.50	0.95	0.75
40-50 Hz	1.25	2.50	2.55	2.60	2.10	1.10	1.10
50-60 Hz	1.60	1.10	1.70	1.65	1.60	1.85	1.15
60-70 Hz	1.00	0.85	0.45	0.90	1.10	1.20	0.35
70-80 Hz	0.60	0.50	0.00	0.67	0.90	0.25	0.10
80-90 Hz	0.00	0.35	0.00	0.35	0.15	0.95	0.20
90-100 Hz	0.00	0.35	0.00	0.35	0.15	0.95	0.20

Table 5-8. Average activity within bilateral area V4 for the luminance pattern viewing. ERD responses are seen in the two lower frequency distributions. Cortical power increases for the middle distributions of gamma (30-60 Hz).

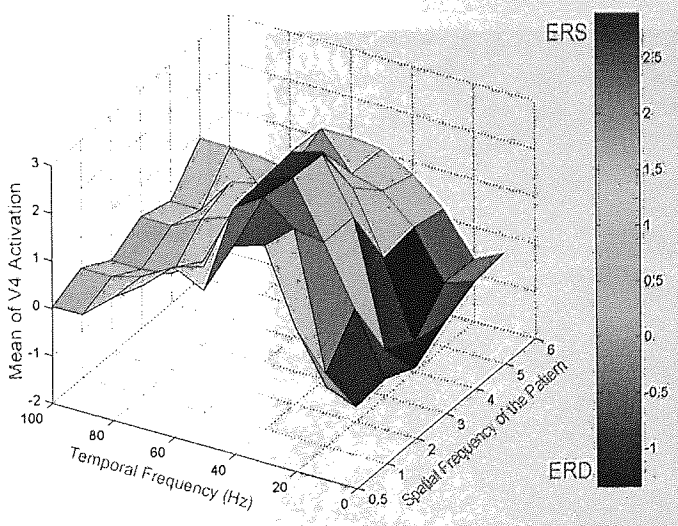

Figure 5-25. A 3D representation of bilateral V4 activity in response to contrast luminance stripe patterns for the group SAM data representing V4 activity as a function of spatial frequency of the stripes in the specified frequency bands. Note that similar to the responses of V4 to the same stripes, the ERS in the gamma range is dependent upon the spatial frequency of the pattern.

Power Spectrum Analysis

It can be seen from the results presented so far that when viewing a chromatic stimulus for 5 seconds, the area known as the human homologue of area V4 is not preferentially activated, either in comparison to the other visual areas or in comparison to non-chromatic stimuli. What these activations reflect, however, is the average of cortical activity in any given region for the entire duration of stimulus presentation. Therefore, in one subject (FAM), time-frequency analysis was performed using two virtual electrodes placed at two different locations. The location of these voxels and their Talairach co-ordinates are given in figure 5-27. The first represented the voxel showing the peak of cortical activation between the active and passive SAM states in response to a chromatic grating of 1cpd in the 10-20 Hz band, which was manifest as ERD. The location of this voxel was in proximity to the primary visual cortex. The second voxel represented the highest magnitude of stimulus-related power change in area V4, which also occurred as ERD. The time-frequency spectrograms spanned for 10 s with the first and the second 5 s representing the passive (control stimulus) and the active (chromatic grating) states respectively.

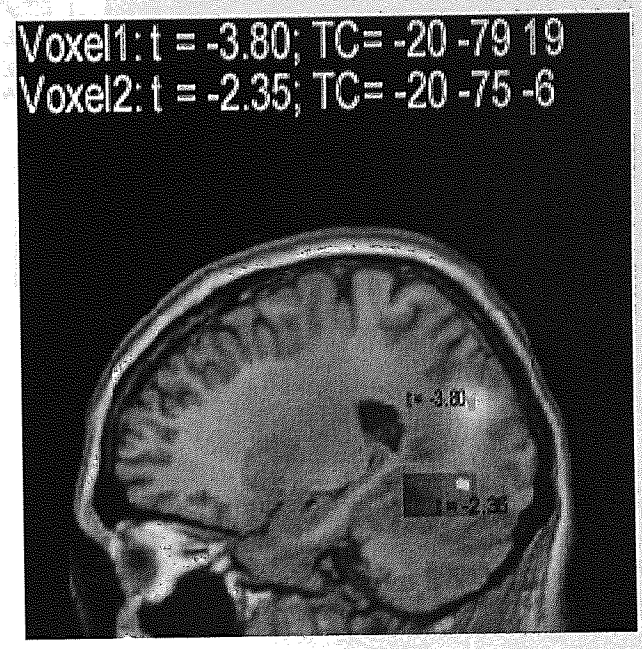

Figure 5-26. The location of the two virtual electrodes used to investigate the time-series of the event-related power changes in the cortex. The t values and the Talairach co-ordinates are given inset. Both voxels are within the same cluster that resulted from the viewing of an isoluminant colour grating at 1cpd in subject FAM. Note the voxel in yellow is within the box-shaded area corresponding to the human homologue of area V4.

The results of the spectrograms are shown in figure 5-28. Figure 5-28a shows the spectrogram for the voxel near V1 that represents the highest magnitude of cortical response. The top panel shows an increase in power at approximately 20 Hz, which initially disappears with the onset of the active state. For the remainder of the active state the power at 20 Hz is reduced compared to that in the passive state. This is clearly demonstrated in the bottom panel, which shows the amount of power in the 10-30 Hz band plotted as a function of time. Figure 5-28b shows the spectrogram for the voxel in area V4. Similar to the voxel at the location of the peak response shown in 5-28a, decrease in power is noticeable around the 20 Hz band with the onset of the active state (top panel). The bottom panel plots the amount of power in the 10-30 Hz band as a function of time.

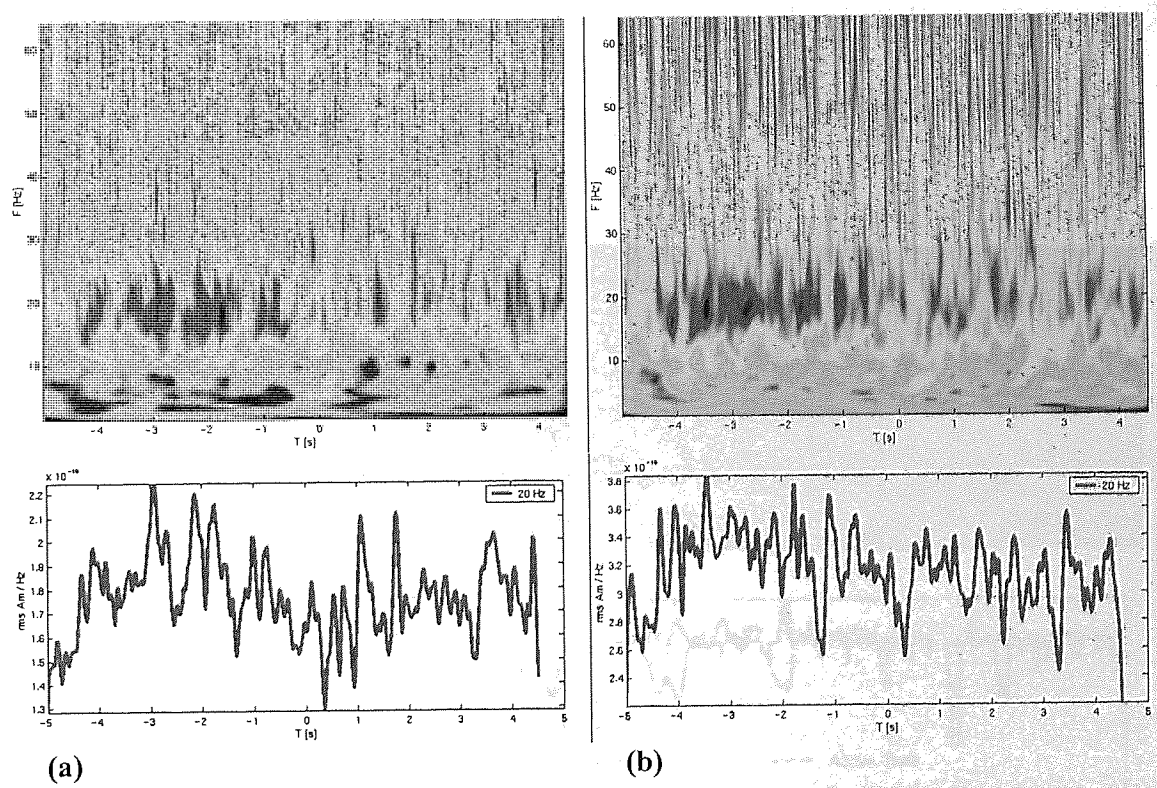

Figure 5-27. Time-frequency spectrograms of a single subject (FAM) data for the responses to a chromatic grating of 1cpd. They show the amount of power change as a function of time between the passive and active states for a voxel representing the highest magnitude of event-related power change **(a)**, and a voxel in V4 **(b).** Note that the responses in both areas are similar with the only difference being that the magnitude of the decrease in cortical power in first voxel is greater.

These spectrograms depict the amount of task-related changes that occur during the passive and active states, but do not relate a measure of statistical significance for this change. A Bootstrap statistical test was performed on the spectrograms in order to determine the statistically significant changes in cortical power at the location of the virtual electrodes. The results are the spectrograms shown in the top panels of figures 5-29a and 5-29b showing calculated for the 2 voxels in the visual cortex. Clearly there is little significant difference in the amount of power change between the active and passive states in the selected voxels, such that the amount of activity in the active state is not markedly different from that in the passive state. For each voxel, the only noticeably significant difference can be seen in the 10-20 Hz band, which does not occur with any consistency during the 5 s. The two panels at the bottom of each spectrogram plot the amount of significant difference between the active and passive states in the 10-25 Hz range.

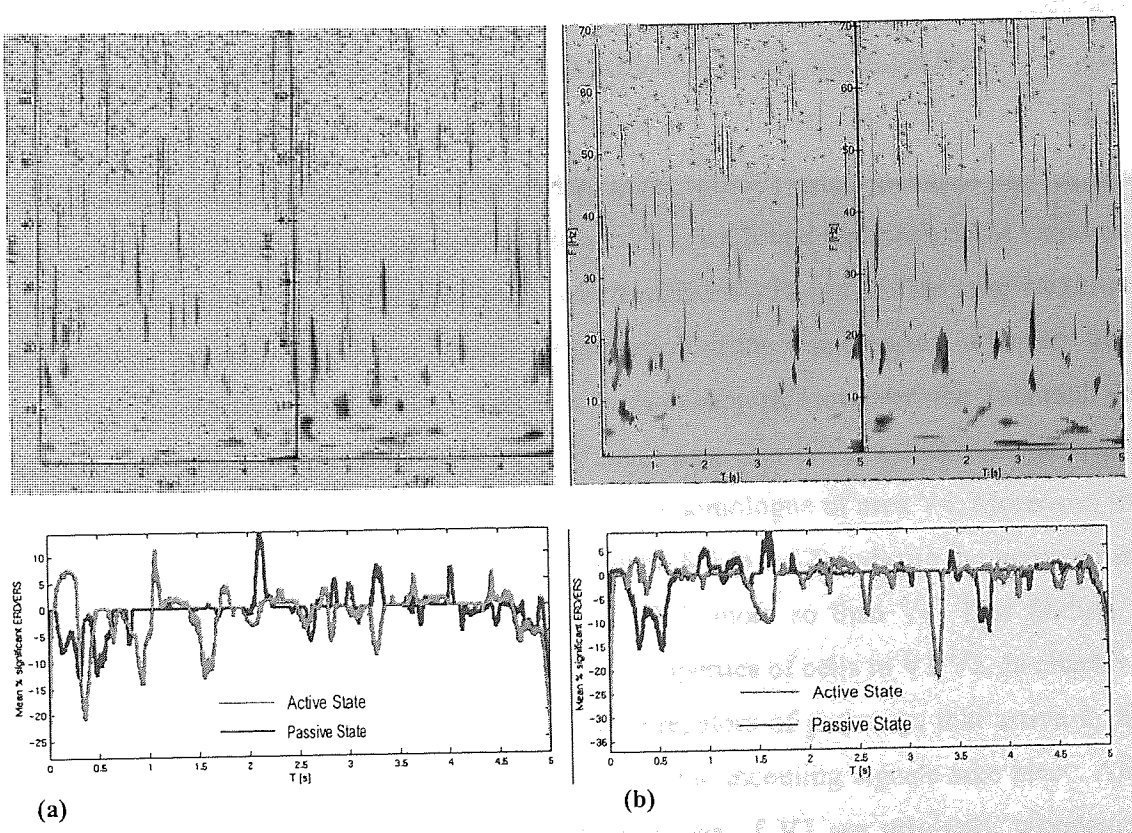

Figure 5-28. Bootstrap analysis of the amount of significant power change between the passive and active states in the voxel representing peak cortical activity near V1 **(a)**, and one representing the highest magnitude of ERD in V4 **(b)**. In each case there is little noticeable amount of significant power change between the active and the passive state. In the 10-20 Hz band, there is a small effect of the stimulus occurring as ERD, although the bottom panels show that the amount of this significant difference is neither sustained nor noticeably high.

5.8 Discussion

In this study, an attempt was made to use the novel MEG analysis technique of SAM to study responses from that part of the human brain thought to be responsible for perception of colour (area V4), using isoluminant colour contrast stimuli. The results show that the cortical region identified as human homologue of V4 was not preferentially activated by the design employed in this study. Desynchronised activation in the 10-20 Hz band was a prominent feature of visual cortex responses to the chromatic stimuli and there is some evidence to suggest that the optimal spatial frequency to produce the highest magnitude of ERD are gratings of 2 and 3cpd. In the gamma frequency range, the responses of the visual cortex were often ERS and confined to a small area within the visual cortex. In what follows, the principal findings of this study are discussed further.

The responses of visual areas and colour specialisation in the visual cortex

Contrary to the MEG study of Fylan et al. (1997) who localised the evoked responses to isoluminant chromatic gratings in area V1, we found that peak SAM responses to similar stimuli occur most frequently in the extrastriate visual cortex. Because we do not have information regarding the retinotopic organisation of the visual cortex, it has not been possible to identify the most active visual area in each subject. However, the Talairach co-ordinates for the peak activations for the group SAM data clearly show that none emanated from the region that has been identified as the human homologue of area V4. Moreover, the investigation of visual areas for subject KDS (figures 5-6 to 5-12) indicate the involvement of extrastriate areas, particularly V2 followed by V3, more so than V4. This finding is interesting in the light of what is known about the properties of cells in V1/V2. In chapter 3 it was described how V1/V2 are thought of as segregators of pathways that arrive in the visual cortex where certain amount of processing of the incoming signals take place. Also recall from sections 3.6.2 and 3.7 that the thin stripes of V2 are primarily wavelength selective (Shipp and Zeki, 1985) and receive their input from the blobs of layers 2 and 3 in V1, which are also wavelength selective. The parvocellular pathway, which conveys colour signals, has been shown to project to the blobs of V1, then to the thin stripes of V2 and then

V4, finally terminating in the ITC (Livingstone and Hubel, 1988). Hence it is very likely that the heightened activity in V2 seen in subject KDS reflects the processing of colour signals by the thin stripes. We have no reason to suspect that the activation of visual areas in other subject is much different from that of subject KDS since the responses of visual cortex are strikingly similar for all subjects.

One surprising feature of the visual cortex responses was the appearance of lateralised activity in response to the binocular viewing of full-field stimulus presentations, with a tendency to occur more often in the left hemisphere. This phenomenon has also been observed in fMRI studies where chromatic stimuli are viewed binocularly (e.g. McKeefry and Zeki, 1997). As described in section 1.6, SAM is incapable of detecting sources with perfectly synchronous time courses. Therefore, it is possible that some activity in one hemisphere is cancelled by stronger activations that are perfectly synchronous, occurring in the opposite hemisphere.

Activations of V1 and V4

Activations of V1/V2 was a consistent feature of the responses to all conditions of the isoluminant chromatic stimuli in the 7 subjects, a fact that is also reflected in the group SAM tuning functions (table 5-4, figure 5-14). This characteristic response of V1/V2 has also been noted in other brain imaging studies into colour vision (e.g. Lueck et al., 1989; Corbetta et al., 1989; McKeefry et al., 1997; Bartels and Zeki, 2000). The involvement of these areas is to be expected given what is known about the anatomy of the colour pathways (see sections 3.6 and 3.7). But the tuning functions in this study have revealed that the responses of the primary visual cortex are frequency specific. Consistent with the individual and group SAM cortical activations (figures 5-4 and 5-5), ERD in the 10-20 Hz band was a salient feature of V1 responses. This frequency dependent ERD was also observed in all the visual areas for subject KDS (figures 5-6 to 5-12). On the other hand similar to the responses of V1 to the luminance contrast gratings (chapter 4), ERS in the gamma range was also observed in response to all conditions of the isoluminant chromatic stimulus although the magnitude to the latter stimulus was markedly less pronounced. This

finding once again suggests that gamma band ERS is a feature of visual cortex responses to a variety of visual stimuli and it is only the magnitude of this response that is dependent upon stimulus parameters. The fact that the primary visual cortex is activated in response to the chromatic gratings is not a unique finding. What is more surprising, however, is the less pronounced activity in these regions for the first 1-second after the onset of the colour stimuli (table 5-5 and figure 5-15). If, as suggested, V1 were the segregator of the magnocellular and parvocellular pathways that project to the visual cortex, it would be reasonable to expect an initially heightened response of this area to all chromatic stimuli.

In contrast to the activity of the primary visual cortex, the analysis of area V4 revealed weaker activations in response to the chromatic stimuli when compared to the activity generated by the control, non-chromatic stimuli. Further evidence that V4 is not preferentially activated in response to chromatic stimulation was provided in figures 5-6 to 5-12, where the flattened visual cortex map of subject KDS was used to calculate the amount of activity in each visual area. Only for a pattern of 6 cpd, the ERD was most pronounced in the 10-20 Hz.

Frequency specificity of visual cortex activations

One interesting feature of the visual cortex responses to the colour stripes is the ERD in the 10-20 Hz band, which is consistently observed for all subjects (figure 5-4) and is also evident in the group SAM data (figure 5-5). This phenomenon can be explained in one of two ways. One explanation is that event-related desynchronisation is a characteristic response of the visual cortex to visual stimuli in the alpha and beta frequency bands. This frequency-specific decrease in cortical synchronisation was also observed in responses to the luminance contrast stripes (figures 4-5 and 4-6). However, the magnitude of the ERDs to the isoluminant colour stimuli is more pronounced than those that occurred in response to the luminance stripes. Therefore, a second interpretation is possible: that the pronounced ERDs reflect the processing of the particular attributes of the stimuli which were absent from the luminance contrast gratings i.e. the colour variable, rather than one that is the general feature of visual system response to visual stimuli. It has been suggested that low

amplitude desynchronised EEG or MEG activity is caused by increased cellular excitability (Steriade and Llinas, 1988; also see section 3.9.2). Recent evidence provides a close link between haemodynamic responses in fMRI and the underlying neuronal activation (Logothetis et al., 2001). Furthermore, it has been shown that ERD can be thought of as an electrophysiological correlate of increased activation in a cortical area (Pfurtscheller and Lopes da Silva, 1999; Singh et al., 2002). Therefore, it is reasonable to assume that the ERD occurring in the 10-20 Hz band represents the responses of neuronal populations that are brought about by the specific aspects of the stimuli, i.e. the colour component.

Similarly, the responses to both non-chromatic and chromatic sets of gratings in V1 are manifest entirely in ERS in the gamma frequency range of 20-70 Hz (figures 4-8 to 4-14 and 5-13). For the luminance stripes, however, the magnitude of this ERS in V1 is considerably more pronounced than for the chromatic gratings, particularly in response to stripe patterns set between 2-4 cpd (tables 4-2 and 5-5). This indicates that although high frequency synchronisation maybe an intrinsic property of the responses of neuronal assemblies to visual stimuli (Gray and Singer, 1989; Gray et al, 1989; Gray and McCormick, 1996) the magnitude of this response depends on stimulus characteristics. In this case the colour gratings produce less activity than high contrast gratings. Similar pattern of activation was observed in area V4 where luminance stripe patterns produced ERS in response to the isoluminant chromatic as well as the non-chromatic contrast stripes, but once more, the magnitude of the response to the latter was greater. This finding may point to the activity of chattering cells (see the discussion in chapter 4), which respond optimally to specific visual stimuli and are thought to facilitate the high frequency synchrony between groups of neurons (Gray and McCormick, 1996). The high magnitude of this response is clearly produced by critical features of the stimuli, likely to be the maximum luminance, square-wave profile of the patterns.

Interestingly, the results of subject KDS also showed that for the middle spatial frequencies of 2 and 3 cpd, the ERS was most pronounced in the gamma range while the ERD in the 10-20 Hz was equally pronounced both decreasing dramatically in response to higher spatial frequencies. This indicated once again that a principal response characteristic

of the visual cortex to stationary stimuli is the fast oscillations in the gamma 20-70 Hz, which depend on the parameters of the stimulus.

Spatial-frequency characteristics of the SAM responses

It can be recalled from the last chapter, that ERS emanating from V1 in response to luminance contrast gratings are manifest in the gamma range and are stimulus-dependent for all subjects, such that the middle spatial frequencies of 2-4cpd produce the most pronounced activity. These responses attenuate for the lowest and highest spatial frequencies. In this study, although gamma activity is present, they are not strongly modulated by the spatial frequency of the isoluminant chromatic gratings. The absence of such a response could be due to the lack of perception of a clear edge between the borders of each chromatic stripe.

On the other hand there is enough evidence from a number of subjects to suggest that the ERD occurring in the 10-20 Hz is spatial frequency-dependent with gratings of 1-3cpd producing characteristically pronounced responses, which attenuate at higher spatial frequencies. This interesting observation is similar to the magnetic recordings of Regan and He (1995) who found that responses to isoluminant red-green gratings are lowpass with the greatest amplitude of response to the lower spatial frequencies of 1 and 2cpd. These responses attenuate steeply with increasing spatial frequency above 2cpd. Fylan et al. (1997) reported similar results by calculating the maximum global field power of evoked response as a function of grating spatial frequency. They found that the chromatic response properties of area V1 have a characteristic peak at 1-2cpd which fall to noise level at 6-8cpd. Figure 5-30 depicts global field power as a function of grating spatial frequency reported by Fylan et al. (1997). The global field power is a measure of the total power in the detector array (19 MEG channels) placed over the occipital area. Based on the SAM responses to the chromatic gratings, we conclude, as did Regan and He (1995) and Fylan et al. (1997), that chromatic responses are lowpass with respect to spatial frequency. Fylan and colleagues attribute this reduction in field power to the small number of cycles displayed such that attenuation of response occurs for patterns of more than six cycles.

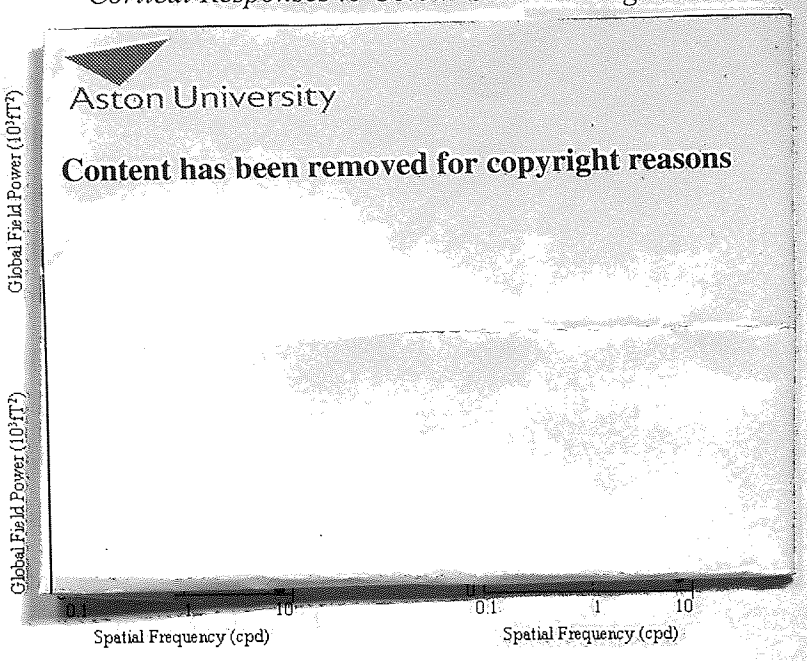

Figure 5-29. Global magnetic field power as a function of spatial frequency of isoluminant chromatic gratings for four subjects. Note the peak responses to spaial frequencies of 1-2cpd. The global field power reflects the total power measured by all the MEG channels (in this case 19) over the occipital area.Reproduced from Fylan et al. (1997).

Are the visual pathways independent?

It was described in chapter 3 that the M and P pathways remain segregated throughout the visual system and are responsible for conveying different types of information to the visual cortex. The M pathway is thought to respond best to motion and luminance, while the P pathway responds to colour and form. The theory of functional specialisation assumes that the P pathway projects via V1 and V2, to area V4, where colour is specifically processed. However, there is some evidence to suggest that although the M and P pathways seem physically and functionally distinct, there is considerable communication between them at all levels (Ramachandran and Gregory, 1978, Ramachandran, 1987). More recently, Zeki (1993) has suggested that when speaking of functional organisation within the visual cortex, it is important to distinguish between the projection of functional pathways and the function of each extrastriate area. In other words, functional specialisation is characterised by the physiological properties of a specific area irrespective of whether it receives input from one or the other pathway, or from both. Consequently, it is perfectly reasonable to suppose that the P pathway may project to V5, or that V4 receives inputs from the M pathway. Indeed the unlikelihood of the two streams remaining fully independent throughout the visual cortex has been substantiated experimentally using anatomical, psychophysical, and lesion studies while the

physiological response properties of the two streams are not entirely dissimilar either. In the first instance, direction selective cells have been found in the P pathway, while the M pathway is also not entirely free from orientation selective neurons (DeYeo and Van Essen, 1988). Secondly, anatomical studies of the macaque have revealed a pattern of connections between V5 and V4 (Maunsell and Ven Essen, 1983). Zeki (1993) has thus conceded that functional specialisation does not imply that each area alone is responsible for each submodality of vision, or that it is the only function of a given area. In other words, although V3, V4 and V5 have been implicated for processing of form, colour and motion, these are not their only function and they are not the only areas involved in their processing. The findings in this study support this latter view that other areas in the visual cortex are involved in processing of colour, more so than V4.

5.9 Conclusion and recommendations

The chromatic stimuli used for identifying the colour-processing regions of the visual cortex did not implicate the human homologue of area V4 as, or the fusiform and lingual gyri, as found in the fMRI studies reviewed earlier. Although the theory of colour specialisation in the visual cortex does not suppose that the colour pathway terminates in V4 (see section 3.7), if one is to believe that V4 is indeed responsible for colour processing in the visual cortex, a much more active involvement of this area in processing of the chromatic stimuli is expected. In any case the results in this study indicate that the area identified as human homologue of V4 is not specialised for processing of colour. The patterns of cortical activations revealed interesting insight into the responses of the visual cortex. It seems that ERS and ERD are characteristic responses of visual cortex to all visual stimuli although the strength of these changes in cortical power are clearly dependent upon the type of stimulations and the parameters of stimulus used.

In the design of the study, certain aspects of the stimulus could be altered in order to eliminate potential inaccuracies in the procedure. As described in chapter 4, in order to record the responses of the brain to colour, all information relating to other aspects of the visual stimulus must be minimised as far as possible such that areas of the brain other than the focus of interest are not activated. For this reason, psychophysical experiments on colour vision use stimuli of equal luminance. In such experiments, isoluminance is achieved by a technique known as heterochromatic flicker photometry (HFP) (Kaiser, 1991). This method is often preferred since isoluminance is a subjective perception. In this technique, each subject adjusts the intensity of light between two chromatic lights that flicker at a rate of 15-20 Hz, until the flicker is no longer perceived. This procedure is ideal when defining the stimuli, and although it is not sufficient to explain the lack of V4 responses, it is a more robust method of defining isoluminance.

References

Achim A. (1995) Cerebral source localisation paradigms: spatiotemporal source modelling. *Brain and Cognition*, **27**, 256-287.

Aine C., George J., Medvick P., Supek S., Flynn E., and Bodis-Wollner I. (1989) Identification of multiple sources in transient visual evoked neuromagnetic responses. In: Advances in Biomagnetism (Eds Williamson, S.J., Hoke, M., Stroink, G., and Kotani, M.) *Plenum Press, New York.*

Aine C.J., (1995) A Conceptual Overview and Critique of Functional Neuroimaging Techniques in Humans: I.MRI/fMRI and PET. *Critical Review of Neurobiology,* **9(2&3),** 229-309.

Ahlfors S., and Ilmoniemi R.J. (1989) Magnetometer position indicator for multi-channel MEG. In: Advances in Biomagnetism (Eds Williamson S.J., Hoke M. Stroink, G., and Kotani M). Plenium Press, New York.

Balish M., and Muratore R. (1990) The Inverse Problem in Electroencephalography and Magnetoencephalography. In: *Advances in Neurology*. (Ed. Susumo Sato). Raven Press, New York.

Bamidis P.D., and Ioannides A.A. (1996) Combination of point and surface matching techniques for accurate registration of MEG and MRI. Tenth International Conference on Biomagnetism – Biomag96, Santa Fe, New Mexico, USA.

Barnes G.R., and Hillebrand A. (2003) Statistical Flattening of MEG Beamformer Images. *Human Brain Mapping*, **18**, 1-12.

Bartels A., and Zeki S. (2000) The architecture of the colour centre in the human visual brain: new results and a review. *European Journal of Neuroscience*, **12(1)**, 172-193.

Basar E., Damirlap T., Schurmann M., Basar-Eroglu C., and Ademoglu A (1999) Oscillatory brain dynamics, wavelet analysis, and cognition. *Brain and Language*, **66**, 146-183.

Berger H. (1930) Uber das Elektrenkephalogramm des Menschen II. J. Psychol. Neurol. 40, 160-179; Cited in: Pfurtscheller G., and Lopes da Silva F.H. (1999a) Event-related EEG/MEG synchronisation: basic principles. *Clinical Neurophysiology*, **110**, 1842-1847.

Blakemore C., and Campbell F.W. (1969) On the existence in the human visual system of neurones selectively sensitive to the orientation and size of retinal images. *Journal of Physiology (London),* **203,** 237-60.

Boycott B.B., and Kolb H. (1973) The horizontal cells of the rhesus monkey retina. *The Journal of Comparative Neurology,* **148**, 115-139.

Boycott B.B., and Wassle H. (1991) Morphological classification of bipolar cells of the primate retina. *European Journal of Neuroscience*, **3,** 1069-1088.

Boynton G.M., Engel S.A., Glover G.H., Heeger D.J. (1996) Linear systems analysis of functional magnetic resonance imaging in human V1. *Journal of Neuroscience,* **16(13),** 4207-21.

Burgess A.P., and Gruzelier J.H. (2000) Short duration power changes in the EEG during recognition memory for words and faces. *Psychophysiology,* **37**, 596-606.

Burkhalter A., and Bernardo K.L. (1989) Organization of corticocortical connections in human visual cortex. *Proceedings of the National Academy of Sciences of the United States of America,* **86**, 1071-1075.

Carelli P., and Fogiletti V. (1983) A second derivative gradiometer integrated with a dc superconducting inferometer. *Journal of Applied Physics*, **54**, 6065-60-67.

Chronicle E.P. and Wilkins A.J. (1991) Colour and visual discomfort in migraineurs. *Lancet,* **338,** 890.

Chatrian G.E., Lettich E., Miller L.H., and Green J.R. (1970) Pattern-sensitive epilepsy. Part 1. An electroencephalographic study of its mechanisms. *Epilepsia,* **15,** 125-49.

Clare M.H., and Bishop G.H. (1954) Responses from an association area secondarily activated from optic cortex. *Journal of Neurophysiology*, **17**, 271-277.

Clarke S., Walsh V., Schoppig A., Assal G., and Cowey A (1998) Colour constancy impairments in patients with lesions of the prestriate cortex. *Experimental Brain Research,* **123**, 154-158.

Cohen D. (1968) Magnetoencephalography: evidence of magnetic fields produced by alpha-rhythm currents. *Science*, **161,** 784-786.

Cohen D., and Cuffin B.N. (1983) Demonstration of useful differences between Magnetoencephalogram and Electroencephalogram. *Electroencephalography and Clinical Neurophysiology,* **56,** 38-51.

Collins R.E.C. (1969) A new escalator injury. *Lancet*, **i**, 1268.

Corbetta M., F. M. Miesin S. Dobmeyer G. L. Shulman and S. E. Petersen (1991) Selective and divided attention during visual discriminations of shape, color and speed: functional anatomy by positron emission tomography. *Journal of Neuroscience,* **11,** 2382-2402.

Cowey A. (1979) Cortical maps and visual perception: the Grindley Memorial Lecture. *The Quarterly Journal of Experimental Psychology,* **31**, 1-17.

Cowey A. and Perry V.H. (1980) The projection of the fovea to the superior colliculus in rhesus monkeys. *Neuroscience,* **5**, 53-61.

Cragg B.G. (1969) The topography of the afferent projections in the circumstriate visual cortex of the monkey studied by the Nauta method. *Vision Research,* **9**, 733-747.

Cuffin B.N. (1986) Effects of measurement errors and noise on MEG moving dipole inverse solustions. *IEEE Transactions on Medical Imaging.* **33,** 854-861.

Cuffin B.N., and Cohen D. (1977) Magnetic Fields of a Dipole in Special Volume Conductor Shapes. *IEEE Transactions in Biomedical Engineering,* **24(4),** 372-381.

Damasio A.R., Damasio H., and Van Hoesen G.W. (1982) Prosopagnosia: anatomic basis and behavioral mechanisms. *Neurology,* **32**, 331-341.

De Valois R.L., and De Valois K.K. (1990) *Spatial Vision.* Oxford University Press.

De Munck J.C. (1989) A mathematical and physical interpretation of the electromagnetic field of the brain. Ph. D. Thesis, University of Amsterdam, The Netherlands.

De Munck J.C., and Spekreijse H. (1989) Dipole localization by VEPs in man. *International Journal of Psychophysiology,* **7**, 177-178.

De Munck J.C., Verbunt J.P.A., Van't Ent D., Van Dijk B.W. (2001) The use of an MEG device as 3D digitizer and motion monitoring system. *Physics in Medicine and Biology,* **46**, 1-12.

De Munck J.C., Vijn P.C., and Spekreijse H. (1991) A practical method for determining electrode positions on the head. *Electroencephalography and Clinical Neurophysiology,* **78**, 85-87.

Desimone R., and Schein S.J. (1987) Visual properties of cells in area V4 of the macaque: sensitivity to stimulus form. *Journal of Neurophysiology*, **57**, 835-868.

Desimone R., Schein S.J., Moran J., and Ungerleider J., (1985) Contour, colour, and shape analysis beyond the striate cortex. *Vision Research*, **25**, 441-452.

DeYoe E.A., and Van Essen D.C. (1988) Concurrent processing streams in monkey visual cortex. *Trends in Neurosciences,* **11**, 219-226.

Dow B.M., and Gouras P (1973) Colour and spatial selectivity of single units in rhesus monkey foveal striate cortex. *Journal of Neurophysiology.* **36**, 79-100.

Dowling J.E. (1987) *The Retina: An Approachable Part of the Brain.* Harvard University Press, Cambridge, MA.

Dubner R., and Zeki S.M. (1971) Response properties and receptive fields of cells in an anatomically defined region of the superior temporal sulcus in the monkey. *Brain Research.* **35**, 528-532.

Engel A.K., König P., Gray C.M., Singer W. (1990) Stimulus-dependent neuronal oscillations in cat visual cortex: intercolumnar interaction as determined by cross-correlation analysis. *Eur J Neurosci* **2,** 588-606.

Engel S.A., Glover G.H., Wandell B.A. (1997a) Retinotopic organization in human visual cortex and the spatial precision of functional MRI. *Cerebral Cortex,* **7(2),** 181-92.

Engel S.A., Rumelhart D.E., Wandell B.A., Lee A.T., Shadlen M., and Glover G. (1994) fMRI of human visual cortex. *Nature,* **369,** 525.

Felleman D. J., and Van Essen D. C. (1991) Distributed hierarchical processing in the primate cerebral cortex. *Cerebral Cortex,* **1,** 1-47.

Fitzpatrick J.M., West J.B. (2001) The Distribution of Target Registration Error in Rigid-Body Point-Based Registration. *IEEE Transactions on Medical Imaging,* **20(9),** 917-927.

Fitzpatrick J.M., West J.B., and Maurer Jr. C.R. Predicting error in Rigid-Body Point-Based Registration. *IEEE Transactions on Medical Imaging.* 1998; **17(5)**, 694-702.

Friedman-Hill S., Maldando P.E., and Gray C.M. (2000) Temporal dynamics of neuronal activity in the striate cortex of alert macaque: I. Incidence and stimulus-dependence of oscillations. *Cerebral Cortex*, **10**, 1105-1116.

Frien A., Eckhorn R., Bauer R., Woelburn T, Kehr H (1994) Stimulus-specific fast oscillations at zero phase between visual areas V1 and V2 of awake monkey. NeuroReport, **5**, 2273-2277.

Fries P., Roelfsema P.T., Engel A.K. König P., & Singer W. (1997). Synchronization of oscillatory responses in visual cortex correlates with perception in interocular rivalry. *Proceedings of the National Academy of Sciences USA,* **94**, 12699-12704.

Fries W. (1981) The projection from the lateral geniculate nucleus to the prestriate cortex of the macaque monkey. *Proceedings of the Royal Society of London. Series B. Biological Sciences,* **213**, 73-86.

Fuchs M., Wischmann H.A., Wagner M., and Kruger J. (1995) Coordinate system matching for neuromagnetic and morphological reconstruction overlay. *IEEE Transactions on Biomedical Engineering.* **42(4)**, 416-420.

Fylan F., Holliday I.E., Singh K.D., Anderson S.J., and Harding F.A. (1997) Magnetoencephalographic investigation of human cortical area V1 using colour stimuli. *Neuroimage*, **6**, 47-57.

George J.S., Jackson P.S., Ranken D.M., and Flynn E.R. (1989) Three-dimensional volumetric reconstruction for neuromagnetic source localisation. In: *Advances in Biomagnetism* (Eds Williamson, S.J., Hoke, M., Stroink, G., and Kotani, M.). Plenum Press, New York.

George J.S., Lewis P.S., Ranken D.M., Kaplan L., and Wood C.C. (1991) Anatomical constraints for neuromagnetic source models. *SPIE Medical Imaging V: Image Physics*, **1443,** 37-51.

Georgeson M.A. (1976) Psychophysical hallucinations of orientation and spatial frequency. *Perception,* **5,** 99-111.

Georgeson M.A. (1980) The perceived spatial frequency, contrast and orientation of illusory gratings. *Perception,* **9,** 695-712.

Gorodnitsky I., George J.S., Schlitt H.A., and Lewis P.S. (1992) A weighted iterative algorithm for neuromagnetic imaging. Satellite Symposium on Neuroscience and Technology, 14th Annual International Conference, Lyon, France.

Gorodnitsky I., and Rao B.D. (1997) Sparse Signal Reconstruction from Limited Data Using FOCUSS: A Re-weighted Minimum Norm Algorithm. *IEEE Transactions in Signal Processing*, **45(3)**, 600-616.

Gouras P. (1968) Identification of cone mechanisms in monkey ganglion cells. *The Journal of Physiology,* **199**, 533-547.

Gray C.M., Engel, A.K., König, P., and Singer. W. (1990) Stimulus-dependent neuronal oscillations in cat visual cortex: receptive field properties and feature dependence. *European Journal of Neuroscience* **2,** 607-619.

Gray C.M., König, P., Engel, A.K., and Singer, W., (1989) Oscillatory responses in cat visual cortex exhibit intercolumnar synchronization which reflects global stimulus properties. *Nature* **338,** 334-337.

Gray C.M., and McCormick D.A. (1996) Chattering cells: Superficial Pyramidal Neurons Contributing to the Generation of Synchronous Oscillations in the Visual Cortex. *Science,* **274,** 109-113.

Gray C.M., and Singer W. (1989) Stimulus-specific neuronal oscillations in orientation columns of cat visual cortex. *Proceedings of the National Academy of Sciences USA,* **86,** 1698-1702.

Gray C.M., and Viana Di Prisco, G., (1997) Stimulus-dependent neuronal oscillations and local synchronization in striate cortex of the alert cat. *J Neurosci 17, 3239-3253.*

Guillery R.W. (1979) A speculative essay on geniculate lamination and its development. *Progress in Brain Research,* **51**, 403-418.

Hadjikhani N., Liu A.K., Dale A., Cavanagh P., and Tootell R.B.H. (1998) Retinotopy and colour sensitivity in human visual cortical area V8. *Nature Neuroscience*, **1**, 235-241.

Hämäläinen M., Hari R., Ilmoniemi R.J., Knuutila J., and Lounasmaa O.V. (1993) Magnetoencephalography – theory, instrumentation, and applications to noninvasive studies of the working human brain. *Reviews in Modern Physics,* **65(2),** 413-497.

Hämäläinen M., and Ilmoniemi R.J. (1984) Interpreting measured magnetic fields of the brain: estimates of current distributions. Helsinki, Helsinki University of Technology, TKK-F-A559.

Hämäläinen M., and Sarvas J. (1989) Realistic Conductivity Geometry Model of the Human Head for Interpolation of Neuromagnetic Data. *IEEE Transactions in Biomedical Engineering,* **36(2),** 165-171.

Harding G.F.A., and Jeavons P. (1994) *Photosensitive Epilepsy*, 2nd Ed. London, Mac Keith Press.

Hari R. (1991) A neurophysiologist's view on biomagnetic source localisation. In: *Biomagnetic Localisation and 3D modelling* (eds. J Nenonen, H-M Rajala and T Katila). Helsinki, Helsinki University of Technology, TKK-F-A559.

Hillebrand A. (2000) The development of constrained source localization algorithms for human imaging. Ph.D. Thesis, Aston University, United Kingdom.

Hillebrand A., and Barnes G.R. (2002) Aquantitative Assessment of the Sensitivity of Whole-Head MEG to Activity in the Adult Human Cortex. *Neuroimage,* **16**, 638-650.

Horton J.C., and Hoyt W.F. (1991) The representation of the visual field in human striate cortex. A revision of the classic Holmes map. *Archives of Ophthalmology* **109**, 816-824.

Hubel D.H., and Wiesel T.N. (1962) Receptive fields, binocular interaction and functional architecture in the cat's visual cortex. *Journal of Physiology (London)*, **160**, 106-154.

Hubel D.H., and Wiesel T.N. (1962) Receptive fields and functionbal architecture of monkey striate cortex. *Journal of Physiology, London*, **195**, 215-243.

Hubel D.H., and Wiesel T.N. (1977) Functional architecture of macaque visual cortex. *Proceeds of the Royal Society of London,* **198,** 1-59.

Hubel D.H., and Wiesel T.N. (1979) Brain mechanisms of vision. *Scientific American,* **241**, 150-162.

Huppertz H-J., Otte M., Grimm C., Kristeva-Feige R., Mergner T., and Luking C. (1998) Estimation of the accuracy of a surface matching technique for registration of EEG and MRI data. *Electroencephalography and Clinical Neurophysiology*. **106**, 409-415.

Irlen, H. (1991) *Reading by the colours: Overcoming Dyslexia and other Reading Disabilities through the Irlen Method.* Avery Publishing Group, New York, USA.

Jeavons P., and Harding G.F.A. (1975) *Photosensitive Epilepsy. Clinics in Developmental medicine No. 56.* London: Spastics International Medical Publications.

Jurgens E., Rosler F., Henninghausen E., and Heil M. (1995) Stimulus induced gamma oscillations; harmonics of alpha activity? *Neuroreport*, **6**, 813-816.

Kolb H. (1994) The architecture of functional neural circuits in the vertebrate retina. The Proctor Lecture. *Investigative Ophthalmology & Visual Science* **35**, 2385-2404.

Kozinska D., Tretiak O.J., Nissonov J., and Ozturk C. (1997) Multidimensional Alignment Using the Euclidean Distance Transform. *Graphical Models and Image Processing*, **59(6)**, 373-387.

Kuffler S.W. (1953) Discharge patterns and functional organisation of the mammalian retina. *Journal of Neurophysiology*, **16**, 37-68.

Lashley K.S. (1948) The Mechanism of vision. XVIII. Effects of destroying the visual 'associative areas' of the monkey. *Genetic Psychology Monographs*, **37**, 107-166.

Livingstone M.S. (1988) Art, illusion and the visual system. *Scientific American* **258,** 78-85.

Livingstone M.S., Hubel D.H. (1984) Anatomy and physiology of a color system in the primate visual cortex *Journal of Neuroscience, 4, 309-356.*

Livingstone M.S., and Hubel D.H. (1987a) Psychophysical evidence for separate channels for the perception of form, colour, movement and depth. *Journal of Neuroscience,* **7(11),** 3416-68.

Livingstone M.S. and Hubel D.H. (1987b) Connections between layer 4B of area 17 and the thick cytochrome oxidase stripes of area 18 in the squirrel monkey. *Journal of Neuroscience,* **7**, 3371-3377.

Livingstone M.S., and Hubel D.H. (1988) Segregation of form, color, movement, and depth: anatomy, physiology, and perception. *Science,* **240**, 740-749.

Livingstone M.S., (1996) Oscillatory firing and interneuronal correlations in squirrel monkey striate cortex. *J Neurophysiol.* **75,** 2467-2485.

Llinas R., Ribary U., Contreras D., and Pedroarena C. (1998) The neural basis for consciousness. *Philosophical Transactions of the Royal Society of London. B. Biological Sciences,* **353(1377)**, 1841-1849.

Logothetis N.K., Schiller P.H., Charles E.R., and Hurlbert A.C. (1990) Perceptual deficits and the activity of the color-opponent and broad-band pathways at isoluminance. *Science,* **247**, 214-217.

Lopes da Silva F.H., van Rotterdam A., Storm van Leeuwen W., and Tielen A.M. (1970) dynamic characteristics of visual evoked potentials in dog. II. Beta frequency selectivity in evoked potentials and background activity. *Electroencephalography and clinical Neurophysiology,* **29**, 260-268.

Lopes da Silva F.H. (1991) Neural mechanisms underlying brain waves: from neural membranes to networks. *Electroencephalography and clinical Neurophysiology.* **110**, 1842-1857.

Lopes da Silva F.H. (1993) Computer-assisted EEG diagnosis: Pattern recognition and brain mapping. In: W Niedermeyer and F. Lopes da Silva (Eds.), *Electroencephalography: Basic Principles, Clinical Applications and Related Fields*, 3rd Edition. Williams and Wilkins, Baltimore, MD, 1063-1086.

Lopes da Silva F.H., van Rotterdam A., Storm van Leeuwen W. and Tielen A.M. (1970) Dynamic characteristics of visual evoked potentials in the dog. II. Beta frequency selectivity in evoked potentials and background activity. *Electroencephalography and clinical Neurophysiology,* **29**, 260-268.

Lueck C.J., Zeki S., Friston K.J., Deiber M-P., Cope P., Cunningham V.J., Lammertsma A.A., Kennard C., and Frackowiack R.S.J. (1989) The colour centre in the cerebral cortex of man. *Nature, London*, **340**, 386-389.

Lund J.S. (1988) Anatomical organization of macaque monkey striate visual cortex. *Annual Review of Neuroscience,* **11**, 253-288.

Lund J.S., Lund R.D., Hendrickson A.E., Bunt A.H., and Fuchs A.F. (1975) The origin of afferent pathways from the primary visual cortex, area 17, of the macaque monkey as shown by retrograde transport of horseradish peroxidase. *Journal of Comparative Neurology*, **164**, 287-303.

Makeig S., Westerfield M., Jung T.P., Enghoff S., Townsend J., Courchesene T., and Sejnowski J. (2002) Dynamic brain sources of visual evoked responses. *Science*, **295**, 690-694.

Maldando P.E., Friedman-Hill S., and Gray C.M. (2000) Temporal dynamics of neuronal activity in the striate cortex of alert macaque: II. Fast time scale synchronisation. *Cerebral Cortex*, **10**, 1117-1131.

Malmivuo J., Suihko V., and Eskola H (1997) Sensitivity Distributions of EEG and MEG Measurements. *IEEE Transactions on Biomedical Engineering*, **44(3)**, 196-208

Mariani A.P. (1981) A diffuse, invaginating cone bipolar cell in the primate retina. *The Journal of Comparative Neurology,* **197**, 661-671.

Maunsell J.H.R., and Newsome W.T. (1987) Visual processing in monkey extrastriate cortex. *Annual Review of Neuroscience*, **10**, 776-783.

Maunsell J.H.R., and Van Essen (1983) The connections of the middle temporal visual area (MT) and their relation to a cortical hierarchy in the macaque monkey. *Journal of Neurophysiology*, **3**, 2563-2586.

Maurer Jr. C.R., Maciunas R.J., and Fitzpatrick J.M. (1998) Registration of Head CT Images to Physical Space Using a Weighted Combination of Points and Surfaces. *IEEE Transactions on Medical Imaging*, **17(5),** 753-761.

McCormick D.A., Connors B.W., Lighthall J.W. and Prince D.A. (1985) Comparative electrophysiology of pyramidal and sparsely spiney neurons of the neocortex. *Journal of Neurophysiology,* **54**, 782-806.

McKeefry D., and Zeki S. (1997) The position and topography of the human colour centre as revealed by functional magnetic resonance imaging. *Brain,* **120**, 2229-2242.

Meadows J.C. (1974a) Disturbed perception of colours associated with localised cerebral lesions. *Brain*, **97**, 615-632.

Meadows J.C. (1974b) The anatomical basis of prosopagnosia. *Journal of Neurology, Neurosurgery and Psychiatry*, **37**, 489-501.

Medvick P.A., Lewis P.S., Aine C., and Flynn E.R. (1989) Monte Carlo analysis of localisation errors in Magnetoencephalography. In: Advances in Biomagnetism (Eds Williamson, S.J., Hoke, M., Stroink, G., and Kotani, M.). *Plenum Press, New York,* 543-546.

Meldrum B.S., and Wilkins A.J. (1984) Photosensitive epilepsy in man and the baboon: integration of pharmacological and psychophysical evidence. In *Electrophysiology of epilepsy* (ed. P.A. Schwartzkroin and H.V. Wheal), pp. 51-77. Academic Press, London.

Menon R.S., Ogawak S., Hu, X., Strupp J.P., Anderson P., and Ugurbil K. (1995) BOLD based functional MRI at 4 tesla includes a capillary bed contribution: echo-planar imaging correlates with previous optical imaging using intrinsic signals. *Magnetic Resonance in Medicine.* **1995**, 453-459.

Merigan W.H. (1989) Chromatic and achromatic vision of macaques: role of the P pathway. *Journal of Neuroscience,* **9**, 776-783.

Merigan W.H., Byrne C.E., and Maunsell J.H.R. (1991). Does primate motion perception depend on the magnocellular pathway? *Journal of Neuroscience,* **11,** 3422-3429.

Merigan W.H., Katz, L.M., and Maunsell, J.H.R. (1989) Contribution of the primate parvocellular pathway to acuity and contrast sensitivity. *Investigative Ophthalmology and Visual Science*, **30,** 53.

Merigan W.H., and Maunsell J.H.R. (1990) Macaque vision after magnocellular lateral geniculate lesion. *Visual Neuroscience*, **5**, 347-352.

Merigan, W.H., and Maunsell J.H.R. (1993) How parallel are the primate visual pathways? *Annual Review of Neuroscience,* **16,** 369-402.

Mishkin M., Ungerleider L.G., and Macko K.A (1983) Object vision and spatial vision: two cortical pathways. *Trends in Neuroscience*, **6**, 414-417.

Mosher J., and Leahy R. (1998) Recursive MUSIC: A framework for EEG and MEG source localisation. *IEEE Transactions in Biomedical Engineering*. **45(11),** 1342-1354.

Mosher J., Lewis P., and Leahy R. (1992) Multiple dipole modelling and localisation from spatio-temporal MEG data. *IEEE Transactions in Biomedical Engineering,* **39**, 541-557.

Mosher J., Lewis P., Lewine J., George J., Leahy R., and Singh M. (1991) Electromagnetic imaging of dynamic brain activity. In *Proceedings of the 1991 IEEE Medical Imaging Conference.*

Nichols T.E., and Holmes A.P. (2002) Nonparametric permutation tests for functional neuroimaging: a primer with examples. *Huuman Brain Mapping*, **15(1)**, 1-25.

Nunez P.L. (1981) *Electric Fields of the Brain*. Oxford University Press, New York.

Nunez P.L. (1986) The brain's magnetic field: some effects of multiple sources on localization methods. *Electroencephalography and Clinical Neurophysiology,* **63,** 75-82.

Nunez P.L. (1995) Neocortical Dynamics and Human EEG Rhythms. *Oxford University Press, New York.*

Okada Y. (1982) Neurogenesis of evoked magnetic fields. In: Biomagnetism: An Interdisciplinary Approach (Eds Williamson, S., Romani, G.L., Kaufman, L., and Modena, I. *Pergamon Press, New York.*

Okada Y.C. (1989) Recent developments on the physiological basis of magnetoencephalography (MEG). In: Advances in Biomagnetism (Eds Williamson, S.J., Hoke, M., Stroink, G., and Kotani, M.). *Plenum Press, New York.*

Panda-Jonas S., Jonas J.B., Jakobczyk M., and Schneider U. (1994) Retinal photoreceptor count, retinal surface area, and optic disc size in normal human eyes. *Ophthalmology,* **101,** 519-523.

Pasqual-Marqui R.D., Michael C.M., and Lehmann D (1994) Low Resolution Electromagnetic Tomography: A new method for localizing electrical activity in the brain. *International Journal of Psychophysiology*, **18**, 49-65.

Pelizzari C.A., Chen G.T., Spelbring D.R., Weichselbaum R.R., and Chen C-T. (1989) Accurate three-dimensional registration of CT, PET, and/or MMR Images of the brain. Journal of Computer Assisted Tomography, **13(1),** 20-26.

Pfurtscheller G. (1992) Event-related synchronisation (ERS): an electrical correlate of cortical areas at rest. *Electroencephalography and clinical Neurophysiology*, **83**, 62-69.

Pfurtscheller, G., Stancák Jr., A. and Edlinger, G. (1997) On the existence of different types of central beta rhythms below 30 Hz. *Electroencephalography and clinical Neurophysiology,* **102,** 316-325.

Pfurtscheller G., and Lopes da Silva F.H. (1999a) Event-related EEG/MEG synchronisation: basic principles. *Clinical Neurophysiology*, **110**, 1842-1847.

Pfurtscheller G., and Lopes da Silva F.H. (1999b) Functional meaning of event-related desynchronisation (ERD) and synchronisation (ERS). (In: Handbook of *Electroencephalography and clinical Neurophysiology.* Pfurtscheller G., and Lopes da Silva F.H. eds.) Elsevier Science.

Poylak S.L. (1941) *The Retina*. University of Chicago Press, Chicago.

Rabin J., Switkes, E., Crognale M., Scheck M.E., and Adams A.J. (1994). Visual evoked potentials in three-dimensional color space: Correlates of spatio-chromatic processing. *Vision Research,* **34,** 2657-2671.

Ramon y Cajal S. (1892) La retine des vertebras. La Cellule, 9: 17-257. In Rodieck R.W. (1973) The Vertebrate Retina. WH Freeman, San Francisco.

Ramachandran V.S. (1987) Interaction between colour and motion in human vision. *Nature*, **328**, 645-647.

Ramachandran V.S., and Gregory R.L. (1978) Does colour provide an input to human motion perception? *Nature*, **275**, 55-56.

Regan D., and He P. (1996) Magnetic and electrical brain responses to chromatic contrast in human. *Vision Research,* **35,** 1-18.

Ribary U., Ioannides A.A., Singh K.D., Hasson R., Bolton J.P.R., Lado F., Mogilner A. and Llinas R. (1991) Magnetic field tomography of coherent thalamocortical 40-Hz oscillations in humans. *Proc. Natl. Acad. Sci. USA,* **88,** 11037-11041.

Roe A.W., and Ts'o D.Y. (1995) Visual topography in primate V2: multiple representation across functional stripes. *The Journal of Neuroscience: the Official Journal of the Society for Neuroscience,* **15**, 3689-3715.

Rockel A.J., Hiorns R.W., and Powell T.P. (1980) The basic uniformity in structure of the neocortex. *Brain,* **103**, 221-244.

Robinson S.E. (1997) Functional imaging of language cortex by MEG. The Japanese Biomagnetism Conference, Japan.

Robinson S.E., and Vrba, J. (1998) Functional Neuroimaging by Synthetic Aperture Magnetometry (SAM). *11th International Conference on Biomagnetism, Sendai, Japan.*

Romani G.L. (1989) Fundamentals on neuromagnetism. In: Advances in Biomagnetism (Eds Williamson, S.J., Hoke, M., Stroink, G., and Kotani, M.) *Plenum Press, New York.*

Sarvas J. (1987) Basic mathematical and electromagnetic concepts of the biomagnetic inverse problem. *Physics in Medical Biology,* **32(1),** 11-22.

Scherg M., and Berg P. (1991) Use of Prior Knowledge in Brain Electromagnetic Source Analysis. *Brain Topography,* **4(2),** 143-150.

Schiller P.H. (1982) Central connections of the retinal ON and OFF pathways. *Nature,* **297**, 580-583.

Schiller P.H. (1986) The central visual system. *Vision Research,* **26**, 1351-1386.

Schiller P.H. (1993) The effects of V4 and middle temporal (MT) area lesions on visual performance in the rhesus monkey. *Visual Neuroscience,* **10(4),** 717-746.

Schiller P.H. (1995) Effect of lesions in visual cortical area V4 on the recognition of transformed objects. *Nature,* **376 (6538),** 342-34.

Schiller P.H., and Logothetis N.K. (1990) The color-opponent and broad-band channels of the primate visual system. *Trends in Neurosciences,* **13**, 392-398.

Schiller P.H., Logothetis N.K., and Charles E.R. (1990a) Functions of the colour-opponent and broad-band channels of the visual system. *Nature,* **343**, 68-70.

Schiller P.H., Logothetis N.K., and Charles E.R. (1990b) Role of the color-opponent and broad-band channels in vision. *Visual Neuroscience,* **5**, 321-346.

Schiller P.H., and Malpeli J.G. (1977). Properties and tectal projections of the monkey retinal ganglion cells. *Journal of Neurophysiology,* **40**, 428-445.

Schiller P.H., Malpeli J.G., and Schein (1979). Composition of geniculostriate input to superior colliculus of the rhesus monkey. *Journal of Neurophysiology,* **42**, 1124-1133.

Schiller P.H., Sandell J.H., and Maunsell J.H. (1986) Functions of the ON and OFF channels of the visual system. *Nature,* **322**, 824-825.

Schaefer M., Muhlnickel W., Grusser S. M., Flor H. (2002) Reproducibility and Stability of Neuroelectric Source Imaging in Primary Somatosensory Cortex. *Brain Topography,* **14(3),** 179-189.

Schwartz D., Lemoine D., Poiseau E., and Barillot C. (1996) Registration of MEG/EEG data with 3D MRI: Methodology and precision issues. *Brain Topography*, **9(2)**, 101-116.

Shapley R.M., Kaplan E., and Soodak R. (1981) Spatial summation and contrast sensitivity of X and Y cells in the lateral geniculate nucleus of the macaque. *Nature* **292**, 543-545.

Shipp S., and Zeki S.M. (1985) Segregation of pathways leading from area V2 to areas V4 and V5 of macaque monkey visual cortex. *Nature, London*, **315**, 322-325.

Shipp S., and Zeki S.M. (1989a) The organisation of connections between areas V5 and V1 in the macaque monkey visual cortex. *European Journal of Neuroscience*, **1**, 309-332.

Shipp S., and Zeki S.M. (1989b) The organisation of connections between areas V5 and V2 in the macaque monkey visual cortex. *European Journal of Neuroscience*, **1**, 333-354.

Singer W. (1993) Synchronization of cortical activity and its putative role in information processing and learning. *Annual Review of Physiology,* **55,** 349-374.

Singer W., and Gray C.M. (1995) Visual feature integration and the temporal correlation hypothesis. *Annual Review of Neuroscience B*, **18**, 555-586.

Singh K.D., Barnes G.R., Hillebrand A., Forde E.M., and Williams A.L. (2002) Task-related changes in cortical synchronisation are spatially coincident with the hemodynamic response. *Neuroimage*, **16(1),** 103-14.

Singh K.D., Barnes G.R. Hillebrand A. (2002) Group Imaging of Task-Related Changes in Cortical Synchronisation using Non-Parametric Permutation Testing. *In Press.*

Singh K.D., Holliday I.E., Furlong P.L., and Harding G.F.A. (1997) Evaluation of MEG/EEG co-registration strategies using Monte Carlo simulation. *Electroencephalography and Clinical Neurophysiology*, **102**, 81-85.

Steriade M., and Llinas R.R. (1988) The functional states of the thalamus and the associated neuronal interplay. *Physiological Reviews,* **68**, 649-742.

Swinney K.R., and Wikswo, Jr. J.P. (1980) A calculation of the magnetic field of a nerve action potential. *Biophysiological Journal*, **32,** 719-732.

Tallon-Baudry C., and Bertrand O. (1999) Oscillatory gamma activity in humans and its role in object representation. *Trends in Cognitive Sciences*, **3**, 151-162.

Tallon-Baudry C., and Bertrand O., Delpeuch C., Pernier J. (1997) Oscillatory γ-Band (30-70 Hz) Activity Induced by a Visual Search Task in Humans. *The Journal of Neuroscience*, **17(2)**, 722-734.

Tallon-Baudry C., and Bertrand O., Delpeuch C., Pernier J. (1996) Sstimulus specificity of phase-locked and non-phase locked 40-Hz visual responses in human. *Journal of Neuroscience*, **16**, 4240-4249.

Tootell R.B.H., Silverman M.S., and De Valois R.L. (1981) Spatial frequency columns in primary visual cortex. *Science*, **214**, 813-815.

Traub R.D., Whittington M.A., Buhl E.H. LeBeau F.E., Bibbig A., and Boyd S. (2001) A possible role for gap junctions in generation of very fast EEG oscillations preceding the onset of, and perhaps initiating seizures. *Epilepsia*, **42**, 153-170.

Ungerleider L. G., and Mishkin M. (1982) Two cortical visual systems. In D. J. Ingle, M. A. Goodale, and R. J. W. Mansfield, Eds. *Analysis of Visual Behavior.* Cambridge, MA: MIT Press, pp. 549-586.

Van Essen D.C. (1985) Functional organization of primate visual cortex. In *Cerebral Cortex*, ed. Peters, A., and Jones, E.G. New York: Plenum Publishing Company.

Van Essen D.C., Felleman, D. J., DeYoe E.A., Olavarria, J. and Knierim J.J. (1990) Modular and hierarchichal organization of extrastriate visual cortex in the macaque monkey. *Cold Spring Harbor Symposium. Quantitative Biology,* **55,** 679.

Van Essen D.C., Felleman, D. J., DeYoe E.A., and Knierim J.J. (1993) Probing the Primate Visual Cortex: Pathways and Perspectives. In: *Functional organization of the human visual cortex.* Ed. Gulyas B., Ottoson D., and Roland P.E. Oxford Pergamon Press.

Van Essen D.C., and Zeki S. (1978) The topographic organisation of rhesus monkey prestriate cortex. *Journal of physiology. London*, **277**, 193-226.

Van Essen D.C., Anderson C.H., and Felleman D.J. (1992) Information processing in the primate visual system: an integrated systems perspective. *Science,* **255**, 419-423.

Van Veen B. D., van Drongelen W., Yuchtman M., and Suzuki A. (1997) Localisation of brain electrical activity via linearly constrained minimum variance spatial filtering. *IEEE Transactions in Biomedical Engineering*, **44(9),** 867-80.

Vrba J. (1997) Baseline optimization for noise cancellation systems. *IEEE-EMBS, Chicago.*

Vrba J. (1998) Optimization of SQUID Detectors for MEG Application. *The Japanese Magnetics Society, Tokyo, Japan.*

Vrba J., Taylor B., Haid G., Cheung T., Cheyne D, Fife A.A., Kubik P.R., Lee S., McCubbin J., and Burbank M.B. (1994) Whole Cortex MEG Systems. Paper presented at NABMAG.

Wade N.J. (1977) Distortions and disappearance of geometrical patterns. *Perception*, **6,** 407-33.

Wade N.J. (1978) Opt art and visual perception. *Perception*, **7**, 21-46.

Wandell B.A., Engel, S.A. and Hel-Or, H.Z. 1996. Creating images of the flattened cortical sheet. *Investigative Opthamology and Vision Science*, **37: S10**, 81.

Wang J-Z (1993) Minimum-Norm Least-Squares Estimation: Magnetic source images for spherical images for a spherical model head. *IEEE Transactions On Biomedical Engineering*, **40**, 387-396.

Wassle H., Grunert U., Rohrenbeck J., and Boycott B.B. (1989) Cortical magnification factor and the ganglion cell density of the primate retina. *Nature,* **341**, 643-646.

Watanabe M., and Rodieck R.W. (1989) Parasol and midget ganglion cells of the primate retina. *The Journal of Comparative Neurology,* **289**, 434-454.

Wiesel T.N., and Hubel D.H. (1966) Spatial and chromatic interactions in the lateral geniculate body of the rhesus monkey. *Journal of Neurophysiology,* **29**, 1115-1156.

Wikswo J.P. (1989) Biomagnetic sources and their models. In: *Advances in Biomagnetism* (Eds Williamson, S.J., Hoke, M., Stroink, G., and Kotani, M.) *Plenum Press, New York.*

Wilkins, A. J. (1986) What is Visual discomfort? *Trends in Neurosciences*, **9**, 343-346.

Wilkins, A. J. (1995) *Visual Stress*, Oxford University Press, Oxford.

Wilkins A.J., Binnie, C.D., and Darby, C.E. (1981). Interhemispheric differences in photosensitivity: I. Pattern sensitivity thresholds. *Electroencephalography and Clinical Neurophysiology*, **5,** 461-8.

Wilkins A.J., Darby, C.E., Stefansson S.F., Jeavons P.M., and Harding G.F.A. (1979). Television epilepsy: the role of pattern. *Electroencephalography and Clinical Neurophysiology*, **47,** 163-71.

Wilkins A.J., and Nimmo-Smith I. (1984). On the reduction of eye-strain when reading. *Ophthalmic and Physiological Optics*, **4(1),** 53-9.

Wilkins A.J., and Nimmo-Smith I. (1987) The clarity and comfort of printed text. *Ergonomics*, **30(12),** 1705-20.

Wilkins A.J., Nimmo-Smith I., Tait, A., McManus C., Della Sala S., Tilley A., Arnold K., Barrie M., and Scott S. (1984). A neurological basis for visual discomfort. *Brain,* **107,** 989-1017.

Wilkins A.J., Patel R., Adjamian P., and Evans B.J.W (2002) Tinted spectacles and visually sensitive migraine. *Cephalalgia*, **22**, 711-719.

Williamson S.J., and Kaufman L. (1981) Magnetic fields of the cerebral cortex, in *Biomagnetism*, (H.D. Hahlbohm and H. Lubbig, Eds.) S.N. Eme, Walter de Gruyter & Co., Berlin New York, 353-401.

Williamson S.J., and Kaufman L. (1987) Analysis of Neuromagnetic Signals. In: *Handbook of Electrencephalography and Clinical Neurophysiology* (Eds Gevins, A.S., and Rémond, A.) *Elsevier, Amsterdam.*

Wood C.C., Cohen D., Cuffin B.N., Yarita M., and Allison T. (1985) Electrical sources in human somatosensory cortex: identification by combined magnetic and potential recordings. *Science,* **277,** 1051-1053.

Zeki S.M. (1969a) Representation of central visual fields in prestriate cortex of monkey. *Brain Research,* **14**, 271-291.

Zeki S.M. (1969b) The secondary visual areas of the monkey. *Brain Research,* **13**, 197-226.

Zeki S.M. (1971) Cortical projections from two prestriate areas in the monkey. *Brain Research, Amsterdam,* **34**, 19-35.

Zeki S.M. (1973) Colour coding in the rhesus monkey prestriate cortex. *Brain Research, Amsterdam,* **53**, 422-427.

Zeki S.M. (1974a) The mosaic organisation of the visual cortex in the monkey. In: *Essays on the nervous system* (Ballairs R, Grey EG, eds.) pp 327-343. Oxford: Clarendon.

Zeki S.M. (1974b) Functional organisation of a visual area in the posterior bank of the superior temporal sulcus in the rhesus monkey. *Journal of Physiology,* **236,** 549-573.

Zeki S.M. (1975) The functional organisation of projections from striate to prestriate areas visual cortex in the rhesys monkey. *Cold Spring Harbor Symposia on Quantitative Biology,* **40**, 591-600.

Zeki S.M. (1977) Colour coding in the superior temporal sulcus of rhesus moneky visual cortex. *Proceedings of the royal society of London, B,* **197**, 195-223.

Zeki S.M. (1978a) Functional specialisation in the visual cortex of the rhesus monkey. *Nature*, **274**, 423-8.

Zeki S.M. (1978b) The cortical projections of foveal striate cortex in the rhesus monkey. *Journal of Physiology*, London, **277**, 227-244.

Zeki S.M. (1978c) The third visual complex of rhesus monkey prestriate cortex. *Journal of Physiology*, London, **277**, 245-272.

Zeki S.M. (1983a) The distribution of wavelength and orientation cells in different areas of monkey visual cortex. *Proceedings of the Royal Society of London, B,* **217**, 449-470.

Zeki S.M. (1983b) Colour coding in the cerebral cortex: the reaction of cells in monkey visual cortex to wavelength and colours. *Neuroscience*, **9**, 741-765.

Zeki S.M. (1990) A century of cerebral achromatopsia. *Brain*, **113**, 1721-1777.

Zeki S.M. (1993). *A Vision of the Brain.* Oxford: Blackwell.

Zeki S.M., and Marini L. (1998) Three cortical stages of colour processing in the human brain. *Brain*, **121**, 1669-1685.

Zeki S.M. and Shipp, S. (1988). The functional logic of cortical connections. *Nature*, **335**, 311-317.

Zeki S.M., Watson, J.D.G., Lueck, C.J., Friston, K.J., Kennard, C., Frackowiak, R.S.J. (1991). A direct demonstration of functional specialisation in human visual cortex. *Journal of Neuroscience,* **11,** 641-649.

Zhuang P., Toro C., Grafman J., Manganotti P., Leocani L., and Hallett M. (1997) Event-related desynchronisation (ERD) in the alpha frequency during development of implicit and explicit learning. *Electroencephalography and clinical Neurophysiology,* **102**, 374-381.

Zihl J., von Cramon D., and Mai N. (1983) Selective disturbance of movement vision after bilateral brain damage. *Brain,* **106**, 313-340.

Zimmerman J.E. (1977) SQUID instruments and shielding for low-level magnetic measurements, *Journal of Applied Physics*, **48**, 702-710.

Appendices

Appendix 1.

Please look at the dot at the centre of the pattern for 5 seconds and tick off the illusions you saw on the checklist below. If you find the pattern aversive, do not force yourself to look at it. If you have photosensitive epilepsy or migraine, do not look at the pattern.

Checklist:

Red

Green

Blue

Yellow

Blurring

Bending of the lines

Shadowy shapes amongst the lines

Shimmering of the lines

Flickering of the whole pattern

Nausea

Dizziness

Pain

Eye-strain

In general, how do you rate the pleasantness of the pattern?

<>Pleasant <>Mildly unpleasant <>Uncomfortable to look at <>I am aversive to it